Hybrid Fibre and Free-space Optical Solutions in Optical Access Networks

Mbah Afamefuna Maduka, MSc.

Thesis submitted to the University of Nottingham

for the degree of Doctor of Philosophy

March 2016

Abstract

This thesis evaluates the potentials of hybrid fibre and free space optical (FSO) communications access networks in providing a possible solution to an all optical access network. In such network architectures, the FSO link can extend the system to areas where an optical fibre link is not feasible, and/or provide limited mobility for indoor coverage. The performance of hybrid fibre and FSO (HFFSO) networks based on digital pulse position modulation (DPPM), for both the indoor and outdoor environments of the optical access network, are compared with the performance of such a network that is based on conventional on-off keying non-return-to-zero (OOK NRZ) modulation using results obtained through computational and analytical modelling. Wavelength division multiplexing (WDM) and/or code division multiple access (CDMA) are incorporated into the network for high speed transmission and/or network scalability.

The impacts of optical scintillation, beam spreading and coupling losses, multiple access interference (MAI), linear optical crosstalk and amplified spontaneous emission noise (ASE) on the performance of hybrid fibre and FSO (HFFSO) access networks are analysed, using performance evaluation methods based on simple Gaussian approximation (GA) and more complex techniques based on moment generating function (MGF), including the Chernoff bound (CB), modified Chernoff bound (MCB) and saddlepoint approximation (SPA). Results in the form of bit error rate (BER), power penalty, required optical power and outage probability are presented, and both the CB and MCB, which are upper bounds, are suggested as safer methods of assessing the performance of practical systems.

The possibility of using a CDMA-based HFFSO network to provide high speed optical transmission coverage in an indoor environment is investigated. The results show a reduction in transmit power of mobile devices of about 9 – 20 dB (depending on number of active users) when an optical amplifier is used in the system compared to a non-amplified system, and up to 2.8 dB improvement over OOK NRZ receiver sensitivity is provided by a DPPM system using integrate and compare circuitry for maximum likelihood detection, and at coding level of two, for minimum bandwidth utilization.

Outdoor HFFSO networks using only WDM, and incorporating CDMA with WDM, are also investigated. In the presence of atmospheric scintillations, an OOK system is required (for optimum performance) to continuously adapt its decision threshold to the fluctuating instantaneous irradiance. This challenge is overcome by using the maximum likelihood detection DPPM system, and necessitated the derivation of an interchannel crosstalk model for WDM DPPM systems. It is found that optical scintillation worsens the effect of interchannel crosstalk in outdoor HFFSO WDM systems, and results in error floors particularly in the upstream transmission, which are raised when CDMA is incorporated into the system, because of MAI. In both outdoor HFFSO networks (with WDM only and with WDM incorporating CDMA), the optical amplifier is found necessary in achieving acceptable BER, and with a feeder fibre of 20 km and distributive FSO link length of 1500 m, high speed broadband services can be provided to users at safe transmit power at all turbulence levels in clear air atmosphere.

Dedication

To Chidi, Tochi and Zara

and

to the loving memory of my beloved sister Amaka Nkay Mbakwe

Acknowledgements

Contents

List of Acronyms

AA	Aperture averaging
ADSL	Asymmetric digital subscriber loop
AEL	Accessible emission limit
ANSI	American National Standards Institute
AON	Active optical network
APD	Avalanche photodiode
ASE	Amplified spontaneous emission
AWG	Arrayed waveguide grating
BEP	Binary error probability
BER	Bit error rate
CB	Chernoff bound
CDM	Code division multiplexing
CDMA	Code division multiple access
CWDM	Coarse wavelength division multiplexing
DBR	Distributed Bragg reflector
Demux	De-multiplexer
DFB	Distributed feedback
DPPM	Digital pulse position modulation
DPSK	Differential phase-shift keying
DWDM	Dense wavelength division multiplexing
EDFA	Erbium-doped fibre amplifier
FA	Frame aligned
FBG	Fibre Bragg grating
FEC	Forward error correction
FET	Field effect transistor
FOV	Field-of-view
FPA	Fabry Perot amplifier
FSO	Free-space optical
FTTH	Fibre-to-the-home

GA	Gaussian approximation
GG	Gamma-gamma
HFFSO	Hybrid fibre and FSO
ICNIRP	International Commission on Non-Ionizing Radiation Protection
IEC	International Electrotechnical Commission
ITU	International Telecommunication Union
KD	K distribution
LASER	Light amplification by stimulated emission of radiation
LED	Light emitting diode
LN	Lognormal
MAI	Multiple access interference
MCB	Modified Chernoff bound
MEMS	Micro-electromechanical system
MGF	Moment generating function
MPE	Maximum permissible exposure
Mux	Multiplexer
MZI	Mach-Zehnder interferometer
NE	Negative exponential
NF	Noise figure
NRZ	Non-return-to-zero
OA	Optical amplifier
OBPF	Optical bandpass filter
OCDM	Optical CDM
OCDMA	Optical CDMA
OLT	Optical line terminator
ONU	Optical network unit
OOC	Optical orthogonal code
OOK	On-off keying
OSA	Only slots aligned
OSNR	Optical signal-to-noise ratio
PAT	Pointing, acquisition and tracking

PCA	Power control algorithm
pdf	Probability density function
P-I-N	Positive-intrinsic-negative
PLL	Phase-locked loop
PON	Passive optical network
PSD	Power spectral density
PSK	Phase-shift keying
RCL	Receiver collecting lens
RF	Radio frequency
RHS	Right-hand side
RN	Remote node
RZ	Return-to-zero
Sig,TurbXT	Signal with no turbulence, interferer with turbulence
Sig,XT	Signal with no turbulence, interferer with no turbulence
SM	Slot misaligned
SOA	Semiconductor optical amplifier
SPA	Saddlepoint approximation
TDM	Time division multiplexing
TDMA	Time division multiple access
TL	Transmitting lens
TurbSig	Signal with turbulence, no interferer
TurbSig,TurbXT	Signal with turbulence, interferer with turbulence
TurbSig,XT	Signal with turbulence, interferer with no turbulence
TWA	Travelling-wave amplifier
VCSEL	Vertical cavity surface emitting laser
VDSL	Very high speed digital subscriber loop
VOA	Variable optical attenuator
WDM	Wavelength division multiplexing
WDMA	Wavelength division multiple access
XT	Crosstalk

List of Figures

xviii

List of Tables

CHAPTER 1   Introduction

1.1 Optical communication – historical overview

Before the advent of the laser, incoherent light was employed in various roles to facilitate telecommunication. In Claude Chappe's invention of the optical telegraph in 1792, the optical wave was used for illumination of coded signals, to enable proper interception at relay stations [1]. About a century later, Alexander Graham Bell experimentally demonstrated the use of an optical wave as a carrier in the first free space communication [2]. However, the transmission distance was just 200 m, and was significantly less than the long distance transmission of about 1000 km provided by electric telegraphy, which had fully replaced Claude Chappe's optical telegraph by 1859 [1-3].

The invention of the laser (originally an acronym LASER for light amplification by stimulated emission radiation) in 1960 [4] was timely for the glass-clad fibres, which were readily available, but with application limited to the medical field because of high attenuation over a long distance caused by impurities present in the glass material [5]. Further work [6, 7] lead to the development of a low loss (about 20 dB/km) multimode optical fibre in 1970, and coupled with the availability of Gallium Arsenide (GaAs) semiconductor laser diodes, stimulated the first boom in optical fibre communication near the 800 nm wavelength, starting with a data rate of 45 Mbps [5]. Several factors, including the development of compact transceivers operating around the 1300 nm wavelength, the realization of single mode fibre and dispersion-shifted fibre and the development of the optical amplifier (e.g. erbium doped fibre amplifier (EDFA)) lead to a full evolution and maturity of optical fibre communication systems and technology, capable of carrying data at terabit per second (Tbps) speed over several thousands of kilometre [1].

Due to the great advances in optical fibre, research and development of free space optical communication systems then focused on deep space and intersatellite applications [8-10]. The resurgence of interest in terrestrial application of free space optical (FSO) communication arguably began around September 2001 [11] due to the terrorist destruction of existing communication links and equipment at the World Trade Center, as Merrill Lynch deployed free

space optical communication links to re-establish connection with some of its offices at a distance of about 2.5 km [11-13]. About a decade later, free space optical communication systems operating at 10 Gbps have been standardized and are commercially available [14].

Thus, the aim of this research work is to investigate and evaluate the performance of optical access networks that use fibre and/or FSO technology, with the primary objectives to:

- review the existing fibre and free space systems, devices and technologies
- identify candidate architectures for future fibre and FSO optical access networks including a multiple access scheme,
- identify the impairments that will exist in these architectures and how they may be modelled,
- identify architectures and/or modelling techniques that are advantageous and novel and study the performance in depth, with emphasis on BER,
- consider the challenges in providing mobility in the optical access networks.

1.2 Optical access networks

At the lowest hierarchy of the telecommunication network is the access network, which broadly covers the entire network between the user's device and the service provider's hub. For most of the last century, the first/last mile of the access network was dominated by copper wire and coaxial cable connections. Digital subscriber loop (DSL) technologies were later introduced to cope with the explosion of internet services and are found in most access networks across Europe, sometimes jointly implemented with radio frequency (RF) and microwave communication technologies for ubiquitous coverage and enhanced mobility [15]. However, the data rates achievable with very high speed digital subscriber loops (VDSLs), RF, millimetre wave and microwave technologies were significantly less than the 10 Gbps which could easily be achieved with an optical carrier [16]. Increasing variation and complexity in user need and greater demand for broadband services led to the deployment of fibre in the last mile of the access network, providing a fibre-to-the-home optical access network.

Optical access networks are grouped into two major categories, that is the active optical network (AON) and passive optical network (PON) [17]. The AON includes point-to-point connections (sometimes referred to as home run [18] when between exchange and the user premises) with a dedicated fibre link directly connecting each home to the optical line termination (OLT) located at the service provider's central office (CO), and the active star configurations which utilize electrically powered switches at the remote node to manage the distribution of steady state traffic to each home [15, 19, 20]. The PON on the other hand is mainly in a tree and branch/point-to-multipoint architecture, and employs passive devices (e.g. optical splitters, couplers or arrayed waveguides (AWG)) at the remote node to separate and forward each end user's signal to the optical network unit (ONU) located at their home or building. PON is more common than AON in fibre optical access networks and offers several advantages over AON such as efficient use of installed infrastructure (e.g. shared fibre pair and fewer transceiver devices compared to multiple fibre pairs in home run connection and additional transceiver devices in active star AON [19]), low maintenance cost and non-requirement of extra power supply for switching devices. However, the use of passive components in PON does result in difficulty in isolating faults as such devices cannot be accessed or diagnosed remotely.

It is problematic to install fibre in some locations within the access network due to environmental reasons or topographical barrier [21]. In addition, provision of access and approvals from local authorities for digging and trenching across sensitive infrastructures may be difficult. Another challenge with an all fibre optical access network is that fibre links terminate at a fixed point (the ONU) in the building which does not provide any kind of mobility for indoor users. This was less of a problem about two decades ago when computing devices were bulky. However, with the miniaturization of most computing and communication devices, users are often demanding one kind of broadband service or the other while moving around in their homes.

An alternative optical access technology, notably FSO, has been advanced to complement existing fibre installations in the optical access network [21, 22]. It is expected that a successfully deployed FSO communication system will provide a viable solution to the bottleneck seen in broadband signal transmission to existing homes where fibre could not be installed. Unlike RF communication, FSO

communication is immune to multipath fading, and offers a more secure transmission within a huge unregulated bandwidth and with reduced power requirement [23-26]. FSO systems can also be deployed in the optical access network as an emergency link, alternative back up link or in a hybrid with fibre (either connecting two feeder fibre links together [27, 28] or just as a distribution link in the last mile). In addition, FSO communication links can be extended to provide all optical broadband service to indoor users, with limited mobility.

A hybrid fibre and FSO (HFFSO) communication link offers several advantages to the optical access network compared to an all fibre link, including easier penetration (e.g. the FSO part of the link could be used for connections between buildings and to bypass difficult barriers), easier deployment (no trenching required for the FSO part of the link) and reduced deployment cost (as fewer fibre installations would be required) [12, 29, 30]. Compared to an FSO only link, a hybrid offers longer reach and thus the potential for greater centralization of the OLT. Both optical fibre and FSO systems are highly compatible, with very similar properties, and use similar device technologies [31]. Therefore a hybrid fibre and FSO (HFFSO) optical access network would benefit immensely from the already mature optical fibre technology, and both systems could seamlessly combine to provide higher bandwidth to users in the optical access network, with excellent quality of service (QoS).

Generally, an optical access network supports many users. From a service provider's perspective, the viability of such a network is highly dependent on its user capacity and possible scalability. Deployment cost in the optical access network is reduced by network resource sharing among users. For example in PON, multiple users' signals are transported through a single optical channel and share one kind of (active or passive) optical component or the other, such as optical amplifiers, multiplexers and demultiplexers or power splitters. Resource management and access protocols are employed for this purpose, with each user assigned a specific time slot, wavelength, code or spatial orientation. Thus PON systems are classified based on the multiplexing/multiple access technique used in its application, e.g. time division multiplexing/time division multiple access (TDM/TDMA) PON, wavelength division multiplexing/wavelength division multiple access (WDM/WDMA) PON, optical code division multiplexing/optical code division multiple access (OCDM/OCDMA) PON, space division

4

multiplexing (SDM) PON [32] or a hybrid of any of the above techniques [17, 18, 33].

A detailed analysis of the performance of HFFSO systems in an optical access network is provided in this thesis with major focus on wavelength division multiplexing (WDM) and code division multiple access (CDMA) techniques and considering PON architecture. The effects of several impairments (such as multiple access interference (MAI), interchannel crosstalk, turbulence induced scintillation, background ambient light and different kinds of noise) on such systems are considered in the analysis. Performance evaluation methods including the Gaussian approximation (GA), and moment generating function (MGF) based techniques such as Chernoff bound (CB), modified Chernoff bound (MCB) and saddlepoint approximation (SPA), are used to facilitate the analysis. Results are obtained using well-known modulation schemes, specifically, on-off-keying non-return-to-zero (OOK NRZ) and digital pulse position modulation (DPPM), and presented in the form of bit error rate (BER), required optical power, power penalties and outage probability.

1.3 Thesis structure

This thesis contains eight further chapters and is organised as follows: In Chapter 2, a detailed review of different optical communication system components (including the receiver and transmitter devices) and optical amplification processes is provided. This chapter also presents a review of popular modulation schemes applied in optical communication systems, specifically the OOK and DPPM modulation formats, and briefly introduces the optical channel. The next chapter presents a detailed study of the nature of optical channels with focus on optical fibre and FSO channels and a general overview of the behaviour of each channel is presented. Multiplexing and multiple access techniques are also covered in this chapter with a full consideration of different kinds of impairments found in HFFSO communication systems. The performance evaluation techniques used in system modelling in this thesis are also studied in this chapter. In Chapter 4, a performance analysis of an optically preamplified HFFSO network using CDMA in an indoor environment is presented for OOK and DPPM systems. A model for the performance evaluation of interchannel crosstalk for a WDM DPPM system is developed in Chapter 5. Numerical results and analysis are presented

under various forms of misalignment between the signal frame and the crosstalk frame in a non-turbulent FSO system and for both single and multiple crosstalk sources. The model developed in Chapter 5 is used to investigate the impact of atmospheric turbulence and interchannel crosstalk in a HFFSO WDM DPPM network in Chapter 6. Numerical results are provided to show how design parameters such as FSO link lengths for both the signal and interferer and demultiplexer adjacent channel rejections affect the network performance. The outage probability in a HFFSO WDM network impaired by turbulence-accentuated interchannel crosstalk is analysed in Chapter 7 for both OOK and DPPM systems. Numerical results are presented to reveal that a system with good average BER could have instantaneous periods of outages which would affect the overall quality of service (QoS). A HFFSO WDM network including optical code division multiple access (OCDMA) technique for improved user capacity is proposed in Chapter 8. The thesis is concluded in Chapter 9 with concise details of the potentials of the HFFSO schemes, and a report of possible areas for future work in the thesis field.

1.4 New contributions to knowledge

This thesis focuses on the application of a hybrid fibre and free space optical (HFFSO) solution to optical access network. An all optical access network requires that optical signals extend to the indoor environment where users with small mobile devices could use this service conveniently in different rooms and offices. Several considerations of an indoor system in the literature reported restrictions in optical power transmission requirement due to eye or skin safety and have generally considered single room architecture [34-37]. This motivated the writing of a paper entitled: '*Indoor Hybrid Fibre and Wireless CDMA System using Optically Preamplified Fibre Coupled Receiver*'. This paper was presented at the 2nd International Workshop on Optical Wireless Communications (IWOW) 2013, published by *IEEE* [38] and it forms the basis of Chapter 4, with the inclusion of a DPPM system analysis. Using flexible system architecture, illustrations of possible scalability in number of users by physical layer upgrade (combiner/splitter replacement) or data link layer upgrade (CDMA code replacement) is provided. Upstream coded optical signals from different rooms and offices in a building are collected through a fibre end assembly located at the

ceiling of each room and connecting into a fibre distributive network. A power combiner is used to join all the users' signals which are amplified by a single optical amplifier before reception or further transmission to the OLT. The amplifier compensates for power combiner losses and reduces the required transmit power of the user devices but introduces amplified spontaneous emission (ASE) noise and amplifies the background ambient noise accompanying the signal. The ASE, and possibly ambient, noise beating with the signal in the presence of multiple access interference (MAI) is considered in detail in the analysis using the GA, CB, MCB and SPA. The BER or required optical power calculations involve finding different optimum values of the *s* parameter for transmitted 1 or 0 (and for all the number of users when using the MGF techniques) and an optimum threshold fixed over the number of interferers for OOK system. The overall BER is obtained by averaging over the MAI effect of all the interfering users. Numerical results obtained in Chapter 4 reveal that an optical amplifier can ease the power constraints on the user devices, and DPPM signalling format can improve the average power efficiency of the system compared to an OOK modulation scheme.

WDM is a very popular multiplexing technique in optical access networks implemented with both OOK and DPPM modulation schemes. Interchannel crosstalk which is common in WDM systems have been investigated for various OOK systems [39-41], but no such analysis has been performed for any realistic WDM DPPM system. This was the motivation for the work presented in Chapter 5 in which a crosstalk model for WDM DPPM system analysis for single and multiple crosstalk sources is developed. During signal frame reception in a realistic WDM DPPM system, crosstalk frames are received as well, either in alignment or misalignment with the signal frame. An MGF, and related BER formulas, are derived for three different forms of (mis)alignment between the signal frame and crosstalk frames during reception including the frames aligned (FA) case, only slots aligned (OSA) case and slots misaligned (SM) case. Although the model could apply to DPPM system in any physical WDM channel, specific analysis for a non-turbulent FSO system is performed in Chapter 5 using the GA, CB and MCB. Analytical results are obtained for single crosstalk sources, while both analytical and Monte Carlo facilitated simulation results are provided for multiple crosstalk sources. The results in this thesis confirm that the effect of a

single crosstalk with high power is worse than that of many crosstalks of equivalent power. In the absence of turbulence and at data rate of 2.5 Gbps on the 1550 nm wavelength, DPPM systems with coding level of 2 provide about 2.8 dB improvement in average power over an equivalent OOK NRZ system while maintaining minimum bandwidth expansion. The analysis performed under the assumption of FA results in the worst BER while the SM case produces a more optimistic BER result. Furthermore, the MCB presents a tighter upper bound than the CB and is more sensitive to optical amplification, although the GA is simpler and computationally quicker. A second paper based on Chapter 5 of the thesis and entitled: '*Performance evaluation of digital pulse position modulation for wavelength division multiplexing FSO systems impaired by interchannel crosstalk*' has been published in *IET Optoelectronics* [42].

Atmospheric channel conditions are random and have a more severe effect on optical signals compared to the indoor FSO environment. In some conditions, extra power margins are required to counter strong signal attenuation and optical scintillation. DPPM is perceived to be more suited for an outdoor FSO system because the FSO channel is non-dispersive. In addition, DPPM has the potential of improving the average power requirement of FSO systems and has no requirement for threshold as seen with OOK signalling format. However, no analysis of a HFFSO WDM optical access network using DPPM exists and there has never been a consideration of outage probability in the case where a turbulence-affected crosstalk interferes with a turbulence-affected signal. This and the earlier development of a crosstalk model for WDM DPPM system motivated the writing of a paper entitled: '*Performance Evaluation of Turbulence-Accentuated Interchannel Crosstalk for Hybrid Fibre and FSO WDM Systems using Digital Pulse Position Modulation*'. This paper is the basis of Chapters 6 and 7 of the thesis and has been published by the *IET Optoelectronics* [43]. In a network architecture similar to WDM PON, free space links are used to distribute signals from a remote node to different ONUs within the last few kilometres of the access network. The analysis, which gives a full consideration of the effects of turbulence and crosstalk (accounting for beam spreading loss, coupling loss, scintillation and attenuation in fibre and free space), also incorporates aperture averaging as a turbulence mitigation technique. Analytical results suggest that the performance of the system is dependent on design parameters such as the distance

of the desired ONU from the remote node, distance of the interfering ONU from the remote node and the demux adjacent signal rejection. The crosstalk effect is exacerbated by the presence of turbulence and limits system performance in the upstream transmission. Specifically in the upstream, when the desired user is located 2000 m from the remote node, it is shown that a demux with adjacent signal rejection ratio greater than or equal to 45 dB is required if an adjacent channel interferer is 500 m away from the remote node and for a BER of 10^{-6} to be achieved in all turbulence regimes. It is also shown that in the presence of turbulence, DPPM systems suffer a minor loss in sensitivity but still maintain a better average power efficiency compared to systems using OOK NRZ format.

Outage probability is an alternative metric to average BER, used in assessing the behaviour of turbulent FSO systems. It has previously only been applied to the case of a turbulence-affected signal with no interferer. The work in Chapter 7 extends outage probability analysis to the case where a turbulence-affected signal is impaired by turbulence-affected crosstalk. This case to the best of the author's knowledge has not been previously considered. Results presented in this thesis show that in the presence of turbulence-affected crosstalk, the outage probability worsens, with more possibility of deep fades as the turbulence becomes stronger.

An extensive network design and analysis of a HFFSO WDM optical access network using OCDMA for multiple user connections and user capacity improvement is proposed in Chapter 8 of this thesis. The purpose of this network design is to facilitate the integration of the indoor system considered in Chapter 4 with the HFFSO WDM optical access network discussed in Chapter 6. WDM OCDMA systems have been studied for all fibre PON systems [33, 44], but no analysis has been provided for such systems including a turbulent FSO link. The performance evaluation considers the combined impact of turbulence-accentuated crosstalk and MAI as well as other network losses incurred in a HFFSO link, and is provided for both OOK and DPPM systems. Numerical results suggest that the combined impact of these impairments in the upstream transmission leads to bit error rate floors occurring at a BER value higher than the typical BER in the presence of MAI alone or turbulence accentuated-crosstalk alone. Trade-off between the number of users and FSO link length may be required in some cases to achieve a target BER in a practical system.

1.5 References

1. Agrawal, G. P. *Fiber-optic communication systems*. 3rd ed. New York: John Wiley & Sons Inc.; 2002.
2. Bell, A. G.: 'On the production and reproduction of sound by light'. *American Journal of Science,* 1880 October 1, 1880, **20**, (118), pp. 305-324
3. Bouchet, O., Sizun, H., Boisrobert, C., De Fornel, F. *Free-space optics: propagation and communication*: John Wiley & Sons; 2010.
4. Maiman, T. H.: 'Stimulated Optical Radiation in Ruby'. *Nature,* 1960, **187**, (4736), pp. 493-494
5. Downing, J. N. *Fiber-optic Communications*. New York, USA: Thomson Delmar Learning; 2005.
6. Kao, K. C., Hockham, G. A.: 'Dielectric-fibre surface waveguides for optical frequencies'. *Proc. Institution of Electrical Engineers,* 1966, **113**, (7), pp. 1151-1158
7. Kapron, F. P., Keck, D. B., Maurer, R. D.: 'Radiation Losses in Glass Optical Waveguides'. *Applied Physics Lett.,* 1970, **17**, (10), pp. 423-425
8. Brookner, E., Kolker, M., Wilmotte, R. M.: 'Deep-space optical communications'. *IEEE Spectrum,* 1967, **4**, (1), pp. 75-82
9. McIntyre, C., Peters, W. N., Chi, C., Wischnia, H. F.: 'Optical components and technology in laser space communications systems'. *Proc. of the IEEE,* 1970, **58**, (10), pp. 1491-1503
10. Jolley, N. E., Patel, B., Hadjifotiou, A.: 'Coherent optical system for inter-satellite communications'. *IEE Colloquium on Opt. Intersatellite Links and On-Board Techniques* 1990, pp. 15/1-15/7
11. Bansal, R.: 'The aftermath of 9/11. What light through yonder window breaks? [free-space laser link]'. *IEEE Antennas and Propagation Mag.,* 2002, **44**, (1), pp. 146
12. Killinger, D. 'Free Space Optics-For Laser Communication Through the Air'. *Optics & Photonics News, OSA*. Oct. 2002: pp. 36-42.
13. Berman, D. K. 'Lasers, Broadband Wireless Hookups Speed Data Around Lower Manhattan'. *The Wall Street Journal*. Oct. 2001.
14. Borah, D. K., Boucouvalas, A. C., Davis, C. C., Hranilovic, S., Yiannopoulos, K.: 'A review of communication-oriented optical wireless systems'. *EURASIP J. Wireless Communs. and Networking,* 2012, **2012**, (1), pp. 1-28
15. Popov, M.: 'The Convergence of Wired and Wireless Services Delivery in Access and Home Networks'. *Optical Fiber Commun. Conf.* 2010: Optical Society of America, pp. OWQ6
16. Ramaswami, R., Sivarajan, K. N., Sasaki, G. H. *Optical Networks: A Practical Perspective*. 3rd ed. Boston: Morgan Kaufmann Publishers; 2010.
17. Breuer, D., Lange, C., Weis, E., Eiselt, M., Roppelt, M., Grobe, K., Elbers, J.-P., et al.: 'Requirements and Solutions for Next-Generation Access'. *Proc. of Photonic Networks, 12. ITG Symp.* 2011, pp. 1-8
18. Chang-Hee, L., Sorin, W. V., Byoung Yoon, K.: 'Fiber to the Home Using a PON Infrastructure'. *J. Lightw. Technol.,* 2006, **24**, (12), pp. 4568-4583
19. Larsen, C. P., Gavler, A., Wang, K.: 'Comparison of active and passive optical access networks'. *9th Conf. on Telecommun. Internet and Media Techno Economics* 2010, pp. 1-5
20. Banerjee, A., Sirbu, M. A.: 'Towards technologically and competitively neutral fiber to the home (FTTH) infrastructure'2003: TPRC;
21. Pei-Lin, C., Shenq-Tsong, C., Shuen-Te, J., Shu-Chuan, L., Han-Hsuan, L., Ho-Lin, T., Po-Hsuan, H., et al.: 'Demonstration of 16 channels 10 Gb/s WDM free space transmission over 2.16 km'. *Digest of the IEEE/LEOS Summer Topical Meetings* 2008, pp. 235-236
22. Kartalopoulos, S. V. *Free space optical networks for ultra-broad band services*: John Wiley & Sons; 2011.

23. Barry, J. R. *Wireless Infrared Communications*. Boston: Kluwer Academic Publishers; 1994 1994.

24. Andrews, L. C., Phillips, R. L. *Laser Beam Propagation Through Random Media*. 2nd ed: SPIE Press, Bellingham, Washington; 2005.

25. Heatley, D. J. T., Wisely, D. R., Neild, I., Cochrane, P.: 'Optical wireless: the story so far'. *IEEE Commun. Mag.,* 1998, **36**, (12), pp. 72-74, 79-82

26. Bayaki, E., Schober, R., Mallik, R. K.: 'Performance Analysis of Free-Space Optical Systems in Gamma-Gamma Fading'. *IEEE Global Telecommun. Conf.* 2008, pp. 1-6

27. Di Bartolo, S., Pizzoleo, A., Penna, S., Beleffi, G. M. T., Matera, F., Pompei, S.: 'Experimental demonstration of a GPON free space optical link for full duplex communications'. *Fotonica AEIT Italian Conf. on Photonics Technol.* 2014, pp. 1-3

28. Shahpari, A., Sousa, A. N., Ferreira, R., Lima, M., Teixeira, A.: 'Free space optical communications for ultra high-capacity PON system'. *2nd Intl. Conf. on Applications of Optics and Photonics* 2014, pp. 92861Y

29. Wakamori, K., Kazaura, K., Oka, I.: 'Experiment on Regional Broadband Network Using Free-Space-Optical Communication Systems'. *J. Lightw.Technol.,* 2007, **25**, (11), pp. 3265-3273

30. Cap, G. A., Refai, H. H., Sluss Jr, J. J.: 'Omnidirectional free-space optical (FSO) receivers'. *Defense and Security Symp.* 2007, pp. 65510O

31. Bloom, S., Korevaar, E., Schuster, J., Willebrand, H.: 'Understanding the performance of free-space optics'. *J. Opt. Netw.,* 2003, **2**, (6), pp. 178-200

32. Richardson, D. J., Fini, J. M., Nelson, L. E.: 'Space-division multiplexing in optical fibres'. *Nature Photonics,* 2013, **7**, (5), pp. 354-362

33. Kitayama, K., Xu, W., Wada, N.: 'OCDMA over WDM PON-solution path to gigabit-symmetric FTTH'. *J. Lightw.Technol.,* 2006, **24**, (4), pp. 1654-1662

34. Ghaffari, B. M., Matinfar, M. D., Salehi, J. A.: 'Wireless optical CDMA LAN: digital design concepts'. *IEEE Trans. Commun.,* 2008, **56**, (12), pp. 2145-2155

35. Khazraei, S., Pakravan, M. R.: 'Analysis of generalized optical orthogonal codes in optical wireless local area networks'. *IEEE J. Sel. Areas Commun.,* 2009, **27**, (9), pp. 1572-1581

36. Ohtsuki, T.: 'Performance analysis of indoor infrared wireless systems using PPM CDMA'. *Electronics and Commun. in Japan* 2002, **85**, (1), pp. 1-10

37. Ke, W., Nirmalathas, A., Lim, C., Skafidas, E.: '4 x 12.5 Gb/s WDM Optical Wireless Communication System for Indoor Applications'. *J. Lightw. Technol.,* 2011, **29**, (13), pp. 1988-1996

38. Mbah, A. M., Walker, J. G., Phillips, A. J.: 'Indoor hybrid fibre and wireless CDMA system using optically preamplified fibre coupled receiver'. *2nd Intl. Workshop on Optical Wireless Communs. (IWOW)* 2013, pp. 94-98

39. Monroy, I. T., Tangdiongga, E. *Crosstalk in WDM Communication Networks*. Norwell, Massachusetts, USA, : Kluwer Academic Publishers; 2002.

40. Ma, R., Zuo, T. J., Sujecki, S., Phillips, A. J.: 'Improved performance evaluation for DC-coupled burst mode reception in the presence of amplified spontaneous emission noise and interchannel crosstalk'. *IET Optoelectron.,* 2010, **4**, (3), pp. 121-132

41. Ke, W., Nirmalathas, A., Lim, C., Skafidas, E.: 'Impact of Crosstalk on Indoor WDM Optical Wireless Communication Systems'. *IEEE Photonics Journal,* 2012, **4**, (2), pp. 375-386

42. Mbah, A. M., Walker, J. G., Phillips, A. J.: 'Performance evaluation of digital pulse position modulation for wavelength division multiplexing FSO systems impaired by interchannel crosstalk'. *IET Optoelectronics,* 2014, **8**, (6), pp. 245-255

43. Mbah, A. M., Walker, J. G., Phillips, A. J.: 'Performance Evaluation of Turbulence-Accentuated Interchannel Crosstalk for Hybrid Fibre and FSO WDM Systems using Digital Pulse Position Modulation'. *IET Optoelectronics,* 2016, **10**, (1), pp. 11-20

44. Huang, J.-F., Chang, Y.-T., Hsu, C.-C.: 'Hybrid WDM and optical CDMA implemented over waveguide-grating-based fiber-to-the-home networks'. *Optical Fiber Technology,* 2007, **13**, (3), pp. 215-225

CHAPTER 2   Optical Communication Systems and Technologies

2.1 Overview

The aim of this chapter is to briefly review the different components of optical communication systems including the transmitter and receiver systems and the physical channels used for optical signal transmission. The basic features of the main signal modulation schemes used in the thesis, namely OOK and DPPM are presented. The general processes of optical amplification and signal detection are also presented in this chapter. A brief review of different structures of the receiver unit is provided, and the effects of any optics included in the receiver unit on signal reception are considered.

2.2 Optical signal generation

Optical signal sources are commonly made from semiconductor materials. In such devices, optical signal generation is a process of complex interaction between electron-hole pairs in the gain medium located between a p-type and an n-type material. At the temperature of 0 K in a pure semiconductor, no electrons exist in the upper energy level called the conduction band and the lower energy level called the ground state or valence band is full of electrons. As the temperature increases to room temperature, electrons in the valence band absorb energy greater than the bandgap energy of the semiconductor material (see Fig.2.1 $E_g = E_2 - E_1 = h\upsilon$ where h is Planck constant and υ is the optical frequency) and are excited to the conduction band leaving holes in the valence band. These electrons can recombine with the holes, spontaneously emitting photons (light 'particles') in the process as shown in Fig. 2.1. In thermal equilibrium there are typically fewer electrons in the conduction band compared to the valence band, and emitted or input photons are easily reabsorbed by other electrons before exiting the device. This is called optical absorption. For the semiconductor to significantly emit a large number of useful photons, one needs to create a thermal imbalance and unsettle the device equilibrium by increasing the electron density in the conduction band and the hole density in the valence band (i.e. population

inversion) through artificial means. This process of providing energy to the semiconductor device through an external source to ensure significant light emission is referred to as pumping. There are various methods of pumping a semiconductor device, but optical and electrical pumping are two of the common methods. However, electrical pumping is more popular with semiconductor devices than optical pumping.
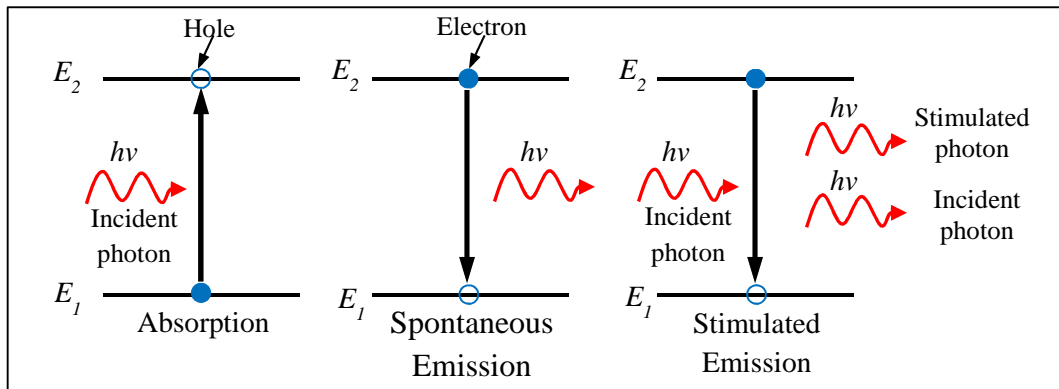
Fig. 2.1 Interaction between photon and electron-hole pair in the gain medium

2.2.1 Laser sources

The output light quality of a laser makes it an important optical source for communication. Laser beams are collimated, spatially and temporally coherent with narrow spectral widths and have high power compared to light emiting diodes (see Table 2.2). Lasers are broadly categorised according to different criteria such as safety of use and type of gain medium. The basic structure of a laser includes an optical gain medium placed within an optically resonant cavity that provides optical feedback and phase selection. The gain medium could be in a solid (insulating crystal or semiconductor), liquid or gaseous form [1]. Semiconductor-based lasers use semiconductor material as their gain medium and are the most popular in optical communication. They are further grouped into different types based on number of longitudinal modes (single mode and multimode), emitter characteristics (edge emitting and surface emitting) and junction composition (homojunction and heterojunction). Semiconductor lasers are compact and small, with typical dimensions of 300 μm length and 50 - 200 μm width, although the dimensions could vary depending on design [2, 3]. They are highly reliable and have high power conversion efficiency (see Fig. 2.2 [4]). Semiconductor lasers generate light through a stimulated emission process as

illustrated in Fig. 2.1. Once population inversion is achieved in a laser, incident photons are more likely to resonate with electron-hole pairs and stimulate the emission of additional photon(s) than be absorbed. The stimulated photons are of the same frequency, phase, direction and polarisation as the incident photon. Population inversion also increases the chances of spontaneous emission. Threshold conditions require that the optical gain must be equal to optical loss (round trip gain equals unity) and that the cavity length must be an integer multiple of the half the wavelength in the cavity. Spontaneous emission dominates the process until these conditions are met. Once lasing starts, the electron-hole density and the gain coefficient are fixed at threshold value.
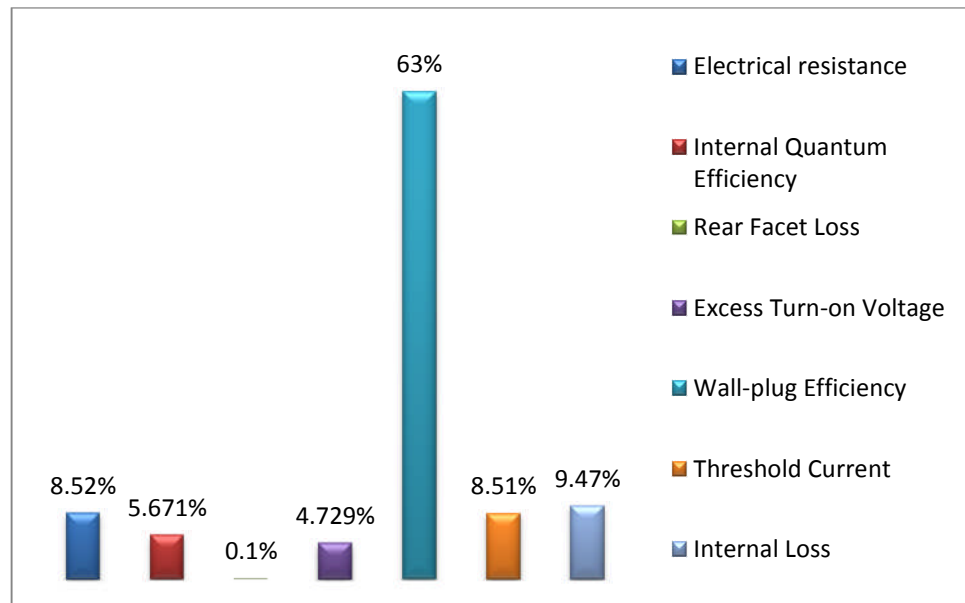
Fig. 2.2 Power conversion efficiency of a typical 100 µm wide, 970 nm laser diode (conversion (wall-plug) efficiency in this case is 63 %) [4]

2.2.1.1 Longitudinal modes

Longitudinal modes are formed at all the wavelengths with optical waves returning to the same point with the same phase after a round trip. In principle, in a homogenously broadened medium like in a semiconductor, only the mode centred at the peak of the gain bandwidth should oscillate after the gain and electron-hole density have been clamped to the threshold value. However in practice, multiple modes attain a round trip gain of unity partly due to spontaneous emission and close wavelength spacing within the gain bandwidth [5], but majorly due to spatial hole burning effects [3, 6, 7]. This effect is a result

of non-uniform spatial distribution of the intensity of the lasing mode due to uneven depletion of the population inversion in laser systems with homogeneously broadened medium [6] as shown in Fig. 2.3. Fabry-Perot lasers are typical examples of multiple longitudinal mode semiconductor lasers. They are easy to fabricate due to their simple structure with feedback provided by reflective facets (mirrors).
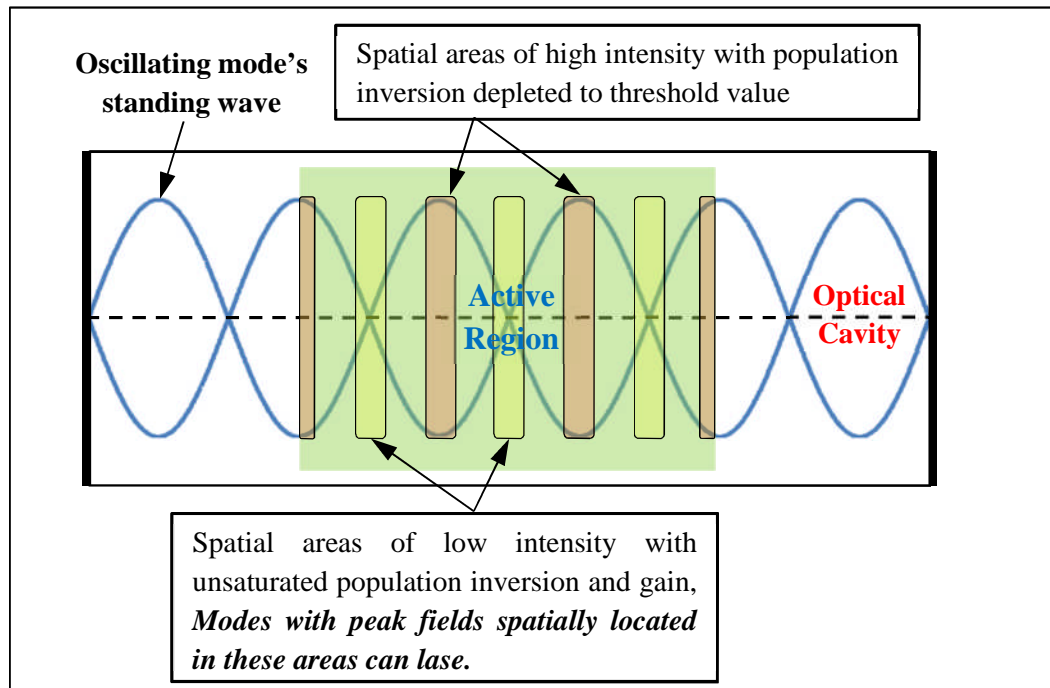
Fig. 2.3 Spatial hole burning in a homogenously broadened medium. Modes with peak field spatially located near the nodes of the oscillating mode's standing wave win the competition for electron-hole pair within that space and grow.

In single mode operation, the cavity loss is mode dependent [8], and is high at every wavelength except the resonant wavelength of the optical cavity as shown by the bottom right sub-figure in Fig. 2.4. This is achieved through additional filtering mechanism and ensures that only a single mode oscillates. Types of single longitudinal mode semiconductor laser include distributed feedback (DFB) lasers, distributed Bragg reflector (DBR) lasers, external cavity lasers and vertical surface emitter lasers (VCSEL). Single longitudinal mode semiconductor lasers emit near-monochromatic light beams and are used as optical sources in long distance communication.
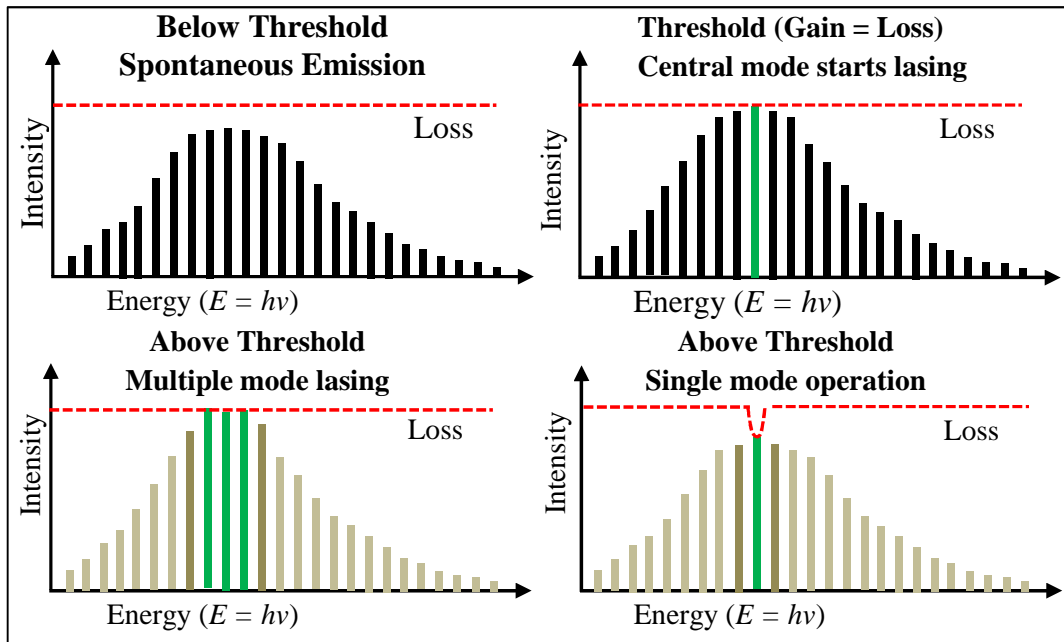
Fig. 2.4 Illustration of lasing processes in a typical semiconductor laser

2.2.2 LED sources

Light emitting diodes (LEDs) are fabricated from semiconductor materials. These materials as shown in Table 2.1 [9] could be binary compound semiconductors such as Gallium Arsenide (GaAs), ternary compound such as Aluminium Gallium Arsenide (AlGaAs) or quaternary compound like Indium Gallium Arsenide Phosphides (InGaAsP). In its basic structure, an LED is a PN junction in a forward-biased connection. LEDs are generally classified based on their emitter configuration as surface-emitting LED (SLED) or edge-emitting LED (ELED). However, they are sometimes categorized based on the frequency of the light they emit such as blue, green, red and infrared LEDs. Light emission in an LED is through spontaneous emission and pumping is through an electrical source. At equilibrium in a PN junction, the conduction band which is on the n-type material is densely populated with electrons while the valence band on the p-type material contains high number of holes as shown in Fig. 2.5a. These carriers are however unable to cross the high barrier into the depletion region where they can be actively involved in recombination. A forward bias of the PN junction lowers the barrier, and minority carriers diffuse across the junction into the depletion layer where they engage in radiative recombination with majority carriers.
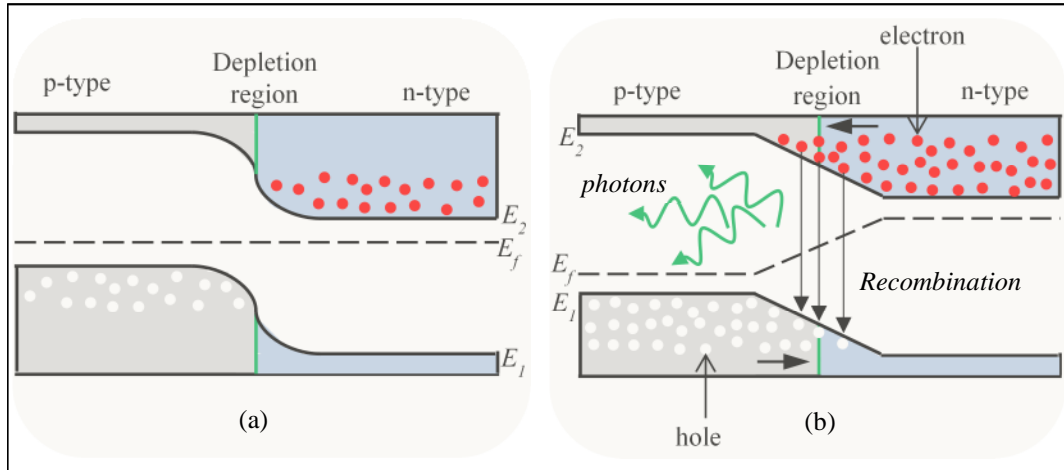
Fig. 2.5 Schematic diagram of light emission process in an LED: (a) Equilibrium condition and (b) Forward biased condition (E_2 = conduction band energy level, E_1 = valence band energy level, E_f = Fermi level and bandgap energy $E_g = E_2 - E_1$)

The energy of the emitted photon is equal to the bandgap energy of the material which could vary depending on the composition. For example, by varying the percentages of arsenide and phosphide in GaAsP, the bandgap energy could vary from 1.43 eV to 2.26 eV [10]. An LED emits light in all directions with random phase. Thus the output light beam is incoherent, with broad spectrum ($\Delta\lambda = 50 - 60$ nm) and wide angular distribution [3, 10]. Due to non-radiative recombination (which increases with temperature) and large solid angle of emission, the overall efficiency of a typical LED is low. For GaAs, an external quantum efficiency of 1.4 % has been reported, with output power ranging between 10 µW -100 µW [3, 11]. Consequently, LEDs are used for short distance transmission and within local area networks (LANs) [3]. However, LEDs are cheaper to fabricate than lasers, and edge-emitting LEDs have higher modulation bandwidth with smaller beam divergence and can generally support high data rate transmission over a longer distance compared to surface-emitting LEDs [3]. Table 2.2 shows a comparison of laser and LED sources (based on [2, 3, 10, 11]).

Table 2.1 Typical LED types and characteristics (adapted from [9])

Active Material	AlGaAs		GaAs		InGaAsP		
Radiating Wavelength (nm)	660	850	850	850	1300	1300	1500
LED type	SLED	ELED	SLED	ELED	SLED	ELED	ELED
Spectral linewidth (nm)	20	35-65	40	35	110	25	40-70
Max. power into fibre (mW)	1.35	0.08	0.14	0.032	0.05	0.15	7.5
Bandgap energy (eV)	1.88	1.46	1.46	1.46	0.95	0.95	0.80

17

Table 2.2 Comparison of laser and LED sources (based on [2, 3, 10, 11]).

Beam quality	Laser	LED
Coherency	Highly coherent	Incoherent
Spectral linewidth	Narrow	Large (about 50 nm)
Directionality	High	Low
Output power	High (up to 100 mW)	Low (less than 7 mW)

Physical properties	Laser	LED
Life span	Short	Long
Ease of use	More complex	Easier to operate
Transmission aperture	Small	Large
Power conversion rate	High	Low efficiency
Cost	Expensive	Low cost

Transmission Application	Laser	LED
Data rate	High (up to 40 Gbps)	Low (about 100 Mbps)
Modulation frequency	High	Low (about 200 MHz)
Transmission range	Long range	Short range
Fibre coupling rate	High	Very Low

2.3 Signal modulation and transmission

Additional to an optical source and its driving circuit (pump energy), the transmitting unit also includes a signal modulator and possibly an encoder. A telescopic transmitting lens is required for most free space transmission. The entire unit functions together to ensure that a data bearing signal is launched into the optical channel with adequate power and signal quality to ensure that the data is recovered at the receiver. Signal modulation is the process of impressing (engraving) the generated light with the data meant for transmission. Light sources such as semiconductor laser diodes are usually modulated directly by varying the drive current to a high (well above threshold) and low (below threshold or just above threshold) values to represent data 1 and data 0 respectively. Since no additional component is required, this method is simple and inexpensive but increases the occurrence of chirping which generally affects the dispersion performance of the system [11]. Chirping may be controlled, and data rate improved, by increasing the drive current well above the threshold value for

data 0 but at the expense of reduced extinction ratio and overall receiver performance [12]. An alternative method is to keep the drive current constantly well above the threshold value to produce a continuous wave and place an external modulator such as a directional coupler or a Mach-Zehnder interferometer (MZI) after the light source to vary the properties of the light in accordance with the data to be transmitted. Compared to direct modulation, external modulation leads to a better system performance in terms of chirp and extinction ratio but at the significant cost of a separate modulation component.

2.3.1 Signal modulation schemes

In modulation of light for optical communication, properties such as amplitude (intensity), phase, frequency and polarization of the signal in passband transmission, and width, position, code and interval of pulse train in baseband transmission could be adjusted in sympathy with the data in various modulation schemes. Some of these modulation schemes which have been applied to optical communication systems are phase shift keying (PSK, with different variants – binary-PSK, quadrature-PSK, differential-PSK), quadrature amplitude modulation (QAM), on-off keying (OOK), and a variety of digital pulse-time modulation schemes including digital pulse position modulation (DPPM), dicode pulse position modulation (DiPPM) [13-17], digital pulse interval modulation (DPIM) and digital pulse width modulation (DPWM) [18-24]. Each of these schemes has various advantages and disadvantages, but in general, it is desirable that a modulation scheme supports efficient power and bandwidth utilization, provides good quality of service and is less complex and inexpensive to implement [25]. The work in this thesis is performed using OOK and DPPM modulation schemes which are among the most common modulation schemes in optical access networks. OOK is particularly simple and DPPM has excellent power utilisation, as discussed below.

2.3.1.1 On-off keying

On-off keying (OOK) is the simplest and most widely used modulation scheme in both optical fibre and FSO communication systems [3, 12, 26, 27]. OOK modulation is implemented in combination with the return-to-zero (RZ) and non-return-to-zero (NRZ) signalling formats. In the OOK-NRZ scheme, data 1 is transmitted by turning on the optical source and sending a pulse of duration equal

to the bit interval and data 0 is transmitted by turning off the light for the same bit interval. The light source is turned on and an optical pulse is sent for a part of the bit duration determined by the duty cycle in order to transmit a data 1 in OOK-RZ scheme as shown in Fig. 2.6. By having a narrower pulse, the OOK-RZ scheme utilizes more bandwidth than the OOK-NRZ. Thus by varying the duty cycle, the bandwidth efficiency of the OOK-RZ scheme could approach that of OOK-NRZ. One major weakness of the OOK scheme is the inability to determine the bit boundaries for the receiver timing recovery when long strings of ones or zeros are transmitted [11]. There is also the issue of lack of DC balance, due to the variation in the average transmitted power over sequences of data bit, but this is only a concern in optical fibre systems where it results in difficulties in setting fixed decision threshold [11]. For FSO systems, atmospheric turbulence effects primarily cause a random fluctuation of the short term average power in a signal previously launched into the atmosphere with constant average transmitted power such that its DC balancing is of no consequence.

2.3.1.2 Digital pulse position modulation

Digital pulse position modulation (DPPM) is one of the schemes that exploit the time-varying properties of a pulse train, with each data binary-word represented by the distinct position of a signal pulse in a time frame. In the DPPM scheme illustrated in Fig. 2.6, a frame of duration equal to MT_b is divided into $n = 2^M$ equal time slots of length $t_s = MT_b/n$, where M is the coding level and is equal to the number of data bits transmitted per DPPM frame. Also, $T_b = 1/R_b$ is the equivalent OOK-NRZ bit period and R_b is the raw bit rate. DPPM is an isochronous modulation scheme with better average power efficiency compared to OOK (see Table 2.3) or other digital pulse time schemes. This advantage is at a cost of additional bandwidth expansion which is more prominent at high coding level or bit resolution. In addition, DPPM requires a separate synchronization unit which adds to receiver complexity and for a dispersive channel such as an optical fibre, guard bands are required to separate each signal frame from another. In practical applications, a trade-off is required in choosing the DPPM coding level. Higher coding levels provide increase in power efficiency, but also result in increase in electronic processing speed, timing recovery challenge and bandwidth utilization (which directly increases filter bandwidths). Thus optimal performance

in practical systems may be obtained at moderate DPPM coding levels. For example, in a system with limited bandwidth, DPPM coding level of 2 may present an optimal trade-off because it provides some improvement in power efficiency over OOK-NRZ at minimal bandwidth utilization (i.e. the same bandwidth expansion with coding level of 1).
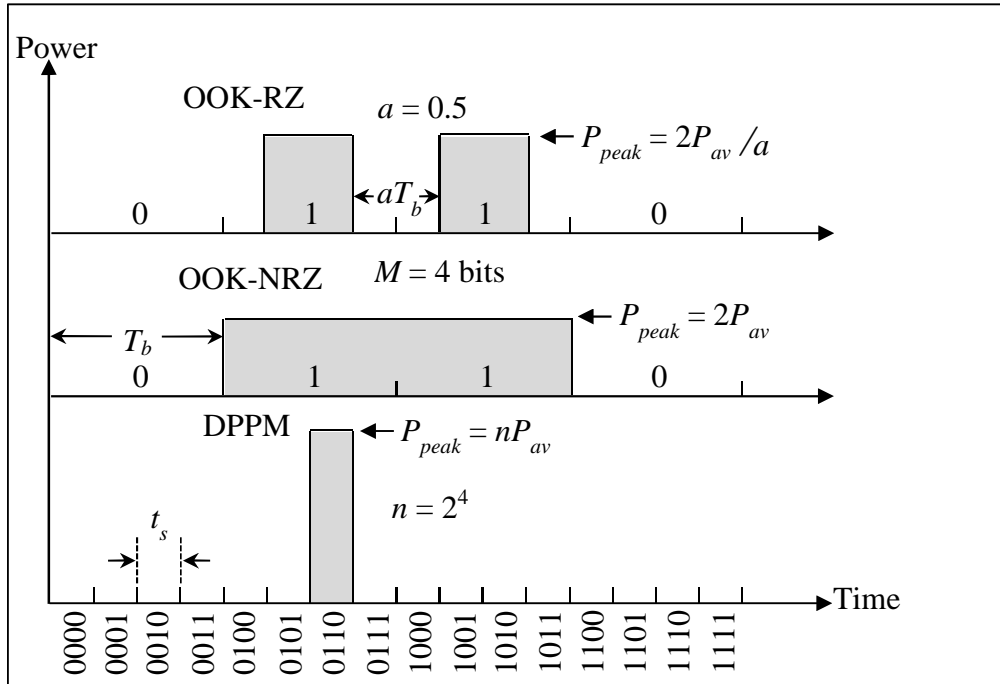
Fig. 2.6 Illustration of OOK and DPPM waveforms (duty cycle $a = 0.5$ for OOK-RZ)

DPPM has been applied in optical fibre, intersatellite and deep space communication systems. Some of the earliest works on the DPPM scheme were reported for deep space applications [28, 29]. Later, studies on DPPM systems were extended to optical fibre communications [18, 30-32]. Analysis for optically preamplified DPPM systems in the intersatellite application, facilitated by moment generating function techniques and the Gaussian approximation (GA), was performed in [33-35]. In addition, the performance of DPPM and some of its hybrids/variants such as differential-PPM, differential-amplitude-PPM and dicode-PPM have been investigated for indoor or non-turbulent FSO links [36-38], and for terrestrial (outdoor) FSO links [21, 25, 27]. The DPPM scheme is considered to be well suited for the FSO (atmospheric) channel because there is no requirement to set and track threshold as in some OOK systems. Furthermore, an FSO channel is dispersion free unlike an optical fibre channel, thus there is an

improvement in bandwidth utilization of DPPM in FSO channels over fibre channels due to non-requirement of guard bands, and there is no dispersion imposed limitations on achievable bit rate and link length as seen in fibre systems. Although when compared to DPPM, some modulation schemes like digital pulse interval modulation (DPIM) and dual-header pulse interval modulation (DH-PIM) offer improved bandwidth efficiency and synchronisation, DPPM offers a better average optical power requirement efficiency which is necessary in complying with eye safety limitations [25], and also provides better error rate performance [39]. Furthermore, at coding level of 2 or 1, DPPM bandwidth efficiency is comparable to that of other digital pulse modulation schemes as shown by results in [25].

Table 2.3 Comparison of OOK and DPPM modulation schemes (duty cycle = a)

Modulation scheme	*Transmission capacity*	*Bandwidth utilization*	*Optical power utilization*
OOK-NRZ	1 bit per symbol	R_b	Pav
OOK-RZ	1 bit per symbol	R_b/a	$Pav\sqrt{a}$
DPPM	M bits per symbol	$R_b(n/M)$	$Pav\sqrt{(2/nM)}$

2.3.2 Signal encoding and decoding

Signals are further encoded before transmission to provide greater tolerance to interference and noise or for error detection and correction [40, 41]. Signal encoding increases the line rate of the system but can improve the system BER performance and aggregate capacity. In this thesis, only encoding for multiple access such as CDMA is directly considered. Such an encoding could be performed in the optical or the electrical domain [42, 43] and has improved over the years due to advances in device technology. Codes are spread in one or more of the temporal, spectral and spatial directions [44-46]. Because of limited electronic processing speed, optical encoding is preferred for long range optical communication although the encoding devices are more expensive. Appropriate decoders are used to retrieve the signal at the receiver unit.

In an FSO system, the slow fading effects of scintillation could result in data sequence being received with long consecutive erroneous bits or at least long runs

of bits with degraded instantaneous BER, such that the transmitted data may not be recovered even with forward error correction (FEC) coding applied. It is also possible that the data sequence could be received in an almost error free condition such that the FEC is not needed. Thus in a randomly poor BER system, FEC is more beneficial if the bits are considered to be interleaved prior to transmission and FEC is then applied upon reception and de-interleaving of the data.

2.4 Eye and skin safety

At all times from the transmission to the reception of an optical signal, it is paramount that the safety of the user or any other person that may come in contact with the signal be guaranteed. For this reason, there are standard guidelines for the use of lasers and LEDs to avoid hazardous exposure to radiation. These guidelines, developed by various standard organisations such as International Commission on Non-Ionizing Radiation Protection (ICNIRP), American National Standards Institute (ANSI) and International Electrotechnical Commission (IEC), state the accessible emission limit (AEL) and maximum permissible exposure (MPE) as well as the procedure for calculating these limits under various conditions and wavelengths. Most LED sources are regarded as safe and when there are safety concerns, the less restrictive exposure limits for incoherent sources should apply [47, 48]. Strict safety regulations apply for laser sources which generally are grouped into classes based on order of hazard, with increasing class number indicating greater possibility of hazard.

2.4.1 Accessible emission limit

According to the IEC, the accessible emission limit (AEL) is the maximum level of accessible emission allowed within a specific class of laser [49]. The AEL is defined for different wavelengths and depends on the exposure duration. Fig. 2.7 shows the AEL for different classes of laser at different optical communication wavelengths for exposure duration between 0.35 - 10 s. The angle subtended by the source from a viewer at least 100 mm away is assumed to be less than 1.5 mrad. The subclass M relates to sources with additional optics such as a lens, in which case the viewer is assumed to be at least 100 mm away from the lens. Class 1 and 1M lasers are considered generally safe with AEL of 10.12 mW at 1550 nm as shown in Fig. 2.7 and are commonly found in indoor applications.

Classes 2 and 2M lasers are specified only for visible light wavelengths and have AEL of 1 mW. Although this class of laser is not as safe as the class 1 laser, it is expected that the reflex action of the eye will prevent any damage in case of exposure. Most semiconductor laser diodes fall within classes 3R and 3B and are potentially hazardous. Extra caution is required when using these classes of laser to avoid direct viewing.
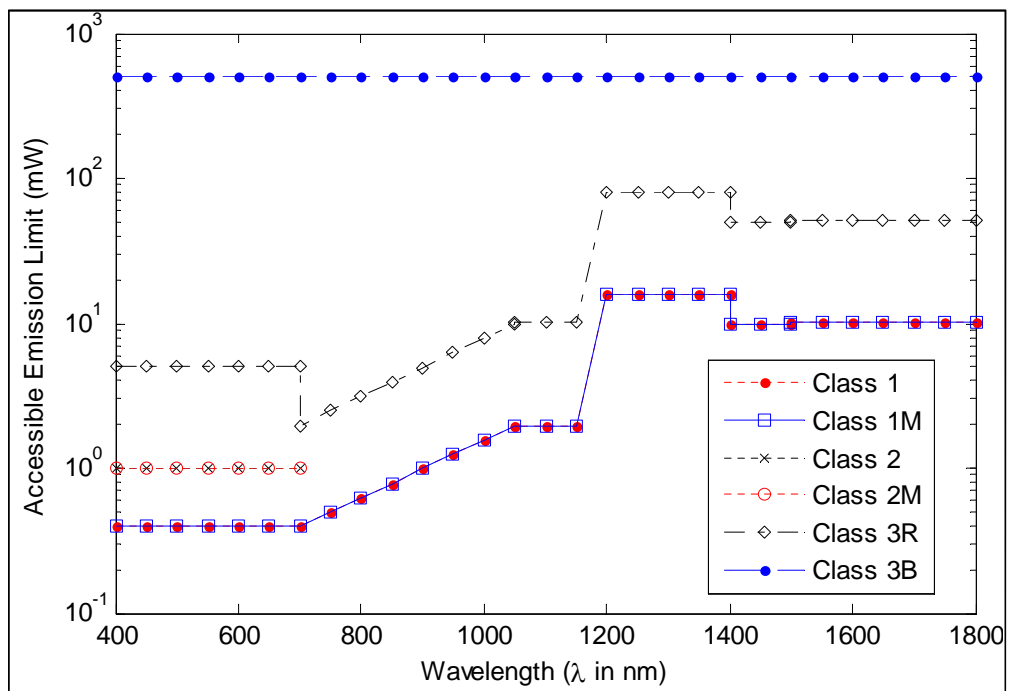
Fig. 2.7 AEL values for different classes of laser at various wavelengths based on [49] (class 4 (not included in the figure) is above 500mW for all wavelengths)

2.4.2 Maximum permissible exposure limit

In some working environments, unavoidable and/or accidental exposures to laser emission occur. The maximum permissible exposure (MPE) defines the maximum level of radiation that a person may be exposed to without any short or long term damage to the eye or skin under normal circumstances [49]. The MPE is dependent on the wavelength, exposure duration and the circular area over which the source irradiance is measured (usually referred to as the limiting aperture) [50]. The MPE values for skin to laser radiation are shown in Table 2.4 [49] for various wavelengths and exposure durations. The MPE values for the skin are high because it is more tolerant to laser emission compared to the eye.

Table 2.4 MPE values (in Wm^{-2}) of skin to laser radiation (adapted from [49])

Wavelength, λ (nm)	MPE (W.m^{-2})	Exposure duration, t (s)	
400 - 700	$\dfrac{11000t^{0.25}}{t}(\text{J.m}^{-2})$	1ms – 10s	$C_4 = 1$ for $\lambda < 700$;
	2000	10s – 1ks	
	2000	1ks – 30ks	$C_4 = 10^{0.002(\lambda-700)}$ for $700 \le \lambda \le 1050$;
700 - 1400	$\dfrac{11000t^{0.25}C_4}{t}$ (J.m^{-2})	1ms – 10s	
	2000 C$_4$	10s – 1ks	
	2000 C$_4$	1ks – 30ks	$C_4 = 5$ for $\lambda > 1050$
1400 - 1800	$\dfrac{5600t^{0.25}}{t}(\text{J.m}^{-2})$ to $\dfrac{10000}{t}$ (J.m^{-2})	1ms – 10s	
	1000	10s – 1ks	
	1000	1ks – 30ks	

The amount of laser light reaching the retina is greater for visible and near infrared light due to the focussing effect of the pupil and the transparent layers of the eye. Thus the MPE at the wavelengths between 400 nm to 1400 nm is particularly low compared to the 1550 nm wavelength as shown in Fig. 2.8. Most of the radiation around 1550 nm is absorbed at the cornea with the thermal effect distributed over the aqueous humour and thus poses less danger to the eye [49].
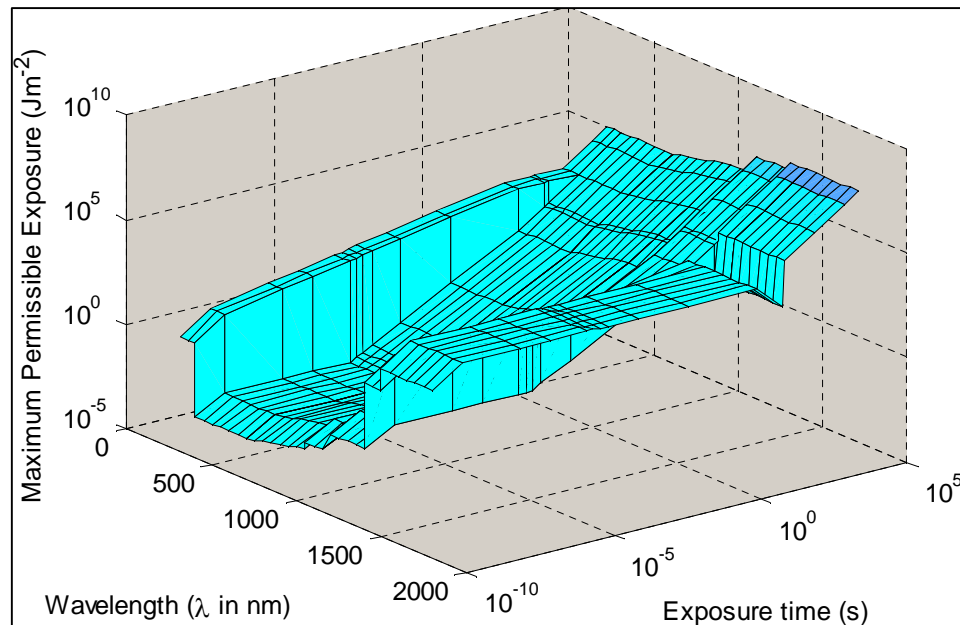
Fig. 2.8 MPE values (in Jm^{-2}) as a function of wavelength and exposure time (based on [49])

2.5 Optical channels

A waveguide is required in optical communication or clear line of sight (if FSO) as optical signals are unable to pass through various barriers (such as wooden furniture, metallic and brick walls) unlike radio frequency signals. Light as an electromagnetic wave possesses different properties from other electromagnetic radiations. It is the unique property of optical signals that causes them to be absorbed by most materials, as their respective photon energies correspond to the quantum energies of the electrons in these materials. It is also for the same reason that some material or medium could make a good or bad optical waveguide or channel. Major optical channels include waveguides like optical fibre, the atmosphere (free space), deep space (for intersatellite optical communication) and water (for deep sea optical communication) [51-53]. The focus of this thesis is on optical fibre and FSO channels.

2.5.1 Optical fibre channel

An optical fibre is a waveguide primarily made of a glass core and enclosed in a glass cladding. Typically in a step index fibre, the cladding is of a lower refractive index compared to the core. Various degrees of reinforcement including an elastic buffer are used to protect the core and cladding during the manufacturing process. Based on geometric optics, light is guided in the fibre core by the principle of total internal reflection which applies only to light that is incident on the fibre core at an angle not greater than the acceptance angle of the fibre. Signals propagating through an optical fibre experience a loss in quality and power mainly due to the attenuating properties of the fibre material and dispersion. These impairments are discussed further in the next chapter.

2.5.2 Free space (outdoor) optical channel

Unlike the optical fibre channel, signals propagating in a free space channel are not guided. They are subject to beam divergence and are exposed to unpredictable atmospheric conditions. A line of sight is also required between the transceivers in an FSO channel, thus in addition to free space attenuation due to atmospheric particles; physical barriers could also cause a loss of signal. Various factors

affecting signal transmission in an FSO channel, including atmospheric turbulence, are discussed in detail in Chapter 3.

2.5.3 Indoor free space optical channel

The indoor FSO channel is more conducive for the propagation of optical signal as the channel is not affected by weather condition or atmospheric turbulence. Some of the challenges facing indoor FSO communications include restrictions in transmitter power due to eye safety, limitation in bandwidth and user data rate due to multipath dispersion and slow receiver response time, limitation in user mobility, provision of multiple user service, and interferences from background ambient radiation [54-56]. Various types of link arrangement including direct, non-direct and hybrid line of sight connections, and transceiver optimisation have been extensively studied in order to find a solution to the mobility and transmission power challenges in indoor FSO communication system [26, 55, 57, 58]. In addition, multiple access schemes such as CDMA, WDM and subcarrier multiplexing have been proposed and studied for the provision of multi-user services [55, 59-61].

Recent advances in LED technology led to increased proposals for indoor FSO systems using LED sources which are cheaper, and have longer lifespan than lasers, and can perform the dual function of communication and illumination, i.e. visible light communications (VLC) [62, 63]. However, additional to the performance advantages of laser over LED as shown in Table 2.2, further benefits of using a laser source in an indoor FSO system include the use of narrowband optical bandpass filters (OBPF) to reduce system noise, and operation at the 1550 nm wavelength which allows for the use of optical amplifier (particularly the erbium doped fibre amplifier (EDFA)), and where both ambient background light interferences and transmitter power restrictions (because light at this wavelength does not reach the retina) are reduced. Despite all the interests in indoor FSO communications, achievable data rates in deployed systems were just about 1 Gbps as of 2012 [62, 64] (although data rates greater than 2.5 Gbps have been demonstrated [65] in the laboratory), and only limited mobility could be supported in proposed or deployed systems [61, 62]. Further details on the indoor FSO channel will be mentioned as the need arises, and a detailed analysis of an indoor FSO system is provided in Chapter 4.

2.6 Optical amplifiers

Before the advent of optical amplifiers, optoelectronic repeaters were employed to counter the loss in signal quality and power over an optical communication link. These repeaters perform a threefold signal regenerating function of reamplification, reshaping and retiming. The major consideration in locating such repeaters is to ensure that the signal is not excessively degraded such that the recovery of the original signal becomes impossible at the repeater. Thus in optical fibre communication links typical repeater spacings of 40 – 60 km were used depending on data rate and fibre dispersion [3, 66]. However, the repeaters are specific to signal modulation, bit rate and wavelength and required optical-to-electrical-to-optical (OEO) conversion [11, 66]. The attendant cost of using many repeaters in close spacing for each wavelength as well as the challenges and cost implication of system scalability and upgrade were the drive for an alternative means of regenerating the signal in the optical domain. Compared to the optoelectronic repeaters, optical amplifiers provide gain over a large range of wavelength and thus are well adapted to wavelength division multiplexing (WDM) and applicable to varying system speed. This capability of network resource sharing among many wavelengths, superior power amplification and ease of upgrade make the optical amplifier a cost effective option to counter signal attenuation in optical communication systems. Optical amplifiers however do not provide the reshaping and retiming functions, and additional optical components are required to compensate for dispersion and timing jitter where necessary. Another drawback of optical amplification is the introduction of amplified spontaneous emission (ASE) noise into the system which generally degrades receiver sensitivity.

2.6.1 Optical amplification process

The process of stimulated emission was discussed in Section 2.2 for optical signal generation in a laser. Unlike lasing which occurs at threshold conditions, optical amplification starts immediately after transparency is attained. At transparency, the electron densities at the upper and ground states are equal as shown in Fig. 2.9 and net absorption equals net emission (stimulated plus spontaneous emission). The photon flux in the gain medium remains unchanged under such condition and an input photon is neither amplified nor lost.

28
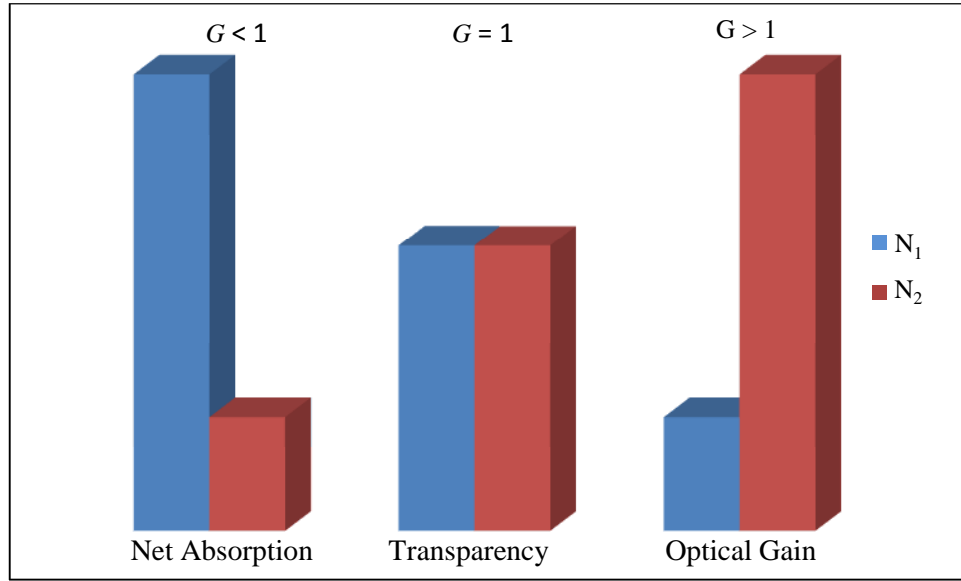
Fig. 2.9 Illustration of optical amplification processes with changes in electron densities in the upper state (N_2) and ground state (N_1)

The optical feedback mechanism required in a laser is not needed for (traveling wave) optical amplification. Thus, as the pump energy is increased beyond the transparency condition, N_2 increases above N_1, and only then can a stimulated emission of photons lead to optical amplification as the optical gain (G) is driven above the cavity losses. This also increases the chance of spontaneous emission which is responsible for the ASE noise. The rate equation for change in the population of photons inside the active region (N_p) is given as [3]

$$\frac{dN_p}{dt} = R_{st}N_p + R_{sp} - \frac{N_p}{\tau_p} \tag{2.1}$$

where R_{st} is the rate of stimulated emission recombination, τ_p is the photon lifetime and the spontaneous emission rate (R_{sp}) is related to the spontaneous emission parameter (n_{sp}), both are respectively written as [3, 11]

$$R_{sp} = R_{st}n_{sp} \tag{2.2}$$

$$n_{sp} = \frac{N_2}{N_2 - N_1} \tag{2.3}$$

Optimum amplifier gain is obtained when $N_1 \approx 0$ and $n_{sp} \approx 1$. The total ASE noise in single polarisation has a power spectral density (PSD) (N_o) written as

$$N_o = n_{sp}(G-1)h\upsilon \tag{2.4}$$

2.6.2 Erbium doped fibre amplifier

The development and deployment of erbium doped fibre amplifiers (EDFAs) marked the evolution of optical communication into what is now known as the third optical communication window. An EDFA is manufactured by doping an optical fibre core with erbium ions (Er^{3+}). Erbium is a rare earth element and unlike other rare earth elements such as praseodymium (Pr^{3+}), ytterbium (Yb^{3+}), neodymium (Nd^{3+}) and thulium (Tm^{3+}), it provides wide spectral bandwidth (about 35 – 40 nm) with high gain (greater than 30 dB) and operates principally around the 1550 nm wavelength (although operations in the L-band (1565 nm – 1625 nm wavelength range) has been exploited) [3, 11, 66]. EDFAs operate with pump energy supplied by semiconductor lasers (mainly operating at 980 nm and 1480 nm, see Fig. 2.10 [11, 67]). They have high pump energy conversion efficiency, and high pump power (up to 20 dBm) could be provided with the 980 nm pumping [3]. EDFAs find their most important application in WDM systems where multichannel amplification highly reduces system cost. Furthermore, they provide a low noise gain that is less sensitive to polarisation, over a wide bandwidth which could accommodate many channels in dense-WDM systems, and their large carrier lifetime aids in mitigating interchannel crosstalk that is common in WDM systems [3]. A major drawback to the application of EDFAs in WDM systems is the non-uniform gain profile over the bandwidth range which results in variable amplification across the channels [3, 11]. A direct approach to solving this problem is through gain flattening by introducing a filtering element after the doped fibre [11, 67] as shown in Fig. 2.10.

IN: signal
OUT: backward ASE, residual counter-propagating pump

Single mode fibre doped with Er^{3+} ions

Long period grating filter

OUT: amplified signal, forward ASE, residual co-propagating pump

Isolator

Isolator

PUMP LASER

PUMP LASER

Co-propagating

Counter-propagating

Coarse wavelength mux/demux

Pump band (980 nm)

Fast non-radiative decay

Decay within band

Upper energy band (metastable)

980 nm

1480 nm

Electrons / ions in the metastable state can return to the ground state either through spontaneous or stimulated emission

Ground state band

Fig. 2.10 Schematic of a single gain stage erbium doped fibre amplifier with gain flattening filter (adapted from [11, 67]), including pumping possibilities.

Fig. 2.10 [11, 67] shows a simple schematic of a single gain stage EDFA with bi-directional pump. EDFAs with single directional or multiple pumping configurations are also available commercially and they may include multiple gain stages, variable optical attenuators (VOAs) and monitoring feedback to maintain the output-to-input power ratio. Isolators are positioned to reduce reflected light and back propagating ASE which could re-enter the gain medium and saturate the amplifier. The bands as shown in Fig. 2.10 are quite broad, thus there are many transitions (levels) and non-uniform distribution of erbium ions within the band due to thermal effect [11]. EDFAs operate as a three energy level system; pump energy excites the ions to higher energy states from where they decay to the metastable state. Then they return to the ground state either through stimulated or spontaneous emission, resulting in either amplification or ASE (with the help of stimulated emission), respectively. The optimum gain of an EDFA is a function of both the pump power and the amplifier length, so both parameters should be chosen carefully during the design process [3].

2.6.3 Semiconductor optical amplifier

Semiconductor optical amplifiers (SOAs) are primarily grouped into two types based on the reflectivity of the cavity end facet. They are the Fabry-Perot amplifiers (FPAs) and travelling wave amplifiers (TWAs). In the Fabry-Perot amplifiers (FPAs), facet reflectivities are in the range of 0.1 - 32 % [3, 66] such that reflections from the facets result in gain ripples with different peak gains at different wavelengths. FPAs are susceptible to polarisation and fluctuations in bias current because of the filtering characteristics of the devices and are more used in pulse reshaping than in amplification [66]. The gain ripples are eliminated in TWAs by reducing the facet reflectivities to less than 0.1% [3]. This is achieved through the use of antireflective coating (and sometimes in combination with angled-facets) and makes the TWA a superior optical amplifier, with a broad gain spectrum that is less sensitive to polarisation and having better noise performance compared to the FPA [3, 11, 66].

SOA gain and optimum linear power is dependent on many factors such as wavelength, bias current, and both the device structure and material [66] (InGaAsP/InP and GaAs/GaAlAs are popular materials). A schematic of the structure of an SOA is shown in Fig. 2.11 [66]. Unlike an EDFA, fewer components are required for its fabrication, but careful engineering is necessary to eliminate the facet reflectivities and to obtain good linear characteristics. The active region is formed at the junction of a p-type and n-type semiconductor. SOAs operate via stimulated emission of photons by recombination of electrons (driven to the conduction band on application of a bias current) with holes in the valence band.
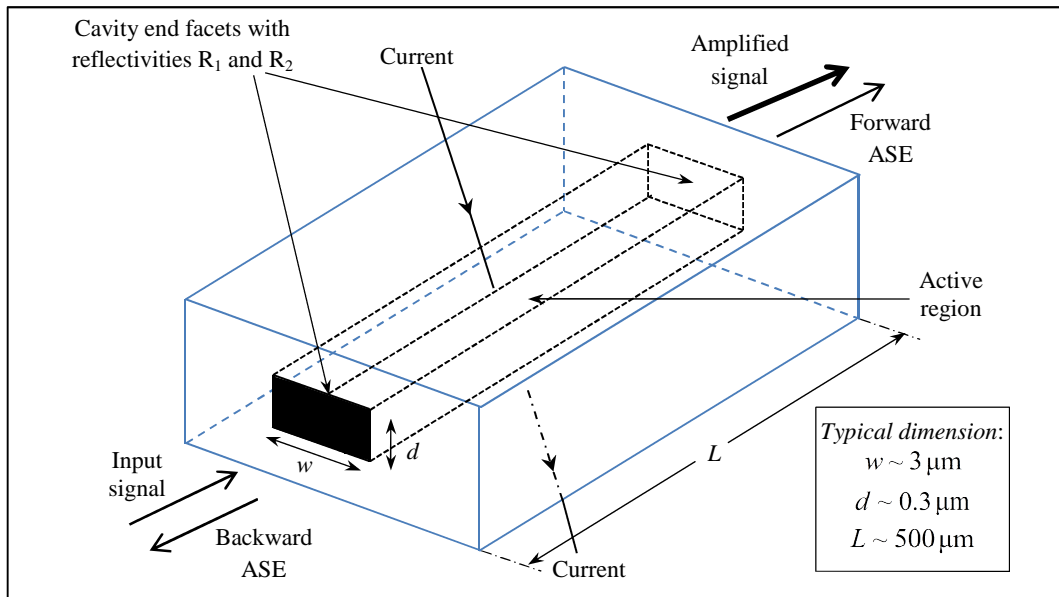
Fig. 2.11 Schematic structure of typical semiconductor optical amplifier (redrawn from [66])

SOAs can be fabricated to operate in different wavelength regions, and can be integrated seamlessly with planar waveguide optical devices. Their gain dynamic effects can be problematic for linear optical amplification, but finds application in other areas of optical communications (functional photonics - optical regeneration, wavelength conversion etc.). Despite these advantages, EDFAs are preferred over SOA, for optical amplification because of their higher gain (30 – 40 dB compared to about 20 dB for SOAs [11, 50]), better noise performance, lower insertion loss and stronger immunity to polarisation [3]. In addition, EDFAs are natural traveling wave amplifiers with no gain ripples and do not distort signals because of their comparably longer gain recovery time.

2.7 Optical receiver systems

An optical receiver module consists of different components which may be grouped into four sub-functional units, namely pre-detection optical processing, detection, post-detection electrical processing and decision circuit. The pre-detection unit is made up of optional components which function to ensure that the optical signal arriving at the photodetector input is of significant power and quality to enable photodetection. They may include passive receiver optics (mainly for FSO systems) such as receiver collecting lens (RCL), concentrators and collimators, and active components like the optical amplifiers and optical bandpass filters (OBPF) which limit the bandwidth of noise in the optical domain

(e.g. ASE noise (if optical amplifier is included) and ambient light (if FSO)) accompanying the signal. The detection unit includes the photodetector which is the main component in a receiver and which converts the optical signal to electrical signal. The post detection electrical processing unit includes electrical amplifiers and filter (which limits the electrical noise bandwidth) and possibly an equalization circuit. Finally, demodulation of the amplified electrical signal and recovery of the transmitted data takes place at the decision circuit which is designed according to the modulation scheme employed in the system [11]. Most practical receivers in optical access networks employ the low cost and simple detection method called direct detection. This method requires the detection of only the optical intensity of the signal and is the approach considered in this thesis. In another, more sophisticated method, referred to as coherent detection, both the optical intensity and phase of the signal is detected.

2.7.1 Principles of photodetection

Photocurrent is generated by a photodetector through the process of photo-electric effect. Most photodetectors are fabricated from semiconductor materials. In such materials, electrons at the ground state (valence band) absorb energy from incident photons with energy greater than the bandgap energy of the material and are moved up to the upper energy level (conduction band) leaving a hole in the valence band. An electric field, created in the depletion region of the photodetector by an applied bias voltage, then causes the electron-hole pair to separate thus generating electrical current. For various reasons all the incident light may not be converted to photocurrent. In most cases part of it is reflected at the surface of the detector, some of the transmitted light is not absorbed depending on the absorption coefficient ($\alpha_a(\lambda)$) of the material (which is also wavelength dependent) and the length of the light absorbing region (d_a), and some of the electron-hole pairs generated by the absorbed light recombine before they reach or leave the depletion region [68]. The external quantum efficiency (η_T) which accounts for all these losses could be written as [68]

$$\eta_T = \kappa \left(1 - R_f \right) \left[1 - e^{-\alpha_a(\lambda)d_a} \right] \tag{2.5}$$

where κ is the percentage of un-recombined electron-hole pairs, R_f is the reflectance of the photodetector material and $\alpha_a(\lambda) = 0$ for $\lambda > \lambda_{\text{cutoff}}$. The last part

of eq. (2.5) is the internal quantum efficiency (η_i) defined as the ratio of the absorbed power to the optical power incident on the photodetector. With careful design and fabrication $\kappa \to 1$, $R_f \to 0$, $\eta_T \approx \eta_i$ and a simplified formula for the quantum efficiency could be written as [11]

$$\eta = 1 - e^{-\alpha_a(\lambda)d_a} \tag{2.6}$$

Also related to the quantum efficiency is the responsivity of the photodetector. The responsivity is dependent on the optical frequency and defined in A/W or C/J as the ratio of the generated photocurrent to the incident optical power. Given an electron charge $q = 1.602 \times 10^{-19}$ C, It is generally written as,

$$R = \frac{\eta q}{h\upsilon} = \frac{\eta\lambda \ (\mu m)}{1.24} \tag{2.7}$$

where q is electron charge, h is Planck constant and υ is the optical frequency

2.7.2 Photodetectors

Two types of photodetectors are commonly used in optical communication receiver systems. They include the positive-intrinsic-negative (PIN) photodiode and the avalanche photodiode (APD). PIN photodiodes are fabricated by implanting an intrinsic semiconductor material of appropriate cut-off wavelength in-between a p-type and n-type semiconductor materials. The intrinsic material forms the depletion region in the PIN photodiode. Common intrinsic semiconductor materials for photodetectors operating at 1550 nm are InGaAs and InGaAsP. The absorption capacity of the PIN photodiode is improved by using an intrinsic material of greater thickness compared to the p- and n-type materials which could both be made of InP to form a double heterojunction device (InP/InGaAs/InP) or InGaAs could be used for the p-type material to form a single heterojunction device (InGaAs /InGaAs/InP). It is worth noting though that the transit time (and consequently the response time) of the device increases with the thickness of the intrinsic material, thus limiting the achievable bandwidth or data rate. Additionally, recombination of electron-hole pairs could increase in the depletion region if the response time is more than the recombination time.

In contrast to a PIN photodiode, an additional semiconductor region called the multiplication layer is required in an APD. Avalanche multiplication of electron-hole pairs occur in this layer due to impact ionization by collision of high energy

primary electrons with other electrons in the valence band causing them to rise to the conduction band. A high electric field is set up in this multiplication layer which accelerates the primary electrons resulting in a transfer of kinetic energy to other electrons [3]. The generation of secondary electron-hole pairs in the multiplication region (commonly made of InP) is a random process, thus the mean number of the secondary photoelectrons (per primary) is termed the APD multiplication factor or gain (M_A) [3, 11]. The multiplicative gain of the APD improves the signal power but the process is accompanied with additional shot noise, although in general, the receiver sensitivity is improved as the receiver thermal noise is not amplified in the gain process. Improvement in the sensitivity of receivers using PIN photodiodes is achieved with the use of optical preamplifiers.

2.8 Receiver optics and configurations

In the most conventional configuration, passive pre-detection optical devices are not included in the optical communication receiver. A small area photodetector preceded by an optical amplifier and OBPF is a common structural part of optical fibre communication receiver systems while large area photodetectors coated with thin-film filters are used in FSO links to enhance signal collecting capability of the system [55]. Large area photodetectors are not suitable for high speed communication because of their large RC time constant which increases the response time of the receiver and limits the achievable bandwidth. Consequently, additional optics are often included in FSO receiver systems to facilitate the collection of signal on to a small area photodetector [65]. In some cases, a short length of fibre preamplifier is included, leading to the various receiver configurations shown in Fig. 2.12. With additional optics included in Figs. 2.12b and 2.12c, the signal collecting apertures are large and both equal to the aperture of the collecting lenses, while the detector areas are relatively small (equal to the output aperture of the concentrator in Fig. 2.12b and about the area of the fibre in Fig. 2.12c). The increase in collecting area is at the expense of reduced field of view (FOV) because of etendue conservation [54]. However, for portable devices used mainly in the indoor environment, both wide FOV and large detector aperture are needed for enhanced mobility. Therefore, a trade-off between the receiver FOV and aperture area is required in the design of

such devices in order to provide a compact communication device that can operate at high speed and support some degree of mobility.
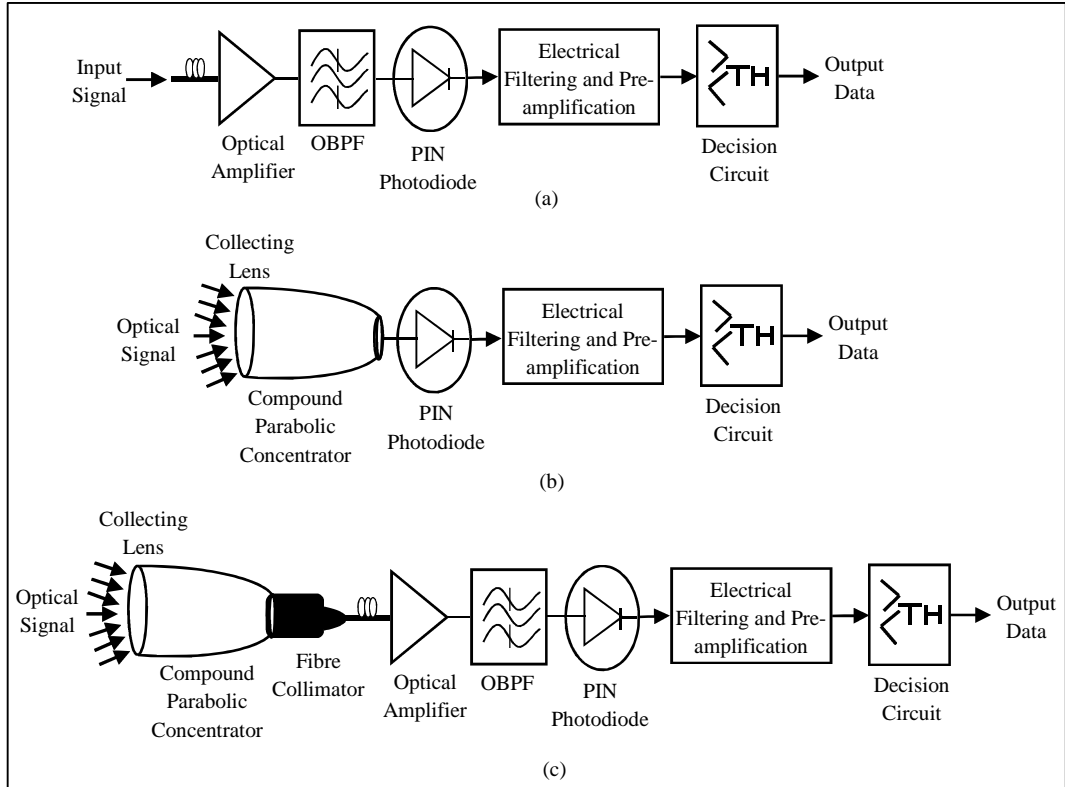
Fig. 2.12 Schematic structure of various optical communication receiver systems: (a) optically preamplified optical fibre receiver system (b) FSO receiver system (c) optically preamplified fibre coupled FSO receiver system

2.8.1 Etendue conservation

The etendue of an optical system defines the geometric limit of how much light it can accept. In theory, the area and solid angle product of the external optics such as the collecting lens is constrained by the etendue of the detector or fibre in the case of Fig. 2.12c. Thus there is a limit to the selection of wide FOV large area collecting lens in an FSO receiver, the FOV gets narrower with larger area. The constraint imposed by the etendue of fibre coupled optical receiver system is illustrated in Fig. 2.13. Considering Fig. 2.13, the optical power incident on the fibre core is related to its etendue which is written as [69]

$$E_f = \pi n_o^2 A_f \sin^2 \theta \tag{2.8}$$

The optical power collected at the collecting lens is also proportional to its area and solid angle product which could be written as

$$E_c = \pi n_a^2 A_c \sin^2 \varphi \tag{2.9}$$

As E_f is required to be equal to E_c, the gain obtained from an ideal concentrator located between the fibre end the collecting lens is written as [55]

$$C_g = \frac{A_c}{A_f} = \frac{n_o^2 \sin^2 \theta}{\sin^2 \varphi} \tag{2.10}$$

where the air index of refraction $n_a = 1$.
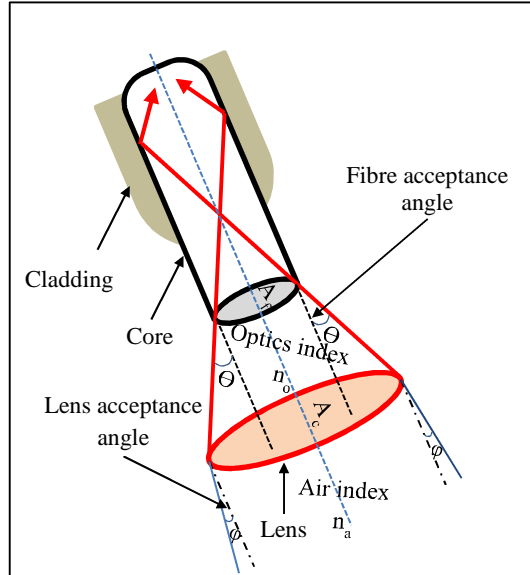
Fig. 2.13 Illustration of the etendue of the fibre coupled receiver systems

2.8.2 Receiver decision devices

A common part of an optical receiver system is a device that facilitates decision making by using defined methods to declare the received data to be a 1 or 0. In OOK systems, this is achieved by setting a decision threshold which is compared with the received signal, and data 1 or 0 is declared for signals above or below the threshold respectively. This decision threshold method is also used in fibre DPPM systems where the first slot in which the leading edge of the signal crosses the threshold is declared as the slot carrying the transmitted data [32, 70]. Although the threshold method could be implemented for FSO DPPM systems, the method that integrates the content of each slot in the frame and compares the output of all the slots, and selects the slot with the highest output as the data carrying slot, has been generally used in both intersatellite and terrestrial FSO systems [35, 71], and will be assumed in this thesis. The integrate and compare decision method outperforms the threshold method in terms of symbol error rate [35], but requires faster and more complex electronic processing because the rate of slot integration and comparison has to match the data arrival rate in the slots.

2.9 Passive optical network

The optical fibre access network is dominated by the passive optical network (PON) which offers numerous advantages compared to the active optical network (AON) such as fewer fibre installation, low power consumption and low maintenance cost. The architecture of a generic PON is shown in Fig. 2.14. The optical line termination (OLT) located at the central office (CO) is connected to the optical network unit (ONU) at the customer's premises through a fibre network consisting of the feeder fibre, passive optical devices including splitters/combiners or/and multiplexers/demultiplexers, and the distribution fibre network. The broadband-PON (BPON) approved by ITU-T G.983 and originally deployed for broadband access could only support up to 32 ONUs, at a distance of about 20 km and data rates of 622 Mbps downstream and 155 Mbps upstream [72, 73]. Since its first deployment, PON has evolved with increase in capacity, reach and data rate, and both Ethernet-PON (EPON) with 1.25 Gbps for both upstream and stream and Gigabit-PON (GPON) which can support up to 64 ONUs at 2.5 Gbps in the upstream and downstream have been deployed [73, 74]. The current focus of research for next generation PON was firstly on SuperPONs, and then (with WDM) long-reach-PONs, which are intended to extend the data rate and reach of PON to about 10 – 40 Gbps and 60 - 100 km, and probably support more than 128 ONUs [73, 74].
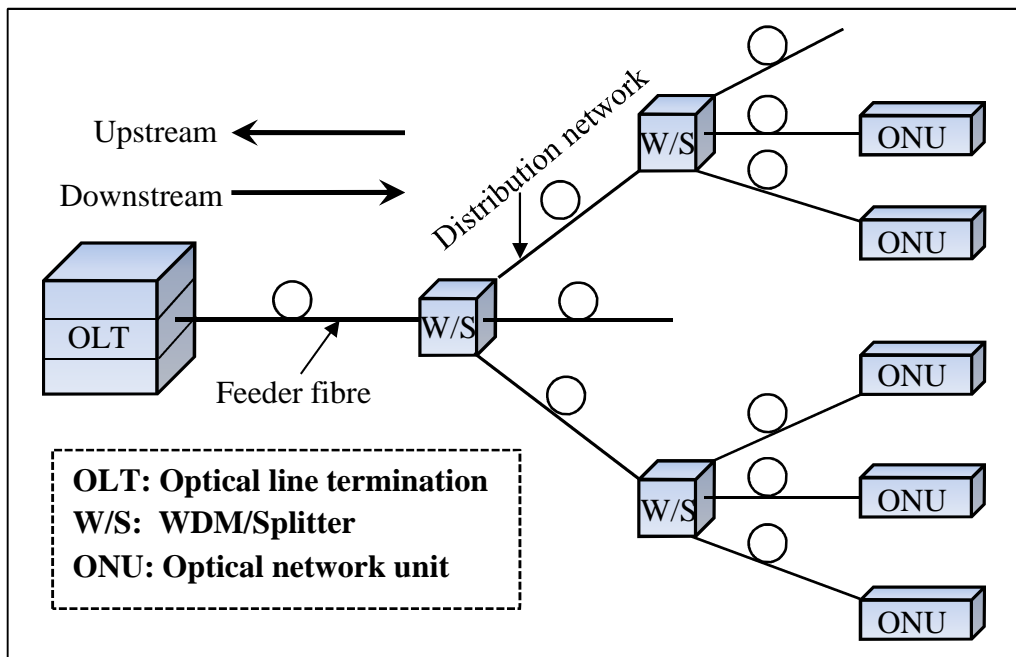
Fig. 2.14 Architecture of a generic passive optical network

2.10 Summary

The functional units of an optical communication system have been discussed in this chapter. Different processes involved in optical signal generation, transmission and reception were discussed in detail, and a general review of laser safety and standards was given. Various receiver configurations and some common modulation schemes in optical communication were discussed. The optical fibre and FSO channels were briefly presented in this chapter. Detailed behaviour of each channel with system impairments and receiver noise are fully discussed in the next chapter.

2.11 References

1. Keiser, G. *Optical Fiber Communications*. 2nd ed: McGrraw-Hill, Inc.; 1991.
2. Hunsperger, R. G. *Integrated Optics Theory and Technology*. 6th ed. New York, USA: Springers; 2010.
3. Agrawal, G. P. *Fiber-optic communication systems*. 3rd ed. New York: John Wiley & Sons Inc.; 2002.
4. Injeyan, H., Goodno, G. D. *High-power Laser Handbook*: McGraw-Hill, Inc; 2011.
5. Kaminow, I. P., Turker, R. S., Tamir, T. *Guided-Wave Optoelectronics: Mode-Controlled Semiconductor Laser*. 2nd ed. Tamir T, editor: Springer-Verlag; 1990.
6. Hooker, S., Webb, C. *Laser Physics*: Oxford University Press; 2010.
7. Parker, A. M. *Physics of Optoelectronics (Optical Science and Engineering)*: Taylor & Francis Group; 2005.
8. Kazovsky, L. G., Cheng, N., Shaw, W.-T., Gutierrez, D., Wong, S.-W. *Broadband Optical Access Networks*. New Jersey, USA: John Wiley & Sons, Inc.; 2011.
9. Lightwave 1999 Worldwide Directory of Fibre-Optic Communications Products and Services. March 31, 1999: pp. 58-61.
10. Streetman, B. G., Banerjee, S. K. *Solid State Electronic Devices*. 6th ed. New Jersey, USA: Pearson Prentice Hall; 2006.
11. Ramaswami, R., Sivarajan, K. N., Sasaki, G. H. *Optical Networks: A Practical Perspective*. 3rd ed. Boston: Morgan Kaufmann Publishers; 2010.
12. Caplan, D. O.: 'Laser communication transmitter and receiver design'. *Journal of Optical and Fiber Commun. Reports,* 2007, **4**, (4-5), pp. 225-362
13. Sibley, M. J. N.: 'Dicode pulse-position modulation: a novel coding scheme for optical-fibre communications'. *IEE Proc. Optoelectron.,* 2003, **150**, (2), pp. 125-131
14. Al-Suleimani, I. H., Phillips, A. J., Woolfson, M. S.: 'Performance evaluation of optically preamplified dicode pulse position modulation receivers'. *European Trans. Telecommun.,* 2008, **19**, (1), pp. 47-52
15. Cryan, R. A., Sibley, M. J. N.: 'Minimising intersymbol interference in optical-fibre dicode PPM systems'. *IEE Proc. Optoelectron.,* 2006, **153**, (3), pp. 93-100
16. Charitopoulos, R. A., Sibley, M. J. N.: 'Slot and frame synchronisation in dicode pulse-position modulation'. *IET optoelectron.,* 2010, **4**, (4), pp. 174-182
17. Charitopoulos, R. A., Sibley, M. J. N., Mather, P. J.: 'Maximum likelihood sequence detector for dicode pulse position modulation'. *IET Optoelectron.,* 2011, **5**, (6), pp. 261-264
18. Garrett, I.: 'Pulse-Position Modulation for Transmission Over Optical Fibers with Direct or Heterodyne Detection'. *IEEE Trans. Commun.,* 1983, **31**, (4), pp. 518-527

19. Ghassemlooy, Z., Hayes, A. R., Seed, N. L., Kaluarachchi, E. D.: 'Digital pulse interval modulation for optical communications'. *IEEE Communs. Magazine,* 1998, **36**, (12), pp. 95-99

20. Kataoka, N., Cincotti, G., Wada, N., Kitayama, K.: 'Demonstration of asynchronous, 40Gbps x 4-user DPSK-OCDMA transmission using a multi-port encoder/decoder'. *Opt. Express,* 2011, **19**, (26), pp. B965-B970

21. Kiasaleh, K.: 'Performance of APD-based, PPM free-space optical communication systems in atmospheric turbulence'. *IEEE Trans. Communs.,* 2005, **53**, (9), pp. 1455-1461

22. Li, J., Liu, J. Q., Taylor, D. P.: 'Optical communication using subcarrier PSK intensity modulation through atmospheric turbulence channels'. *IEEE Trans. Commun.,* 2007, **55**, (8), pp. 1598-1606

23. Popoola, W. O., Ghassemlooy, Z.: 'BPSK subcarrier intensity modulated free-space optical communications in atmospheric turbulence'. *J. Lightw. Technol.,* 2009, **27**, (8), pp. 967-973

24. Zuo, T. J., Ma, R., Phillips, A. J., Sujecki, S.: 'Performance analysis of optically preamplified DC-coupled burst mode receivers'. *European Trans. Telecommun.,* 2009, **20**, (3), pp. 281-286

25. Ghassemlooy, Z., Popoola, W., Rajbhandari, S. *Optical Wireless Communications - System and Channel Modelling with MATLAB*. 1st ed. London: CRC Press; 2013.

26. Gfeller, F. R., Bapst, U.: 'Wireless in-house data communication via diffuse infrared radiation'. *Proc. IEEE,* 1979, **67**, (11), pp. 1474-1486

27. Majumdar, A. K.: 'Free-space laser communication performance in the atmospheric channel'. *J. Opt. Fiber Commun. Rep.,* 2005, **2**, pp. 345 - 396

28. Gagliardi, R. M., Karp, S.: 'M-ary Poisson detection and optical communications'. *IEEE Trans. Commun. Technol.,* 1969, **17**, (2), pp. 208-216

29. Karp, S., Gagliardi, R. M.: 'The design of a pulse-position modulated optical communication system'. *IEEE Trans. Commun. Technol.,* 1969, **17**, (6), pp. 670-676

30. Pires, J. J., Da Rocha, J. F.: 'Digital pulse position modulation over optical fibres with avalanche photodiode receivers'. *IEE Proceedings Journal Optoelectronics,* 1986, **133**, (5), pp. 309-313

31. Cryan, R. A., Unwin, R. T., Garrett, I., Sibley, M. J. N., Calvert, N. M.: 'Optical fibre digital pulse-position-modulation assuming a Gaussian received pulse shape'. *IEE Proceedings J (Optoelectron.)* 1990, pp. 89-96

32. Phillips, A. J., Cryan, R. A., Senior, J. M.: 'Optically preamplified pulse-position modulation for fibre-optic communication systems'. *IEE Proc. - Optoelectron.,* 1996, **143**, (2), pp. 153-159

33. Phillips, A. J., Cryan, R. A., Senior, J. M.: 'An optically preamplified PPM intersatellite system described by a moment-generating function formulation'. *Microwave and Optical Technol. Letters,* 1995, **8**, (4), pp. 200-204

34. Phillips, A. J., Cryan, R. A., Senior, J. M.: 'Novel laser intersatellite communication system employing optically preamplified PPM receivers'. *IEE Proceedings Communications,* 1995, **142**, (1), pp. 15-20

35. Phillips, A. J., Cryan, R. A., Senior, J. M.: 'An optically preamplified intersatellite PPM receiver employing maximum likelihood detection'. *IEEE Photonics Technol. Lett.,* 1996, **8**, (5), pp. 691-693

36. Audeh, M. D., Kahn, J. M., Barry, J. R.: 'Performance of pulse-position modulation on measured non-directed indoor infrared channels'. *IEEE Trans. Commun.,* 1996, **44**, (6), pp. 654-659

37. Sethakaset, U., Gulliver, T. A.: 'Differential amplitude pulse-position modulation for indoor wireless optical channels'. *IEEE Global Telecommun. Conf.* 2004, pp. 1867-1871

38. Menon, M., Cryan, R. A.: 'Optical wireless communications utilizing a dicode PPM PIN-BJT receiver'. *Microwave and optical technol. letters,* 2005, **45**, (4), pp. 273-277

39. Aldibbiat, N. M., Ghassemlooy, Z., McLaughlin, R.: 'Indoor optical wireless systems employing dual header pulse interval modulation (DH-PIM)'. *Int. J. Commun. Syst.,* 2005, **18**, (3), pp. 285-305

40. Stallings, W. *Data and Computer Communications*. 8th ed. New Jersey, USA: Pearson Prentice Hall; 2007.

41. Kim, C., Li, G.: 'Direct-detection optical differential 8-level phase-shift keying (OD8PSK) for spectrally efficient transmission'. *Opt. Express,* 2004, **12**, (15), pp. 3415-3421

42. Kotani, Y., Iwamura, H., Tamai, H., Sarashina, M., Kashima, M.: 'Demonstration of 1.25 Gb/s 8-channels ECDM using eight-chip electrical coding'. *IEEE Photonics Technol. Lett.,* 2010, **22**, (12), pp. 875-877

43. Kitayama, K., Xu, W., Wada, N.: 'OCDMA over WDM PON-solution path to gigabit-symmetric FTTH'. *J. Lightw.Technol.,* 2006, **24**, (4), pp. 1654-1662

44. Guo, C., Huang, L., He, S.: 'Demonstration of 1 Gb/s 15-User CDM Over WDM-PON Using Electrical Spatial Coding and Subcarrier Multiplexing'. *IEEE Photonics Technol. Lett.,* 2011, **23**, (14), pp. 953-955

45. Ghaffari, B. M., Matinfar, M. D., Salehi, J. A.: 'Wireless optical CDMA LAN: digital design concepts'. *IEEE Trans. Commun.,* 2008, **56**, (12), pp. 2145-2155

46. Galdino, L., Raddo, T. R., Sanches, A. L., Bonani, L. H., Moschim, E.: 'Performance comparison of hybrid 1-D WDM/OCDMA and 2-D OCDMA towards future access network migration scenario'. *14th Int'l Conf. on Transparent Optical Networks (ICTON)* 2012, pp. 1-4

47. 'ICNIRP Statements on Light-emitting diodes and laser diodes : Implications for Hazard Assessmen', *Health Physics*, **78**, (6), pp. 744-752, 2000.

48. 'Guidelines on Limits of Exposure to Broadband Incoherent Optical Radiation', *Health Physics Society*, 1997.

49. 'Safety of laser products - part 1: Equipment classification, requirements and user's guide, IEC-60825-1 (Incorporating amendments A1:1997 and A2:2001)', 2001.

50. 'ICNIRP Guidelines - Revision of guidelines on limits of exposure to laser radiation of wavelengths between 400nm and 1.4micro', *Health Physics*, **79**, (4), pp. 431-440, 2000.

51. Kapron, F. P., Keck, D. B., Maurer, R. D.: 'Radiation Losses in Glass Optical Waveguides'. *Applied Physics Lett.,* 1970, **17**, (10), pp. 423-425

52. Karp, S., Gagliardi, R. M., Moran, S. E., Stotts, L. B. *Optical channels: fibers, clouds, water, and the atmosphere*: Springer Science & Business Media; 2013.

53. Mitra-Thakur, S. Deep-sea optical communications system launches. *IET Engineering and Technology Magazine*. March 2012.

54. O'Brien, D.: 'Indoor optical wireless communications: recent developments and future challenges'. *Proc. of SPIE,* 2009, **7464**, pp. 74640B

55. Barry, J. R. *Wireless Infrared Communications*. Boston: Kluwer Academic Publishers; 1994 1994.

56. Ghassemlooy, Z., Boucouvalas, A. C.: 'Indoor optical wireless communication systems and networks'. *Intl. J. Commun. Syst.,* 2005, **18**, (3), pp. 191-193

57. Kahn, J. M., Barry, J. R.: 'Wireless infrared communications'. *Proc. IEEE,* 1997, **85**, (2), pp. 265-298

58. Ntogari, G., Kamalakis, T., Sphicopoulos, T.: 'Analysis of Indoor Multiple-Input Multiple-Output Coherent Optical Wireless Systems'. *J. Lightw. Technol.,* 2012, **30**, (3), pp. 317-324

59. Matsuo, R., Matsuo, M., Ohtsuki, T., Udagawa, T., Sasase, I.: 'Performance analysis of indoor infrared wireless systems using OOK CDMA on diffuse channels'. *IEEE Pacific Rim Conf. on Commun., Comput. and Signal Processing* 1999, pp. 30-33

60. Ohtsuki, T.: 'Performance analysis of indoor infrared wireless systems using PPM CDMA'. *Electronics and Commun. in Japan* 2002, **85**, (1), pp. 1-10

61. Ke, W., Nirmalathas, A., Lim, C., Skafidas, E.: '4 x 12.5 Gb/s WDM Optical Wireless Communication System for Indoor Applications'. *J. Lightw. Technol.,* 2011, **29**, (13), pp. 1988-1996

62. Elgala, H., Mesleh, R., Haas, H.: 'Indoor optical wireless communication: potential and state-of-the-art'. *IEEE Commun. Mag.,* 2011, **49**, (9), pp. 56-62

63. Komine, T., Nakagawa, M.: 'Fundamental analysis for visible-light communication system using LED lights'. *IEEE Trans. Consum. Electron.,* 2004, **50**, (1), pp. 100-107

64. Borah, D. K., Boucouvalas, A. C., Davis, C. C., Hranilovic, S., Yiannopoulos, K.: 'A review of communication-oriented optical wireless systems'. *EURASIP J. Wireless Communs. and Networking,* 2012, **2012**, (1), pp. 1-28

65. Ke, W., Nirmalathas, A., Lim, C., Skafidas, E.: 'High-Speed Optical Wireless Communication System for Indoor Applications'. *IEEE Photonics Technol. Lett.,* 2011, **23**, (8), pp. 519-521

66. Senior, J. M. *Optical Fiber Communications Principles and Practice*. 3rd ed. Essex, England: Pearson Prentice Hall; 2009.

67. Wysocki, P. F., Judkins, J. B., Espindola, R. P., Andrejco, M., Vengsarkar, A. M.: 'Broad-band erbium-doped fiber amplifier flattened beyond 40 nm using long-period grating filter'. *IEEE Photonics Technology Letters,* 1997, **9**, (10), pp. 1343-1345

68. Liu, J.-M. *Photonic devices*: Cambridge University Press; 2005.

69. Ho, K.-P., Kahn, J. M.: 'Compound parabolic concentrators for narrowband wireless infrared receivers'. *OPTICE,* 1995, **34**, (5), pp. 1385-1395

70. Zuo, T. J., Phillips, A. J.: 'Performance of burst-mode receivers for optical digital pulse position modulation in passive optical network application'. *IET Optoelectron.,* 2009, **3**, (3), pp. 123-130

71. Aladeloba, A. O., Phillips, A. J., Woolfson, M. S.: 'Performance evaluation of optically preamplified digital pulse position modulation turbulent free-space optical communication systems'. *IET Optoelectron.,* 2012, **6**, (1), pp. 66-74

72. Van de Voorde, I., Van der Plas, C.: 'Full service optical access networks: ATM transport on passive optical networks'. *IEEE Commun. Mag.,* 1997, **35**, (4), pp. 70-75

73. Trojer, E., Dahlfort, S., Hood, D., Mickelsson, H.: 'Current and next-generation PONs: A technical overview of present and future PON technology'. *Ericsson Review,* 2008, **2**, pp. 64-69

74. Gianordoli, S., Rasztovits-Wiech, M., Stadler, A., Grabenhorst, R.: 'Next generation PON'. *Elektrotechnik und Informationstechnik,* 2006, **123**, (3), pp. 78-82

CHAPTER 3   Performance Evaluation
and Multi-user Schemes

3.1 Overview

This chapter discusses the devices and techniques commonly used in the implementation of multiple user services in optical access networks. Various channel characteristics and attendant impairments in an optical communication system, including multi-access interference and crosstalk, and different receiver noises, are analysed. Performance evaluation methods used in facilitating the analysis of different optical communication systems considered in this thesis are also described.

3.2 Multiplexing and demultiplexing

Commonly in optical access networks, multiple users' information is transported together in a single physical medium such as a single mode fibre or a direct atmospheric link. Network designers have to devise means of managing the data over the single channel with minimum compromise to data integrity and to enable proper separation of each user's data at the receiver. The processes of combining multiple signals together for transmission through a single medium and separating them into its original component signals for reception are respectively called multiplexing and demultiplexing. Signal multiplexing provides an economic advantage to the system by enabling the sharing of system resources such as channel bandwidth and network components, like the optical amplifier, among many users [1].

3.2.1 Optical power splitters and combiners

Optical power splitters are often used in optical communication systems to split an optical signal into two or more parts. They are referred to as beam splitters in FSO systems where a single beam may be split into different parts and sent to either the receiver system or the tracking subsystem or both [2, 3], but are generally known as power splitters in optical fibre systems. Splitters are passive devices, and can act as power combiners for transmission in the reverse direction. Optical power splitters are mostly made from 3 dB couplers by fusing fibre ends

together and terminating unwanted ends to prevent back reflection. These are referred to as fused biconical taper (FBT) splitters. Another type of power splitter is the planar lightwave circuit (PLC) splitter, which is fabricated through a more complex and expensive process, from lithium niobate (LiNbO$_3$) or silica based waveguides [4]. Because of the advanced fabrication technique used in PLC power splitters, they are compact and more reliable and can provide higher splitting ratio. Power splitters are sometimes fabricated to have fixed and equal percentage splitting, but recent splitters with variable percentage splitting exist [5, 6]. The insertion loss of a power splitter ranges from 3 dB to 4 dB per 2-way split including excess losses and depending on the splitting ratio and fabrication process [1, 4, 7].

3.2.2 Wavelength multiplexers and demultiplexers

A wavelength multiplexer (mux) selects signals of different wavelengths from different input ports and combines them onto one output port for transmission in a single medium such as an optical fibre. Wavelength demultiplexers (demux) are generally made by connecting a wavelength multiplexer in reverse order enabling combined multiple wavelength input signals to be separated into different wavelength output signals in different ports. Multiplexers and demultiplexers are mainly fabricated based on three major technologies, namely thin film multicavity filters (TFMF), arrayed waveguide gratings (AWG) and fibre Bragg gratings (FBG), though diffraction grating (also called Stimax grating) based multiplexers have been demonstrated and deployed [1, 8-10]. A thin film multicavity filter transmits signal of a particular wavelength based on the length of the filter cavity and reflects all other wavelength signals. By assembling many such filters on a glass substrate, a low loss multiplexer with a flat top passband and insensitive to signal polarisation could be made [1].

Alternatively, an array of waveguides etched on silica or germanium-doped silica is connected to a multiport coupler on both ends and fabricated on a silicon substrate to produce an AWG multiplexer. Multiple wavelength signals from one port of the input coupler are distributed (through diffraction [10]) among the waveguide array which is structured such that a constant path length difference exists between adjacent waveguides. The periodic gratings formed by the path length difference result in constructive or destructive interferences between the

signals from all the waveguides with signals of different wavelengths being isolated at different ports of the output coupler. AWG is fabricated using advanced technology (e.g. planar lightwave circuit) and is compact with uniform insertion loss over all wavelengths and could be cascaded with MZIs to obtain narrow flatter top passband [10, 11], with 1 dB bandwidth of about 0.22 nm as shown in Table 3.1 [1].

Table 3.1 Comparison of different wavelength multiplexer technologies assuming 16 channels spaced at 100 GHz [1]

Multiplexer filter Property	FBG based	TEMF based	AWG based	Diffraction (Stimax) grating based
1 dB bandwidth (nm)	0.3	0.4	0.22	0.1
Adjacent channel rejection (dB)	25	25	25	30
Insertion Loss (dB)	0.2	7	5.5	6
Polarisation dependent loss (dB)	0	0.2	0.5	0.1
Temperature coefficient (nm/$^\circ$C)	0.01	0.0005	0.01	0.01

FBG technology creates a grating inside the core of a photosensitive fibre by subjecting it to ultraviolet light or using a phase mask to create a variation in refractive index [1]. FBGs are used in combination with circulators as optical add drop multiplexers. As shown in Fig. 3.1, input signals on port 1 are transmitted out on port 2 by the circulator. In this case, the grating is tuned to the desired wavelength λ_3 which it reflects back to the circulator and the circulator transmits it out on port 3. As shown in Table 3.1, FBG based multiplexers have the lowest insertion loss with flat top passband but imperfect grating reflection could increase crosstalk [1].
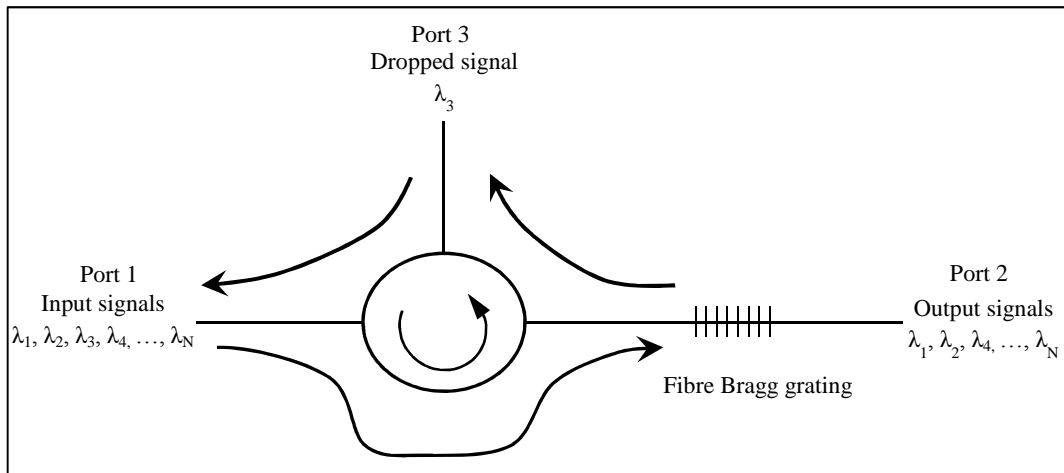
Fig. 3.1 Schematic diagram of the optical add drop multiplexer based on FBG

The diffraction grating based multiplexers are made with gratings etched on bulk semiconductor material like silica and fabricated on silicon substrate. They are implemented with lenses at the input and output fibres and are expensive because of difficult fabrication processes [1, 8].

3.3 Multiplexing and multiple access techniques

Signal multiplexing was described in Section 3.2. Multiple access techniques are related to multiplexing because they provide means by which many users can utilize the resources in a common transmission channel. Multiplexing and multiple access are implemented by sharing the wavelength, time and space in the channel among the users, or by assigning a unique code to each user. Resource allocation may be performed dynamically (allocation on demand) or fixed resources allotted to each user in the system. Dynamic allocation of resources for multiple access requires protocols. Common multiplexing and multiple access techniques in optical access networks include TDM/TDMA, WDM/WDMA and CDM/CDMA.

3.3.1 Time division multiplexing/multiple access

Time division multiplexing (TDM) is an established multiplexing technique in which a specific time slot in a frame is allotted to each of the different signals meant for transmission over a common channel. In the downstream of the optical access networks, each independent data stream is sent to the designated network unit either through an active switching and routing mechanism where only the

data for each network unit is sent to its destination, or through a network broadcast as in PON where a passive power splitter is used to split the signals and each ONU receives other ONU's data but selects only the data that is occupying its time slot [12, 13]. The TDMA technique is used for upstream transmission in PON with access granted to each ONU at a specific time slot determined by an OLT controlled protocol. All the data from the ONUs are joined together at the combiner in a time frame with guard bands separating each ONU's data from the other and forwarded to the OLT. The TDM/TDMA technique is simple and offers efficient average use of power because signals are transmitted with low duty cycle [14], but the signals incur splitting losses, require synchronisation and each users' transmission capacity is reduced compared to overall system capacity [14, 15]. Upstream data are not synchronised and signals are of different amplitudes, resulting in bursty data packets and the requirement of burst mode receivers at the OLT [16, 17].

3.3.2 Wavelength division multiplexing/multiple access

In wavelength division multiplexing (WDM), a range of wavelengths within the bands in the International telecommunication union-telecommunication (ITU-T) grid is used and each fixed central wavelength is assigned for the transmission of a specific signal in a common channel. Adequate spacing is provided between the central wavelength assigned for the transmission of each signal and the central wavelength assigned for the transmission of the next adjacent signal, just like the guard band in a TDM/TDMA PON, with wider spacing required for coarse-WDM (CWDM) applications than dense-WDM (DWDM) [7, 18]. In a WDM PON, a dedicated central wavelength is used for both the upstream and downstream transmission of signal between the OLT and the ONU. However, in some systems that employ WDMA, wavelengths are assigned based on demand for either the upstream or downstream transmission. Dynamic allocation of wavelengths in WDMA systems contributes to efficient utilization of the channel resources as wavelengths are freed when they are not in use by an OLT or ONU. However, WDM is more preferred in PON because it simplifies the operation of the system compared to WDMA. A hybrid of both technologies could also be used in a PON. WDM/WDMA implementation is enabled by optical amplifiers which could

provide significant signal amplification over all the wavelengths in the channel, generally reducing the system cost [19].
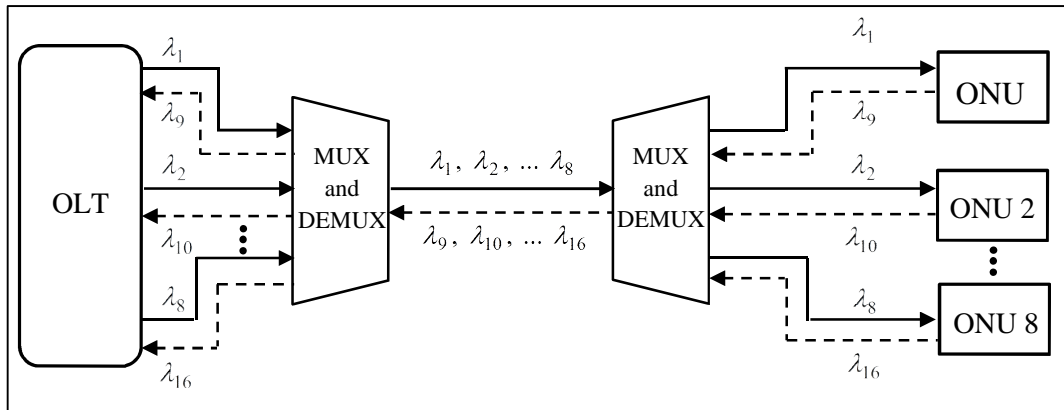
Fig. 3.2 Illustration of WDM application in PON (adapted from [19])

Traditionally in WDM/WDMA PONs, separate wavelength bands are used for the upstream and downstream transmission [18], (e.g. about 1260 – 1285 nm and 1310 - 1350 nm in the O-band for upstream and 1526 - 1560 nm for downstream in 10 Gbps GPON [20]). However, bidirectional WDM systems using reflective SOAs have been proposed [21, 22]. Wavelength mux/demux are used in WDM/WDMA technology to overcome the splitting power loss incurred in TDM/TDMA systems as shown in Fig. 3.2. In addition, WDM/WDMA provides high bandwidth transmission between the OLT and ONUs without any need for time sharing. Furthermore, because each ONU's data is sent to that ONU on its own wavelength in WDM PON systems, it provides greater security and privacy compared to TDM PON where all the ONU's data are sent as a broadcast on a single wavelength and each ONU sees other ONU's data. The technique however requires optical network components that are capable of operating at multiple wavelengths, probably wavelength tunable and selective devices which are expensive and which increase system complexity [7, 18]. Bidirectional transmission and several alternative devices aimed at reducing the cost of WDM PON systems including the use of less expensive transmitters (e.g. VCSEL lasers) and colourless ONUs have been proposed [18, 21, 23].

3.3.3 Code division multiplexing/multiple access

Different users' signals are transmitted using a unique code sequence in a common channel and in an overlapping time and wavelength when code division

multiplexing/multiple access (CDM/CDMA) is employed in a communication system. In the primary approach, a fixed code is assigned to each user for both upstream and downstream transmission, but dynamic allocation of codes to users has been proposed in [24, 25]. CDM/CDMA is a spread spectrum based technology originally used for military communication because of its enhanced security features and has been fully adapted for use in RF and microwave communications, but limited implementation has been reported in optical communications due to major concerns regarding the cost and availability of high speed encoding and decoding devices [26-28]. Typically, a single bit period in a CDMA system is divided into a code length dependent number of equal intervals called chips as shown in Fig. 3.3a for an OOK system and Fig. 3.3b for a binary DPPM system. Signal pulses are transmitted in one or more chips according to the code sequence for each user and depending on the modulation scheme employed and the data to be transmitted.

CDMA in optical communications is classified as coherent or incoherent and as one dimensional (1D) or two dimensional (2D) depending respectively on the method of detection (or type of optical source) and which domain the signal pulses are encoded (temporal, spectral or both temporal and spectral) [26, 29-31]. Data encoding/decoding in CDMA can be performed in electrical or optical domain (optical CDMA (OCDMA)) and system implementation could be synchronous and asynchronous [32-34]. Optical encoding/decoding is preferred for high speed transmission to avoid the electronic processing burden that would be placed on encoders and decoders when encoding/decoding is performed in the electrical domain. In synchronously implemented CDMA systems, the electronic processing burden is reduced and the code cardinality is improved because a pulse is transmitted only in a single chip position to represent each user's signal, whereas a number of pulses depending on the code weight are simultaneously transmitted in several chip positions to represent each user's signal in asynchronous CDMA systems [26]. Full system synchronisation is however challenging, therefore, additional resistance to multiple access interference (MAI) is obtained in 'synchronous' CDMA systems by simultaneously transmitting more than one pulse in several chip positions for each users signal as in asynchronous CDMA. Asynchronous CDMA is sometimes preferred for easier implementation.
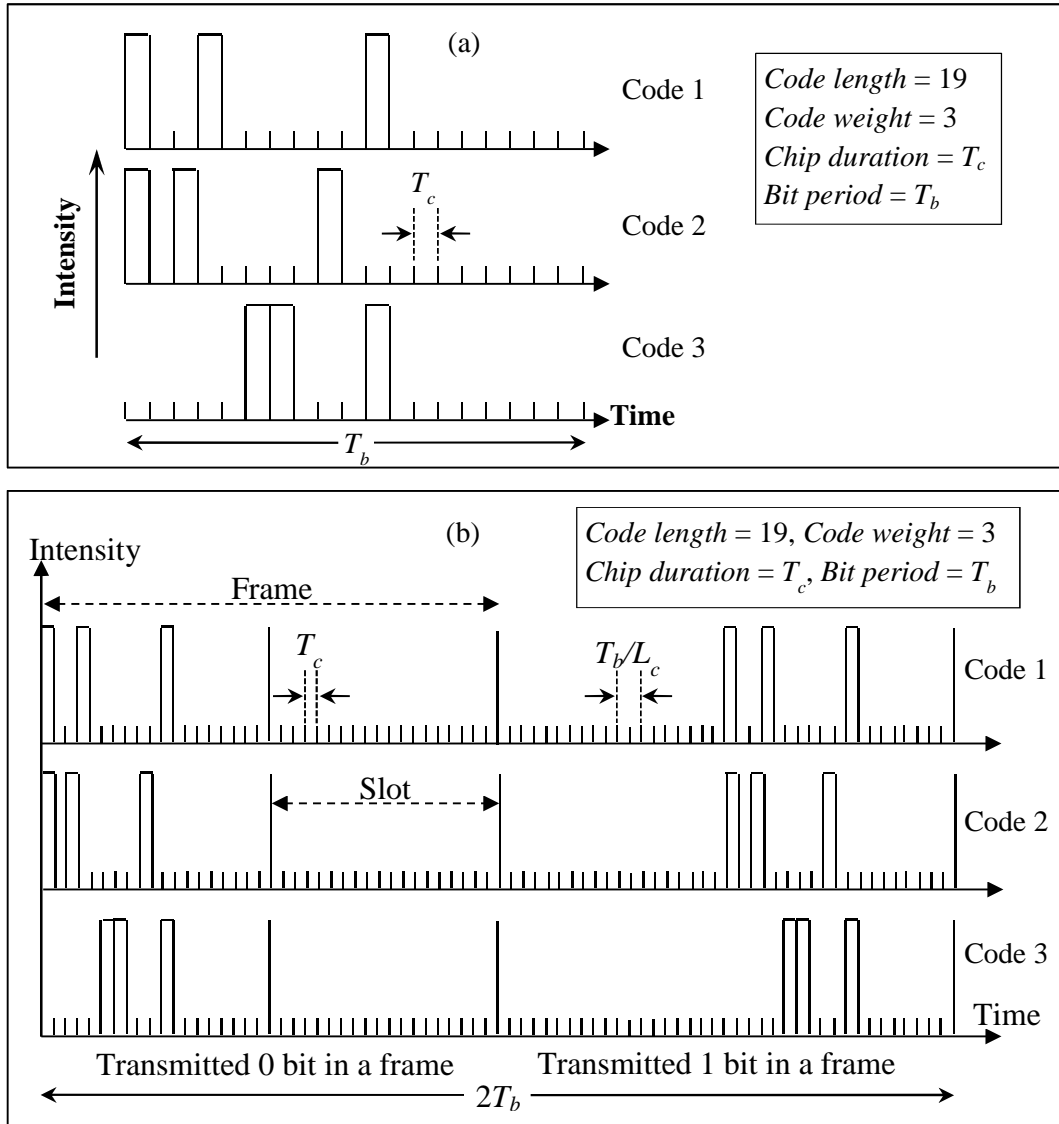
Fig. 3.3 Illustration of unipolar 1D time encoded signal (L_c = code length): (a) OOK CDMA and (b) binary (M = 1) DPPM CDMA

Both bipolar and unipolar codes are used in CDMA. A bipolar code such as a Gold sequence is represented in both positive and negative components (i.e. 1, -1), while unipolar codes such as optical orthogonal codes (OOC) and prime codes are represented with only positive components (i.e. 1, 0) [26, 35]. A general requirement is that code sequences in a family of code are distinguishable from one another to enable detection of different user's signals at the receiver with acceptable error rate. CDM/CDMA has been well researched in both optical fibre [29, 34, 35] and free space communication systems [27, 36, 37], and presents some advantages over WDM/WDMA and TDM/TDMA which include improved data security, ease of upgrade and capacity scalability, and simultaneous

51

transmission by all users in overlapping wavelength and time without requirement for a protocol [26, 38, 39]. The initial concern about implementation devices is gradually easing with advances in optical device technology which has made available high performing encoders and decoders such as super structured fibre Bragg gratings (SSFBG) and planer lightwave circuits (PLC) [29]. Similar to TDM/TDMA, CDM/CDMA however does increase the system repetition rate above the average user data rate. In this thesis, only incoherent 1D time encoded CDMA which is easy to realize, cost effective and well suited for intensity modulation/direct detection (IM/DD) system [26] is considered. Highly orthogonal unipolar codes, namely OOC, is used with encoding/decoding performed in the optical domain in Chapter 4 for an indoor system and in Chapter 8 for an outdoor system.

One dimensional unipolar optical encoders and decoders for IM/DD systems could be implemented using optical fibre tapped delay lines [40, 41]. For signal encoding, the optical data pulse is split into a number of arms equal to the code weight (w), with each arm including fibre delay lines corresponding to the periodic delay before the pulse mark chip positions in the code sequence. For example, for code 2 in Fig. 3.3a, the data pulse is split into $w = 3$, with $i_1 T_c$ delay in the 1st arm, $i_2 T_c$ delay in the 2nd arm and $i_w T_c$ delay in the 3rd arm as shown in Fig. 3.4a [40], (where i_1, i_2, and i_w are respectively equal to 0, 2 and 8 for the case illustrated). The delayed pulses in the 3 arms are combined together to obtain a coded data signal of the same sequence as code 2 in Fig. 3.3a. Similarly, optical signal decoding could be performed using a simple correlator at the receiver which includes fibre tapped delay lines with mirrored periodic delays of the code sequence to be detected (see Fig. 3.4b [40]), i.e. as in a simple match filtering process. Recent encoders and decoders are based on FBGs (incorporating a circulator) [42, 43]. In this approach, low reflectivity gratings are written at the chip durations corresponding to the pulse mark chip positions in the code sequence, e.g. at chip positions 1, 3 and 9 for code 2 in Fig. 3.3a. An input signal is only reflected at the period of the grating, thus resulting in the preferred coded signal. At the decoder, the gratings are written in a time-reversed direction to the encoder gratings, producing a mirror of the coded signal.
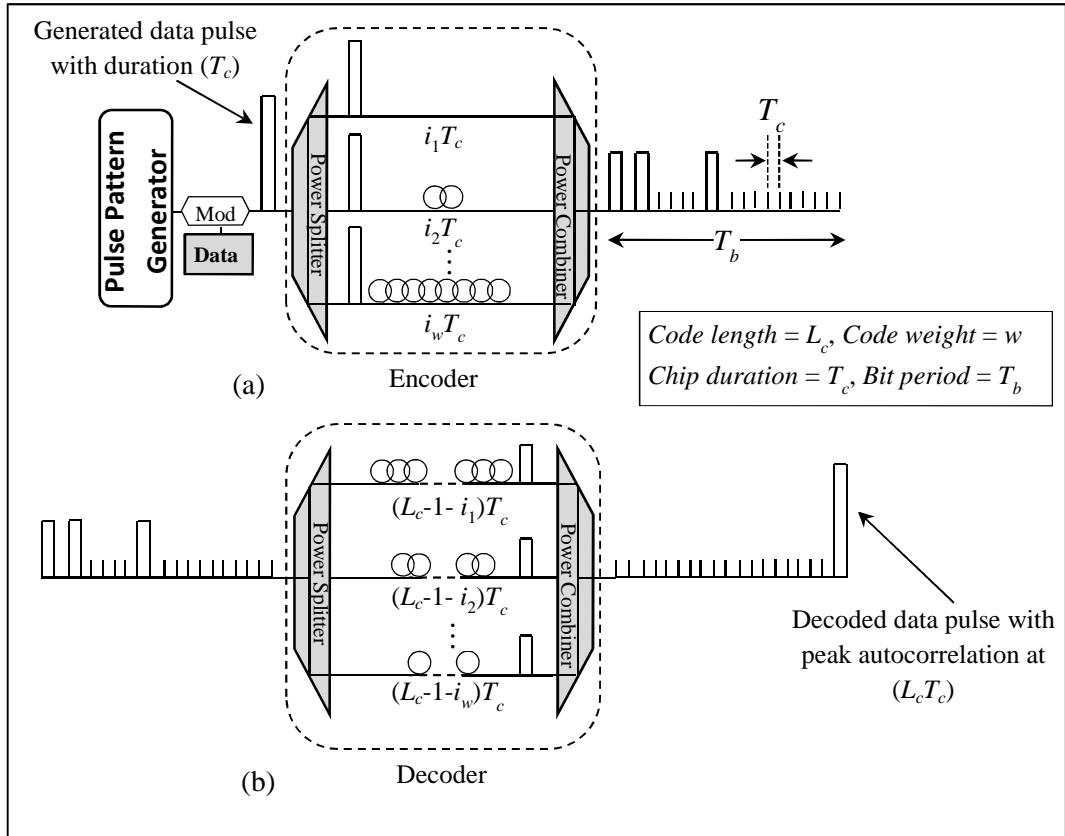
Fig. 3.4 Schematic of unipolar 1D optical CDMA encoder and decoder using fibre tapped delay lines: (a) Encoder and (b) Decoder (adapted from [40])

3.4 Impairments in optical communication

Optical signals propagating in a channel are subject to various forms of channel effects that degrade the signal quality and overall system performance. In addition, different kinds of noise sources are found in the optical communication systems, and they all combine to decrease the signal-to-noise ratio (SNR) of the system. While the severity of these impairments may depend on the transmitter or receiver system, some of them are channel specific and are discussed under optical fibre and FSO channels in the sub-sections below.

3.4.1 Impairments in optical fibre channel

Although light is confined in the core of an optical fibre, several factors affect its propagation through the channel including attenuation, dispersion and other component losses. These limitations generally affect the system data rate and link length.

3.4.1.1 Fibre attenuation and component losses

Attenuation in optical fibre is primarily due to Rayleigh scattering and different absorption mechanisms at different wavelengths. Absorption losses are caused by the interaction of light photons with the particles of the silica glass in the ultraviolet or infrared wavelength regions which result in the loss of photons. Furthermore, the absorption of impurities such as hydrogen or hydroxide ions by the silica glass could increase the fibre attenuating properties at different wavelengths. Rayleigh scattering is a result of some glass particles that are smaller than the wavelength of the optical signal splitting the light in the fibre into different parts in different directions. The overall effects result in loss of transmitted optical power. Imperfections in the manufacturing processes such as random variations in the radius of the fibre core, and both macro and micro bending losses contribute to attenuation in optical fibre [28]. The attenuation in fibre is written as

$$L_f = 10^{(\alpha_f l_f)/10} \tag{3.1}$$

where the fibre attenuation coefficient $\alpha_f \approx 0.2$ dB/km at 1550 nm and l_f is the fibre length. Other passive components including couplers/splitters, connectors and splices also contribute additional (insertion) loss to the optical fibre link. Thus for a long reach transmission over the fibre, optical amplifiers are used to compensate for these losses.

3.4.1.2 Fibre dispersion

Dispersion is the differential broadening of spectrum experienced by different components of light during propagation in a channel such as an optical fibre. Signals in single mode fibre experience only intra-modal dispersion while both intra-modal and inter-modal dispersions occur in multimode fibre. In a single mode fibre (SMF), the effective modal refractive index is a function of angular frequency. Signal pulses propagating in the SMF have a spectrum and thus are made up of different frequency components. These frequencies components travel at different speeds because the refractive index of the mode changes with their angular frequencies. This results in temporal broadening of the pulse and is called group velocity dispersion (GVD). GVD is from two different sources, namely material dispersion and waveguide dispersion. Material dispersion is as a result of change in the refractive index of the fibre core material with respect to

wavelength, which causes light of different frequency components in the same mode to travel at different speeds. Waveguide dispersion is as a result of some part of the light coupled into the cladding of a single mode fibre. Because of the refractive index difference between the fibre core and cladding, the light in the cladding and core travel at different speeds. Dispersion (D) limits the bit rate length product obtainable in an SMF and is estimated as

$$D = -\frac{2\pi c \beta_2}{\lambda^2} \tag{3.2}$$

where c is the speed of light and β_2 is referred to as the GVD parameter. At 1550 nm the high frequency components of the signal travel faster than the low frequency components, resulting in typical values of D ranging from 16 to 20 ps nm^{-1} km^{-1} [7, 28]. Although this value is higher than the value of dispersion at 1300 nm (about 1 ps nm^{-1} km^{-1} [28]), dispersion shifted/flattened single mode fibre (particularly non-zero dispersion shifted fibre [7]) with low dispersion at 1550 nm is available for optical fibre communication at 1550 nm where WDM operation with optical amplifiers (particularly EDFA) is possible. Dispersion shifting/flattening in fibre is realised by adjusting the refractive index profile of the fibre core relative to specific wavelengths, however, in a HFFSO system, the fibre will be typically short enough that we can neglect the impact of fibre dispersion.

3.4.2 Impairments in FSO channel

An outdoor FSO channel is exposed to various forms of impairment due to harsh weather conditions and the turbulent nature of the atmosphere. Optical signals are subjected to heavy attenuation and optical turbulence as a result of varying atmospheric conditions. The effects of optical turbulence include random fluctuations in irradiance and phase of the optical beam (scintillation), random fluctuation in the position of the geometric centre of the beam (beam wandering) and increase in beam spreading [44] as illustrated in Fig. 3.5. Indoor FSO systems (optical wireless systems) are not affected by optical turbulence or changes in atmospheric weather conditions but do experience beam spreading due to signal diffraction. Additionally factors that affect the performance of both outdoor and indoor FSO communication systems are external interferences from other light sources and systems, and physical blockages.
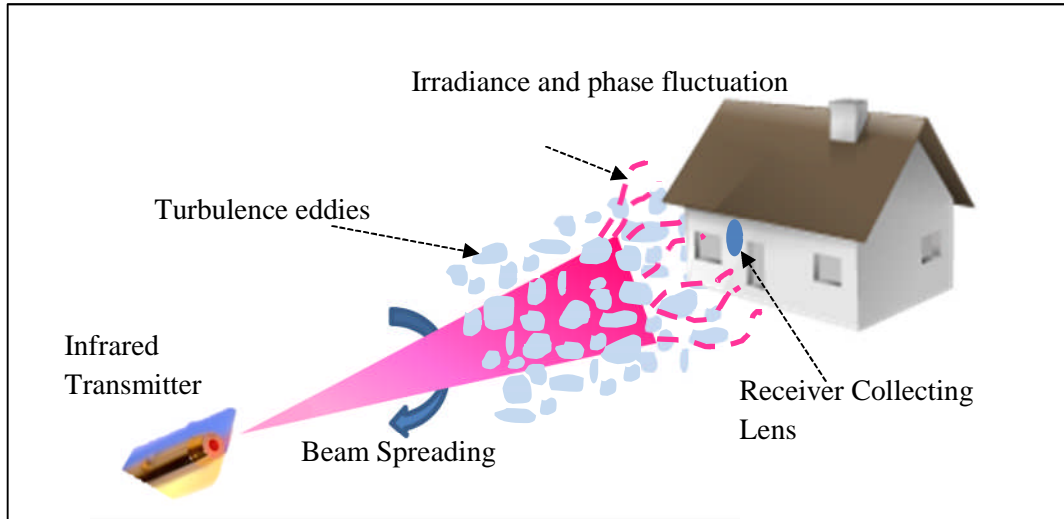
Fig. 3.5 Illustration of turbulence effects in an outdoor FSO channel

3.4.2.1 FSO attenuation

Absorption and scattering are the two factors contributing to attenuation in FSO channels. Both natural and artificial processes result in an abundance of different gaseous molecules including carbon dioxide (CO_2), ozone (O_3) and water vapour (H_2O) in the atmosphere, which interact with and absorb propagating photons at different wavelengths. Because the rate of absorption is dependent on both the concentration of these gases and wavelength, FSO communications are established at wavelengths around 780 - 1550 nm where absorption is relatively low [45, 46]. Scattering however is an unavoidable source of power loss in the atmosphere. The presence of micro and macro particles in the atmosphere leads to different scattering processes which attenuate the optical power of the propagating signal. These micro particles including air molecules and aerosol (dust, haze or fog) contribute to Rayleigh scattering or Mie scattering depending on their sizes and the wavelength of the optical beam. Particle size parameter $x_0 = 2\pi r_n / \lambda$ [47], where r_n is the particle radius. The scattering process by macro particles such as rain, mist or snow are described using the geometry of such particles and the rate of precipitation. The FSO attenuation is written as

$$L_{fs} = 10^{(\alpha_{fso} l_{fso})/10}$$
(3.3)

where α_{fso} is the atmospheric attenuation coefficient (shown in Table 3.2 [48] at 1550 nm) and l_{fso} is the free space link length. Optical amplifiers and power

efficient modulation schemes are necessary to mitigate the attenuating effect of an FSO channel.

Table 3.2 Attenuation coefficient and visibility range at 1550 nm for various atmospheric conditions [48]

Atmospheric condition	Particle size parameter, x_0	Visibility range (m)	Attenuation (dB/km)
Clear air	0.0004	23000	0.2
		10000	0.4
Haze	0.04 – 4.05	4000	2
		2000	4
Fog	4.05 – 81.07	500	34
		200	85
		50	340

3.4.2.2 Optical scintillation

The random fluctuations in signal intensity of an optical beam propagating in the atmosphere which are caused by turbulence are generally referred to as optical scintillation. A common approach used in describing the effect of scintillation along most horizontal paths in the atmosphere is the extended medium model in which the whole range of the signal propagation path is treated as a random medium [44]. Turbulent eddies of varying refractive indices are created in the atmosphere due to constant changes in air temperature over the atmospheric channel [44, 49]. These eddies are of different sizes as explained in the Kolmogorov theory of turbulence [50] and the distortion experienced by a signal propagating in the atmosphere is dependent on the scale size of the turbulent eddies on its path. The small scale eddies (or inner scale of turbulence) are of the size l_0 less than the smaller of the spatial coherence radius of the optical wave ρ_c and the Fresnel zone defined as $\sqrt{l_{fso}/k}$, and have diffractive (scattering) effects on the optical beam which results in beam spreading and irradiance fluctuations [44, 51]. In contrast, the large scale eddies (or outer scale of turbulence) are of the size L_0 greater than the larger of the Fresnel zone and the scattering disk defined as $l_{fso}/k\rho_c$ (where $k = 2\pi/\lambda$ is the optical wave number), and their refractive

(focusing) effect on the optical beam results in fluctuations in phase and drift in the centroid of the beam [44, 51]. Between the least size of the large scale eddies and the largest size of the small scale eddies exist several scale sizes where the medium is considered isotropic and the effect of turbulence on the optical beam is insignificant [44, 51, 52].

The total scintillation index σ_I^2 including the large scale and small scale scintillations is expressed as a function of the variance of the natural logarithm of the irradiance $\sigma_{\ln I}^2$, given as [44]

$$\sigma_I^2 = \exp(\sigma_{\ln I}^2) - 1 \tag{3.4}$$

Equation (3.4) can be written in terms of a turbulence parameter called the Rytov variance σ_R^2 as [44]

$$\sigma_I^2 = \exp\left[\frac{0.49\sigma_R^2}{\left(1+1.11\sigma_R^{12/5}\right)^{7/6}} + \frac{0.51\sigma_R^2}{\left(1+0.69\sigma_R^{12/5}\right)^{5/6}}\right] - 1 \tag{3.5}$$

where $\sigma_R^2 = 1.23 C_n^2 k^{7/6} l_{fso}^{11/6}$ and C_n^2 is the atmospheric refractive index structure constant. The Rytov variance increases with C_n^2 and the FSO link length l_{fso}, and indicates an increasing strength of turbulence. However, it has been shown experimentally [44] that the scintillation index does not always increase with the Rytov variance. The scintillation index as shown in Fig. 3.6 increases with both the C_n^2 and l_{fso} (and consequently σ_R^2) and reaches a maximum (above unity) with the strongest fluctuations at the so called focusing regime where the focusing effect of the outer scale of turbulence near the transmitter completely dominates the scattering effect of the inner scale of turbulence near the receiver [50]. As both or either the C_n^2 and l_{fso} is increased beyond this point, the beam becomes partially coherent with most scale sizes unable to focus the beam, and the scintillation index normalises to unity at the turbulence saturation regime [44, 50].
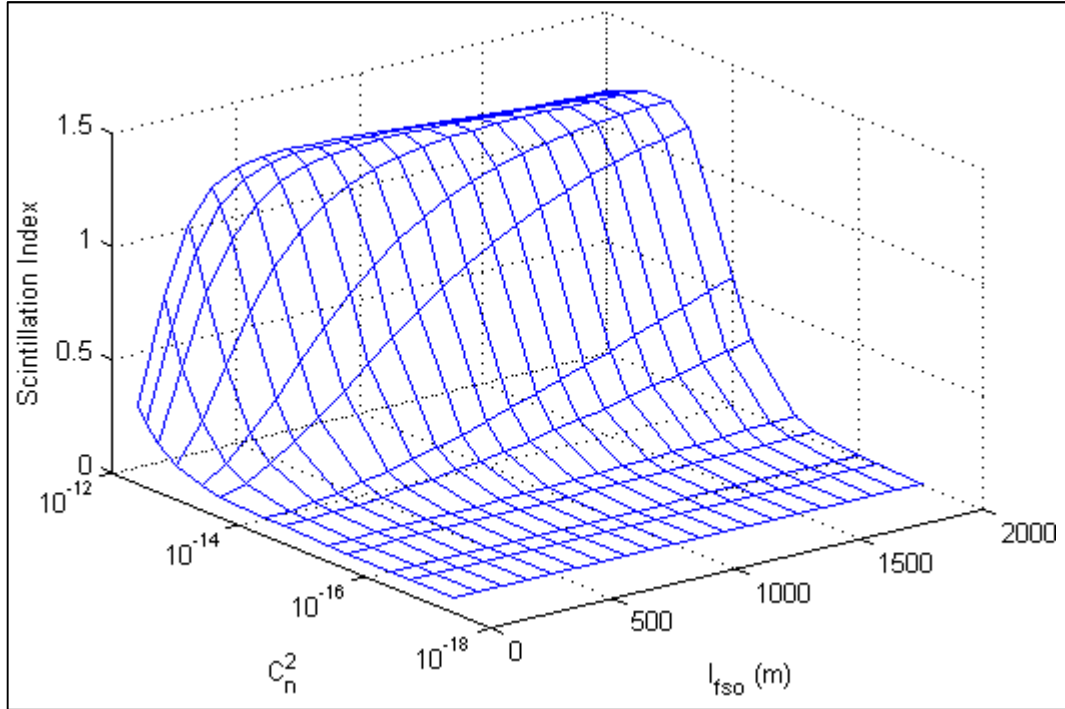
Fig. 3.6 Scintillation index as a function of refractive index structure constant
($C_n{}^2$) and FSO link length (l_{fso}) for a point source receiver.

3.4.2.3 Atmospheric turbulence modelling

Some of the probability distribution functions (pdfs) used to describe the irradiance fluctuations by atmospheric turbulence include the lognormal (LN), modified Rician, lognormally modulated Rician or Beckmann's, lognormally modulated exponential, negative exponential (NE), gamma-gamma (GG) and K or I-K distributions [44, 50, 53-56]. Among all these pdf models, the gamma-gamma distribution is the most popular model because it may be written in a close form expression that is directly related to turbulence parameters describing the number of eddies of different sizes involved in the scattering processes, is closely fitted to experimentally obtained turbulence pdf's, and could be used to describe a wide range of turbulence effects from weak regime to strong regime [44, 50, 54]. The cumulative distribution function (cdf) of the gamma-gamma distribution is sometimes used for the turbulence modelling instead of the pdf, in which case the generalised hypergeometric function [44] or the Meijer G-function [57, 58] is utilised. The lognormal distribution model is also common because of ease of computation and finds more use in the weak turbulence regime where the turbulence pdf gets narrower and complex approximations are required for the gamma-gamma distribution, whereas the K and NE distributions are generally

59

applied in the modelling of strong and saturated turbulence regimes respectively [44, 56]. The effect of irradiance fluctuations in this thesis is covered using mainly the gamma-gamma distribution model fully developed by Andrews and Phillips in [44], with the lognormal distribution used for comparison purposes where necessary.

Gamma-Gamma distribution model

The gamma-gamma distribution model was developed by considering the irradiance fluctuations due to the large scale and small scale size eddies as two gamma distributions. The normalised optical field irradiance I could be written in terms the component irradiance fluctuations contributed by both scale sizes as

$$I = \frac{I_{inst}}{\langle I \rangle} = I_s I_l \tag{3.6}$$

where I_{inst} is the instantaneous irradiance of the optical wave, $\langle I \rangle$ is an ensemble average of the irradiance of the optical wave, while I_s and I_l are small scale and large scale irradiance fluctuations respectively, and each represented by a gamma distribution [53]

$$p_s(I_s) = \frac{\alpha(\alpha I_s)^{\alpha-1}}{\Gamma(\alpha)} \exp(-\alpha I_s), \qquad \alpha > 0, I_s > 0, \tag{3.7}$$

$$p_l(I_l) = \frac{\beta(\beta I_l)^{\beta-1}}{\Gamma(\beta)} \exp(-\beta I_l), \qquad \beta > 0, \ I_l > 0, \tag{3.8}$$

where α and β are the effective numbers of large-scale and small-scale eddies of the scattering process respectively and $\Gamma(\bullet)$ is the gamma function. By transformation of random variables using eq. (3.6), eq. (3.8) can be written as a different pdf conditional on I_s as

$$p_l(I|I_s) = \frac{\beta\left(\beta\dfrac{I}{I_s}\right)^{\beta-1}}{I_s\Gamma(\beta)} \exp\left(-\beta\frac{I}{I_s}\right), \qquad I > 0, \tag{3.9}$$

The conditionality is removed to obtain a gamma-gamma (GG) pdf by averaging eq. (3.9) over eq. (3.7), thus [44, 52, 53]

$$
\begin{aligned}
p_{GG}(I) &= \int_0^\infty p_l(I|I_s) p_s(I_s) dI_s \\
&= \frac{2(\alpha\beta)^{(\alpha+\beta)/2}}{\Gamma(\alpha)\Gamma(\beta)} I^{\frac{(\alpha+\beta)}{2}-1} K_{\alpha-\beta}\left(2\sqrt{\alpha\beta I}\right), \qquad I > 0,
\end{aligned}
\tag{3.10}
$$

where $K_n(\bullet)$ represents the modified Bessel function of the second kind, order n.

Aperture averaging

Among the numerous techniques proposed for the mitigation of turbulence effects which include aperture averaging (AA) [54, 59, 60], diversity systems [61] and wave front reconstruction [62], aperture averaging presents the simplest and most cost effective option applicable to direct detection systems. The basic idea in aperture averaging is to increase the receiving aperture above the cell size of the turbulent eddies responsible for irradiance fluctuations so that such fluctuations are averaged out over a large receiver aperture [54, 59, 60]. Practically, most fluctuations produced by the large scale eddies (which could be up to few meters in size [52]) are not averaged out as there is a limitation to the physical size of the collecting lens or receiver that could be used in a system [63]. The scintillation is however reduced as most fluctuations produced by small scale eddies are averaged out.

In an aperture averaged FSO system, the parameters α and β for a plane wave are given as [44, 60, 64]

$$\alpha = \left\{ \exp\left[\frac{0.49\sigma_R^2}{\left(1+0.65d^2+1.11\sigma_R^{12/5}\right)^{7/6}} \right] - 1 \right\}^{-1} \tag{3.11}$$

$$\beta = \left\{ \exp\left[\frac{0.51\sigma_R^2\left(1+0.69\sigma_R^{12/5}\right)^{-5/6}}{1+0.90d^2+0.62d^2\sigma_R^{12/5}} \right] - 1 \right\}^{-1} \tag{3.12}$$

where $d = \sqrt{kD_{RX}^2/4l_{fso}}$ is the normalised radius of the collecting lens (CL) aperture, D_{RX} is the CL aperture diameter and $\sigma_R^2 < 1$ for weak turbulence, $\sigma_R^2 \approx 1$ for moderate turbulence, $\sigma_R^2 > 1$ for strong turbulence and $\sigma_R^2 \to \infty$ for saturated turbulence. The GG pdf model of weak to strong turbulence with and without aperture averaging is shown in Fig. 3.7.

Lognormal distribution model

The lognormal distribution model is based on the logarithm amplitude of the optical field (derived from the first-order Rytov approximation) which indicates that the logarithm irradiance of the optical field follows a normal distribution [44, 65]. The log amplitude fluctuation of the optical field is written as [52]

$$X - E[X] = \frac{\ln(I/I_0)}{2} \tag{3.13}$$

where $E[X] = \langle X \rangle$ is the ensemble average of the log amplitude, I is the irradiance of the optical field and I_0 is the turbulence free irradiance. A normal distribution of the log amplitude fluctuations with variance σ_X^2 is written as

$$p_X(X) = \frac{1}{\sqrt{(2\pi\sigma_X^2)}} \exp\left\{-\frac{(X - E[X])^2}{2\sigma_X^2}\right\} \qquad (3.14)$$

It could be straightforwardly shown that $dX/dI = 1/2I$ from eq. (3.13). By substituting eq. (3.13) into eq. (3.14), and performing variable transformation, the lognormal distribution of the fluctuating irradiance is written as

$$P_{LN}(I) = p_X(X)\frac{1}{2I} = \frac{1}{I\sqrt{(8\pi\sigma_X^2)}} \exp\left\{-\frac{\left(\frac{1}{2}\ln\left(\frac{I}{I_0}\right)\right)^2}{2\sigma_X^2}\right\} \qquad (3.15)$$

Under weak fluctuation conditions $\sigma_{\ln I}^2 \approx 4\sigma_X^2$ [44], and from eq. (3.13) $\langle I \rangle = I_0 \exp(2\sigma_X^2)$ [52], thus eq. (3.15) can be written as

$$P_{LN}(I) = \frac{1}{I\sqrt{(2\pi\sigma_{\ln I}^2)}} \exp\left\{-\frac{\left[\ln\left(\frac{I}{\langle I \rangle}\right) + \frac{\sigma_{\ln I}^2}{2}\right]^2}{2\sigma_{\ln I}^2}\right\}, \qquad I > 0 \qquad (3.16)$$

The LN pdf model of weak to strong turbulence with and without aperture averaging is shown in Fig. 3.7. As seen in Fig. 3.7a, the LN pdf is closely fitted to the GG pdf in weak fluctuation conditions although some difference may exist in the pdf tails. The pdfs become narrower as the turbulence weakens. With increasing σ_R^2 and turbulence as shown in Fig. 3.7b, discrepancies are seen between the GG and LN pdfs. This result is in agreement with already established experimental and analytical results in the literature which confirms that the LN pdf model is accurate for weak turbulence regime alone [44, 54]. In Fig. 3.7b, the pdfs are skewed to the left, with higher degree of skewness indicating the strength of turbulence. Comparing Figs. 3.7b, 3.7c and 3.7d, the effect of aperture averaging (AA) could be seen as the pdfs without AA (indicating more turbulence effect) are more skewed to the left than the pdfs with AA, with the difference becoming clearer in Fig. 3.7d where a larger aperture with RCL diameter of 50 mm have been used.
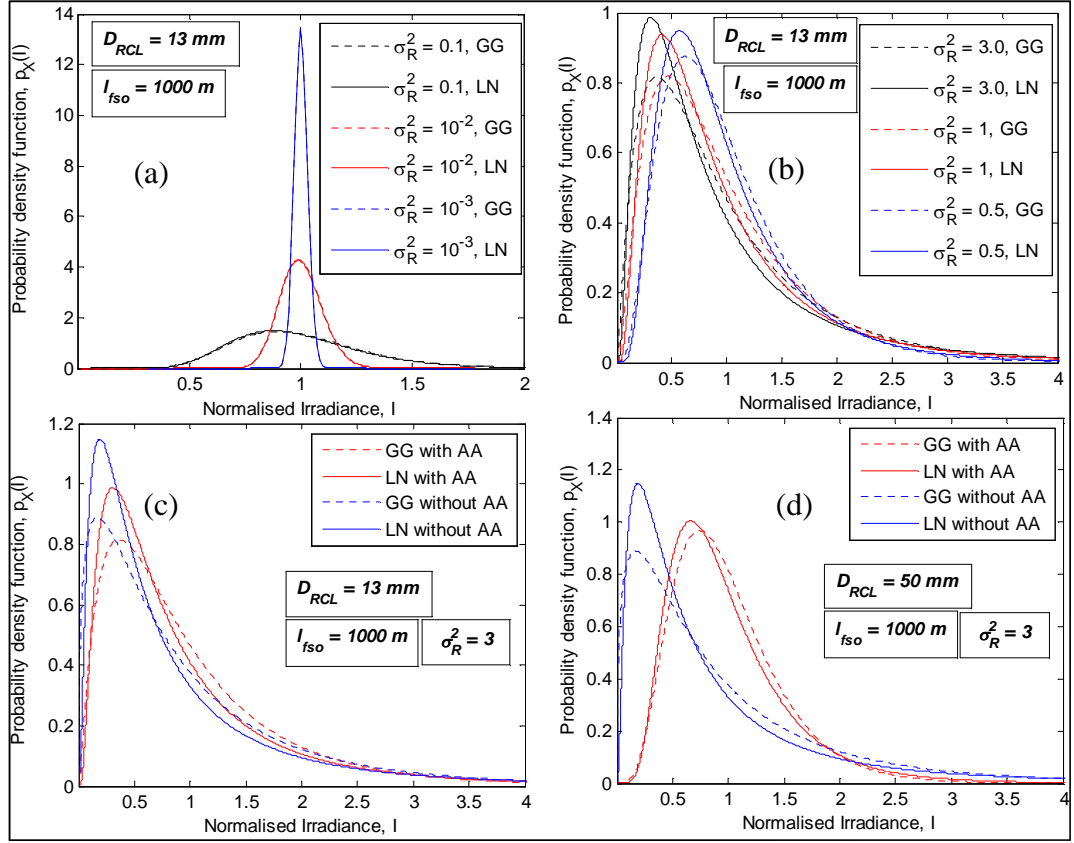
Fig. 3.7 pdf of irradiance fluctuations as a function of normalised irradiance using the GG and LN model, (a) weak turbulence regime only with AA, (b) weak to strong turbulence regimes with AA, (c) strong turbulence with AA (RCL diameter = 13 mm) and without AA and (d) strong turbulence with AA (RCL diameter = 50 mm) and without AA

3.4.2.4 Beam spreading

An optical beam propagating in a free space channel is affected by diffraction limited divergence described by the beam divergence angle (φ_{TX}), transmitter aperture diameter (D_{TX}) and the propagation distance [49, 64]. The beam spot size or diameter d_l after a distance l_{fso} due to diffraction is written as [49]

$$d_l = D_{TX} + (\varphi_{TX} l_{fso}) \tag{3.17}$$

The presence of atmospheric turbulence along the path of the beam, causes the beam to spreads more than the diffraction limited divergence [44] as illustrated in Fig. 3.5. The total spot size of the beam is written as [44, 66]

$$D_e = d_l \left[1+1.33\sigma_R^2 \left(\frac{2l_{fso}}{k(d_l/2)^2}\right)^{5/6}\right]^{1/2}$$ (3.18)

For a receiver using a collecting lens with diameter larger than the D_e, the entire beam could still be collected assuming the centroid of the beam corresponds with the optical axis of the lens. However as discussed in Chapter 2, there is a practical limitation on the size of the receiver collecting lens (RCL) and a beam spreading loss is incurred at the receiver. For an RCL of diameter D_{RX}, this loss (in dB) is written as [49, 64]

$$L_{bs} = 20\log_{10}\left(\frac{D_{RX}}{D_e}\right)$$ (3.19)

3.4.2.5 Coupling loss

Similar to the insertion losses experienced in fibre systems, FSO signals incur coupling losses when being coupled to a different medium at various interfaces. In a HFFSO system, such losses are experienced at FSO-to-fibre interfaces either at the receiver end or at the remote node. For a laser signal propagating through the atmosphere, turbulence induced fluctuations in its phase affect the coherence of the signal and leads to a mismatch between the field of the beam and the back propagated fibre mode field. As a result, the optical signal collected at the lens is coupled into the fibre at a coupling efficiency [67]

$$\eta_c = 8a^2 \int_0^1 \int_0^1 \left(\exp\left[-\left(a^2 + \frac{A_{RX}}{A_c}\right)(x_1^2 + x_2^2)\right] I_0\left(2\frac{A_{RX}}{A_c}x_1 x_2\right)x_1 x_2\right)dx_1 dx_2$$ (3.20)

where $a = \pi W_f D_{RX}/2f\lambda$ is the coupling geometry parameter, expressed as the ratio of the RCL radius to the back-propagated fibre mode radius, and optimum for a fully coherent incident plane wave in the absence of turbulence [68], $A_{RX} = \pi D_{RX}^2/4$ is the RCL area, $A_c = \pi\rho_c^2$ is the spatial coherence area of the incident optical wave, with radius $\rho_c = (1.46C_n^2 k^2 l_{fso})^{-3/5}$, $I_0(\bullet)$ is a modified Bessel function of the first kind, order zero.

3.4.2.6 Other FSO impairments

So far, we have discussed only FSO impairments that are due to the inherent nature of the atmosphere. Physical obstacles (such as low flying objects and birds,

high rising buildings and mountainous terrains), and external interferences from background ambient signals can be problematic to the propagation of an optical signals in the atmosphere. Additionally, thermal expansion and small movements of buildings caused by high velocity winds, vibrations by heavy machinery and minor earthquakes can increase misalignment and pointing errors above that originally caused by beam wandering [44, 49, 69]. The challenges posed by physical obstacles are mitigated by adequate link path planning during installations, but for FSO links greater than about 100 m range, an automatic pointing, acquisition and tracking (PAT) sub-system is required to mitigate pointing and tracking errors [49, 70, 71]. The PAT subsystem optimises the divergence angle of the transmitted optical beam, and utilises multiple lenses of varying properties in adjustable positions to focus or expand the beam, while maintaining an alignment between the transmitter and receiver optical axis. Automation is implemented with the aid of micro-electromechanical system (MEMS), stepping motor system or mechanical gimbals [70, 72]. The effect of background ambient light which, when unchecked, degrades the performance of the system as shot noise is discussed in the next sub-section.

3.4.3 Optical system interference and noises

Interference and noise in an optical system can combine with the signal at various stages of transmission, and they all compound to degrade the performance of the receiver. The presence of noise during signal reception leads to erroneous decisions in the receiver and increases the bit error rate (BER) of the system. Generally, there is an acceptable optical signal-to-noise ratio (OSNR) corresponding to targeted BER performance of an optical communication systems. Typically, most systems are designed to provide OSNR of about 20 dB at the receiver [1], with the ASE noise power calculated using a standard bandwidth (B_{OSNR}) over which the ASE PSD N_o is approximately constant (often, 0.1 nm is used for 1550 nm wavelength region). Shot noise is inherent with the signal and thermal noise originates due to various components at the receiver. Other interference and noises, such as ASE noise, crosstalk and interference from multiple access and background ambient signal originate outside the receiver circuitry [28].

3.4.3.1 Thermal noise

The random movement of thermally excited electrons flowing through resistive elements in the receiver circuitry generates a thermal noise signal. Sources of thermal noise in the receiver include photodetector electrodes and resistors used for coupling, feedback and post amplification. Thermal noise is also called Nyquist noise or Johnson noise and is signal independent, statistically described as a Gaussian process with zero mean. The variance of the thermal noise current with power in a single sided spectral density is given as [1, 7]

$$\sigma_{th}^2 = \left(\frac{4K_B T}{R_L}\right) F_n B_e \tag{3.21}$$

where K_B is Boltzmann constant, $K_B = 1.38 \times 10^{-23}$ J/K, T is absolute temperature in Kelvins, R_L is the receiver load resistance, F_n is the noise figure of the electrical amplifier and B_e is the electrical noise equivalent bandwidth of the receiver.

3.4.3.2 Shot noise

Shot noise is the result of inherent fluctuations in the flow of photoelectrons which are randomly distributed during photodetection. These fluctuations also exist in the flow of photons and are transferred to shot noise current by photoelectric effects. Shot noise is described by the Poisson distribution, but is usually approximated as Gaussian for large values of the mean [28]. The variance of the shot noise current for a receiver with PIN photodetector is written as

$$\sigma_{sh}^2 = 2qiB_e \tag{3.22}$$

where the average generated photocurrent by the photodetector $i = RP$ for receiver without an optical preamplifier and $i = RGP$ for an optical preamplifier receiver. P is the optical power incident on the photodetector, G is the optical amplifier gain and R is the photodetector responsivity.

For a receiver with an APD, the shot noise current variance is written as [7]

$$\sigma_{sh}^2 = 2qM_A^2 F(M_A)RPB_e \tag{3.23}$$

where $F(M_A) = k_A M_A + (1 - k_A)(2 - 1/M_A)$ is the excess noise of the APD, M_A is the APD multiplicative factor or gain and k_A is the ionization coefficient relating the ionization rates of holes and electrons in the APD material and ranges between 0 and 1 [28].

3.4.3.3 Amplified spontaneous emission noise

The generation of amplified spontaneous emission during optical amplification was discussed in Chapter 2 and the single-sided power spectral density of the total ASE noise was written as eq. (2.4) which relates the spontaneous emission parameter n_{sp} to the optical amplifier gain G. The amplifier noise is described in terms of its noise figure NF which also relates to n_{sp} and G as

$$NF = \frac{SNR_{in}}{SNR_{out}} = 2n_{sp}\left(\frac{G-1}{G}\right) + \frac{1}{G} \qquad (3.24)$$

where, for $G \gg 1$, $NF \approx 2n_{sp}$, and $N_o = \frac{1}{2}NF(G-1)h\upsilon$. The ASE noise accompanies the signal to the receiver where photocurrent is generated by square law detection. Considering a receiver with a PIN photodetector, the resulting photocurrent is given as

$$i(t) = R\overline{\left(E_{\text{sig}}(t) + E_{\text{spe}}(t)\right)^2} = R\overline{\left(\left[E_{\text{sig}}(t)\right]^2 + 2E_{\text{sig}}(t)E_{\text{spe}}(t) + \left[E_{\text{spe}}(t)\right]^2\right)} \qquad (3.25)$$

where the bar above the equation means time averaging, and both $E_{\text{sig}}(t)$ and $E_{\text{spe}}(t)$ are the signal and spontaneous emission optical fields (defined in units of $\sqrt{W}$ for direct relationship to signal and noise power in watts). As shown in eq. (3.25), squaring the sum of two input waves (signal and ASE) at different frequencies generates two noise components due to the signal beating with the ASE (second term on the right hand side (RHS) of eq. (3.25)) and the ASE beating with itself (last term on the right hand side (RHS) of eq. (3.25)). Thus the optical amplifier is responsible for three noise components (including the shot noise generated by the ASE direct current) namely ASE shot noise, signal-spontaneous beat noise and spontaneous-spontaneous beat noise which can respectively be written as [16, 73, 74]

$$\sigma_{\text{sh,ASE}}^2 = 2m_t qRN_o B_o B_e \qquad (3.26)$$

$$\sigma_{\text{sig-sp}}^2 = 4R^2 N_o PB_e \qquad (3.27)$$

$$\sigma_{\text{sp-sp}}^2 = 2m_t R^2 N_o^2 B_o B_e\left(1 - \frac{B_e}{2B_o}\right) \qquad (3.28)$$

where B_o is the bandwidth of the OBPF and the number of polarisation states of ASE noise is m_t. For linear optical amplifiers, the amplitude of the ASE field is

considered Gaussian in the optical domain [74], but the beat noises are non-Gaussian and are best described by non-central chi-square statistics [16].

3.4.3.4 Linear optical crosstalk

Optical crosstalk occurs in a WDM system when signals of different wavelength division from the desired signal are received along with the desired signal. It could also arise from signals of the same wavelength with the desired signal, but from different optical source and/or different propagation path, being received along with the desired signal. Different kinds of crosstalk that can occur in a WDM system are shown in Fig. 3.8. In a WDM or DWDM system, the wavelength spacing is in the range of 25 GHz – 200 GHz on the ITU-T grid [75, 76]. Crosstalk that results from a signal of entirely different wavelength on the ITU-T grid being received along with the desired signal is referred to as interchannel crosstalk while the crosstalk caused by a signal of the same ITU-T wavelength with the desired user is called intrachannel or co-channel crosstalk. Interchannel crosstalk is independent of the signal polarisation while intrachannel crosstalk is polarisation dependent (in which case, to perform worst case calculations, the crosstalk is usually assumed to be polarisation aligned with the desired signal). When the intrachannel crosstalk signal originates from the same source as the desired signal but propagated through a different path, it is referred to as co-channel homodyne, while intrachannel crosstalk that originates from a different source as the desired signal is called co-channel heterodyne. Depending on whether the time delay between the crosstalk signal and the desired signal is less than or greater than the coherence time of the optical source, co-channel homodyne crosstalk is termed phase correlated or phase uncorrelated. Non-linear crosstalk also occurs in WDM systems and is caused by non-linear effects such as cross-phase modulation (XPM) and four-wave mixing (FWM) [7].
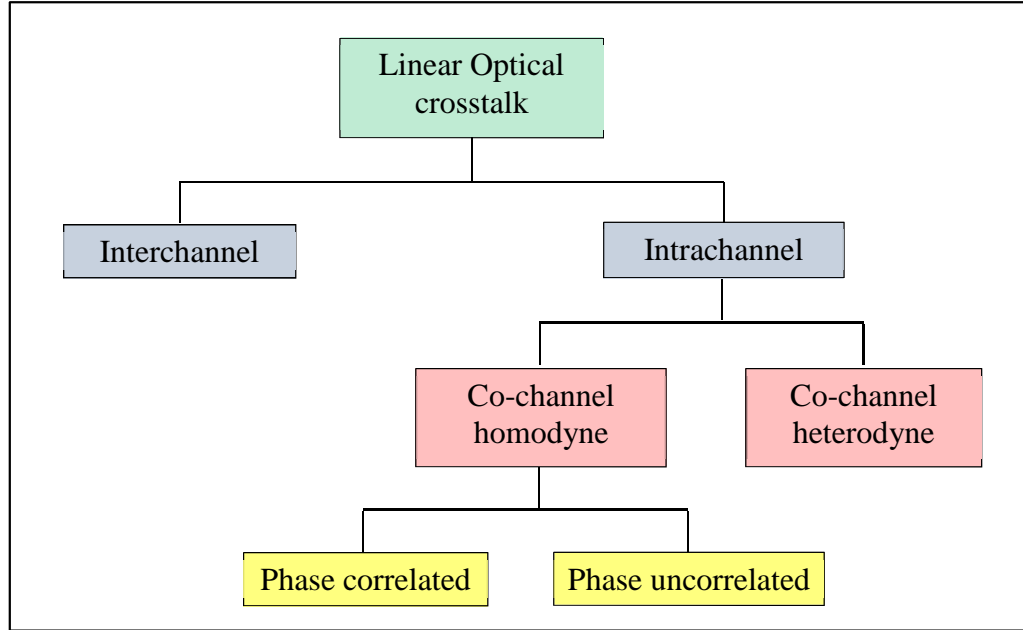
Fig. 3.8 Types of linear crosstalk in a WDM system

Crosstalk consideration is also based on square law detection. Both the signal and crosstalk optical fields can be written as

$$E_{\text{sig}}(t) = (2P_s(t))^{1/2} \cos(\omega_s t + \phi_s) \tag{3.29}$$

$$E_{\text{int}}(t) = (2P_i(t))^{1/2} \cos(\omega_i t + \phi_i) \tag{3.30}$$

where P_s and P_i, ω_s and ω_i, ϕ_s and ϕ_i, are the signal and crosstalk optical powers, optical frequencies, and phases respectively. By replacing the spontaneous emission optical field in eq. (3.25) with the crosstalk optical field $E_{\text{int}}(t)$, and substituting eqs. (3.29) and (3.30) in eq. (3.25), we can write

$$i(t) = R\left[P_s(t) + P_i(t) + 2(P_s(t)P_i(t))^{1/2} \cos((\omega_s - \omega_i)t + \phi_s - \phi_i) \right] \tag{3.31}$$

where terms that are twice the optical frequencies have averaged to zero. Equation (3.31) represents the exact photocurrent that is incident on the decision device at the receiver in the case of co-channel heterodyne, while for a co-channel homodyne the angular frequency part of the cosine term equals zero ($\omega_s = \omega_i$). In the case of interchannel crosstalk, the electrical filter (which has a smaller bandwidth than the beat term) prevents the beat frequency from reaching the decision device leaving only the first two terms in eq. (3.31).

69

3.4.3.5 Multiple access interference

Multiple access interference (MAI) is a limiting factor in the performance of CDMA systems. MAI can be likened to co-channel crosstalk in WDM systems because it arises from interfering signals of the same nominal wavelength as the desired user but of different optical orthogonal code (OOC). The interfering signals may be from the same laser source or not and may have propagated through the same path with the desired user or not.

Consider Fig. 3.3a for an OOK system and assume that the desired user is assigned Code 1 while two other users (interferers) are each assigned Code 2 or Code 3. In the absence of noise and any other impairment, if both interferers have transmitted a data 1, the time waveform of the signal pulse train at the desired user's decision device (e.g. a correlator) is shown in Fig. 3.9a and Fig. 3.9b for when the desired user transmitted data 1 and data 0 respectively (assuming the bits are synchronised). The correlator sample chips 1, 4 and 11 which are the pulse mark chip positions of the desired user and with the threshold set equal to the code weight, correct decisions are made for both data 1 and 0 irrespective of the MAI. However in realistic systems noise or other impairments are capable of introducing additional pulses or attenuating the intensity of existing pulses, thus leading to errors.
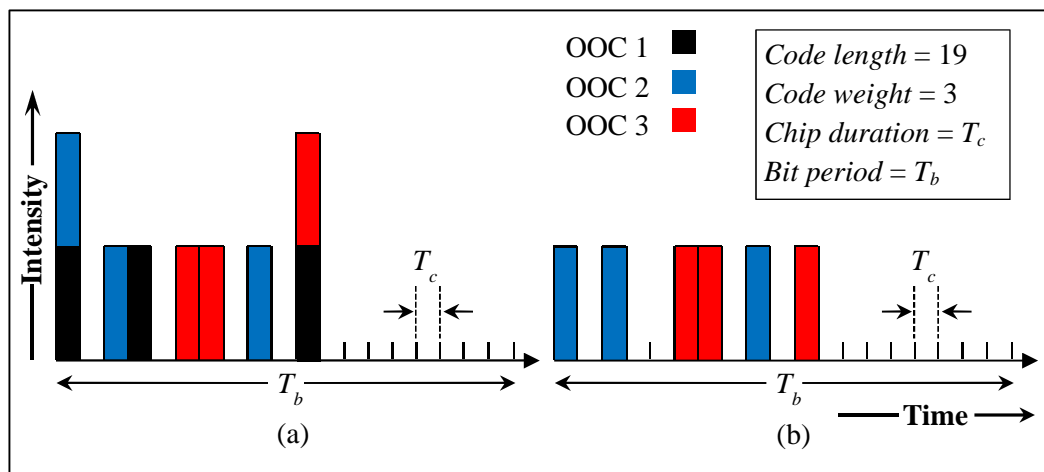
Fig. 3.9 Illustration of signal reception in the presence of multiple access interference in an OOK CDMA system, desired user transmitting with OOC 1: (a) desired user transmitted data 1 (b) desired user transmitted data 0

For a DPPM CDMA system, MAI could occur whether the interferer's transmitted data is 0 or 1. Using the same code parameters that were exemplified in Fig. 3.3b and assuming that the desired user is assigned Code 1, the time waveforms of a binary DPPM system where the desired user and the interferers have transmitted the same data are shown in Fig. 3.10a for data 0 and Fig. 3.10c for data 1. The integrate and compare circuitry integrates the contents of the desired users pulse mark chip positions (chips 1, 4 and 11) in the two slots and compare the output of both slots to decide which slot bears the signal pulse. For Figs. 3.10a and 3.10c, the comparison is between 5 pulses and 0 pulses in the absence of noise and other impairments. In Fig. 3.10b the desired user transmitted data 0 and the interferers transmitted data 1 while in Fig. 3.10d, the desired user transmitted data 1 and the interferers transmitted data 0. In this case, the comparison is between 3 pulses and 2 pulses in the absence of any other impairments or noise. Similar to the OOK system, error due to MAI does not occur in all the cases when there is no noise or other sources of system impairments.
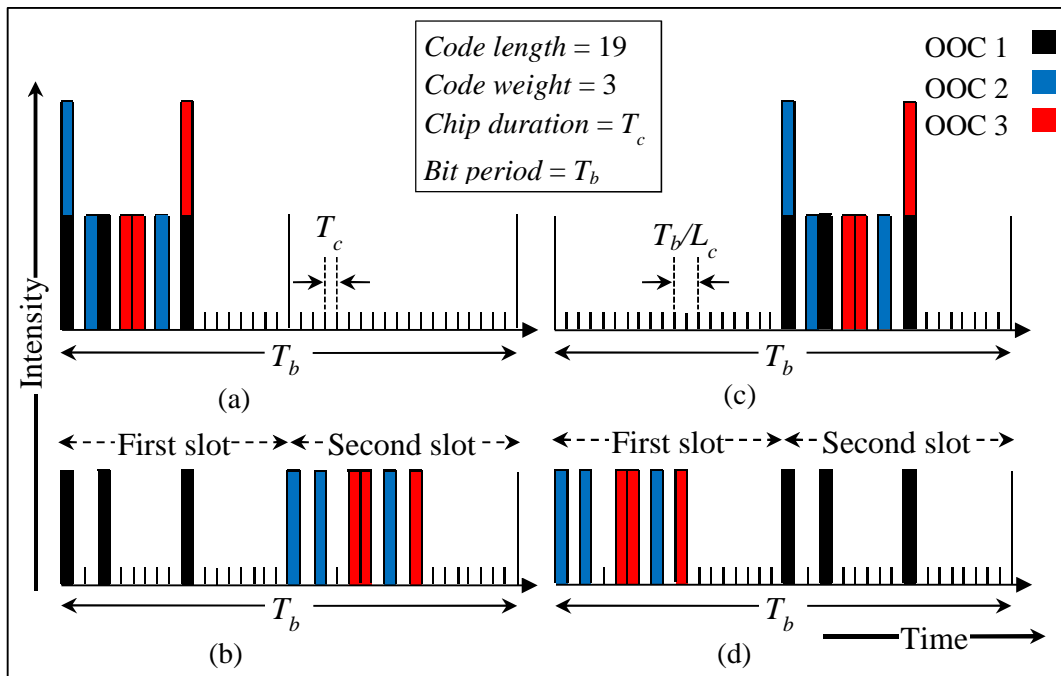
Fig. 3.10 Illustration of signal reception in the presence of multiple access interference in a binary ($M = 1$) DPPM CDMA system, desired user transmitting with OOC 1: (a) and (b) desired user transmitted data 0, (c) and (d) desired user transmitted data 1

71

The illustrations in Figs. 3.9 and 3.10 are for cases where all the users in the network are active. However, in a realistic system, some users may be inactive, and the exact number of users contributing MAI is a random variable. Additionally, all the interferers may not transmit the same data. For an OOK CDMA system, there is no MAI impact when an interferer transmits data 0 (which in an ideal case means that the transmitter is off), so the analysis assumes that all active interferers transmit data 1. However, for a DPPM CDMA system, the transmitter is not off for data 0 transmission, but rather sends pulses in the pulse mark chip positions of the slot corresponding to data 0 for the particular user. Although some DPPM CDMA analysis [37, 77, 78] does not consider cases where the interferers transmit in the same slot as the desired user, e.g. in Figs. 3.10a and 3.10c, such approach simplifies the BER calculations and results in upper bound on the BER, but the DPPM CDMA analyses that will be performed in Chapters 4 and 8 consider all the cases and are thus more detailed.

Cross correlation and auto correlation constraints

The degree of similarity between two different codes is specified by the cross-correlation between the two codes, while the auto-correlation specifies the degree of similarity between the same codes. OOCs are designed so that there is a minimum cross-correlation between different codes, minimum auto-correlation between a code and its delayed copy, and maximum auto-correlation between a code and its exact copy. Considering Fig. 3.3, the maximum cross-correlation γ_c between two different codes and maximum auto-correlation γ_a between each code and its shifted version are both equal to one, and since there are only two interferers, a maximum of two pulses can contribute to the pulse mark chip positions of the desired user as MAI, thus it is easier for decision to be made at the receiver (e.g. in Figs. 3.9 and 3.10), by setting the threshold equal to 3 (i.e. the code weight). For a CDMA system that is not properly designed, high values of γ_c, γ_a and number of users would greatly increase the impact of MAI and limit the system performance.

For cross correlational values $z = \{1, 2, \dots, \gamma_c\}$ between the desired user's OOC and an interferer's OOC, if corresponding probabilities of MAI between the two OOCs for each cross correlational values is defined as $p'_z = \{p'_1, p'_2, \dots, p'_{\gamma_c}\}$, with p'_1 as the probability that only a single pulse of the interfering user's OOC

coincides with the pulse chip positions of the desired user's OOC, $p_2^{'}$ as the probability that only two pulses of the interfering user's OOC coincide with the pulse chip positions of the desired user's OOC and $p_{\gamma_c}^{'}$ as the probability that only γ_c pulses of the interfering user's OOC coincide with the pulse chip positions of the desired user's OOC, then generally, one can write that the interference probability between the interfering user's OOC and the desired user's OOC is [79, 80]

$$P_I = \sum_{z=1}^{\gamma_c} z\, p_z = p_1 + 2p_2 + ... + \gamma_c p_{\gamma_c} \tag{3.32}$$

where $p_z = p_z^{'}\left(\dfrac{w!}{z!(w-z)!}\right)$ is the total probability of interference for each cross correlational values, considering all the combinations of the interferer's pulses coinciding with the pulse chip positions of the desired user's OOC. Equation (3.32) shows that for code words designed with specific γ_c, interferences could practically occur with cross-correlation values $\leq \gamma_c$ and a consideration of the exact performance of the system using eq. (3.32) requires prior knowledge of all the code words in the OOC family used in the system, which seems unfeasible [81]. In addition, such analysis is specific to the particular code family used and may not be generally applied to systems using a different OOC. A straight forward approach that results in an upper bound for the system performance and is assumed in Chapters 4 and 8 of this thesis is to set $p_z = 0$ for $1 \leq z \leq \gamma_c - 1$ and $p_{\gamma_c} \neq 0$ [79-81]. In that case, eq. (3.32) reduces to $P_I = \gamma_c p_{\gamma_c}$. Since there are only w pulse mark chip positions out of L_c chip positions in each OOC, two OOCs can interfere with each other in w^2/L_c ways and $P_I = \gamma_c p_{\gamma_c} = w^2/L_c$. For OOK CDMA, $p_{\gamma_c} = w^2/2\gamma_c L_c$, with the factor of 1/2 representing the probability of transmitting data 1 or data 0.

3.4.3.6 Background ambient light

Background ambient radiation from artificial sources such as lamps, fluorescent tubes and LEDs used for illumination, and natural sources such as the sun, can couple into FSO systems and overload the receiver. The ambient light turns into shot noise at the receiver which can be written as

$$\sigma_{sh,A}^2 = 2qRP_b B_e \tag{3.33}$$

where P_b is the background ambient light power incident on the photodetector. In outdoor systems, the major source of ambient light is from the sun. A proper link layout is required to ensure that the transceiver is not mounted directly facing the sun or other light source. For indoor systems, the ambient light from the sun is mostly diffused but the presence of incandescent lamps and other lighting fittings contribute to additional background ambient light. In some cases where a preamplifier has been used, the ambient light could be amplified with the signal, thus exacerbating its impact. The spectrum of the background ambient light produced by the sun, fluorescent and incandescent lamps are shown in Fig. 3.11 [14]. The radiation from the sun is low at 1550 nm compared to the visible light wavelengths, but incandescent lamps emits the highest radiation at 1550 nm and should be a source of concern for indoor systems. However, LEDs are replacing incandescent lamps as lighting fittings in many homes and offices and they emit less ambient radiation in comparison [47]. In most FSO systems, an OBPF is placed before the receiver to reduce the ambient light reaching the receiver.
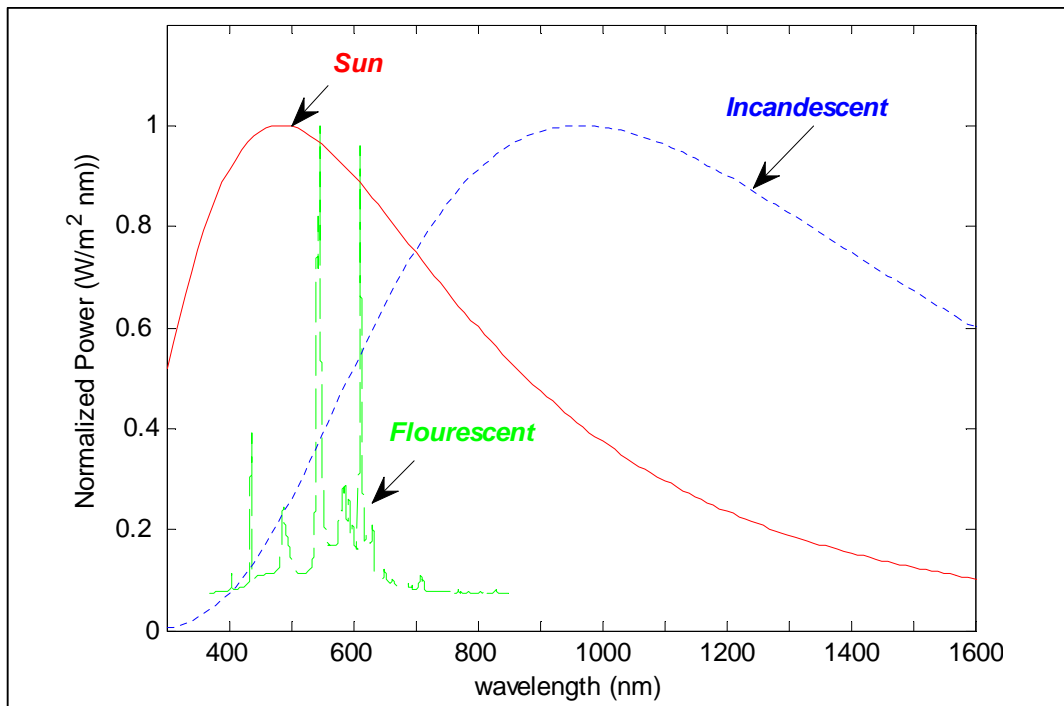
Fig. 3.11 Background ambient light spectrum for different sources (adapted from [14])

3.5 Performance evaluation methods

In the presence of noise and other impairments the performance of an optical communication system is degraded. The predictability of the behaviour of the system under such conditions is dependent on a good understanding of both the signal and the statistics that describe the noise processes. The bit error rate (BER) is a major criterion for expressing the performance of digital optical communication systems and it signifies what fractions of the received bits are erroneous. Therefore BER of 10^{-3} to 10^{-12} have been quoted in the literature [1, 7, 28], with forward error correction required to improve communication systems operating at BER above 10^{-6} [82, 83]. In the exact sense, the BER is the realized measured result of a BER test experiment, while the binary error probability (BEP) model attempts to predict the experimental outcome assuming the BER test experiment runs for the length of time required to achieve a stated BER value. Thus the BER is always an approximation of the BEP because it is usually not feasible to run the BER experiment for long enough time to get the exact value predicted using the BEP model. However, the approximation can be improved by increasing the experimental run-time, and it is frequently the case in modelling sectors that people refer to the BEP as the BER because it is the quantity being predicted. Different methods of varying complexity and accuracy have been established in the literature for estimating the BER of digital optical communication systems, including the Gaussian approximation, and moment generating function techniques such as the Chernoff bound, modified Chernoff bound and saddlepoint approximation [74, 84, 85]. These computational methods have been used in quantifying the BER in this thesis with calculations involving probability distributions facilitated by numerical integration and Monte Carlo simulation. They are now discussed below for a simple OOK NRZ system.

3.5.1 Gaussian approximation

The Gaussian approximation (GA) is based on the mean and variance of the noise contaminated signal and gives a more accurate BER for systems dominated by Gaussian thermal noise than for systems where non-Gaussian noises are dominant. In an optically preamplified system, the ASE noise changes the overall statistics of the noise in a way that cannot be fully described by the first and second moments of the distribution, and the GA loses some accuracy. However,

the GA is commonly used in the literature to approximate the BER because it is simple and easy to compute.

The Gaussian distribution pdf is of the same form as eq. (3.14) with $E[X] = i_X$ and σ_X^2 as the mean and variance of the continuous random variable X. Assuming equiprobable ones and zeros, the BER can be written as

$$BER_{GA} = P(0|1)P(1) + P(1|0)P(0) = \frac{1}{2}\left[\frac{1}{2}\operatorname{erfc}\left(\frac{i_1 - i_D}{\sigma_1 \sqrt{2}}\right)\right] + \frac{1}{2}\left[\frac{1}{2}\operatorname{erfc}\left(\frac{i_D - i_0}{\sigma_0 \sqrt{2}}\right)\right] \qquad (3.34)$$

where the RHS of eq. (3.34) has been obtained by definite integral of the tails of the Gaussian distribution pdf in eq. (3.14) over the ranges of the decision threshold current i_D to ∞ and $-\infty$ to i_D, i_0 and i_1 are the mean current level for transmitted 0 and 1 while σ_0^2 and σ_1^2 are the total variances of the noise experienced by transmitted 0 and 1 at the sampling instant. The optimum value of i_D that reduces eq. (3.34) to a minimum is obtained by solving $dBER_{GA}/di_D = 0$. A sub-optimal threshold is sometimes obtained, by assuming a binary symmetric channel $(P(0|1) = P(1|0))$, which is given as

$$i_D = \frac{\sigma_0 i_1 + \sigma_1 i_0}{\sigma_0 + \sigma_1} \qquad (3.35)$$

3.5.2 Moment generating function

A general representation of a distribution from which all of its existing moments could be found is referred to as the moment generating function (MGF) of that distribution. By using an MGF, a fuller statistical description of the signal and noise is provided compared to the GA [86]. Where X is a discrete random variable, for example in a Poisson process with distribution $p_r = P(X = r)$, the MGF is written as

$$M_X(s) = E\left(e^{sX}\right) = \sum_{r=0}^{\infty} p_r e^{sr} \qquad (3.36)$$

Assuming that X is a continuous random variable, such as in a Gaussian process with distribution $P_X(x)$, the MGF is

$$M_X(s) = E\left(e^{sx}\right) = \int_{-\infty}^{\infty} p_X(x) e^{sx} dx \qquad (3.37)$$

The MGFs describing the statistics of the signal and noise for an optically preamplified system were developed from successive works in [74, 84, 87, 88],

with the derivations in [74] closely agreeing with previously established GA results in [89]. The total MGF derived in [74] including the MGF for the Gaussian thermal noise, and modified to include the number of ASE noise polarisation states m_t is written as

$$M_Z(s) = M_Y(s)M_{th}(s) = \frac{\exp\left[\int_{-\infty}^{\infty}\left\{\frac{R'G\left(e^{sqh_r(t-\tau)}-1\right)h_p(\tau)}{1-R'N_o\left(e^{sqh_r(t-\tau)}-1\right)}\right\}d\tau\right]}{\exp\left[\int_{-\infty}^{\infty}m_tB_o\,\ln\left\{1-R'N_o\left(e^{sqh_r(t-\tau)}-1\right)\right\}d\tau\right]}\exp\left[\frac{\sigma_{th}^2s^2}{2}\right] \quad (3.38)$$

where $R' = \eta/h\upsilon$, $h_p(\tau)$ is the optical power incident on the optical amplifier, $h_r(t)$ is the filter impulse response and the Gaussian thermal noise MGF is $M_{th}(s) = \exp\left(\sigma_{th}^2s^2/2\right)$.

3.5.2.1 Chernoff bound

The Chernoff bound (CB) is based on the MGF of a distribution and is a safer technique than the GA because it provides a sure upper bound on the BER. For a single independent observation, the original statistical formulation of the CB as derived by Herman Chernoff [90] can be written as

$$P(X < \vartheta) \le e^{-s\vartheta}M_X(s), \qquad s < 0 \quad (3.39)$$

$$P(X > \vartheta) \le e^{-s\vartheta}M_X(s), \qquad s > 0 \quad (3.40)$$

The probability that a 0 is received given that a 1 is transmitted $P(0|1)$ and the probability that a 1 is received given that a 0 is transmitted $P(1|0)$ can both be bounded using the CB, and written as

$$P(0|1) = P(i_1 < i_D) \le e^{s_1 i_D}M_{i_1}(-s_1), \qquad s_1 > 0 \quad (3.41)$$

$$P(1|0) = P(i_0 > i_D) \le e^{-s_0 i_D}M_{i_0}(s_0), \qquad s_0 > 0 \quad (3.42)$$

Assuming equiprobable ones and zeros, the BER bounded by the CB is given as [74]

$$BER_{CB} = \frac{1}{2}\left[P(0|1) + P(1|0)\right] \le \frac{1}{2}\left[e^{s_1 i_D}M_{i_1}(-s_1) + e^{-s_0 i_D}M_{i_0}(s_0)\right], \qquad s_1, s_0 > 0 \quad (3.43)$$

The optimum value of i_D that reduces eq. (3.43) is obtained by solving $dBER_{CB}/di_D = 0$, while s_1 and s_0 are independently optimised to obtain the tightest bound. In the days of computer processing power scarcity, setting $s_1 = s_0 = s$ would facilitate an acceptable optimisation. A search algorithm is used to find the

values of i_D, s_1 and s_0 that minimises the BER in the work presented in this thesis.

3.5.2.2 Modified Chernoff bound

The modified Chernoff bound (MCB) was developed as a method of evaluating communication systems impaired by additive zero mean Gaussian noise and interference, both originating from a statistically independent process [91, 92]. The MCB provides a tighter upper bound compared to the CB and has been used in the analysis of optically preamplifed communication systems [74, 76, 92]. The derivation for the MCB follows similar steps to the CB above with the random variable X in eqs. (3.39) and (3.40) split into Gaussian and non-Gaussian components. The standard form of the MCB for the conditional probabilities $P(0|1)$ and $P(1|0)$ is given as [74, 92]

$$P(0|1) = P(i_1 < i_D) \leq \frac{e^{s_1 i_D}}{s_1 \sigma_{th} \sqrt{2\pi}} M_{i_1}(-s_1), \qquad s_1 > 0 \qquad (3.44)$$

$$P(1|0) = P(i_0 > i_D) \leq \frac{e^{-s_0 i_D}}{s_0 \sigma_{th} \sqrt{2\pi}} M_{i_0}(s_0), \qquad s_0 > 0 \qquad (3.45)$$

Assuming equiprobable ones and zeros, the BER bounded by the MCB is given as [74, 92]

$$BER_{MCB} = \frac{1}{2}\left[P(0|1) + P(1|0) \right] \leq \frac{1}{2\sigma_{th}\sqrt{2\pi}}\left[\frac{e^{s_1 i_D}}{s_1} M_{i_1}(-s_1) + \frac{e^{-s_0 i_D}}{s_0} M_{i_0}(s_0) \right], \; s_1, s_0 > 0 \; (3.46)$$

3.5.2.3 Saddlepoint approximation

The saddlepoint approximation (SPA) was developed by expanding the Taylor series of the exponential of the MGF and as a result involves high order differentiations of the MGF [92, 93]. For equiprobable ones and zeros, the BER formulation using the SPA is given as [74, 76, 92]

$$BER_{SPA} = \frac{1}{2}\left[P(0|1) + P(1|0) \right] \leq \frac{1}{2\sqrt{2\pi}}\left[\frac{e^{[\psi_1(s_1)]}}{\sqrt{\psi_1''(s_1)}} + \frac{e^{[\psi_0(s_0)]}}{\sqrt{\psi_0''(s_0)}} \right], \; s_1, s_0 > 0 \; (3.47)$$

where $\psi_1(s_1)$ and $\psi_0(s_0)$ are respectively written as

$$\psi_1(s_1) = \ln\left(\frac{M_{i_1}(-s_1)\exp(s_1 i_D)}{s_1} \right) \qquad (3.48)$$

$$\psi_0(s_0) = \ln\left(\frac{M_{i_0}(s_0)\exp(-s_0 i_D)}{s_0}\right) \tag{3.49}$$

The SPA is more complex and computationally intensive compared to the other evaluation methods considered in this thesis, but it does produce a lower BER as shown by results in [74, 92].

3.6 Summary

This chapter describes the common techniques and optical devices used for signal multiplexing and multiple access in optical communication systems. The effects of atmospheric turbulence in outdoor FSO systems, dispersion in fibre systems and other losses experienced in both fibre and FSO systems are presented. Various types of noise and interference that degrade the performance of the receiver are also discussed. Finally, evaluation methods commonly used in analysing the performance of optical communication systems including the GA and MGF based methods such as the CB, MCB and SPA, which will be used in the analysis performed in the later chapters of this thesis, are presented.

3.7 References

1. Ramaswami, R., Sivarajan, K. N., Sasaki, G. H. *Optical Networks: A Practical Perspective*. 3rd ed. Boston: Morgan Kaufmann Publishers; 2010.
2. Jin, X., Wang, X., Hsu, C. Y.: 'Design and implementation of mobile free space optical communication system'. *IEEE Avionics, Fiber-Optics and Photonics Technol. Conf.* 2008: IEEE, pp. 37-38
3. Kazaura, K., Kazunori, O., Suzuki, T., Matsumoto, M., Mutafungwa, E., Murakami, T., et al.: 'Performance evaluation of next generation free-space optical communication system'. *IEICE Trans. on Electronics,* 2007, **90**, (2), pp. 381-388
4. Doerr, C. R., Okamoto, K.: 'Advances in silica planar lightwave circuits'. *J. Lightw. Technol.,* 2006, **24**, (12), pp. 4763-4789
5. Shaohua, T., Bingchu, Y., Hui, X., Hua, W., Guo-Qiang, L.: 'An Optical Power Splitter With Variable Power Splitting Ratio'. *IEEE Photonics Technol. Lett.,* 2011, **23**, (14), pp. 1004-1006
6. Zeng, Y., Liu, W., Long, C., Luo, Y., Xiao, Q.: 'A 1 x 2 variable optical power splitter development'. *J. Lightwave Technol.,* 2006, **24**, (3), pp. 1566-1570
7. Senior, J. M. *Optical Fiber Communications Principles and Practice*. 3rd ed. Essex, England: Pearson Prentice Hall; 2009.
8. Yu, C. X., Neilson, D. T.: 'Diffraction-grating-based (de)multiplexer using image plane transformations'. *IEEE J. Selected Topics in Quantum Electronics,,* 2002, **8**, (6), pp. 1194-1201
9. Janz, S., Balakrishnan, A., Charbonneau, S., Cheben, P., Cloutier, M., Delage, A., Dossou, K., et al.: 'Planar waveguide echelle gratings in silica-on-silicon'. *IEEE Photonics Technol. Lett.,* 2004, **16**, (2), pp. 503-505

10. Dutta, A. K., Dutta, N. K., Fujiwara, M. *WDM Technologies: Passive Optical Components: Passive Optical Components*: Academic press; 2003.

11. Maru, K., Mizumoto, T., Uetsuka, H.: 'Demonstration of Flat-Passband Multi/Demultiplexer Using Multi-Input Arrayed Waveguide Grating Combined With Cascaded Mach-Zehnder Interferometers'. *J. Lightw. Technol.,* 2007, **25**, (8), pp. 2187-2197

12. Frigo, N. J.: 'Local access optical networks'. *IEEE Network,* 1996, **10**, (6), pp. 32-36

13. Kramer, G., Pesavento, G.: 'Ethernet passive optical network (EPON): building a next-generation optical access network'. *IEEE Commun. Mag.,* 2002, **40**, (2), pp. 66-73

14. Kahn, J. M., Barry, J. R.: 'Wireless infrared communications'. *Proc. IEEE,* 1997, **85**, (2), pp. 265-298

15. Elgala, H., Mesleh, R., Haas, H.: 'Indoor optical wireless communication: potential and state-of-the-art'. *IEEE Commun. Mag.,* 2011, **49**, (9), pp. 56-62

16. Ma, R., Zuo, T. J., Sujecki, S., Phillips, A. J.: 'Improved performance evaluation for DC-coupled burst mode reception in the presence of amplified spontaneous emission noise and interchannel crosstalk'. *IET Optoelectron.,* 2010, **4**, (3), pp. 121-132

17. Zuo, T. J., Phillips, A. J.: 'Performance of burst-mode receivers for optical digital pulse position modulation in passive optical network application'. *IET Optoelectron.,* 2009, **3**, (3), pp. 123-130

18. Banerjee, A., Park, Y., Clarke, F., Song, H., Yang, S., Kramer, G., Kim, K., et al.: 'Wavelength-division-multiplexed passive optical network (WDM-PON) technologies for broadband access: a review [Invited]'. *J. Opt. Netw.,* 2005, **4**, (11), pp. 737-758

19. Chang-Hee, L., Sorin, W. V., Byoung-Yoon, K.: 'Fiber to the Home Using a PON Infrastructure'. *J. Lightw.Technol.,* 2006, **24**, (12), pp. 4568-4583

20. Trojer, E., Dahlfort, S., Hood, D., Mickelsson, H.: 'Current and next-generation PONs: A technical overview of present and future PON technology'. *Ericsson Review,* 2008, **2**, pp. 64-69

21. Kim, T.-Y., Han, S.-K.: 'Reflective SOA-based bidirectional WDM-PON sharing optical source for up/downlink data and broadcasting transmission'. *IEEE Photonics Technol. Lett.,* 2006, **18**, (22), pp. 2350-2352

22. Wooram, L., Mahn Yong, P., Seung Hyun, C., Jihyun, L., Byoung Whi, K., Geon, J.: 'Bidirectional WDM-PON based on gain-saturated reflective semiconductor optical amplifiers'. *IEEE Photonics Technol. Lett.,* 2005, **17**, (11), pp. 2460-2462

23. Payoux, F., Chanclou, P., Genay, N.: 'WDM-PON with colorless ONUs'. *Proc. of OFC* 2007; Annaehim, CA, Paper OTuG5

24. Stok, A., Sargent, E. H.: 'Lighting the local area: optical code-division multiple access and quality of service provisioning'. *IEEE Network,,* 2000, **14**, (6), pp. 42-46

25. Baby, V., Bres, C. S., Xu, L., Glesk, I., Prucnal, P. R.: 'Demonstration of differentiated service provisioning with 4-node 253 Gchip/s fast frequency-hopping time-spreading OCDMA'. *Electronics Letters,* 2004, **40**, (12), pp. 755-756

26. Ghafouri-Shiraz, H., Karbassian, M. M. *Optical CDMA networks: principles, analysis and applications*: John Wiley & Sons; 2012.

27. Prasad, R. *CDMA for wireless personal communications*: Artech House, Inc.; 1996.

28. Agrawal, G. P. *Fiber-optic communication systems*. 3rd ed. New York: John Wiley & Sons Inc.; 2002.

29. Kitayama, K., Xu, W., Wada, N.: 'OCDMA over WDM PON-solution path to gigabit-symmetric FTTH'. *J. Lightw.Technol.,* 2006, **24**, (4), pp. 1654-1662

30. Xu, W., Kitayama, K.: 'Analysis of beat noise in coherent and incoherent time-spreading OCDMA'. *J. Lightw. Technol.,* 2004, **22**, (10), pp. 2226-2235

31. Shurong, S., Yin, H., Wang, Z., Xu, A.: 'A New Family of 2-D Optical Orthogonal Codes and Analysis of Its Performance in Optical CDMA Access Networks'. *J. Lightwave Technol.,* 2006, **24**, (4), pp. 1646-1653

32. Kotani, Y., Iwamura, H., Tamai, H., Sarashina, M., Kashima, M.: 'Demonstration of 1.25 Gb/s 8-channels ECDM using eight-chip electrical coding'. *IEEE Photonics Technol. Lett.,* 2010, **22**, (12), pp. 875-877

33. Rosas-Fernandez, J. B., Ingham, J. D., Penty, R. V., White, I. H.: '18 Gchips/s electronic CDMA for low-cost optical access networks'. *J. Lightwave Technol.,* 2009, **27**, (3), pp. 306-313

34. Kwong, W. C., Perrier, P., Prucnal, P. R.: 'Performance comparison of asynchronous and synchronous code-division multiple-access techniques for fiber-optic local area networks'. *IEEE Trans. Commun.,* 1991, **39**, (11), pp. 1625-1634

35. Yang, G.-C., Kwong, W. C.: 'Performance comparison of multiwavelength CDMA and WDMA+ CDMA for fiber-optic networks'. *IEEE Trans. Commun.,* 1997, **45**, (11), pp. 1426-1434

36. Ghaffari, B. M., Matinfar, M. D., Salehi, J. A.: 'Wireless optical CDMA LAN: digital design concepts'. *IEEE Trans. Commun.,* 2008, **56**, (12), pp. 2145-2155

37. Ohtsuki, T.: 'Performance analysis of atmospheric optical PPM CDMA systems'. *J. Lightw. Technol.,* 2003, **21**, (2), pp. 406-411

38. Fouli, K., Maier, M.: 'OCDMA and Optical Coding: Principles, Applications, and Challenges [Topics in Optical Communications]'. *IEEE Commun. Mag.,* 2007, **45**, (8), pp. 27-34

39. Stok, A., Sargent, E. H.: 'The role of optical CDMA in access networks'. *IEEE Commun. Mag.,* 2002, **40**, (9), pp. 83-87

40. Yin, H., Richardson, D. J. *Optical Code Division Multiple Access Communication Networks: Theory and Applications*. Berlin: Springer; 2008.

41. Salehi, J. A.: 'Emerging OCDMA communication systems and data networks [Invited]'. *Journal of optical networking,* 2007, **6**, (9), pp. 1138-1178

42. Teh, P. C., Petropoulos, P., Ibsen, M., Richardson, D. J.: 'A comparative study of the performance of seven-and 63-chip optical code-division multiple-access encoders and decoders based on superstructured fiber Bragg gratings'. *J. Lightw. Technol.,* 2001, **19**, (9), pp. 1352

43. Geiger, H., Fu, A., Petropoulos, P., Ibsen, M., Richardson, D. J., Laming, R. I.: 'Demonstration of a simple CDMA transmitter and receiver using sampled fiber gratings'. *Tech. Proc. ECOC,* 1998, **98**, pp. 337-338

44. Andrews, L. C., Phillips, R. L. *Laser Beam Propagation Through Random Media*. 2nd ed: SPIE Press, Bellingham, Washington; 2005.

45. Plank, T., Leitgeb, E., Pezzei, P., Ghassemlooy, Z.: 'Wavelength-selection for high data rate Free Space Optics (FSO) in next generation wireless communications'. *17th Euro. Conf. on Networks and Optical Commun. (NOC)* 2012; Barna., Spain, pp. 1-5

46. Willebrand, H. A., Ghuman, B. S. *Free-space optics: enabling optical connectivity in today's networks*. Indiana USA: Sams Publishing; 2002.

47 Ghassemlooy, Z., Popoola, W., Rajbhandari, S. *Optical Wireless Communications - System and Channel Modelling with MATLAB*. 1st ed. London: CRC Press; 2013.

48. Kim, I. I., McArthur, B., Korevaar, E.: 'Comparison of laser beam propagation at 785 nm and 1550 nm in fog and haze for optical wireless communications'. *Proc. SPIE,* 2001, **4214**, pp. 26 - 37

49. Bloom, S., Korevaar, E., Schuster, J., Willebrand, H.: 'Understanding the performance of free-space optics'. *J. Opt. Netw.,* 2003, **2**, (6), pp. 178-200

50. Andrews, L. C., Phillips, R. L., Hopen, C. Y. *Laser Beam Scintillation with Applications*: SPIE Press; 2001.

51. Majumdar, A. K. *Advanced Free Space Optics (FSO): A Systems Approach*: Springer; 2014.

52. Zhu, X., Kahn, J. M.: 'Free-space optical communication through atmospheric turbulence channels'. *IEEE Trans. Commun.,* 2002, **50**, (8), pp. 1293-1300

53. Al-Habash, M. A., Phillips, R. L., Andrews, L. C.: 'Mathematical model for the irradiance probability density function of a laser beam propagating through turbulent media'. *Opt. Eng.,* 2001, **40**, (8), pp. 1554-1562

54. Vetelino, F. S., Young, C., Andrews, L., Recolons, J.: 'Aperture averaging effects on the probability density of irradiance fluctuations in moderate-to-strong turbulence'. *Applied Optics,* 2007, **46**, (11), pp. 2099-2108

55. Borah, D. K., Voelz, D. G.: 'Pointing error effects on free-space optical communication links in the presence of atmospheric turbulence'. *J. Lightwave Technol.,* 2009, **27**, (18), pp. 3965-3973

56. Churnside, J. H., Frehlich, R. G.: 'Experimental evaluation of log-normally modulated Rician and IK models of optical scintillation in the atmosphere'. *Journal of Opt. Soceity of America* 1989, **6**, (11), pp. 1760-1766

57. Nistazakis, H. E., Tsiftsis, T. A., Tombras, G. S.: 'Performance analysis of free-space optical communication systems over atmospheric turbulence channels'. *IET Commun.,* 2009, **3**, (8), pp. 1402-1409

58. Tsiftsis, T. A., Sandalidis, H. G., Karagiannidis, G. K., Sagias, N. C.: 'Multihop free-space optical communications over strong turbulence channels'. *IEEE Intl. Conf. on Commun.* 2006: IEEE, pp. 2755-2759

59. Churnside, J. H.: 'Aperture averaging of optical scintillations in the turbulent atmosphere'. *Applied Optics,* 1991, **30**, (15), pp. 1982-1994

60. Khalighi, M. A., Aitamer, N., Schwartz, N., Bourennane, S.: 'Turbulence mitigation by aperture averaging in wireless optical systems'. *10th Intl. Conf. on Telecommun.* 2009, pp. 59-66

61. Navidpour, S. M., Uysal, M., Kavehrad, M.: 'BER Performance of Free-Space Optical Transmission with Spatial Diversity'. *IEEE Trans. on Wireless Commun.,* 2007, **6**, (8), pp. 2813-2819

62. Tyson, R. K.: 'Bit-error rate for free-space adaptive optics laser communications'. *J. Opt. Soc. of America* 2002, **19**, (4), pp. 753-758

63. Andrews, L. C., Phillips, R. L., Hopen, C. Y.: 'Aperture averaging of optical scintillations: power fluctuations and the temporal spectrum'. *Waves in Random Media,* 2000, **10**, (1), pp. 53-70

64. Majumdar, A. K.: 'Free-space laser communication performance in the atmospheric channel'. *J. Opt. Fiber Commun. Rep.,* 2005, **2**, pp. 345 - 396

65. Kiasaleh, K.: 'On the probability density function of signal intensity in free-space optical communications systems impaired by pointing jitter and turbulence'. *OPTICE,* 1994, **33**, (11), pp. 3748-3757

66. Kopeika, N. S., Zilberman, A.: 'Vertical profiles of aerosol and optical turbulence strength and their effects on atmospheric propagation'2000: Proc. of SPIE, pp. 232-239

67. Dikmelik, Y., Davidson, F. M.: 'Fiber-coupling efficiency for free-space optical communication through atmospheric turbulence'. *Appl. Opt.,* 2005, **44**, (23), pp. 4946-4952

68. Winzer, P. J., Leeb, W. R.: 'Fiber coupling efficiency for random light and its applications to lidar'. *Optics Letters,* 1998, **23**, (13), pp. 986-988

69. Sandalidis, H. G., Tsiftsis, T. A., Karagiannidis, G. K., Uysal, M.: 'BER performance of FSO links over strong atmospheric turbulence channels with pointing errors'. *IEEE Commun. Letters,* 2008, **12**, (1), pp. 44-46

70. Ho, T.-H., Trisno, S., Smolyaninov, I. I., Milner, S. D., Davis, C. C.: 'Studies of pointing, acquisition, and tracking of agile optical wireless transceivers for free-space optical communication networks'. *Remote Sensing* 2004: Intl. Society for Optics and Photonics, pp. 147-158

71. Killinger, D. 'Free Space Optics-For Laser Communication Through the Air'. *Optics & Photonics News, OSA*. Oct. 2002: pp. 36-42.

72. Harris, A., Sluss Jr, J. J., Refai, H. H., LoPresti, P. G.: 'Comparison of active beam steering elements and analysis of platform vibrations for various long-range FSO links'. *Defense and Security* 2005: Intl. Soc. for Optics and Photonics, pp. 474-484

73. Olsson, N. A.: 'Lightwave systems with optical amplifiers'. *J. Lightwave Technol.,* 1989, **7**, (7), pp. 1071-1082

74. Ribeiro, L. F. B., Da Rocha, J. R. F., Pinto, J. L.: 'Performance evaluation of EDFA preamplified receivers taking into account intersymbol interference'. *J. Lightw. Technol.,* 1995, **13**, (2), pp. 225-232

75. Nasu, H., Mukaihara, T., Takagi, T., Oike, M., Nomura, T., Kasukawa, A.: '25-GHz-spacing wavelength-monitor integrated DFB laser module for DWDM applications'. *IEEE Photonics Technol. Lett.,* 2003, **15**, (2), pp. 293-295

76. Monroy, I. T., Tangdiongga, E. *Crosstalk in WDM Communication Networks*. Norwell, Massachusetts, USA, : Kluwer Academic Publishers; 2002.

77. Ohba, K., Hirano, T., Miyazawa, T., Sasase, I.: 'A symbol decision scheme to mitigate effects of scintillations and MAIs in optical atmospheric PPM-CDMA systems'. *IEEE Global Telecommuns. Conf.* 2005, pp. 1999-2003

78. Ohtsuki, T.: 'Performance analysis of indoor infrared wireless systems using PPM CDMA'. *Electronics and Commun. in Japan* 2002, **85**, (1), pp. 1-10

79. Mashhadi, S., Salehi, J. A.: 'Code-division multiple-access techniques in optical fiber networks - part III: optical AND logic gate receiver structure with generalized optical orthogonal codes'. *IEEE Trans. Commun.,* 2006, **54**, (8), pp. 1457-1468

80. Ghaffari, B. M., Salehi, J. A.: 'Multiclass, Multistage, and Multilevel Fiber-Optic CDMA Signaling Techniques Based on Advanced Binary Optical Logic Gate Elements'. *IEEE Trans. Commun.,* 2009, **57**, (5), pp. 1424-1432

81. Khazraei, S., Pakravan, M. R.: 'Analysis of generalized optical orthogonal codes in optical wireless local area networks'. *IEEE J. Sel. Areas Commun.,* 2009, **27**, (9), pp. 1572-1581

82. Lowery, A., Armstrong, J.: 'Orthogonal-frequency-division multiplexing for dispersion compensation of long-haul optical systems'. *Opt. Express,* 2006, **14**, (6), pp. 2079-2084

83. Cano, I. N., Omella, M., Prat, J., Poggiolini, P.: 'Colorless 10 Gb/s extended reach WDM PON with low BW RSOA using MLSE'. *Optical Fiber Communication Conference* 2010: Optical Society of America, pp. OWG2

84. Personick, S. D.: 'Applications for quantum amplifiers in simple digital optical communication systems'. *Bell Sys. Tech. J.,* 1973, **52**, (1), pp. 117-133

85. O'Reilly, J. J., Da Rocha, J. R. F., Schumacher, K.: 'Optical fiber direct detection receivers optimally tolerant to jitter'. *IEEE Trans. Commun.,* 1986, **34**, (11), pp. 1141-1147

86. Phillips, A. J., Cryan, R. A., Senior, J. M.: 'An optically preamplified PPM intersatellite system described by a moment-generating function formulation'. *Microwave and Optical Technol. Letters,* 1995, **8**, (4), pp. 200-204

87. O'Reilly, J. J., Da Rocha, J. F.: 'Improved error probability evaluation methods for direct detection optical communication systems'. *IEEE Trans. on Info. Theory,* 1987, **33**, (6), pp. 839-848

88. Fyath, R. S., O'reilly, J. J.: 'Comprehensive moment generating function characterisation of optically preamplified receivers'. *IEE Proceedings J (Optoelectronics),* 1990, **137**, (6), pp. 391-396

89. Yamamoto, Y.: 'Noise and error rate performance of semiconductor laser amplifiers in PCM-IM optical transmission systems'. *IEEE Journal of Quantum Electronics,* 1980, **16**, (10), pp. 1073-1081

90. Chernoff, H.: 'A measure of asymptotic efficiency for tests of a hypothesis based on the sum of observations'. *The Annals of Mathematical Statistics,* 1952, pp. 493-507

91. Prabhu, V. K.: 'Modified Chernoff bounds for PAM systems with noise and interference'. *IEEE Trans. on Info. Theory,* 1982, **28**, (1), pp. 95-100

92. O'Reilly, J. J., Mitchell, J. E.: 'Simplified derivation of the modified Chernoff upper bound'. *IEE Proc. Commun.,* 2005, **152**, (6), pp. 850-854

93. Helstrom, C. W.: 'Approximate evaluation of detection probabilities in radar and optical communications'. *IEEE Trans. on Aerospace and Electronic Systems,* 1978, (4), pp. 630-640

CHAPTER 4   Indoor Hybrid Fibre and Optical Wireless CDMA System using Optically Preamplified Fibre Coupled Receiver

4.1   Introduction

Recent advances in indoor optical wireless communication could lead to high speed all optical transmission from the service provider's hub to user devices. However, many challenges remain in the realization of full duplex high speed indoor optical wireless links. These include the mobility constraint, multiuser access and stringent power requirements. Fibre coupled receivers have recently been considered in some free space and indoor optical wireless systems [1, 2]. The potential benefits of improving the received optical power and data rate by the use of a fibre amplifier and a small area detector make such receiver systems attractive. However, the issue of air-fibre coupling losses, especially for indoor systems with mobility requirement, necessitates that direct line of sight be established between the transmitter and the receiver. The optically amplified network proposed in this chapter could provide multiuser access and ease both power and mobility constraints in indoor optical wireless communication systems. With inclusion of a fibre splitter, many users share the cost of the optical amplifier, and the system operational unit for all the users could be centralized at a remote and convenient location, thus reducing the system cost and providing greater flexibility for the system architecture [3].

The etendue of an optical system limits the amount of light passing from a source into the optical system [4]. Thus for a fibre coupled receiver, the fibre numerical aperture (NA) and the core diameter (about 0.15 and 10 μm respectively for a single mode fibre) determine the effective collecting area of the system as shown by Fig. 2.13 in Chapter 2. Given the small area of the fibre, it is very difficult for significant power to be coupled into the receiver in a non-directed transmission link, so a directed line of sight link is considered.

Several techniques of varying complexity and advantages have been proposed to overcome the mobility constraints in indoor optical wireless systems. One is the

use of micro-electromechanical system (MEMS) controlled mirrors and image
sensors or tracking systems to establish a direct line of sight transmission between
the receiver and the transmitter [2]. This technique in [2] increases the system
complexity and is adapted for only a single user device. An indoor localization
system using optical signals or radio frequency (RF) profiling and smart antennas
could also be used to locate the position of a mobile target [5-7]. These
localization systems could be combined with steering mirror and adaptive lenses
to establish direct optical wireless communication indoors with limited mobility
as in [7]. The technique involves using a separate (non-signal) wavelength to
communicate with the user devices connected to the link (based on request), in
order to establish their positions with respect to the ceiling transceiver, before a
directed high speed connection is made with protocols required to resolve multiple
request [7]. With the fibre coupled receiver, this model assumes that free mobility
is provided by a sub-system of tracking/localization devices and steering mirrors
as shown in Fig. 4.1 [8], and system coverage of a room does not have the same
constraints as in a fixed alignment ceiling unit system.
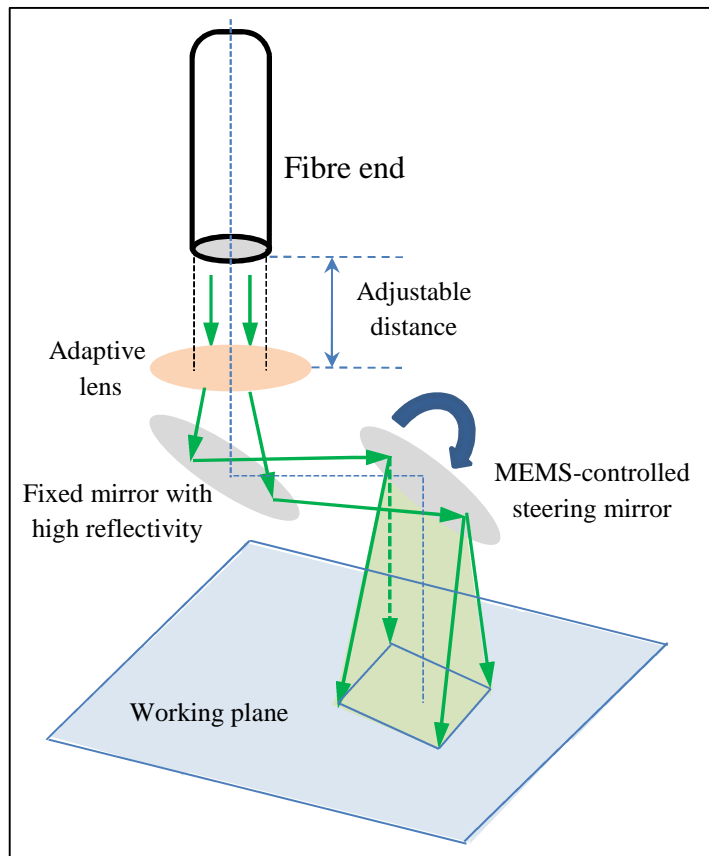
Fig. 4.1 Ceiling unit fibre transmitter (redrawn from [8])

The transmitter unit shown in Fig. 4.1 can be used with most mobile devices, but is better suited for devices that are used with occasional slow movements from one location in the room or cubicle to the other, such as laptops, and when only one device is used within a room or cubicle, there is no need for protocol services.

The downstream receiver architecture could include a collecting lens with a wide field of view (FOV) and a large area photodetector [9], although a fibre coupled receiver with a small area photodiode was used in the experimental work in [7]. Wide FOV receivers are well suited for moderate speed systems as found in the indoor environment and provide additional robustness for mobility, while the fibre coupled receiver is better for fixed high speed optical communication systems.

Code division multiple access (CDMA) can provide a flexible and robust network and is suited for application in the indoor optical wireless environment [10]. In [11], we have considered electrical CDMA with data rates in the range of 20 - 25 Mbps, however in this chapter, optical CDMA (OCDMA) capable of providing higher speed (about 132 Mbps) per user is considered. With OCDMA, signals are encoded and decoded in the optical domain, this primarily requires that the OCDMA signals be decoded before photodetection, as opposed to the electrical CDMA considered in [11] where decoding occur after photodetection. Optical CDMA encoders and decoders can be implemented using fibre tapped delay lines as illustrated in Fig. 3.4 or using FBG with a circulator [12, 13]. Since all the users transmit on the same wavelength and in overlapping time, the signals reaching the decoder (e.g. a correlator) include all users' coded signals. The correlator applies a copy of the desired user's OOC to the received signals and separates the desired user's signal which produces a maximum auto-correlation from other user's signals which produce minimum cross-correlation. In the downstream of such a system, multiple access interference (MAI) which generally limits system performance could be eliminated by proper code selection and arrangement as shown in [9]. The restriction is thus in the upstream and this analysis will focus more on the upstream transmission.

Receiver analysis of an optically amplified CDMA system is fairly complex. The optical amplifier introduces amplified spontaneous emission (ASE) noise which beats with the signal and itself to produce signal-spontaneous and spontaneous-spontaneous emission noise [14] while the CDMA introduces MAI,

all of which combine to impair the system. Furthermore, there is the issue of ambient noise which is optically amplified with the signal and could also be involved in beating with the ASE noise. Such impact is accounted for in the moment generating function (MGF) model described here.

4.2 Receiver system

A schematic diagram of an optically preamplified CDMA ceiling unit network architecture is shown in Fig. 4.2. The user devices are located in different cells which could be separate rooms in a building or separate cubicles in a large office space. The mobile devices access the localization system to know the position of the ceiling unit relative to their different positions in each room, and align their transmitting lenses with the ceiling unit collecting lens establishing a direct line of sight transmission upstream [7]. With the optical amplifier, the required power to achieve a target bit error rate (BER) is reduced, and it is easier to operate within the eye safety limit (10 dBm for indoor applications at 1550 nm [15-17]).
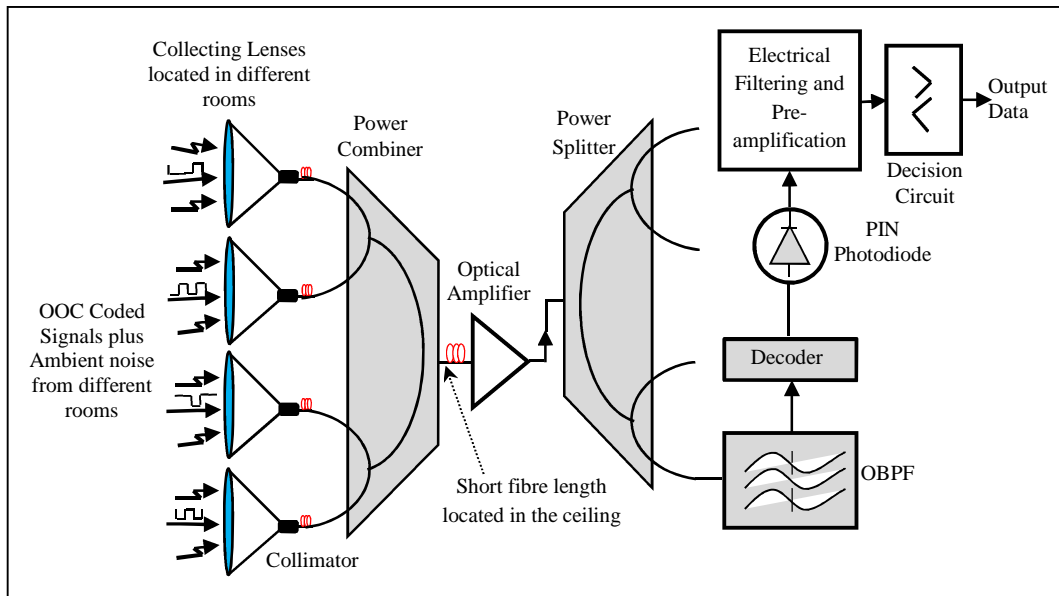
Fig. 4.2 Optically preamplified CDMA receiver system: ceiling unit network architecture

Optical orthogonal coded (OOC) signals are transmitted from different users and are coupled into a fibre with background ambient light via a collimator. The signals, combined with noise propagate over a short fibre length before optical amplification and subsequent splitting into signals of equal power for all the users. Each user's signal is decoded after optical bandpass filtering, and before

photodetection. The signal is then electrically processed (filtering and amplification) before decision is made. The optical bandpass filter (OBPF) is positioned after the optical amplifier to limit the ASE noise following optical amplification. In the configuration shown in Fig. 4.2, a splitter/combiner with 1 x 4 splitting ratio has been used. This provides simultaneous connections to 4 users only, but in some deployed networks, a splitting ratio of 1 x 32 has been achieved [18, 19]. However, in a large network, the system capacity could be limited by the practical number of splits that could be provided by the power splitter/combiner.

In Fig. 4.2, the desired signal (with ambient) enters the system from a collecting lens in one room while other users' signals (with ambient) enter from collecting lenses in other rooms. Fibre loss is negligible over tens of meters, but the splitting loss will effectively degrade the user signals. However, the ambient noise at amplifier input is approximately fixed relative to the number of splits as additional ambient funnelled through the other lenses will compensate for the ambient power loss due to the splitter. The additional dBs gained through optical amplification is used to counter the splitting loss incurred in collecting the signal from other users in different rooms or cells. The architecture of the network shown in Fig. 4.2 could be modified to easily connect to a bigger PON in several ways. The pre-detected signal may be used to drive a laser transmitter in an OEO converter, and the optical signal may be launched out to an outdoor HFFSO network or an outdoor all fibre network. Alternatively, the boosted signal may be launched out to an outdoor network immediately after optical amplification.

4.3 System model

4.3.1 CDMA analysis

The code length, code weight and correlation constraint of an optical orthogonal code (OOC) can be defined as (L_c, w, γ) with $\gamma = \max(\gamma_a, \gamma_c)$ if $\gamma_a \neq \gamma_c$, where γ_a and γ_c are the maximum autocorrelation constraint between shifted versions of the same code and cross-correlation constraint between two different codes respectively [20]. The impulse response of the OOC chip pulse with chip duration T_c can be written as

$$h_{R_c}(t) = \begin{cases} 1 & 0 \leq t < T_c \\ 0 & Otherwise \end{cases} \tag{4.1}$$

The chip rate $R_c = 1/T_c$ is related to the on-off keying (OOK) data rate as $R_b = R_c/L_c$. For a digital pulse position modulation (DPPM) system, additional bandwidth expansion is incurred such that $R_b = R_c/B_{exp}L_c$, where $B_{exp} = 2^M/M$ is the DPPM bandwidth expansion factor [21] and M is the DPPM coding level which is related to the number of slots (n) in the DPPM frame as $n = 2^M$. The OOC chips are spread over a bit period in OOK and over slot duration in DPPM. The number of users K that the OOCs can simultaneously support with almost perfect orthogonality is upper bounded by the Johnson bound on constant weight codes, and expressed in the following relationship [20, 22]

$$K \leq \left\lfloor \frac{(L_c - 1)(L_c - 2)...(L_c - \gamma)}{w \ (w - 1)...(w - \gamma)} \right\rfloor \tag{4.2}$$

Thus the CDMA system is limited by split when the OOC code cardinality is greater than the number of splits and limited by code when the OOC code cardinality is less than the number of splits. It has been shown in [22, 23], that by increasing γ, CDMA system could be optimised to improve performance and code cardinality, although for an on-off-keying system, OOCs with $\gamma_a = \gamma_c = 1$ are considered most appropriate in terms of synchronization [23]. Since only w out of L_c chip positions of the OOCs are pulse mark chips, for $\gamma_a = \gamma_c = 1$, the interference between two OOCs occurs with the probability $p_1 = w^2/L_c$. A more detailed formula for the interference probability between two OOCs for a given value of γ_c is derived in Section 3.4. Generally for OOK and DPPM systems, the interference probabilities between two OOCs are, $p_o = p_{\gamma_c} = w^2/2\gamma_c L_c$ and $p_d = p_{\gamma_c} = w^2/n\gamma_c L_c$ respectively, with the factor of $1/2$ in p_o accounting for the probability of transmitting data 1 or data 0 in an OOK system, and the factor of $1/n$ in p_d accounting for the probability that data could be transmitted in any of the n slots in the DPPM frame.

In OOK transmission, the threshold decision method is used and the same set of interferers impairs the system whether data 1 or data 0 is transmitted. While in the DPPM transmission which uses integrate and compare decision method, an interferer could impair the signal slot or an empty slot, so two sets of interferers exist. Generally the number of interferers impairing the system can be represented as $l_b = (0, 1, ..., K - 1)$ for $b \in \{1, 0\}$, where l_0 and l_1 are the number of interferers

transmitting on an empty slot and the signal slot of the desired user's DPPM frame respectively, and for OOK transmission, $l_0 = l_1 = l$.

4.3.2 BER analysis

The MGF describing the random variable for the signal plus noise is conditional on the number of interferers l_b, and for an integrating over T_c, it can be written as a modification of the MGF in [25],

$$M_{Y_b}(s|l_b) = \frac{\exp\left\{\dfrac{\left[R'G(e^{sq/T_c} - 1)F_b(w,l_b)\displaystyle\int_{T_c} h_{P_c}(\tau)d\tau\right]}{1 - \left[R'(N_o + GN_a)(e^{sq/T_c} - 1)\right]}\right\}}{\left\{1 - \left[R'(N_o + GN_a)(e^{sq/T_c} - 1)\right]\right\}^L} \tag{4.3}$$

where the total number of pulses from both the desired user and interferers that are on the desired user's pulse mark chip positions for received data 1 or signal slot and data 0 or empty slot is $F_b(w,l_b) = wb + \gamma l_b$ for $b \in \{1,0\}$, $h_{P_c}(\tau) = 2L_c P_{av}/w$ is the peak signal pulse power, P_{av} is the average signal pulse power at the preamplifier input, G is optical amplifier gain, $R' = \eta/h\upsilon$, η is quantum efficiency of photodetector, h is Planck's constant, υ is optical carrier frequency, q is electron charge, $N_o = \frac{1}{2}(NF \times G - 1)h\upsilon$ is the single sided ASE noise power spectral density (PSD) in single polarisation, N_a is the background ambient noise PSD, B_o is OBPF bandwidth, $L = m_t B_o T_c$ is the product of spatial and temporal modes [26], m_t is the number of ASE noise polarisation state and s is the MGF arguments.

The system thermal noise is signal independent and its MGF is included separately as:

$$M_{th}(s) = \exp\left(\frac{\sigma_{th}^2 s^2}{2}\right) \tag{4.4}$$

where the thermal noise variance σ_{th}^2 for an OOK CDMA system is $\sigma_{th-OOK_C}^2 = S_{pa}B_e$, and for DPPM CDMA system is $\sigma_{th-DPPM_C}^2 = B_{exp}\sigma_{th-OOK_C}^2$, $B_e = 1/2T_c$ is the single sided electrical bandwidth of the receiver, S_{pa} is the thermal noise single sided power spectral density. The overall signal plus noise MGF conditioned on l_b is given by

$$M_{TOT_b}(s|l_b) = M_{Y_b}(s|l_b) \ M_{th}(s) \qquad (4.5)$$

The mean current $i_b(l_b)$ and noise variance $\sigma_b^2(l_b)$ which are the first and second moments of the MGF are obtained through the first and second derivatives of the total MGF respectively, with s set equal to 0. The mean and the variance are expressed as $E\{TOT_b\} = \left. \dfrac{\partial M_{TOT_b}(s|l_b)}{\partial s} \right|_{s=0}$ and $V\{TOT_b\} = E\{TOT_b^2\}-[E\{TOT_b\}]^2$

respectively, where $E\{TOT_b^2\} = \left. \dfrac{\partial^2 M_{TOT_b}(s|l_b)}{\partial^2 s} \right|_{s=0}$. The variance is thus written as

$$\sigma_b^2(l_b) = \sigma_{SIRN}^2 + \sigma_{SN,b}^2(l_b) + \sigma_{SIBN}^2 + \sigma_{SDBN,b}^2(l_b) \qquad (4.6)$$

σ_{SIRN}^2 is the signal independent receiver thermal noise variance. $\sigma_{SN,b}^2(l_b)$ is the shot noise variance and includes ASE shot noise $\sigma_{ASE,sh}^2 = 2m_t B_o N_o q^2 R' B_e$, ambient shot noise $\sigma_{A,sh}^2 = 2m_t B_o G N_a q^2 R' B_e$ and signal shot noise $\sigma_{s,sh,b}^2(l_b) = 2q^2 R' G \mu_P F_b(w,l_b) B_e$. The signal independent beat noise variance is σ_{SIBN}^2 and includes the beat noises generated by the ASE-ambient, ASE-ASE and ambient-ambient noise beatings, jointly written as $\sigma_{n-n}^2 = 2m_t (qR')^2 (N_o + G N_a)^2 B_o B_e$. The signal dependent beat noise variance $\sigma_{SDBN,b}^2(l_b)$ includes both the signal-ambient beat noise variance $\sigma_{s-A,b}^2(l_b) = 4(qR')^2 G^2 N_a \mu_P F_b(w,l_b) B_e$ and signal-spontaneous beat noise variance $\sigma_{s-sp,b}^2(l_b) = 4(qR')^2 G N_o \mu_P F_b(w,l_b) B_e$, where $\mu_P = 2L_c P_{av}/w$. The flowchart for the upstream BER calculations for both OOK and DPPM systems is shown as Fig. 4.3 for easy understanding of the BER evaluation processes.
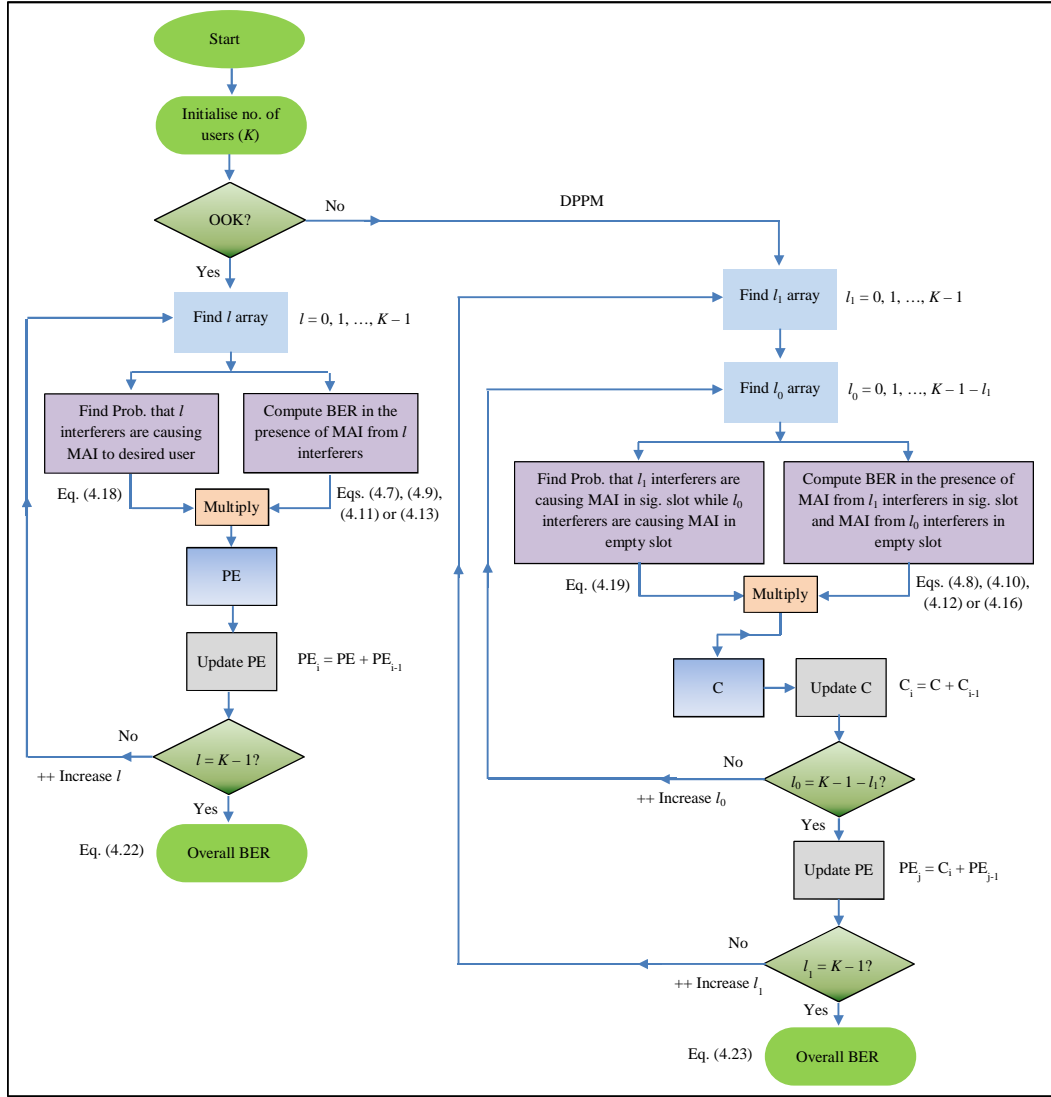
Fig. 4.3 Flowchart for upstream BER calculations

For the Gaussian approximation (GA), the bit error rate (BER) conditioned on the number of interferers $(l_0 = l_1 = l)$ for an OOK system is given by [14, 25],

$$BER_{GA}(l) = \frac{1}{2}\left[\frac{1}{2}\text{erfc}\left(\frac{i_D - i_0(l)}{\sigma_0(l)\sqrt{2}}\right) + \frac{1}{2}\text{erfc}\left(\frac{i_1(l) - i_D}{\sigma_1(l)\sqrt{2}}\right)\right] \tag{4.7}$$

and for a DPPM system [22]

$$P_{WE-GA}(l_0, l_1) = \frac{1}{2}\text{erfc}\left[\frac{i_1(l_1) - i_0(l_0)}{\sqrt{2\left(\sigma_1^2(l_1) + \sigma_0^2(l_0)\right)}}\right] \tag{4.8}$$

where $i_0(l)$ and $i_1(l)$ are the mean currents for data 0 and data 1 respectively in the presence of interferers, i_D is the decision current which is fixed over the number of interferers, $i_0(l_0)$ and $i_1(l_1)$ are the mean currents for the empty slot and the signal slot in the presence of l_0 and l_1 set of interferers respectively,

92

Following [25], the Chernoff bound (CB) on the BER for both OOK and DPPM systems are respectively written as,

$$BER_{CB}(l) = \frac{1}{2}\left[e^{-s_0 i_D} M_{TOT_0}(s_0|l) + e^{s_1 i_D} M_{TOT_1}(-s_1|l) \right], \qquad (s_0, s_1 > 0) \qquad (4.9)$$

$$P_{WE-CB}(l_0, l_1) = M_{TOT_0}(s|l_0) \; M_{TOT_1}(-s|l_1), \qquad (s_0 = s_1 = s > 0) \qquad (4.10)$$

$M_{TOT_0}(s_0|l)$ and $M_{TOT_1}(-s_1|l)$ are defined in eq. (4.5)

In addition, a modified Chernoff bound (MCB) on the BER is derived for both OOK and DPPM systems following [25, 27] and are respectively written as

$$BER_{MCB}(l) = \frac{1}{2\sigma_{th-OOK_C}\sqrt{2\pi}}\left[\frac{e^{-s_0 i_D}}{s_0} M_{TOT_0}(s_0|l) + \frac{e^{s_1 i_D}}{s_1} M_{TOT_1}(-s_1|l) \right], \; (s_0, s_1 > 0) \quad (4.11)$$

$$P_{WE-MCB}(l_0, l_1) = \frac{1}{2s\sigma_{th-DPPM_C}\sqrt{\pi}}\left[M_{TOT_0}(s|l_0) \; M_{TOT_1}(-s|l_1) \right], \; (s_0 = s_1 = s > 0) \qquad (4.12)$$

The Saddle point approximation (SPA) for an OOK system for $s_0, s_1 > 0$, is written as [25]

$$BER_{SPA}(l) = \frac{1}{2}\left[\frac{e^{-s_0 i_D} M_{TOT_0}(s_0|l)}{s_0\sqrt{2\pi\psi_0''(s_0)}} + \frac{e^{s_1 i_D} M_{TOT_1}(-s_1|l)}{s_1\sqrt{2\pi\psi_1''(s_1)}} \right] \qquad (4.13)$$

where $\psi_0(s_0)$ and $\psi_1(s_1)$ are respectively written as,

$$\psi_0(s_0) = \ln\left(\frac{e^{-s_0 i_D} M_{TOT_0}(s_0|l)}{s_0} \right) \qquad (4.14)$$

$$\psi_1(s_1) = \ln\left(\frac{e^{s_1 i_D} M_{TOT_1}(-s_1|l)}{s_1} \right) \qquad (4.15)$$

For a DPPM system the SPA is,

$$P_{WE-SPA}(l_0, l_1) = \left[\frac{M_{TOT_0}(s|l_0) \; M_{TOT_1}(-s|l_1)}{s\sqrt{2\pi\psi''(s)}} \right] \qquad (s_0 = s_1 = s > 0) \qquad (4.16)$$

where $\psi(s)$ is written as,

$$\psi(s) = \ln\left(\frac{M_{TOT_0}(s|l_0) \; M_{TOT_1}(-s|l_1)}{s} \right) \qquad (4.17)$$

The conditionality of the error probability on l or l_b is removed from the total BER by averaging over the MAI contributions of all the interferers.

The MAI effect is cumulative, and is a binomial random variable with parameters $K-1$ as the total number of interferers and $p_o = w^2/2\gamma_c L_c$ as the interference occurrence probability between the desired user's OOC and the

93

interferer's OOC in an OOK system. The probability that l out of $K-1$ interferers are causing MAI in the system or the probability that the interference random variable at decision time equals l is written as [28],

$$P(l) = \binom{K-1}{l} (p_o)^l (1-p_o)^{K-1-l} \tag{4.18}$$

Equation (4.18) gives the probability of a particular interference state pattern occurring in the OOK CDMA system. Illustrations of signal reception in the presence of the interference pattern when $l = 2$ are shown as Figs. 3.9a and 3.9b for when the desired user transmitted data 1 and data 0 respectively.

The effect of MAI in DPPM CDMA systems is as a result of interferers in both the signal slot and the empty slots of the desired user. The distribution is a multinomial with parameters $K-1$ and $p_d \in \{p_1, p_2\}$. Following the same approach in [29, 30], but easing the constraint that no interference occurs in the signal slot of the desired user, the MAI distribution is written as [22, 31, 32]

$$P(l_0, l_1) = \frac{(K-1)!}{l_0! l_1! (K-1-l_0-l_1)!} \, p_r(l_0, l_1) \tag{4.19}$$

where, for $M = 1$,

$$p_r(l_0, l_1) = p_1^{l_0+l_1} (1-2p_1)^{K-1-l_0-l_1} \tag{4.20}$$

and for $M = 2$,

$$p_r(l_0, l_1) = p_1^{l_1} (1-p_1)^{K-1-l_1} p_2^{l_0} (1-p_2)^{K-1-l_1-l_0} \tag{4.21}$$

where $p_1 = w^2/n\gamma_c L_c$ and $p_2 = w^2/(n-1)\gamma_c L_c$ are the probabilities of interference between the desired user's OOC and the interfering users OOC occurring in the signal slot (which could be any of the n slots) and in an empty slot (which could be any of the $n-1$ slots) respectively. Similar to eq. (4.18), eq. (4.19) gives the probability of a particular interference state pattern occurring in the DPPM CDMA system, and illustrations of signal reception in the presence of the interference pattern when $l_1 = 2$ and $l_0 = 0$ are shown as Figs. 3.10a and 3.10c for when the desired user transmitted data 0 and data 1 respectively while illustrations of signal reception in the presence of the interference pattern when $l_1 = 0$ and $l_0 = 2$ are shown as Figs. 3.10b and 3.10d for when the desired user transmitted data 0 and data 1 respectively. The overall BER for an OOK system is calculated as [9],

$$BER_{OOK} = \sum_{l=0}^{K-1} P(l) \; BER_Z(l) \tag{4.22}$$

where Z represents the GA, CB, MCB and SPA. While for a DPPM system, the overall BER is written as [22, 31, 32]

$$BER_{DPPM} = \frac{n}{2(n-1)}(n-1)\sum_{l_1=0}^{K-1}\sum_{l_0=0}^{K-1-l_1} P(l_0,l_1)\ P_{WE-Z}(l_0,l_1) \qquad (4.23)$$

The downstream transmission is controlled by the ceiling unit with proper cyclic shifts which ensure that there is no multiple access interferences between users, provided that $\gamma_a = \gamma_c = 1$ and the code length L_c is greater than the number of times interfering pulse (from all the interferers) occur on the desired user's pulse mark chip positions in a continuous cyclic shift [9]. Since there are w^2 ways in which interference could occur between two different OOCs, MAI could be eliminated in a synchronised downstream transmission provided that $w^2(K-1) < L_c$, and both eqs. (4.18) and (4.19) could be replaced with a Dirac delta function [9], with $l = l_0 = l_1 = 0$ in eqs. (4.22) and (4.23). In addition, the ambient noise is not amplified downstream, although some level of beating with other light may occur.

4.4   Results and discussion

Table 4.1: Parameters used for calculations

Parameter	Description	Value
λ	Optical wavelength	1550 nm
B_o	OBPF channel bandwidth	70 GHz
G	Optical amplifier gain	26 dB (or 8 dB)
NF	Amplifier noise figure	4.77 dB
η	Receiver quantum efficiency	0.7
A_{RX}	Receiver collecting lens area	1 cm^2
m_t	Polarisation states of ASE noise	2 (no polarisation filtering)

The parameters used in the calculations are presented in Table 4.1. In the result section, DPPM1 and DPPM2 refer to DPPM with $M = 1$ and DPPM with $M = 2$ respectively while OOK CDMA and DPPM CDMA are referred to as OOK_C and $DPPM_C$ respectively. The received average power in the plots which follow is defined at the receiver collecting lens, and the ambient intensity is estimated from the background spectral irradiance of diffused sky given as 4.3 $\mu W/(cm^2 sr\ nm)$ [33]. A splitter loss of 3 dB per 2 way split is assumed. The thermal noise variance is back calculated using the CDMA chip rate such that $\sigma^2_{th-OOK_C} = R_c \sigma^2_{thBL}/R_b$, with σ^2_{thBL} estimated from a model of a non-CDMA PIN receiver at BER of 10^{-12} using sensitivities of -36 dBm, -32 dBm and -23 dBm which correspond to data rates of 155 Mbps, 622 Mbps and 2.5 Gbps respectively [34]. These data rates are chosen to obtain good estimates of the thermal noise at chip rates of 256 Mcps, 512Mcps and 2.56 Gcps. A coupling efficiency of 20% is used in the calculations, this is consistent with the experimental work performed in [35] using a compound lens arrangement with a fibre collimator. Diffraction limited beam spreading over the (approximately) 2 m distance between the ceiling and a working plane is considered negligible, but longer distances are possible with the beam steering mechanism. The optimum threshold which minimizes the overall BER in principle is obtained by solving $\partial BER_Z/\partial i_D = 0$, but for straightforwardness, the values of i_D, s_1 and s_0 that give the minimum BER are obtained using a search algorithm. For fair comparison, perfect extinction is assumed for both OOK_C and $DPPM_C$ systems. Different CDMA parameters including code lengths and weights are used in the model and can be found in [9, 22, 29, 36, 37] and will be stated for the plots that follow. The CDMA receiver circuitry operates at the chip rate, and the maximum chip rate considered in the model is 2.56 Gcps and 5.12 Gcps for OOK_C and $DPPM_C$ systems respectively. However, the data rate per user, ranging from about 20-132 Mbps, is comparable to already deployed indoor wireless communication systems (though a single point-point link with no multiple access certainly can do better).
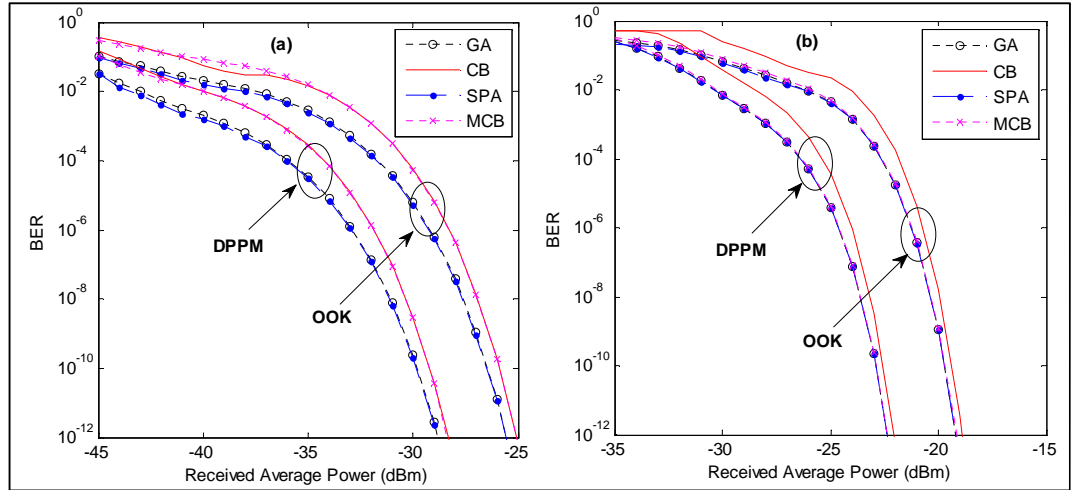
Fig. 4.4 Upstream BER against received average power for 3 users in both OOK_C and $DPPM_C$ ($M = 2$) systems using $\{L_c, w, \gamma_c, \gamma_a\} = \{19, 3, 1, 1\}$ with 1 x 4 splitter (user restricted by code): (a) G = 26 dB and (b) G = 8 dB

The upstream BER for both OOK_C and $DPPM_C$ systems is shown in Fig. 4.4 as a function of the received average power for low amplifier gain ($G = 8$ dB) and high amplifier gain ($G = 26$ dB) using the GA, CB, MCB and SPA. The data rate per user is 132 Mbps (equivalent to 2.5 Gcps for OOK_C system and 5 Gcps for $DPPM_C$ system with $M = 1$ and 2). Although the 1 x 4 way power splitter/combiner (6 dB splitter loss) can support 4 users, the maximum number of users is restricted to 3 due to the code parameters. The BER results obtained using $DPPM_C$ with $M = 2$ are shown to be better than the results for systems using OOK_C. The GA and SPA predict a better BER than the CB which maintain an upper bound, exceeding the other methods. The MCB BER curve coincides with the CB at high gain but moves closer to the GA and SPA BER curves at lower gain. This shift in MCB BER curve with respect to change in amplifier gain (and consequently the signal dependent noise) is well known in non-CDMA systems and seen in [25, 26, 38]. In CDMA system, the MCB results in an upper bound sometimes tighter than the CB and comparable to SPA, provided that the Gaussian thermal noise is non-negligible compared to the non-Gaussian noise contributions from the signal and MAI [27, 39].

In Fig. 4.5, the downstream BER for both OOK_C and $DPPM_C$ is shown as a function of the received average power for $G = 8$ dB and $G = 26$ dB using the GA, CB, MCB and SPA. In the absence of MAI as previously explained for downstream transmission, the GA sometimes exceeds known upper bounds (i.e.

the CB and MCB) as seen in Figs. 4.5a and 4.5b. Similar behaviour is also shown
by the GA in non-CDMA systems (e.g. [1, 25]). The GA is thus inconsistent,
although the accuracy penalty is compensated by its simplicity and the ease of
computation. The SPA however consistently presents a lower BER both in the
upstream and downstream results in Figs. 4.4 and 4.5 respectively.
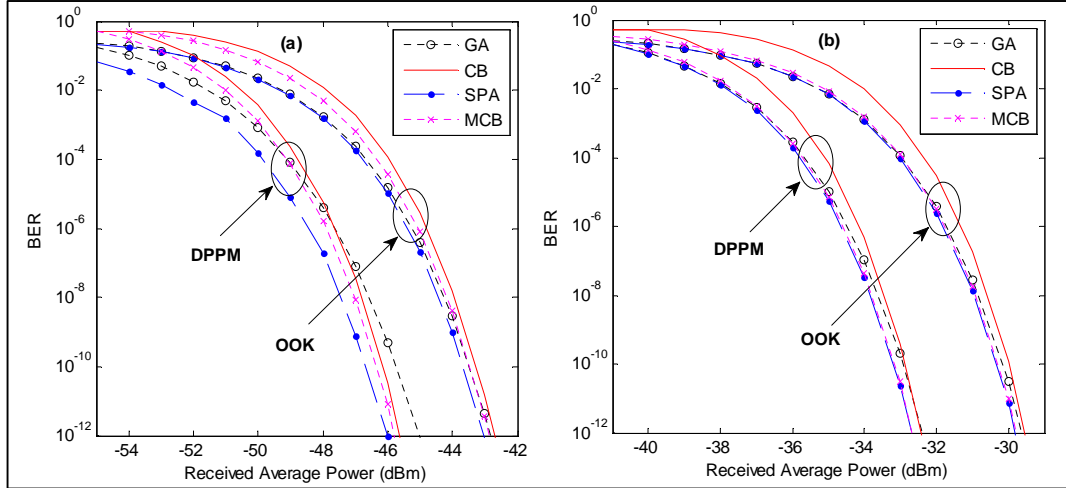
Fig. 4.5 Downstream BER against received average power for 3 users in both
OOK_C and $DPPM_C$ ($M = 2$) systems using $\{L_c, w, \gamma_c, \gamma_a\} = \{19, 3, 1, 1\}$ with 1 x 4
splitter (user restricted by code): (a) G = 26 dB and (b) G = 8 dB

The MCB is used in Fig. 4.6 to compare the downstream and upstream BER
performance of both OOK_C and $DPPM_C$ systems. The presence of MAI in the
upstream is seen to worsen the system performance compared to the downstream
where MAI is absent. The BER curve for $DPPM_C$ at $M = 1$ coincides with the
OOK_C BER curve in the downstream but shows an improvement over OOK_C in
the upstream. This shows that $DPPM_C$ systems are more resistant to MAI
compared to OOK_C systems. This is so partly because of the probability that MAI
is distributed over many slots in $DPPM_C$ systems, but mostly due to the imperfect
threshold acquisition in OOK_C systems which is not necessary in $DPPM_C$ systems
using the integrate and compare receiver. The MCB which is an upper bound has
been used here and has resulted in a tighter upper bound compared to the CB for
the parameters used thus far in the analysis.
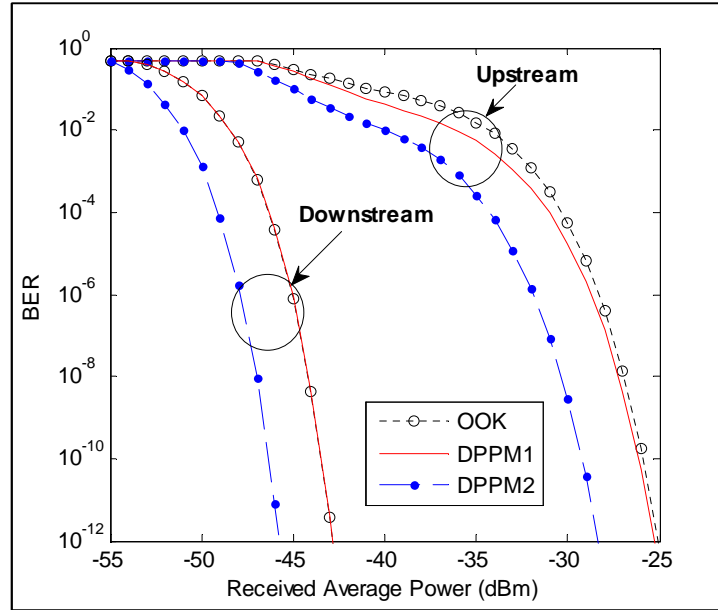
Fig. 4.6 BER against received average power for 3 users in both OOK_C and $DPPM_C$ systems using the MCB and for $\{L_c, \text{w}, \gamma_c, \gamma_a\} = \{19, 3, 1, 1\}$ with 1 x 4 splitter (user restricted by code)

Fig. 4.7 shows the upstream BER against average received power using the GA, CB, MCB and SPA for 4 users at different chip rates with 1 x 4 way splitter. The maximum number of users calculated from the code parameters is 6; however the number of users is limited to 4 due to the splitting ratio. With increasing number of users, the effect of MAI is more prominent in this result and others that follow. The increased effect of MAI results in steeper BER curves in areas where the system is noise dominated, and some leveling effects or floors in the BER curves when MAI is dominant as seen Fig. 4.7 and the rest of the results. The system performance degrades with increasing chip rate resulting in increased system noise. As shown in Fig. 4.7b, $DPPM_C$ still maintains a better BER performance over OOK_C irrespective of the system data rate. However, as the effect of MAI becomes more prominent compared to the thermal noise (e.g. at lower chip rate), the MCB suffers a little loss in tightness.
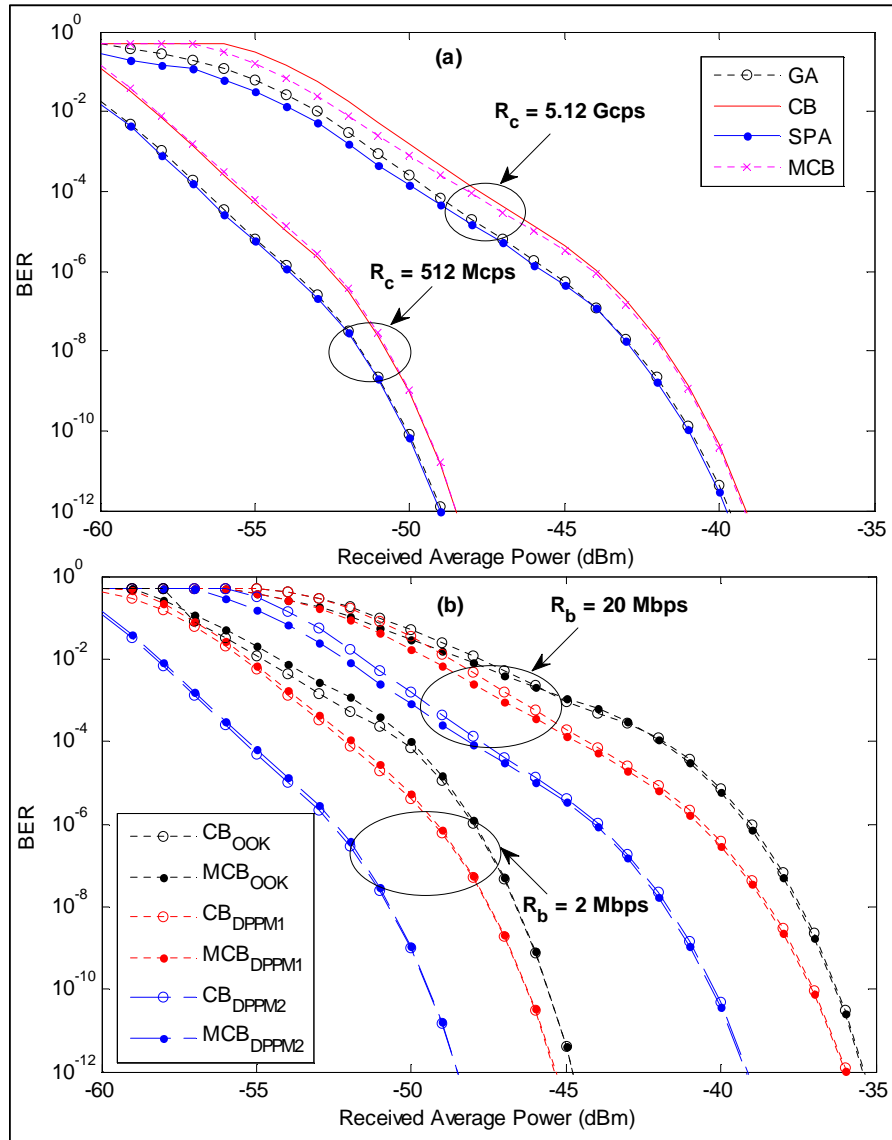
Fig. 4.7 Upstream BER against received average power for 4 users using {L_c, w, γ_c, γ_a} = {128, 5, 1, 1} with 1 x 4 splitter at different chip rates (user restricted by split): (a) DPPM$_C$ system, $M = 2$ and (b) OOK$_C$ and DPPM$_C$ systems

So far, we have considered systems with number of users limited to 4. The MAI effect increases with the number of interferers, and for some code parameters, the system performance could be limited by MAI. In Fig. 4.8, a 1 x 8 way splitter is used for the same code parameters used in Fig. 4.7, allowing the system to accommodate the maximum number of users specified by the CDMA codes, while maintaining the data rate at 20 Mbps per user. Thus in this case, the number of users is limited by code. The MAI effect becomes more prominent and results in an error floor when all 6 users are connected to the system, with a minimum BER greater than 10^{-6} for both OOK$_C$ and DPPM$_C$ systems. The floor

disappears once the number of simultaneously connected users $K < 6$ as the system becomes noise limited rather than MAI limited. The bumps seen in OOK_C BER curves when MAI is prominent are due to the optimization of the decision threshold in order to obtain the minimum BER for the system. They actually disappear when an average decision threshold (e.g. half way between the powers for a transmitted 1 and a transmitted 0) is used, but such decision threshold results in sub-optimal BER curves.
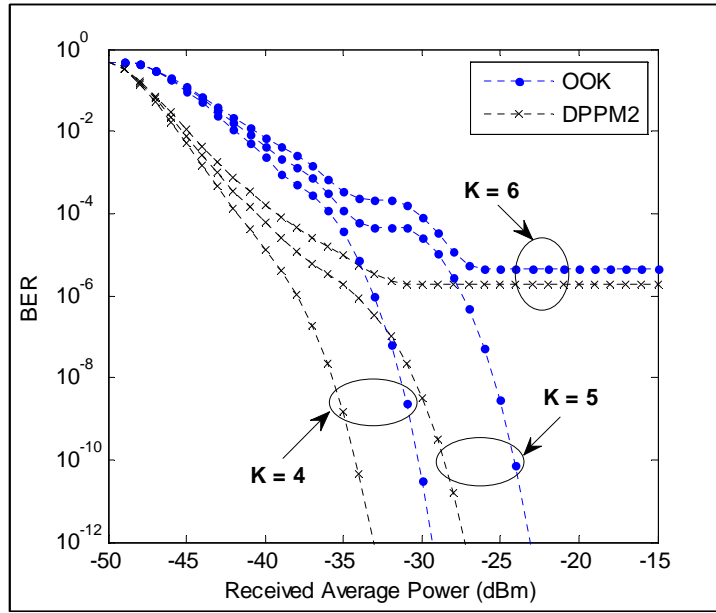
Fig. 4.8 Upstream BER against received average power for maximum of 6 users in both OOK_C and $DPPM_C$ ($M = 2$) systems using the CB and for $\{L_c, \text{w}, \gamma_c, \gamma_a\} = \{128, 5, 1, 1\}$ with 1 x 8 splitter (user restricted by CDMA code).

Results for systems with maximum cross correlation constraint $\gamma_c = 2$, implying more users and MAI in these systems are shown for the remaining results. Fig. 4.9 shows the result for BER against received average power using the same splitter (1 x 8 way) as in Fig. 4.8 but with code parameters that calculates the maximum number of users as 9. Hence the number of users for the system is restricted by split. The code cardinality in Fig. 4.9 is improved by the change of γ_c to 2, and with the code length reduced to 100, the data rate increased to 25.6 Mbps per user while the same chip rate is maintained for either the OOK_C or $DPPM_C$ system. Error floors occurred for both $K = 8$ and 7 in Fig. 4.9, but occurred particularly for $K = 7$ at a lower BER. Generally the error floors occurred at a lower BER for the $DPPM_C$ system in Fig. 4.9b compared to the OOK_C system shown in Fig. 4.9a.
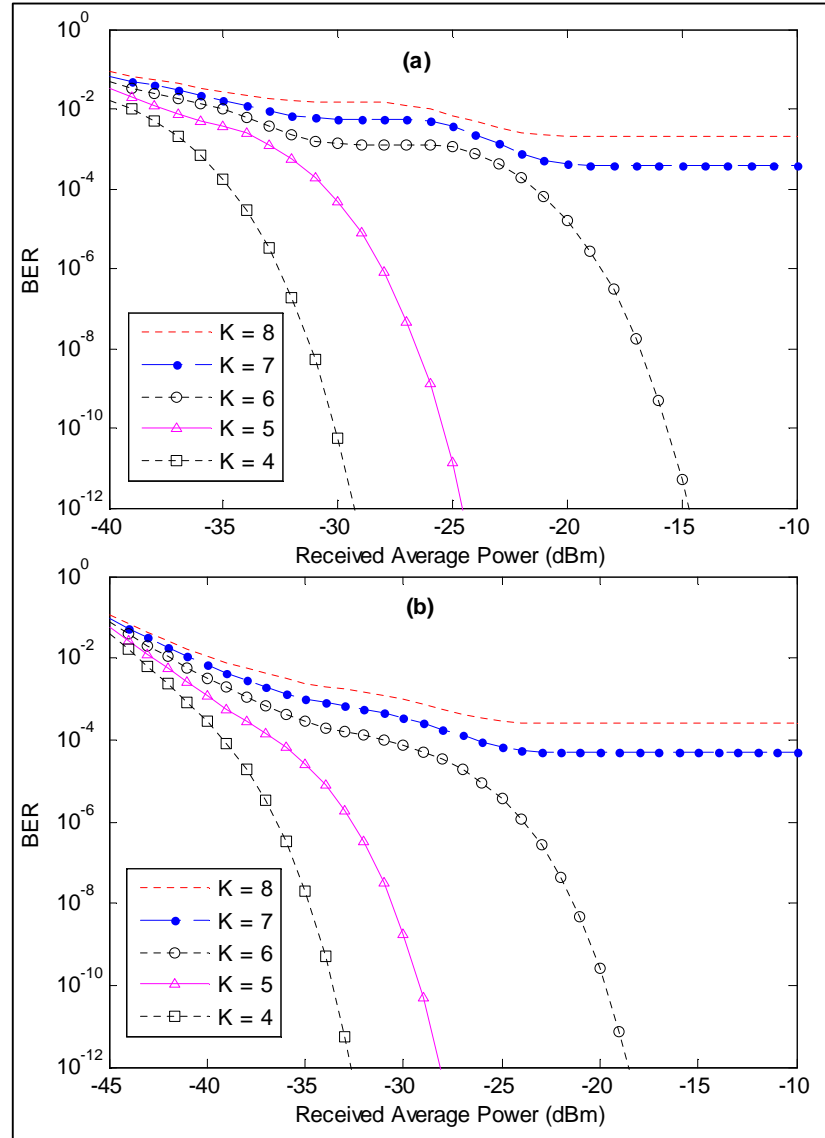
Fig. 4.9 Upstream BER against received average power for maximum of 8 users
using the CB and for $\{L_c, w, \gamma_c, \gamma_a\} = \{100, 11, 2, 1\}$ with 1 x 8 splitter (user
restricted by split): (a) OOK$_C$ system and (b) DPPM$_C$ system, $M = 2$

In Fig. 4.10, a 1 x 16 way splitter is used with double the code length used in
Fig. 4.8, and with $\gamma_c = 2$. The maximum number of users increased to 11, limited
by the CDMA code. However, the chip rate remained the same thus the data rate is
reduced to 10 Mbps per user. There is error floor only when $K = 11$ whilst for $K =$
4 the system is seen to predict a better BER than the other systems considered in
Figs. 4.8 and 4.9, however, at a lower data rate per user. The BER floors in Figs.
4.8 - 4.10 are due to MAI and occur when the number of interfering pulses from
other users occurring at the desired user's pulse mark chip position is greater or

equal to the code weight i.e. $\gamma(K-1) \geq w$. Forward error correction (FEC) may be employed to eliminate the error floor caused by MAI as in some fibre systems [40].
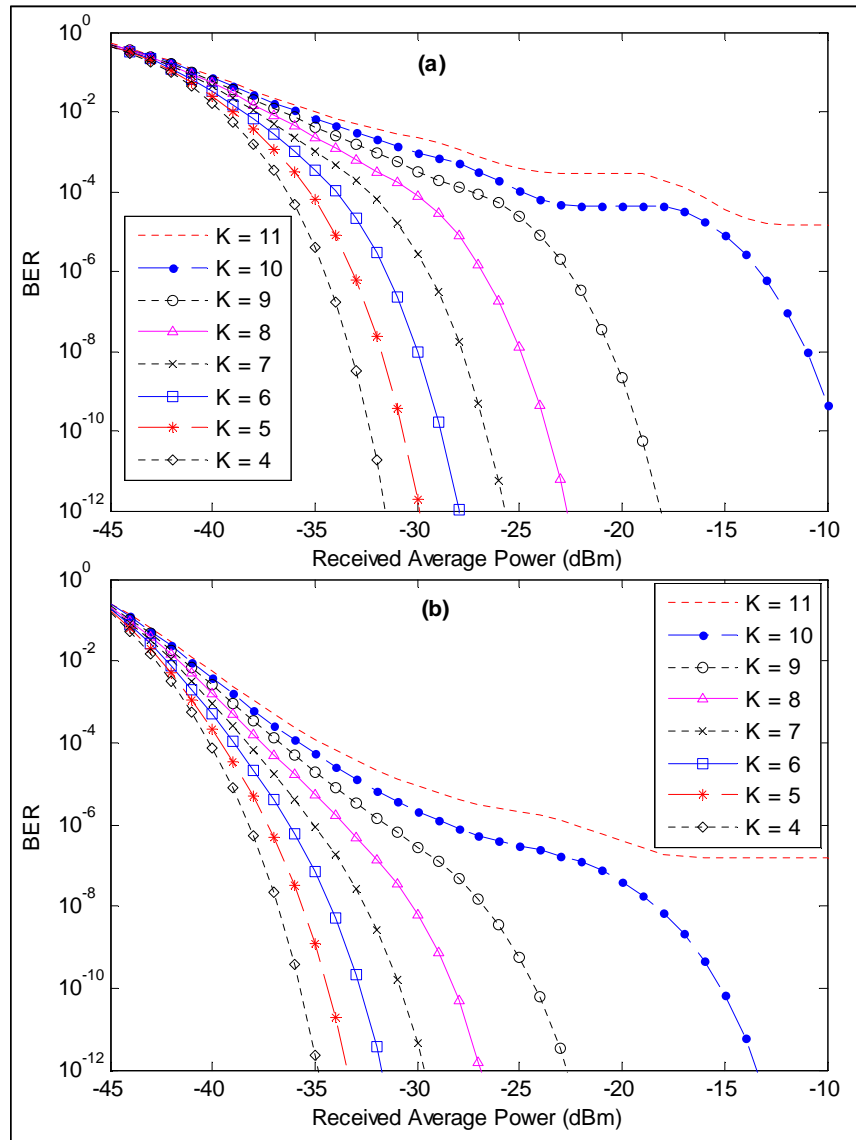
Fig. 4.10 Upstream BER against received average power for maximum of 11 users using the CB and for $\{L_c, w, \gamma_c, \gamma_a\} = \{256, 19, 2, 1\}$ with 1 x 16 splitter (user restricted by CDMA code): (a) OOK_C system and (b) $DPPM_C$ system, $M = 2$

The required received average power to achieve a BER of 10^{-9} in both the upstream and downstream are shown in Fig. 4.11 for an optically preamplified system using the same parameters as in Fig. 4.10, and a non-optically amplified system with the same configuration, i.e. with the amplifier turned off by setting the gain $G = 1$ and ASE noise power spectral density (PSD) $N_0 = 0$. The preamplified system is clearly shown to require less average power in both the upstream and downstream. The $DPPM_C$ system at $M = 2$ shows an improvement

in upstream required optical power over OOK$_C$ system ranging from 2.9 dB when 1 user is connected to 6.2 dB when 10 users are connected in the preamplified system. While for the unamplified upstream transmission, DPPM$_C$ at $M = 2$ showed only about 4.7 dB improvement over OOK$_C$. Depending on the number of active users, the preamplified system shows an improvement in required power ranging from 9 – 22 dB over the non-amplified system as is shown in Fig. 4.11.
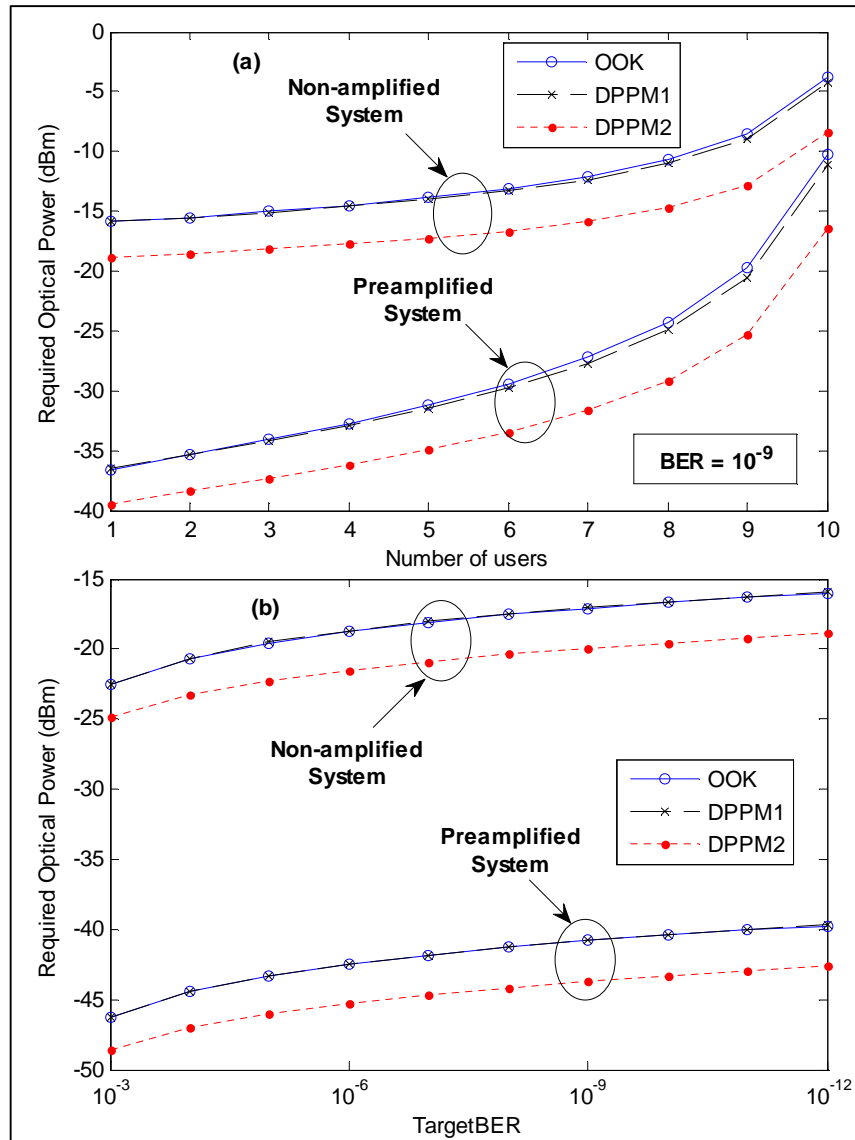
Fig. 4.11 Required received average power for both preamplified and non-amplified OOK$_C$ and DPPM$_C$ systems using the CB and for $\{L_c, w, \gamma_c, \gamma_a\} = \{256, 19, 2, 1\}$ with 1 x 16 splitter: (a) Upstream, target BER = 10^{-9} and (b) Downstream, target BER ranging from 10^{-3} to 10^{-12} (independent of user number)

The resulting power penalties caused by MAI at various target BER values are shown in Fig. 4.12. For a target BER of 10^{-9}, the MAI penalty is about 1.05 dB

and 23 dB when 2 users and 10 users are connected to the DPPM$_C$ preamplified
system respectively (i.e. relative to when one user is active on the system) as
shown in Fig. 4.12b. This value is better than the OOK$_C$ system which reports a
MAI penalty of about 1.2 dB and 26.3 dB when 2 users and 10 users are active on
the preamplified system respectively as shown in Fig. 4.12a. In addition, while the
target BER of 10^{-6} is achievable with 11 users active on the DPPM$_C$ system, only
a BER of about 10^{-4} could be achieved with the OOK$_C$ system.
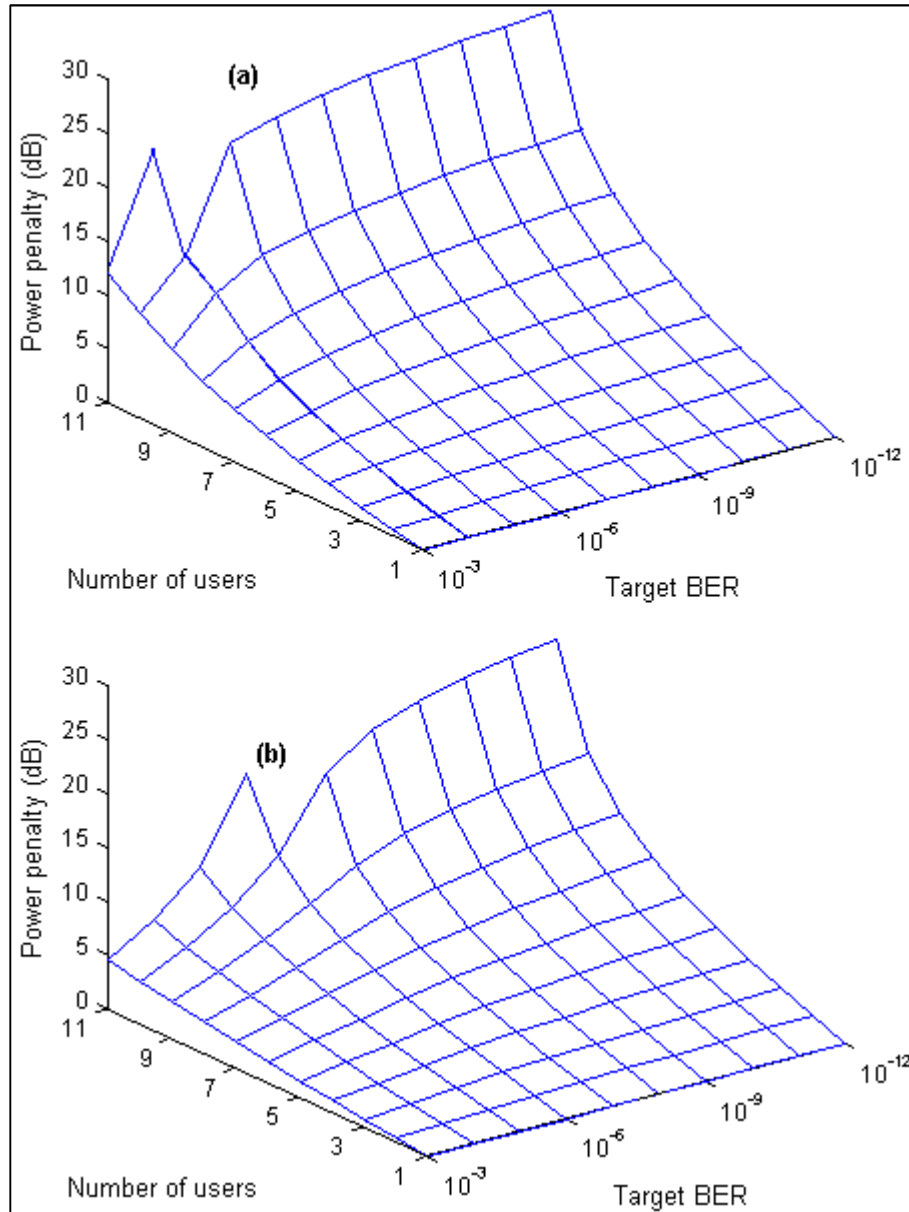
Fig. 4.12 MAI power penalty in the upstream as a function of target BER and
number of users for the preamplified system using the CB and for $\{L_c, w, \gamma_c, \gamma_a\} =$
$\{256, 19, 2, 1\}$ with 1 x 16 splitter (The case for 11 users terminates prematurely
due to error floor, i.e. BER can't be obtained): (a) OOK$_C$ and (b) DPPM$_C$, $M = 2$

4.5　Summary

This chapter analyses the performance of indoor optically preamplified hybrid fibre and wireless CDMA network using both OOK and DPPM formats. The integrate and compare decision circuitry used in $DPPM_C$ systems shows better tolerance to MAI compared to the imperfect threshold acquisition device used in OOK_C systems. In addition, the $DPPM_C$ systems shows improved average power efficiency compared to the OOK_C systems. It is also shown that the optical amplifier reduces the average optical power required from user devices and the system can support many users at moderate data rate. With less required optical power, the battery life of the user device is preserved and the stringent eye safety requirement for indoor power transmission is less difficult to satisfy. The system restricted by code is easily upgradable and more feasible for practical application. Also, full mobility could be provided for the users if the system is supported with tracking/localization devices and steering mirrors. For CDMA systems where MAI could easily dominate the system, the CB is suggested as the safest method of system performance evaluation. Having considered an indoor system with CDMA and DPPM in this chapter, it is now necessary to move our attention to larger outdoor WDM networks with longer FSO links and also to consider the impacts of optical crosstalk and turbulence on such links.

4.6   References

1. Aladeloba, A. O., Phillips, A. J., Woolfson, M. S.: 'Improved bit error rate evaluation for optically pre-amplified free-space optical communication systems in turbulent atmosphere'. *IET Optoelectron.,* 2012, **6**, (1), pp. 26-33
2. Kolev, D. R., Wakamori, K., Matsumoto, M., Kubo, T., Yamada, T., Yoshimoto, N.: 'Gigabit indoor laser communication system for a mobile user with MEMS mirrors and image sensors'. *Int. Workshop on Optical Wireless Commun. (IWOW)* 2012, pp. 1-3
3. Aladeloba, A. O., Woolfson, M. S., Phillips, A. J.: 'WDM FSO Network with Turbulence-Accentuated Interchannel Crosstalk'. *J. Opt. Commun. Netw.,* 2013, **5**, (6), pp. 641-651
4. O'Brien, D.: 'Indoor optical wireless communications: recent developments and future challenges'. *Proc. of SPIE,* 2009, **7464**, pp. 74640B
5. Haque, I. T., Nikolaidis, I., Gburzynski, P.: 'A Scheme for Indoor Localization through RF Profiling'. *IEEE Int. Conf. on Commun. Workshops,* 2009, pp. 1-5
6. Chin-Heng, L., Yahong, W., Ng, B.-P., See, C. M. S.: 'A Real-Time Indoor WiFi Localization System Utilizing Smart Antennas'. *IEEE Trans. Consum. Electron.,* 2007, **53**, (2), pp. 618-622
7. Ke, W., Nirmalathas, A., Lim, C., Skafidas, E.: '4 x 12.5 Gb/s WDM Optical Wireless Communication System for Indoor Applications'. *J. Lightw. Technol.,* 2011, **29**, (13), pp. 1988-1996
8. Ke, W., Nirmalathas, A., Lim, C., Skafidas, E.: 'High-Speed Optical Wireless Communication System for Indoor Applications'. *IEEE Photonics Technol. Lett.,* 2011, **23**, (8), pp. 519-521
9. Ghaffari, B. M., Matinfar, M. D., Salehi, J. A.: 'Wireless optical CDMA LAN: digital design concepts'. *IEEE Trans. Commun.,* 2008, **56**, (12), pp. 2145-2155
10. Chan, H. H., Elmirghani, J. M. H., Cryan, R. A.: 'Performance analysis of indoor infrared wireless networks utilising PPM CDMA'. *IEEE Int. Conf. on Commun., (Conf. Record, Converging Technol. for Tomorrow's Applicat.) 1996* 1996, pp. 1467-1471
11. Mbah, A. M., Walker, J. G., Phillips, A. J.: 'Indoor hybrid fibre and wireless CDMA system using optically preamplified fibre coupled receiver'. *2nd Intl. Workshop on Optical Wireless Communs. (IWOW)* 2013, pp. 94-98
12. Geiger, H., Fu, A., Petropoulos, P., Ibsen, M., Richardson, D. J., Laming, R. I.: 'Demonstration of a simple CDMA transmitter and receiver using sampled fiber gratings'. *Tech. Proc. ECOC,* 1998, **98**, pp. 337-338
13. Yin, H., Richardson, D. J. *Optical Code Division Multiple Access Communication Networks: Theory and Applications*. Berlin: Springer; 2008.
14. Zuo, T. J., Ma, R., Phillips, A. J., Sujecki, S.: 'Performance analysis of optically preamplified DC-coupled burst mode receivers'. *European Trans. Telecommun.,* 2009, **20**, (3), pp. 281-286
15. 'Safety of laser products - part 1: Equipment classification, requirements and user's guide, IEC-60825-1 (Incorporating amendments A1:1997 and A2:2001)', 2001.
16. O'Brien, D., Katz, M.: 'Optical wireless communications within fourth-generation wireless systems [Invited]'. *J. Optical Networking,* 2005, **4**, (6), pp. 312-322
17. Al Hajjar, H., Fracasso, B., Leroux, D.: 'Fiber-distributed indoor high bitrate optical wireless system'. *Wireless personal communications,* 2013, **72**, (3), pp. 1771-1782
18. Vaughn, M. D., Kozischek, D., Meis, D., Boskovic, A., Wagner, R. E.: 'Value of reach-and-split ratio increase in FTTH access networks'. *J. Lightwave Technol.,* 2004, **22**, (11), pp. 2617-2622
19. Kramer, G.: 'What is Next for Ethernet PON?'. *The Joint Intl. Conf. on Optical Internet and Next Generation Network* 2006, pp. 49-54
20. Fan, C., Salehi, J. A., Wei, V. K.: 'Optical orthogonal codes: design, analysis and applications'. *IEEE Trans. Inf.Theory,* 1989, **35**, (3), pp. 595-604

21. Sibley, M. J. N. *Optical Communications : components and systems*. 2nd ed. London: Macmillian Press Ltd; 1995.

22. Khazraei, S., Pakravan, M. R.: 'Analysis of generalized optical orthogonal codes in optical wireless local area networks'. *IEEE J. Sel. Areas Commun.,* 2009, **27**, (9), pp. 1572-1581

23. Mashhadi, S., Salehi, J. A.: 'Code-division multiple-access techniques in optical fiber networks - part III: optical AND logic gate receiver structure with generalized optical orthogonal codes'. *IEEE Trans. Commun.,* 2006, **54**, (8), pp. 1457-1468

24. Ribeiro, L. F. B., Da Rocha, J. R. F., Pinto, J. L.: 'Performance evaluation of EDFA preamplified receivers taking into account intersymbol interference'. *J. Lightw. Technol.,* 1995, **13**, (2), pp. 225-232

25. Aladeloba, A. O., Phillips, A. J., Woolfson, M. S.: 'Performance evaluation of optically preamplified digital pulse position modulation turbulent free-space optical communication systems'. *IET Optoelectron.,* 2012, **6**, (1), pp. 66-74

26. O'Reilly, J. J., Mitchell, J. E.: 'Simplified derivation of the modified Chernoff upper bound'. *IEE Proc. Commun.,* 2005, **152**, (6), pp. 850-854

27. Salehi, J. A., Brackett, C. A.: 'Code division multiple-access techniques in optical fiber networks. II. Systems performance analysis'. *IEEE Trans. Commun.,* 1989, **37**, (8), pp. 834-842

28. Ohtsuki, T.: 'Performance analysis of indoor infrared wireless systems using PPM CDMA'. *Electronics and Commun. in Japan* 2002, **85**, (1), pp. 1-10

29. Ohtsuki, T.: 'Performance analysis of atmospheric optical PPM CDMA systems'. *J. Lightw. Technol.,* 2003, **21**, (2), pp. 406-411

30. Khazraei, S., Pakravan, M. R.: 'Analysis of Generalized Optical Orthogonal Codes in Wireless Optical Networks Using BPPM'. *15th IEEE Intl. Conf. on Networks* 2007, pp. 170-175

31. Shalaby, H. M. H.: 'Performance analysis of optical CDMA communication systems with PPM signaling'. *IEEE Global Telecommun. Conf.* 1993, pp. 1901-1905

32. Djahani, P., Kahn, J. M.: 'Analysis of infrared wireless links employing multi-beam transmitters and imaging diversity receivers'. *Global Telecommun. Conf.* 1999, pp. 497-504 vol. 491a

33. Ramaswami, R., Sivarajan, K. N., Sasaki, G. H. *Optical Networks: A Practical Perspective*. 3rd ed. Boston: Morgan Kaufmann Publishers; 2010.

34. Ke, W., Nirmalathas, A., Lim, C., Skafidas, E.: 'Experimental Demonstration of a Full-Duplex Indoor Optical Wireless Communication System'. *IEEE Photonics Technol. Letters,* 2012, **24**, (3), pp. 188-190

35. Ghaffari, B. M., Matinfar, M. D., Salehi, J. A.: 'Wireless optical CDMA LAN: digital implementation analysis'. *IEEE J. Sel. Areas Commun.,* 2009, **27**, (9), pp. 1676-1686

36. Matsuo, R., Matsuo, M., Ohtsuki, T., Udagawa, T., Sasase, I.: 'Performance analysis of indoor infrared wireless systems using OOK CDMA on diffuse channels'. *IEEE Pacific Rim Conf. on Commun., Comput. and Signal Processing* 1999, pp. 30-33

37. Ma, R., Zuo, T. J., Sujecki, S., Phillips, A. J.: 'Improved performance evaluation for DC-coupled burst mode reception in the presence of amplified spontaneous emission noise and interchannel crosstalk'. *IET Optoelectron.,* 2010, **4**, (3), pp. 121-132

38. Lam, A. W., Hussain, A. M.: 'Performance analysis of direct-detection optical CDMA communication systems with avalanche photodiodes'. *IEEE Trans. Commun.,* 1992, **40**, (4), pp. 810-820

39. Azmi, P., Nasiri-Kenari, M., Salehi, J. A.: 'Low-rate super-orthogonal channel coding for fiber-optic CDMA communication systems'. *J. Lightw. Technol.,* 2001, **19**, (6), pp. 847-855

CHAPTER 5   Performance Evaluation of Digital Pulse Position Modulation for WDM FSO Systems Impaired by Interchannel Crosstalk

5.1 Introduction

One of the popular modulation schemes widely applied in free space optical (FSO) communications is digital pulse position modulation (DPPM). This scheme is well known to be attractive in different FSO environments including intersatellite, atmospheric and indoor wireless channels [1-3]. Apart from the power efficiency advantage that is well reported in several research works, and also shown in Chapter 4, there is the additional advantage that there is no need to set and track a decision threshold in many DPPM systems [4, 5]. DPPM has been proposed and intensively investigated for optical fibre systems [6, 7], however, DPPM is particularly attractive in an FSO channel relative to an optical fibre channel because the FSO channel is dispersion free [1]. The advantages of DPPM however do come at the expense of a bandwidth expansion, but with a moderately low coding level, DPPM can combine with most multiplexing/multiple access techniques without considerable bandwidth expansion. In addition, some hybrids of DPPM with other modulation schemes such as phase shift keying (PSK) and frequency shift keying (FSK) have been proposed for point-to-point fibre communication systems [8, 9] and could be alternative options to improve the DPPM bandwidth efficiency.

With the availability of bandwidth-intensive services such as video on demand (VoD), Internet Protocol television (IPTV), IP telephony and interactive gaming/videoconferencing, there has been a rapid rise in bandwidth demand from users [10-12]. In response to this increase in bandwidth demand, wavelength division multiplexing (WDM) systems have been investigated and/or deployed for optical fibre, atmospheric and indoor wireless optical networks [13-15]. WDM could also be applied in multiple user access networks, for example WDM passive optical network (PON) is generally considered as a good solution to the

109

bandwidth requirement for future access networks, with potential for higher data rate, improved data security and longer reach [13, 16]. The drivers for WDM deployment remain the same whether conventional on-off keying (OOK) modulation or DPPM format is used in the system (as long as the bandwidth expansion can be accommodated). DPPM has been considered for use in WDM systems in [17, 18], and for PON systems in [19], but would have a better application in coarse WDM systems where the additional bandwidth expansion is less problematic.

However, in a multiple wavelength communication link, imperfect optical components (e.g. demultiplexers, filters, etc. [20, 21]), and possibly asymmetric losses, necessitate the evaluation of the impact of interchannel crosstalk [22, 23]. This is well known for OOK systems, and crosstalk in WDM OOK systems has been investigated for optical fibre, intersatellite and FSO links [20, 22, 24-26]. But such a performance evaluation for DPPM interchannel crosstalk has not yet been provided (for any of the realistic WDM DPPM scenarios whether intersatellite, atmospheric, indoor, multi-user, PON or point to point). Thus the analysis performed in this chapter is intended to remedy this shortfall. It should be noted though, that necessarily this evaluation is somewhat more complex than the equivalent for OOK.

Specifically, an optically preamplified WDM DPPM FSO system impaired by interchannel crosstalk is investigated in this chapter. The presence of an optical amplifier (OA) further improves the receiver sensitivity, but introduces amplified spontaneous emission (ASE) noise. The ASE noise beats with the signal and itself to produce signal-spontaneous and spontaneous-spontaneous beat noises which degrade the system performance. The GA, and other techniques based on MGF which gives a full statistical description of the signal and noise [7], including the CB and MCB, are applied in the BER evaluation of the system. Analytically obtained results (and in the case of multiple crosstalk verified with Monte Carlo simulations) are compared with WDM OOK results and presented.

5.2 Optically preamplified WDM DPPM receiver

In DPPM signal transmission scheme, a frame of duration equal to MT_b is divided into $n = 2^M$ equal time slots of length $t_s = MT_b/n$, where M is the coding level and equal to the number of data bits transmitted per DPPM frame, $T_b = 1/R_b$

is the equivalent on-off keying non-return-to-zero (OOK NRZ) bit period and R_b is the bit rate. The maximum likelihood detection receiver is preferred for the best performance in DPPM FSO systems [1]. The decision circuitry is required to integrate over each slot in a frame and the decision is made by comparing the results and selecting the slot with the largest signal as the pulse position [4]. Therefore faster electronic processing speed is required compared to the threshold method used in OOK systems.

A general WDM DPPM system that might require evaluation of crosstalk impact could include a fibre or free space (or hybrid) system and may be in a point-to-point, multipoint-to-point or PON configuration. Different sources and levels of crosstalk could arise in a WDM DPPM system depending on the link configuration. In most point-to-point systems with all signal wavelengths originating from the same place, the major source of crosstalk is imperfect optical bandpass filter (OBPF)/demultiplexer (demux) rejection and since most realistic systems will employ OBPF/demux with good rejection ratio, unless there is a power drop in the signal wavelength compared to the interfering wavelengths (or some relative spectral shift of passband and signal), the crosstalk level will be fairly small. This is also the case in point-to-multipoint fibre systems (like WDM PON downstream) with all signal wavelengths originating from the same place. But in multipoint-to-point links such as upstream transmission in HFFSO systems as shown in Fig. 5.1a or in PON (where signals could experience asymmetric splitting loss, fibre and/or FSO attenuation, beam spreading and coupling loss), signals at different wavelengths will arrive at the OBPF/demux at different power levels (see PON architecture in Fig. 2.14). Under this condition, the crosstalk in the system is no longer dependent only on the OBPF/demux channel rejection but could rise much higher depending on the difference between the signal power of the interfering wavelengths and the desired wavelength at the input of the optical filter. Other cases where asymmetry could affect the level of crosstalk include point-to-multipoint systems with signal wavelengths having different powers prior to multiplexing.

A generic system structure which could be easily adapted to all the different scenarios above is shown in Fig. 5.1b. DPPM signals from different wavelengths are multiplexed and transmitted over an FSO link to a receiving lens (not shown

in Fig. 5.1b). They could also in principle arise from different physical locations as long as they can be collected and coupled effectively into the optical amplifier (OA) which is done by collimating them into a short fibre length at the amplifier input before being demultiplexed into different wavelengths for detection by a PIN photodiode. The optical preamplifier is just treated as a linear gain block generating noise as in Fig. 5.1b. Thus saturation based effects, and other nonlinearities, that may justify a more sophisticated treatment to include the contribution of certain optical amplifiers to the overall crosstalk at the receiver, are not considered. The demux/OBPF provides an effective bandpass filtering which helps to reduce the ASE noise prior to detection, and the detected signal is passed through electrical amplifier and filter before integrate and compare circuitry is used to decide which DPPM slot contains the signal pulse. Finally, the M bit word corresponding to the chosen slot is selected as the receiver output.
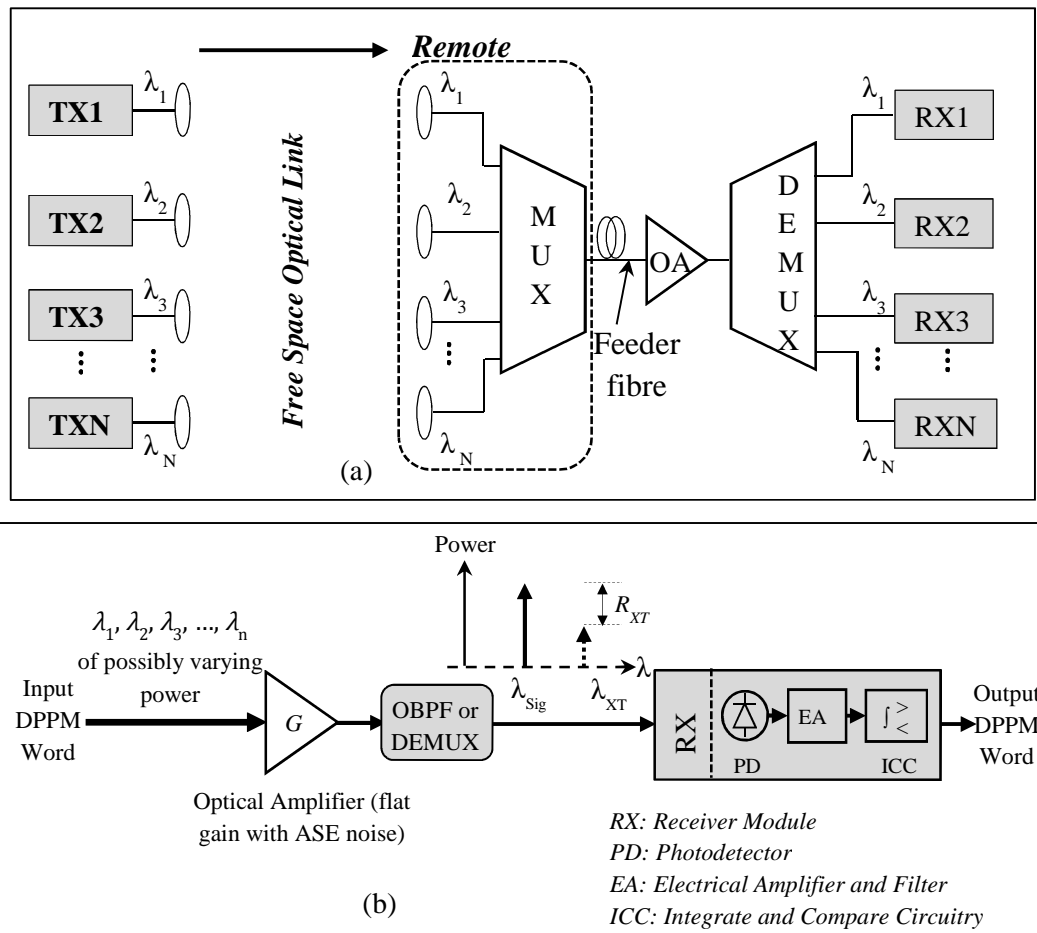
Fig. 5.1 Structure for optically preamplified WDM DPPM system: (a) Specific system architecture for crosstalk evaluation and (b) Generic receiver system

5.3 Crosstalk modelling

The analysis of crosstalk in a DPPM system requires some consideration to ensure that the different scenarios that could arise during frame reception are taken into account. For example, there may be an alignment of frames (and evidently slots) or only slots between the signal and crosstalk (XT) as shown in Figs. 5.2a and 5.2b respectively. The assumption of frame or slot alignment in this analysis is generally for mathematical convenience. However, in a practical system, it is more likely that there is a misalignment of slots (and evidently frames) between signal and crosstalk during signal reception (see Fig. 5.2c). In Fig. 5.2, the case where signal and crosstalk frames are aligned is referred to as FA (Fig. 5.2a), the case where the signal and crosstalk have only their slots aligned is referred to as OSA (Fig. 5.2b) while the case where there is a misalignment between the signal and crosstalk slots is referred to as SM (Fig. 5.2c). Consider Fig. 5.2, $\{n_1, n_2\} \in \mathbb{Z}$ (integer) are the number of whole slots in the earlier and later transmitted crosstalk frames that overlap the signal frame under consideration, while t_1 (or t_2) is the slot offset between the slots in a particular signal frame and the slots in the earlier (or later) transmitted crosstalk frame that overlap with the signal frame, also $t_2 = t_s - t_1$. Thus both t_1 and t_2 define the fractional or partial crosstalk that could affect the signal slots. Furthermore, in the case of both OSA and SM there is the possibility in some systems that the misalignment is maintained for a long time period and thus performance would be calculated for the specific misalignment. Equally in many realistic systems the misalignment will change sufficiently frequently that the proper evaluation approach is to average over all different (mis)alignments.
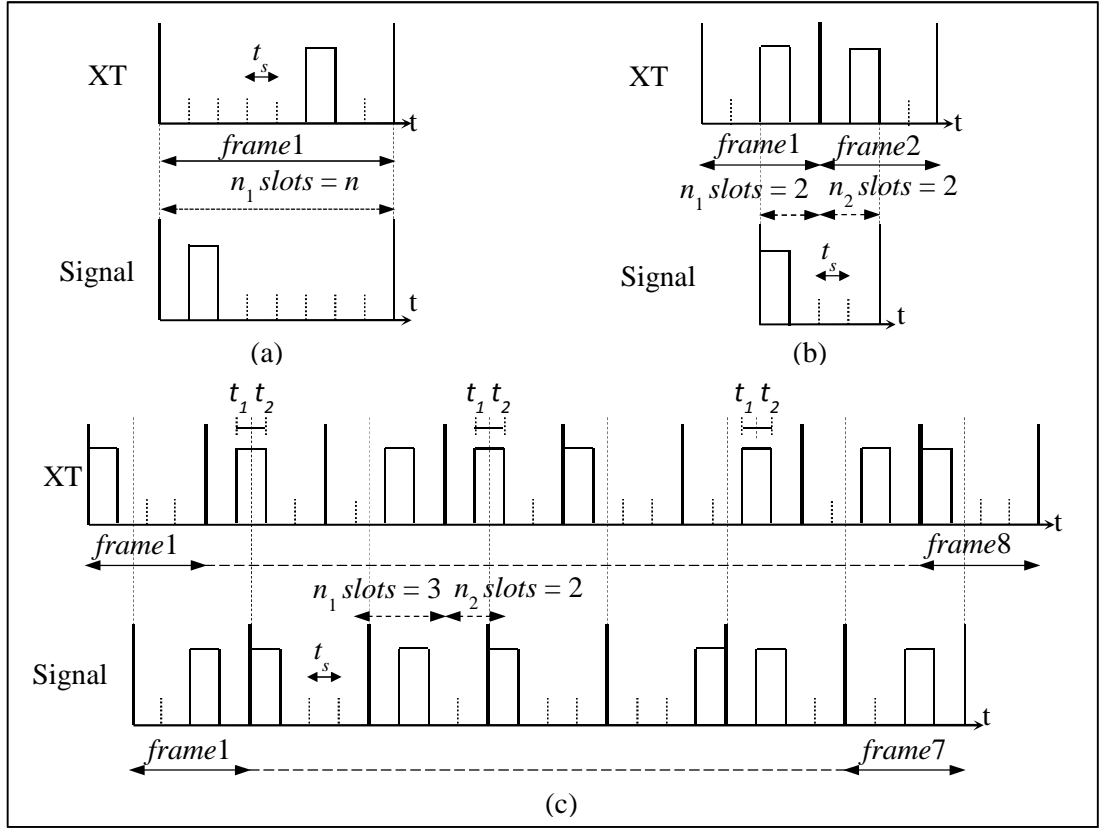
Fig. 5.2 Illustration of crosstalk in WDM DPPM receiver: (a) Frames aligned (FA) for $M = 3$, (b) Only slots aligned (OSA) for $M = 2$ and (c) Slots (and frames) misaligned (SM) for $M = 2$

The moment generating function (MGF) describing the random variable of the current $Y_{sig}(\Delta t)$ (where $sig \in \{0,1\}$ depending on pulse transmitted or not , Δt is the duration of the crosstalk pulse overlap with the slot under consideration) for a general slot which contains ASE, possibly a signal pulse and possibly a single XT pulse (or some fraction of one) is derived using the same treatment as [23, 27, 28]. It is written as:

$$M_{Y_{sig}(\Delta t)}(s) = \frac{\exp\left\{\dfrac{R^{'}G\left(e^{sq/t_s}-1\right)\int\limits_{t_s} sigP_{tr}(t)\,dt}{1-R^{'}N_o\left(e^{sq/t_s}-1\right)}\right\}\exp\left\{\dfrac{R_i^{'}G\left(e^{sq/t_s}-1\right)\int\limits_{\Delta t} P_{XT}(t)dt}{1-R_i^{'}N_{o\_XT}\left(e^{sq/t_s}\right)}\right\}}{\left[1-R^{'}N_o\left(e^{sq/t_s}-1\right)\right]^{L}} \qquad (5.1)$$

where $\Delta t = t_s$ if XT slots align with signal slots otherwise t_1 or t_2 , and for no crosstalk in the slot, $\Delta t = 0$. In addition, P_{tr} and P_{XT} are the DPPM rectangular

114

pulse and the crosstalk pulse power respectively, both defined at the photodetector input, $R^{'} = \eta/h\upsilon$, $R^{'}_i = \eta/h\upsilon_i$, η is the photodetector quantum efficiency, h is Planck's constant, υ and υ_i are the optical frequencies of the signal and crosstalk wavelengths respectively, q is the electron charge, $N_o = 0.5(NF \times G - 1)h\nu$ is the single polarisation ASE power spectral density (PSD) at the amplifier output (and also at the photodetector input if demultiplexer nominal loss is neglected), G and NF are the optical amplifier gain and noise figure respectively, $L = B_o m_t t_s$ is the product of spatial and temporal modes [2], B_o is the demux channel optical noise bandwidth and m_t is the number of ASE noise polarisation states. N_{o_XT} is the ASE PSD at the photodetector at crosstalk wavelength and $R_{XT} = P_{tr}/P_{XT}$ is the signal-to-crosstalk ratio, fixed at the output of the demux. The MGF has been modified to account for crosstalk–ASE beat noise assuming the crosstalk and the desired signal experiences the same ASE noise at the amplifier output [22]. The overall MGF including the zero mean Gaussian thermal noise is given as:

$$M_{X_{sig}(\Delta t)}(s) = M_{Y_{sig}(\Delta t)}(s) \exp\left(\frac{s^2 \sigma^2_{th-DPPM}}{2}\right) \tag{5.2}$$

where $\sigma^2_{th-DPPM}$ is the DPPM thermal noise variance.

Following [1, 2], the means and variances of the random variables representing the integration over the slot that contains only the signal pulse, only crosstalk pulse, both signal and crosstalk pulses and no pulses (i.e. empty slot) are derived from the overall MGF, through its first and second derivatives respectively, with s set equal to 0. They are respectively generally written as:

$$\mu_{X_{sig}(\Delta t)} = \frac{LR^{'}qN_o}{t_s} + R^{'}Gq\left(sigP_{tr} + \frac{P_{XT}\Delta t}{t_s}\right) \tag{5.3}$$

$$\sigma^2_{X_{sig}(\Delta t)} = \sigma^2_{th-DPPM} + \left(\frac{LR^{'}q^2 N_o(1 + R^{'}N_o)}{t_s^2}\right) + R^{'}Gq^2\left[(1 + 2R^{'}N_o)\frac{sigP_{tr}}{t_s}\right]$$
$$+ R^{'}_i Gq^2\left[(1 + 2R^{'}_i N_{o\_XT})\frac{P_{XT}\Delta t}{t_s^2}\right] \tag{5.4}$$

Given that each symbol has equal probability of being transmitted in a slot, the probability that a symbol is successfully received in the presence of crosstalk $P_{ws(l_i\_r_i)} = 1 - P_{we(l_i\_r_i)}$ where $P_{we(l_i\_r_i)}$ is the symbol error probability in the presence of crosstalk, r_i and l_i $(i \in \{s,1,2\})$ denote the number of crosstalk (of duration t_s, t_1

or t_2) occurring in the signal pulse slot and signal frame respectively. Thus for single crosstalk case, $r_i \in \{0,1\}$ while $l_i \in \{0,1,2\}$. Following the same treatment as [1], one can write that:

$$P_{ws(l_i - r_i)} \geq \prod_{\substack{j=1 \\ j \neq \text{sig slot}}}^{n} P(X_1(\Delta t) > X_j)\}$$
(5.5)

where X_j represents the content of the non-signal slot $X_0(\Delta t_j)$ and Δt_j is the crosstalk overlap with the jth (empty) slot.

Assuming that the random variables $X_1(\Delta t)$ and $X_0(\Delta t_j)$ are Gaussian, the expression $P\{X_0(\Delta t_j) > X_1(\Delta t)\}$ using the Gaussian approximation (GA) of the ASE beat noises, is of the general form [1, 2]

$$P\{X_0(\Delta t_j) > X_1(\Delta t)\} = 0.5 \, \text{erfc}\left(\frac{\mu_{X_1(\Delta t)} - \mu_{X_0(\Delta t_j)}}{\sqrt{2(\sigma_{X_1(\Delta t)}^2 + \sigma_{X_0(\Delta t_j)}^2)}}\right)$$
(5.6)

For the CB we have that the general form for random variable X and a fixed threshold ϑ is $P(X > \vartheta) \leq E\{\exp[s(X - \vartheta)]\}$, $s > 0$. Thus $P(X > \vartheta) \leq M_X(s)e^{-s\vartheta}$, and manipulation of this for the difference of two random variables implies that,

$$P\{X_0(\Delta t_j) > X_1(\Delta t)\} \leq M_{X_1(\Delta t)}(-s) M_{X_0(\Delta t_j)}(s) \qquad (s > 0)$$
(5.7)

For the MCB [2], $P(X > \vartheta) \leq M_X(s)e^{-s\vartheta} / s\sigma_{th}\sqrt{\pi}$. Modifying this inequality for the difference of two random variables for $X_0(\Delta t_j)$ and $X_1(\Delta t)$ which both have the same thermal noise contribution then yields,

$$P\{X_0(\Delta t_j) > X_1(\Delta t)\} \leq \frac{M_{X_1(\Delta t)}(-s) M_{X_0(\Delta t_j)}(s)}{2s\sigma_{th}\sqrt{\pi}} \qquad (s > 0)$$
(5.8)

Table 5.1: List of Probability Parameters

Notation	Description
ς, ς_1	Number of crosstalk pulses (from crosstalk sources with frames misaligned with signal frame) that occur in signal slot (ς) and empty slot (ς_1) of the signal frame.
$\ni$, $\ni_1$	Number of crosstalk pulses (from crosstalk sources with frames aligned with the signal frame) that occur in the signal slot ($\ni$) and empty slot ($\ni_1$) of the signal frame.
l_i	Number of full (l_s) or partial (l_1, l_2) crosstalk pulses occurring in the entire signal frame.
n_1, n_2	Number of full slots in the earlier (n_1) and later (n_2) transmitted crosstalk frames that overlap with the signal frame under consideration.
$p_{f(l_i)}(n_1)$	Probability of l_i (l_s, l_1 and/or l_2) crosstalk occurring in the signal frame when n_1 slots overlap that particular signal frame.
$p_{s(l_i)}(r_i)$	Probability of r_i (r_s, r_1 and/or r_2) crosstalk occurring in the signal pulse slot when l_i (l_s, l_1 and/or l_2) crosstalk occur in the signal frame.
$P_{we(l_i\_r_i)}$	Symbol error probability with l_i (l_s, l_1 and/or l_2) crosstalk in the signal frame and r_i (r_s, r_1 and/or r_2) crosstalk in the signal pulse slot.
r_i	Number of full (r_s) or partial (r_1, r_2) crosstalk pulse(s) occurring in the signal pulse slot.
t_1, t_2	Offset between the slots in a particular signal frame and the slots in the earlier (t_1) and later (t_2) transmitted crosstalk frame that overlaps with that signal frame.
Δt	Duration of crosstalk pulse overlap with a general slot.
Δt_j	Duration of the crosstalk overlap with the jth empty slot.

For the frames aligned (FA) and only slots aligned (OSA) cases the symbol error probability in the presence of a specific crosstalk combination is written as,

$$P_{we(l_s\_r_s)} \leq 1 - \left[1 - P\{X_0(0) > X_1(\Delta t)\} \right]^{n-1-(l_s-r_s)} \left[1 - P\{X_0(t_s) > X_1(\Delta t)\} \right]^{l_s-r_s} \qquad (5.9)$$

where l_s and r_s are the number of crosstalk of duration t_s occurring in the signal frame and signal pulse slot respectively, $\Delta t = t_s$ if crosstalk hits signal pulse slot, otherwise $\Delta t = 0$.

117

Similarly, the symbol error probability in the presence of crosstalk for the slot misaligned (SM) case is written as,

$$P_{we(l_1,l_2-r_1,r_2)} \leq 1 - \left[1 - P\{X_0(0) > X_1(\Delta t)\}\right]^{n-1-\chi}$$
$$\times \left[1 - P\{X_0(t_1) > X_1(\Delta t)\}\right]^{l_1-r_1} \left[1 - P\{X_0(t_2) > X_1(\Delta t)\}\right]^{l_2-r_2} \quad (5.10)$$

where l_1, l_2 and r_1, r_2 are the number of crosstalk of duration t_1, t_2 occurring in the signal frame and signal pulse slot respectively, $\chi = l_1 + l_2 - r_1 - r_2$, $\Delta t = t_1$ or t_2 if crosstalk of duration t_1 or t_2 respectively hits the signal pulse slot, otherwise $\Delta t = 0$. Note that in writing eq. (5.10) part crosstalk pulses are counted. So, for example, a whole crosstalk pulse in the frame will nevertheless count as a unit contribution to both l_1 and l_2 as shown in Fig. 5.2c. The list of probability parameters is shown in Table 5.1.

5.4 BER analysis (single crosstalk)

For a single interferer, only one crosstalk pulse can hit the signal slot or an empty slot, although more than one crosstalk pulse can impair the signal frame if there is a misalignment between the signal and crosstalk frames. Clearly, for FA and OSA, only a full crosstalk pulse with overlap duration $\Delta t = t_s$ may occur. Let $p_{f(l_s)}(n_1)$ denote the probability of l_s crosstalk pulses hitting the signal frame where n_1 is the number of whole slots in crosstalk frame 1 that overlap the signal frame. Additionally, let $p_{s(l_s)}(r_s)$ denote the probability of r_s out of l_s crosstalk pulses hitting the signal slot so that the probability that a full crosstalk pulse hits the signal pulse slot $p_{s(l_s)}(1) = l_s/n$ and the probability that full crosstalk pulse(s) hit an (unspecified) empty slot $p_{s(l_s)}(0) = (n-l_s)/n$. Furthermore, once there is slot misalignment (SM), any or both partial crosstalk pulse(s) with overlap durations $\Delta t = t_1$ and $\Delta t = t_2$ (where $t_s = t_1 + t_2$) could occur. Thus, $p_{f(l_1,l_2)}(n_1)$ denote the probability of l_1 and l_2 crosstalk pulses hitting the signal frame and $p_{s(l_1,l_2)}(r_1,r_2)$ denote the probability of r_1 out of l_1 and r_2 out of l_2 crosstalk pulses hitting the signal slot. In order to simplify the understanding of the BER calculation processes, a flowchart for the BER calculations has been included and is shown as Fig. 5.3 (for the SM case, the flowchart continues in Appendix A).
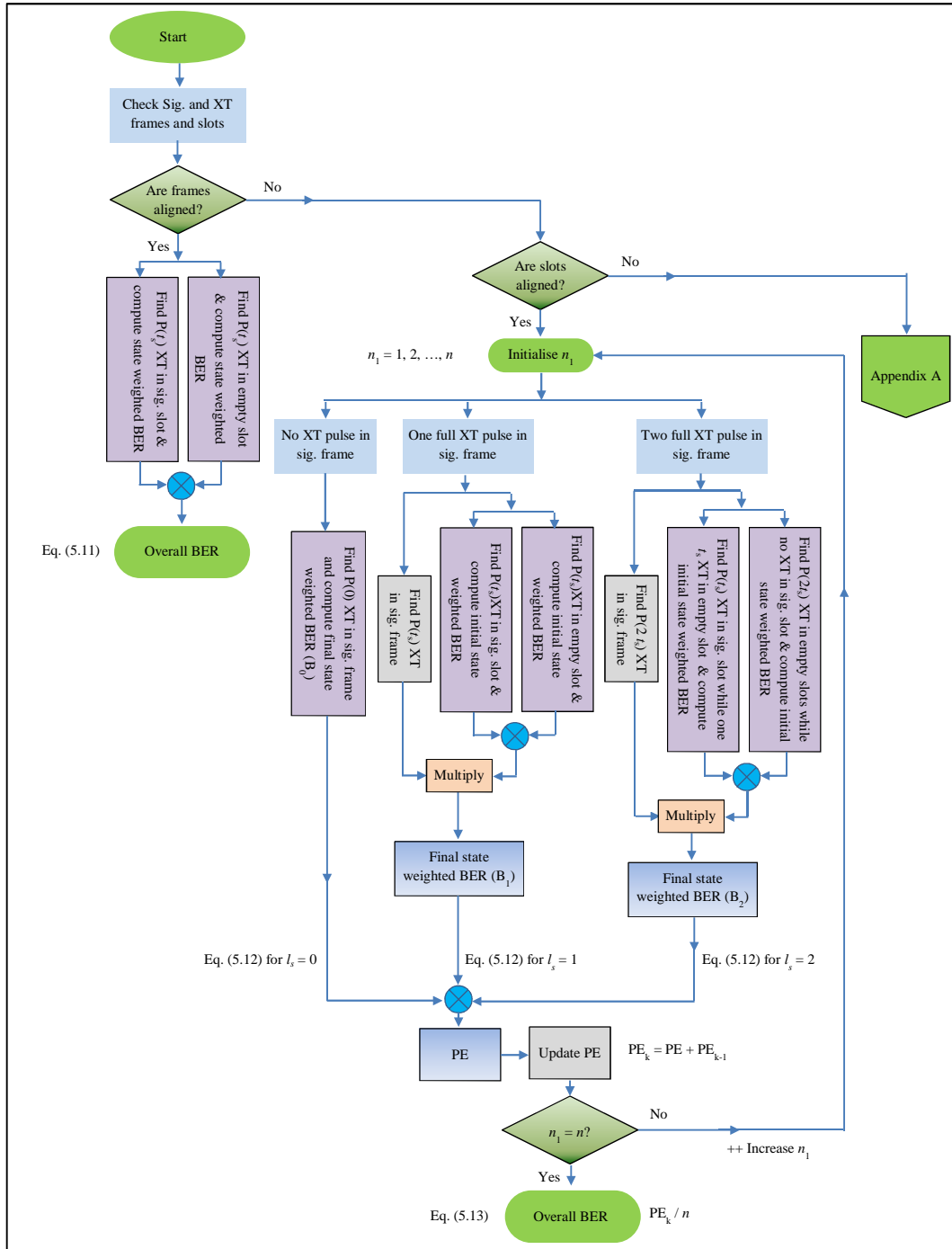
Fig. 5.3 Flowchart for BER calculations

5.4.1 Frames aligned (FA)

Since there is only one pulse in a frame, it may be seen in Fig. 5.2a that for FA only one full crosstalk pulse can impair the signal frame and $p_{f(1)}(n)=1$ (seen from the special case of $p_{f(1)}(n_1) = \left(n_1^2 + (n-n_1)^2\right)/n^2$ with $n_1 = n$ in OSA below). As every frame's pulse has equal likelihood of being in any slot, the probability that a

crosstalk pulse hits the signal slot for FA $p_{s(1)}(1) = 1/n$, and the probability that a crosstalk pulse hits an empty slot $p_{s(1)}(0) = (n-1)/n$. The overall BER in the presence of crosstalk for frames (and slots) aligned is given as [29],

$$BER = \frac{n}{2(n-1)} \left[p_{s(1)}(1)P_{we(1\_1)} + p_{s(1)}(0)P_{we(1\_0)} \right]$$ (5.11)

$P_{we(1\_1)}$ and $P_{we(1\_0)}$ are calculated from eq. (5.9) for $r_s = 1$ and 0 respectively

5.4.2 Only slots aligned (OSA)

Once there is a frame misalignment, it is possible for zero, one or two crosstalk pulses to impair the signal frame. Fig. 5.2b shows a typical example of how two crosstalk pulses from a single interferer can impair the signal frame, however, these two crosstalk pulses can only be in different slots in the signal frame as only one crosstalk can hit a slot for single crosstalk case. Typically, for $M = 2$, the crosstalk frame can possibly misalign with the signal frame by 1, 2 or 3 slots, or fully align with the signal frame (i.e. $n_1 = 1$, 2, 3 or 4 as shown in Fig. 5.4). Thus during signal frame reception, the interfering signal frame is also being received either in full alignment with the signal frame or misaligned by 1, 2 or 3 slots. And, although there is only one pulse in the interfering signal frame, the desired signal may be impaired by zero (Fig. 5.4, $n_1 = 1$), one (Fig. 5.4, $n_1 = 2$ and 4) or two (Fig. 5.4, $n_1 = 3$) crosstalk pulses depending on the position of the pulse in the interfering signal frame and the pattern of (mis)alignment with the desired signal frame.

Using Fig. 5.4, with $n_1 + n_2 = n$, the occurrence probabilities $p_{f(l_s)}(n_1)$ for the three different possibilities of a hit on the signal frame are found as $p_{f(0)}(n_1) = p_{f(2)}(n_1) = n_1(n-n_1)/n^2$ and $p_{f(1)}(n_1) = (n_1^2 + (n-n_1)^2)/n^2$. In addition, the bit error rate contributions for the different possibilities are conditional on n_1 and generally written as,

$$BER_{l_s}(n_1) = p_{f(l_s)}(n_1) \frac{n}{2(n-1)} \left[p_{s(l_s)}(1)P_{we(l_s\_1)} + p_{s(l_s)}(0)P_{we(l_s\_0)} \right]$$ (5.12)

where $l_s \in \{0,1,2\}$ and the no crosstalk symbol error probability $P_{we(0\_0)}$ is treated the same as in [1, 2]. $P_{we(l_s\_1)}$ and $P_{we(l_s\_0)}$ are calculated from eq. (5.9) for $r_s = 1$ and 0 respectively as in the FA case. However, since there could be two crosstalk

in the signal frame under OSA, the overall BER in the presence of crosstalk for only slots aligned is calculated by summing up all the error contribution calculated from eq. (5.12) for all values of l_s and the conditioning on n_1 is removed through averaging (assuming signal and crosstalk walking away from each other sufficiently fast). It is written as

$$BER = \frac{1}{n} \sum_{n_1=1}^{n} \sum_{l_s=0}^{2} BER_{l_s}(n_1) \qquad (5.13)$$
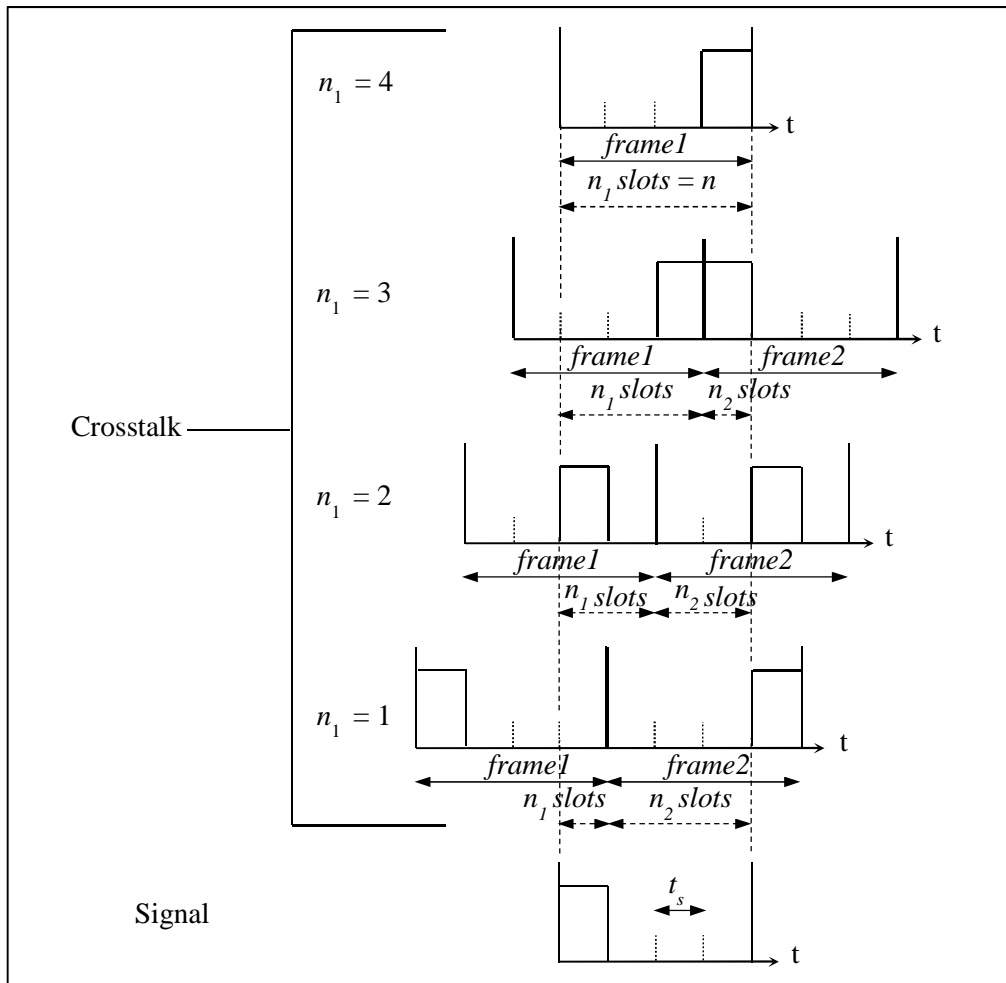
Fig. 5.4 Illustration of different frame misalignments between crosstalk and signal in DPPM WDM receiver for $M = 2$ under the OSA constraint, ($n_1 = 1$, 2, 3 and 4 are optional misalignment forms)

5.4.3 Slots misaligned (SM)

The number of different crosstalk combinations occurring in the signal frame increases with slot misalignment, with the detailed analysis becoming

complicated. Considering Fig. 5.2c, with $n_1 + n_2 = n + 1$ (note the difference to the
OSA case), there are seven different crosstalk distribution possibilities each with
different occurrence probability $p_{f(l_1,l_2)}(n_1)$ calculated from a given n_1
(contributing to the overall symbol error probability) regarding how much
crosstalk hits a frame as follows:

   i) *No crosstalk in the signal frame with probability*
   $p_{f(0,0)}(n_1) = (n_1 - 1)(n - n_1)/n^2$: e.g. as shown when the pulses in XT frame 5
   and frame 6 respectively occur before the signal frame 5 begins and after
   the signal frame 5 ends.

   ii) *Only one t_1 partial crosstalk pulse in the signal frame with probability*
   $p_{f(1,0)}(n_1) = (n_1 - 1)/n^2$: e.g. as shown when XT frame 2 pulse occurs at
   signal frame 1 end while the XT frame 1 pulse occurs before the start of
   signal frame 1.

   iii) *Only one t_2 partial crosstalk pulse in the signal frame with probability*
   $p_{f(0,1)}(n_1) = (n - n_1)/n^2$: e.g. as shown when XT frame 3 pulse occurs after
   signal frame 2 ends while the XT frame 2 pulse occurs at the start of signal
   frame 2.

   iv) *One each of t_1 and t_2 partial crosstalk pulse in the signal frame with
   occurrence probability* $p_{f(1,1)}(n_1) = ((n-1)^2 + 1) - (2(n_1 - 1)(n - n_1))/n^2$: e.g. as
   shown when XT frame 6 pulse occurs within signal frame 6. The other
   possibilities (not shown) are, (a) when XT frame 7 pulse occurs within
   signal frame 6 while XT frame 6 pulse occurs before the start of signal
   frame 6 and (b) where each of XT frames 6 and 7 contribute a part pulse at
   the start and end of signal frame 6 respectively.

   v) *One t_1 and two t_2 partial crosstalk pulses in the signal frame with
   probability* $(p_{f(1,2)}(n_1) = (n_1 - 1)/n^2)$: e.g. as shown when whole XT pulse
   from XT frame 5 occurs within signal frame 4 and XT frame 4 pulse
   occurs at the start of signal frame 4.

   vi) *Two t_1 and one t_2 partial crosstalk pulses in the signal frame with
   probability* $(p_{f(2,1)}(n_1) = (n - n_1)/n^2)$: e.g. as shown when whole XT pulse

from XT frame 3 occurs in signal frame 3 and XT frame 4 pulse occurs at the end of signal frame 3.

vii) *Two each of t_1 and t_2 partial crosstalk pulses in the signal frame with occurrence probability* $(p_{f(2,2)}(n_1) = (n_1 - 1)(n - n_1)/n^2)$: e.g. as shown when whole XT pulses from both XT frames 7 and 8 occur within signal frame 7.

Additionally, at the slot level for the SM, the probabilities that partial crosstalk pulses of duration $\Delta t = t_1$ and $\Delta t = t_2$ hit the signal slot are $p_{s(l_1,l_2)}(1,0) = l_1/n$ and $p_{s(l_1,l_2)}(0,1) = l_2/n$ respectively, and for a hit on empty slot, $p_{s(l_1,l_2)}(0,0) = (n - l_1 - l_2)/n$.
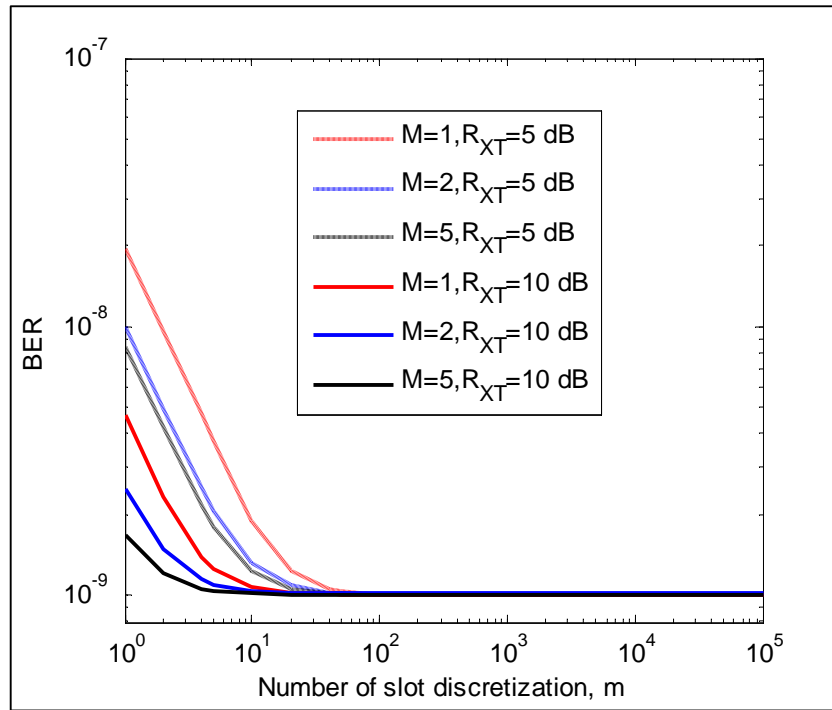
Fig. 5.5 BER as a function of number of slot discretization (*m*) for SM using MCB, $G = 27$ dB, for single crosstalk with received power corresponding to BER $= 10^{-9}$, (*m* is a dimensionless modelling artefact)

Assuming the slot is discretized into *m* small units of length $t_c = t_s/m$ such that the minimum slot offset equals t_c, then t_1 takes values from $\{t_c, 2t_c, 3t_c \dots mt_c\}$ where $t_1 + t_2 = t_s = mt_c$. As shown in Fig. 5.5, for values of $m \geq 100$, the target BER of 10^{-9} is achieved while the BER becomes worse for $m \leq 100$, especially for lower coding levels and higher crosstalk power. For definiteness, $m = 100$ is used in the calculations, as seen in Fig. 5.5, higher values of *m* do not show any significant

change on the BER, but rather increases the computational time. The OSA case is
recovered for $m = 1$, although a higher received power than those used in Fig. 5.5
would be required to attain the BER of 10^{-9}. Note that m is only a modelling
artefact introduced to facilitate the analysis for the SM case.

The bit error rate contribution when there is no crosstalk is written as,

$$BER(n_1) = p_{f(0,0)}(n_1) \frac{n}{2(n-1)} P_{we(0,0\_0,0)} \tag{5.14}$$

while for the other possibilities, it is generally written as :

$$BER_{l_1,l_2}(n_1) = \frac{1}{m} \sum_{t_1=t_c}^{t_s} p_{f(l_1,l_2)}(n_1) \frac{n}{2(n-1)}$$
$$\times \left\{ \begin{array}{l} \left[p_{s(l_1,l_2)}(1,0) P_{we(l_1,l_2\_1,0)} \right] + \left[p_{s(l_1,l_2)}(0,1) P_{we(l_1,l_2\_0,1)} \right] \\ + \left[p_{s(l_1,l_2)}(0,0) P_{we(l_1,l_2\_0,0)} \right] \end{array} \right\} \tag{5.15}$$

The no crosstalk symbol error probability $P_{we(0,0\_0,0)}$ is calculated the same as
$P_{we(0\_0)}$ in the SA case, and $l_1, l_2 \in \{0,1,2\}$ excluding the case where $(l_1, l_2) = (0,0)$.
The other symbol error probabilities $P_{we(l_1,l_2\_1,0)}$, $P_{we(l_1,l_2\_0,1)}$, and $P_{we(l_1,l_2\_0,0)}$ are
calculated using eq. (5.10) for $(r_1, r_2) =$ (1,0), (0,1) and (0,0).

The overall BER in the presence of crosstalk for slots misaligned is calculated
by summing up all the error contributions calculated from eqs. (5.14) and (5.15)
with the conditioning on n_1 removed by averaging. It is written as

$$BER = \frac{1}{n} \sum_{n_1=1}^{n} \left\{ BER(n_1) + BER_{0,1}(n_1) + BER_{1,0}(n_1) + \sum_{l_1=1}^{2} \left[BER_{l_1,1}(n_1) + BER_{l_1,2}(n_1) \right] \right\} \tag{5.16}$$

5.5 Single crosstalk results

The physical parameters used in the model are listed in Table 5.2. N_{o_XT} is
fixed by N_o/R_{XT} at the receiver with $R_{XT} > 1$, i.e. assuming that the crosstalk and
the accompanying ASE have been attenuated by the demultiplexer upon coupling
to the desired signal photodetector. The same data rate is assumed for both
crosstalk and signal. The DPPM thermal noise variance is back calculated using a
bandwidth expansion factor such that $\sigma_{th-DPPM}^2 = B_{exp} \sigma_{th-OOK}^2$ where $B_{exp} = 2^M/M$ is
the DPPM bandwidth expansion factor [30] and $\sigma_{th-OOK} = 7 \times 10^{-7}$ A is obtained
from a model of a PIN-FET receiver with $R_b = 2.5$ Gbps at BER of 10^{-12} assuming
a sensitivity of -23 dBm [21]. The demux (or OBPF) channel bandwidth is 76

GHz with 100 GHz adjacent channel spacing, this is about the same with those
seen in [31, 32] and will easily accommodate the slot rate of 45.7 GHz for
maximum DPPM coding level of $M = 7$ considered [2]. Typical values for
adjacent channel rejection ratio ranges from -20 dB to -30 dB [31-33], however in
the work presented in this chapter, the level of crosstalk (relative to signal at the
photodiode) which could be worsened by asymmetric demux input powers is
allowed to vary from negligible case of -30 dB to a very worse case of -5 dB and
the resulting crosstalk effect is calculated and shown for each case. A target BER
of 10^{-9} is considered for systems without forward error correction coding (FEC)
[34, 35], and 10^{-3} is considered for systems with FEC. Furthermore, the required
optical power is defined as the average power at the input of the optical amplifier
required to achieve the target BER.

Table 5.2: Physical parameters used for calculations

Parameters	Description	Value
R_b	binary data rate	2.5 Gbps
B_o	demux channel optical noise bandwidth	76 GHz
λ_{sig}	signal wavelength	1550 nm
η	receiver quantum efficiency	0.9 [36]
G	optical preamplifier gain	27 dB or 8 dB
NF	optical preamplifier noise figure	4.77 dB [2]
m_t	ASE noise polarisation states	2

Fig. 5.6 shows the single crosstalk BER curves using the MCB technique for
FA, OSA, SM and no crosstalk cases with signal-to-crosstalk ratios $R_{XT} = 10\,\text{dB}$
and $R_{XT} = 5\,\text{dB}$, and at coding levels $M = 1$ and $M = 5$. The curves for the GA and
CB techniques (not shown) are similar to the MCB, just offset by less than 0.3 dB
at a BER of 10^{-9}.

The BER for FA case is seen to exceed all other cases in all the methods considered and thus results in the worst case power penalty. The OSA BER coincides with the FA BER at $M = 5$, while the SM case produces the best BER curves at all coding levels. The similarity between the OSA and the FA (which also is a special and dominant subcase of the OSA, occurring at maximum overlap of a particular crosstalk frame with the signal frame) can be understood from the probabilities of the OSA crosstalk distribution. For example, at $n_1 = 1$ the OSA probabilities are dominated by the probability of one crosstalk hitting the signal frame $p_{f(1)} = (1 + (n-1)^2)/n^2 > (p_{f(0)} = p_{f(2)} = (n-1)/n^2)$. It is easily seen that as n gets larger, $p_{f(1)} \to 1$ while $p_{f(0)} = p_{f(2)} \to 0$ and OSA approximates to FA.
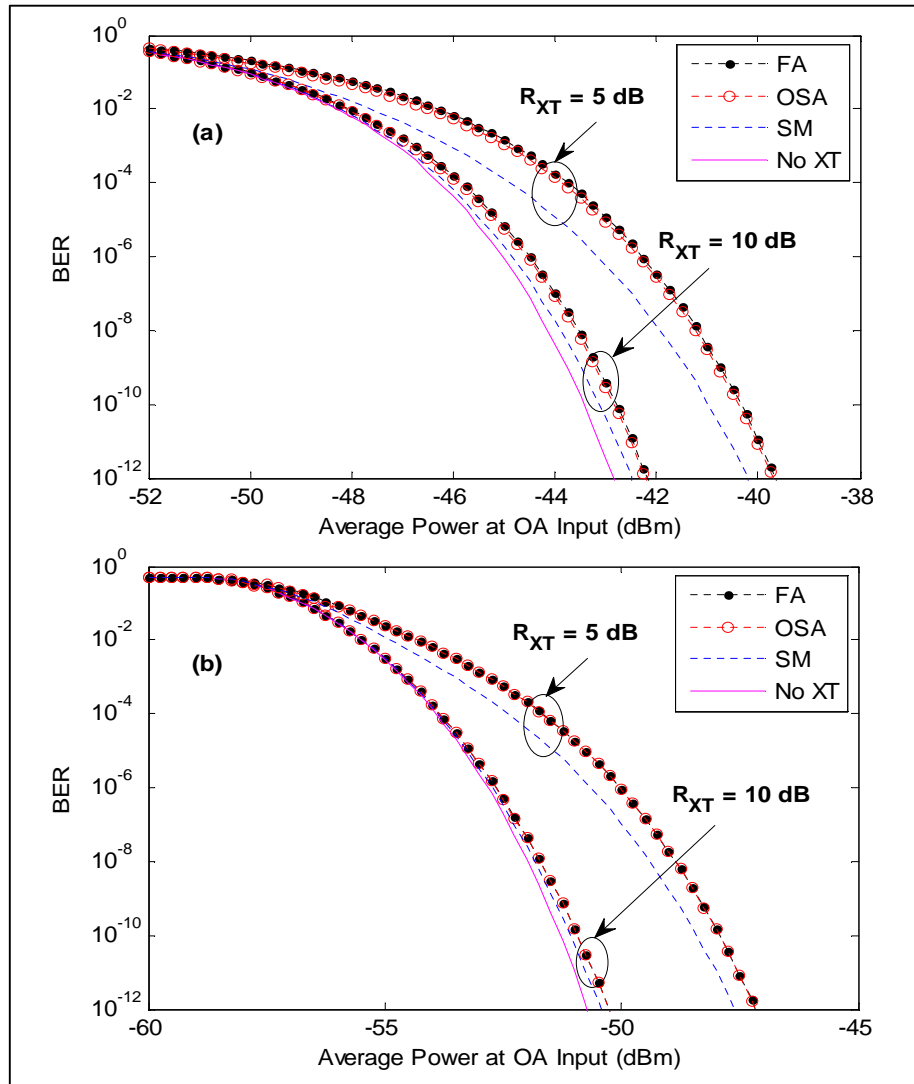
Fig. 5.6 BER against average power at OA input (dBm) using MCB, $G = 27$ dB, for single crosstalk with $R_{XT} = 10$ dB and 5 dB: (a) $M = 1$ and (b) $M = 5$

Fig. 5.7 shows a comparison of the GA, CB and MCB performance at low gain $G = 8$ dB and high gain $G = 27$ dB with a single crosstalk source and $M = 2$. The MCB coincides with the GA at low gain, but shifts close to the CB at high gain as the ASE noise reduces the significance of the thermal noise. The GA on the other hand is seen to exceed the CB and MCB (which are upper bounds) at high gain with no crosstalk and in the presence of crosstalk. The margin with which the GA exceeds the MCB and CB widens as the coding level and the noise equivalent bandwidth B_e of the DPPM receiver increases. This inconsistent behaviour of the GA is well reported for both OOK and DPPM systems [2, 27], but it has the advantage of being a simple and quick performance evaluation technique.
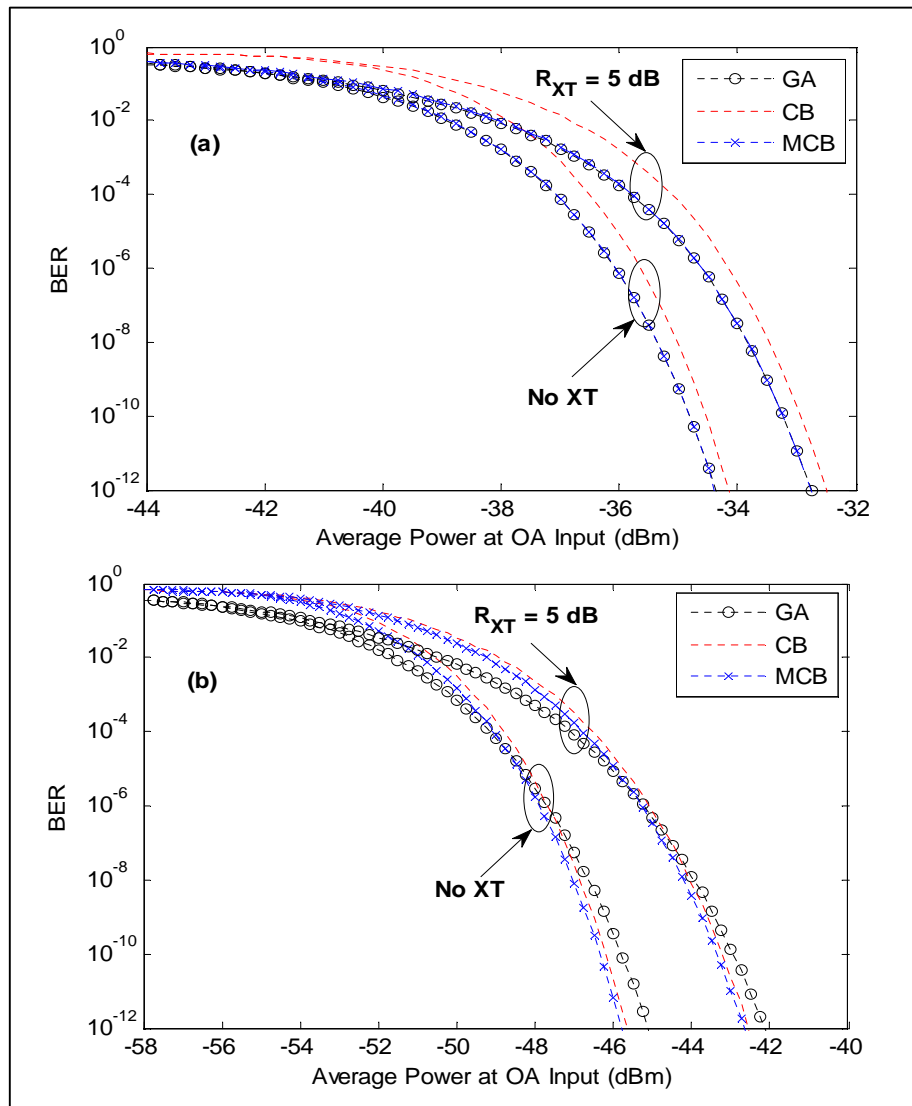
Fig. 5.7 BER against average power at OA input (dBm) using $M = 2$, for FA single crosstalk with $R_{XT} = 5$ dB: (a) $G = 8$ dB and (b) $G = 27$ dB

To further understand the single crosstalk system, consider Fig. 5.8 which shows the result of power penalty as a function of fixed misalignment. Each point in Fig. 5.8a presents the power penalty for the different fixed slot alignments (subcases) that is averaged to obtain the overall power penalty for the OSA case. The penalty at $n_1 = 8$ corresponds to the penalty for FA. The best performance for the fixed slot alignments is attained at $n_1 = 4$, this is because the probability of no crosstalk impairing the signal frame $p_{f(0)}(n_1)$ is highest for such misalignment. Fig. 5.8b presents the power penalty for fixed frame and slot misalignment SM and gives a better insight of a more practical system. The result highlights the importance of the averaging approach for realistic systems as recommended earlier. All the points in Fig. 5.8b are averaged to obtain the overall power penalty for the SM case as per eq. (5.16). The points along the n_1 axis at $t_1 = 1$ are the fixed slot alignment points and are the same as the result presented in Fig. 5.8a. The FA point occurs at $n_1 = 8$, $t_1 = 1$, and is seen to present the worst penalty. Optimum points also occur along the t_1 axis at $t_1 = 0.5$ and implicitly, at $t_2 = 0.5$. This is because the maximum power of either partial crosstalk i.e. $max\{P_{t_1}, P_{t_2}\}$ is lowest at that point. On the left of this optimum point, $t_2 > 0.5$ and on the right $t_1 > 0.5$. Thus, it is clearly seen that the impact of a single high power crosstalk is worse than that of many crosstalk of equivalent power. The result in Fig. 5.8 could be of practical importance in a non-dispersive channel like in free space where fixed misalignment may persist for a longer duration that averaging may not be required.

The remaining results for single crosstalk analysis are obtained assuming the FA case (which has just been shown as the worst case performance).
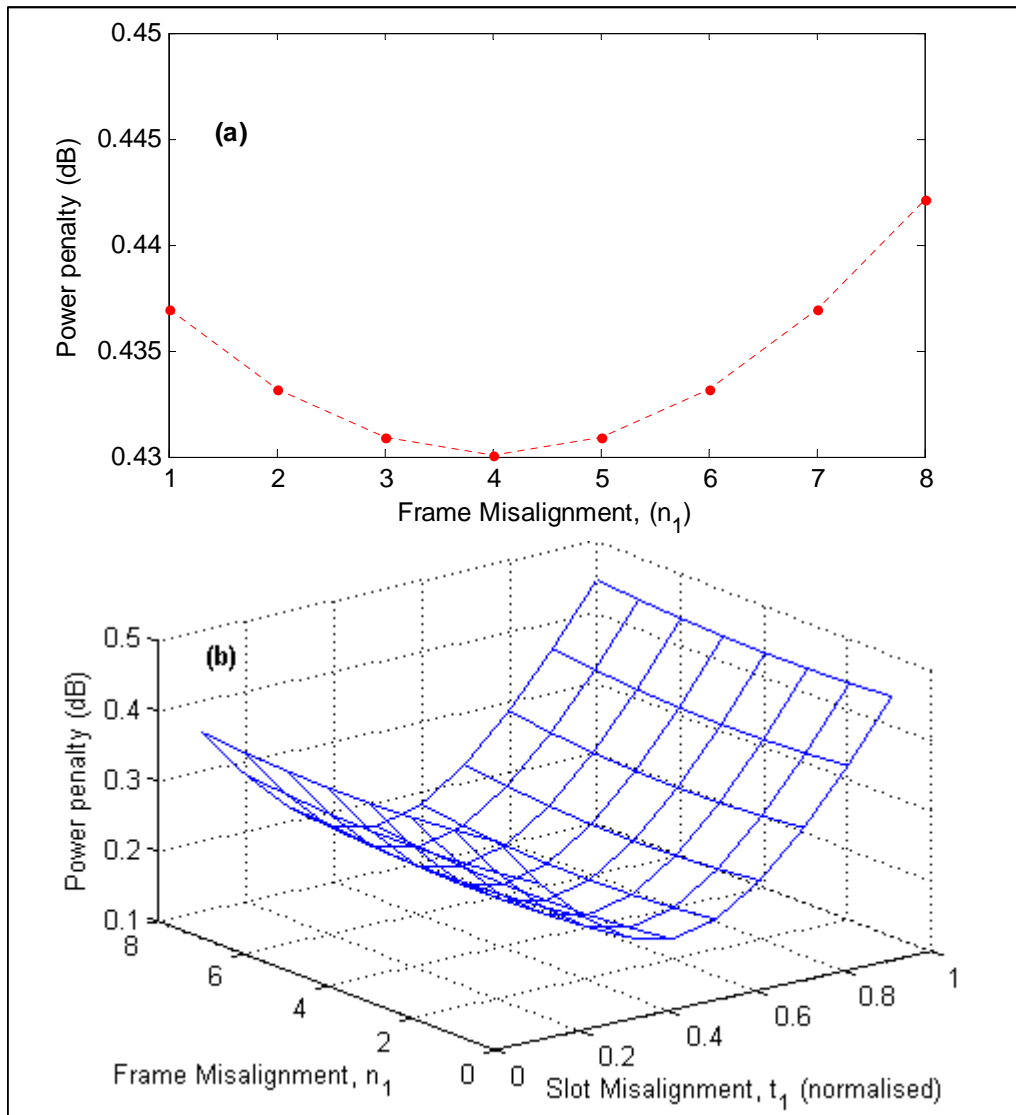
Fig. 5.8 Power penalty as a function of fixed misalignment using MCB (single crosstalk) for $M = 3$ and $R_{XT} = 10$ dB at BER = 10^{-9}: (a) Frame misalignment in OSA case and (b) Frame and slot misalignment in SM case

In Fig. 5.9, the result of the required signal power or power penalty as a function of DPPM coding level and signal-to-crosstalk ratio is shown using the MCB. The required signal power in Fig. 5.9a is seen to decrease as the coding level increases for all values of signal-to-crosstalk ratio, but at each coding level, the required signal power increases as the crosstalk power increases. The same pattern is also seen in Fig. 5.9b with the power penalty increasing as the crosstalk power increases for each coding level. The OOK power penalty at extinction ratio $r \to \infty$ coincides with the DPPM power penalty for $M = 1$ as shown in Fig. 5.9c. However, the DPPM becomes better than OOK as the coding level increases.
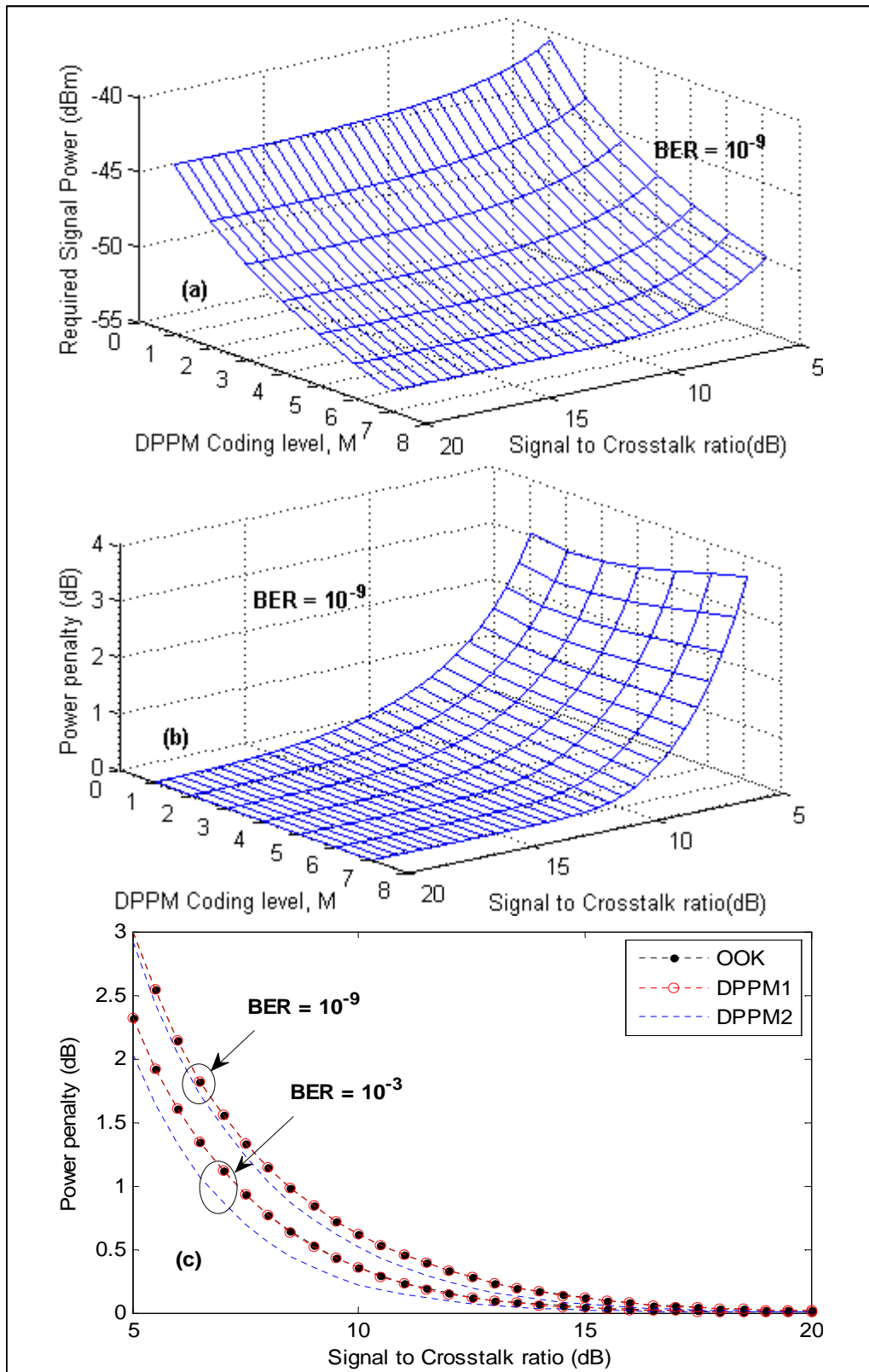
Fig. 5.9 Required signal power or Power penalty using MCB (FA single crosstalk): (a) Required signal power and (b) Power penalty as functions of both DPPM coding level and signal-to-crosstalk ratio, and (c) Power penalty versus signal-to-crosstalk ratio

5.6 BER analysis (multiple crosstalk)

5.6.1 General formulation

Under the constraint that the signal frames and crosstalk frames are aligned, the following derivation for multiple crosstalk holds for number of crosstalk pulses (N), number of slots (n) and number of crosstalk that hit signal slot ($v \in \{0,1,2,..., N\}$). Generally, the probability that for N crosstalk signals, v of them hit the signal slot while $d = N - v$ of them hit an empty slot is defined by the binomial:

$$p_s(N - v, v) = \binom{N}{v} \left(\frac{1}{n}\right)^v \left(\frac{n-1}{n}\right)^{N-v} \tag{5.17}$$

where $d = d_1, d_2, d_3, ..., d_{n-1}, \in \{1,2,3,..., N - v\}$ and $d_0 = 0$, occurring at the same time as v. The probability distribution of the d crosstalk that hit the empty slots are derived as follows, the probability that:

d_1 crosstalk constitute the first hit on empty slot

$$p_s(d_1|0) = \binom{N - v}{d_1} \left(\frac{1}{n-1}\right)^{d_1} \left(\frac{n-2}{n-1}\right)^{N-v-d_1} \left(\frac{n-1}{1}\right) \tag{5.18a}$$

d_2 crosstalk constitute the second hit on empty slot (i.e. given d_1 crosstalk hit the first empty slot)

$$p_s(d_2|d_1) = \binom{N - v - d_1}{d_2} \left(\frac{1}{n-2}\right)^{d_2} \left(\frac{n-3}{n-2}\right)^{N-v-d_1-d_2} \left(\frac{n-2}{2}\right) \tag{5.18b}$$

d_3 crosstalk constitute the third hit on empty slot (i.e. given d_1 and d_2 crosstalk hit the first and second empty slots respectively)

$$p_s(d_3|d_1, d_2) = \binom{N - v - d_1 - d_2}{d_3} \left(\frac{1}{n-3}\right)^{d_3} \left(\frac{n-4}{n-3}\right)^{N-v-d_1-d_2-d_3} \left(\frac{n-3}{3}\right) \tag{5.18c}$$

Thus the probability that for $d = N - v$ crosstalk, d_1 crosstalk constitute the first hit on empty slot and d_2 crosstalk constitute the second hit on empty slot and d_3 crosstalk constitute the third hit on empty slot is equal to the product of eqs. (5.18a), (5.18b) and (5.18c).

Without loss to generality, and for $N \geq 2$ and $n - 1 \geq g \leq N - v$, one can write that, if $u \in \{1, 2, 3, ..., g\}$ represents the $\{1^{st}, 2^{nd}, 3^{rd}, ..., g_{th}\}$ hit on empty slot, and $d = \{1,2,3,..., N - v\}$ constitute the number of crosstalk involved in a hit on empty

slot, then d_u defines the number of crosstalk pulse(s) involved in the u_{th} hit on an empty slot. Therefore the probability of d_1 crosstalk being the 1st hit on an empty slot is the same as eq. (5.18a) and can be rewritten as

$$p_s(d_1|0) = \binom{N-v}{d_1} \left(\frac{1}{n-1}\right)^{d_1} \left(\frac{n-(1+1)}{n-1}\right)^{N-v-d_1} \binom{n-1}{1} \qquad (5.19)$$

Generalizing, the probability that d_u crosstalk pulse(s) is the u_{th} hit on an empty slot (i.e. given $d_1, d_2, d_3, ..., d_{u-1}$ crosstalk pulse(s) are already involved in hit on other empty slots) is written as:

$$p_s\left(d_u|d_1, d_2, d_3, ..., d_{u-1}\right) = \binom{N - v - \sum_{t=1}^{u} d_{t-1}}{d_u} \left(\frac{1}{n-u}\right)^{d_u} \left(\frac{n-(u+1)}{n-u}\right)^{N-v-\sum_{t=1}^{u} d_t} \frac{n-u}{u} \qquad (5.20)$$

Consequently, the probability that $d_1, d_2, d_3, ..., d_g$ crosstalk pulse(s) are the $1^{st}, 2^{nd}, 3^{rd}, ..., g_{th}$ hit on the empty slots respectively is written as

$$p_s((d_1|0), (d_2|d_1), (d_3|d_1, d_2), ..., (d_g|d_1, d_2, d_3, ..., d_{g-1})) =$$
$$\frac{(N-v)!}{k_1! k_2! k_3! ... k_{N-v}!} \prod_{u=1}^{g} p_s(d_u|d_1, d_2, d_3, ..., d_{u-1}) \qquad (5.21)$$

where k_i is the number of empty slots hit by i crosstalk pulse(s).

Finally, the probability that $d_1, d_2, d_3, ..., d_g$ crosstalk pulse(s) are the $1^{st}, 2^{nd}, 3^{rd}, ..., g_{th}$ hit on the empty slots respectively, and v crosstalk pulse(s) hit the signal slot is written as

$$p_s(d_1, d_2, d_3, ..., d_g, v) = p_s(N-v, v)$$
$$\times \left(\frac{(N-v)!}{k_1! k_2! k_3! ... k_{N-v}!}\right) \prod_{u=1}^{g} p_s(d_u|d_1, d_2, d_3, ..., d_{u-1}) \qquad (5.22)$$

The term $\left(\dfrac{(N-v)!}{k_1! k_2! k_3! ... k_{N-v}!}\right)$ accounts for the order of the hit on empty slots (i.e. assuming the position of the empty slots with the hits by crosstalk is shuffled), and since all the crosstalk have equal power, the denominator in the term accounting for the indistinguishability of some hits.

The multiple crosstalk probability distribution analysis performed above ignores empty slots with no crosstalk, and hence considers only the distribution of crosstalk in empty slots with at least one crosstalk. The advantage of this method of analysis is that the distribution could be calculated for any DPPM coding level

(i.e. any value of M). However, it becomes more difficult to calculate as the number of crosstalk (N) increases since it requires identifying at least all the ways the crosstalk that missed the signal slot could hit the empty slots disregarding the order and with repetition. This difficulty however is somewhat reduced because empty slots are not considered, thus limiting the number of ways required to be found for N crosstalk.

An alternative way of performing the multiple crosstalk probability distribution analysis is by the use of multinomial. This method facilitates the calculation of all the likely distribution of crosstalk including slots with no signal or crosstalk pulse. However, it becomes more difficult and computationally intensive as the DPPM coding level increases. For example, for $M = 2$ (i.e. $n = 4$), eq. (5.22) can simply be written as,

$$p_s dist = p_s(N-v,v) \; p_s(d_1,d_2,d_3) \tag{5.23}$$

where d_1, d_2 and d_3 are the contents of non-signal slots 1,2 and 3 respectively, $d_3 = N - v - d_1 - d_2$ and

$$p_s(d_1,d_2,d_3) = \binom{N-v}{d_1,d_2} \left(\frac{1}{n-1}\right)^{N-v} \tag{5.24}$$

where $\binom{N-v}{d_1,d_2} = \dfrac{(N-v)!}{d_1!d_2!(N-v-d_1-d_2)!}$.

Thus the general formula for the multiple crosstalk distribution for any value of M can be written as,

$$p_s dist = p_s(N-v,v) \; p_s(d_1,d_2,d_3,...,d_{n-1}) \tag{5.25}$$

where,

$$p_s(d_1,d_2,d_3,...,d_{n-1}) = \binom{N-v}{d_1,d_2,d_3,...,d_{n-1}} \left(\frac{1}{n-1}\right)^{N-v} \tag{5.26}$$

Calculating eq. (5.25) just for $M = 3$ (i.e. $n = 8$) is computationally intensive even for low values of N.

With the probability distribution known, all that remains is to sum up all the BER contribution under each distribution of crosstalk weighted by the probability of occurrence for each distribution.

Under the constraint of slot or frame misalignment, the derivation of the probability of crosstalk distribution for N crosstalk signals arising from different wavelength channels in the system could be more complex than the above derivation for FA. It will require examining the content of each slot under every possible misalignment of slots and/or frame for all the crosstalk in order to determine their occurrence probabilities and symbol error probability contributions. However, the possibility of all frames aligning (FA) (acceptable as argued previously for a single crosstalk) becomes less likely with increasing N such that imposing such constraint may overestimate the BER or power penalty for large N values. The approach with only slots aligned (OSA) seems to be the most sensible for multiple crosstalk (at least for low values of M), as it is also much quicker than the SM approach, and is considered below for $M \leq 2$.

5.6.2 Specific cases ($M = 1$ and $M = 2$)

The multiple crosstalk analysis below is considered for coding levels $M = 1$ and $M = 2$, which are more practical cases for WDM DPPM systems and the analysis is facilitated by the GA for computational ease. The probabilities for the OSA approach have been validated by Monte Carlo simulation and are presented analytically only for $M = 1$. For simplicity, the probability of crosstalk distribution for $M = 2$ is generated by Monte Carlo simulation. The steps for the Monte Carlo simulations are detailed in Appendix B. All the crosstalk pulses are assumed to have equal power. This is the case when there is symmetry in the transmission link. Alternatively, when the crosstalk power in individual wavelengths are different or there is a single dominant crosstalk in the system it may be more convenient to add all the interfering crosstalk power together and treat the equivalent crosstalk power as if it is from a single wavelength using the single crosstalk model discussed earlier. This at least provides an upper bound for the crosstalk power penalty.

5.6.2.1 Frames aligned (FA)

Under FA and for $M = 1$, there are only two slots in the frame and crosstalk pulses can either hit the signal slot or the empty slot. The probability that for N crosstalk signals, v of them hit the signal slot while $d = N - v$ of them hit an empty slot is defined by the binomial,

$$p_s(v,d) = \binom{N}{v} \left(\frac{1}{2}\right)^v \left(\frac{1}{2}\right)^d \tag{5.27}$$

and the overall BER in the presence of N crosstalk pulses for $M = 1$ is written as:

$$BER = \frac{n}{2(n-1)} \sum_{v=0}^{N} p_s(v,d) \left[1 - \{1 - P(X_0(dt_s) > X_1(vt_s))\} \right] \tag{5.28}$$

In addition, for $M = 2$, the probability distribution of crosstalk between the signal slot and the three empty slots is a binomial while the distribution of crosstalk within the three empty slots is a trinomial. The total probability distribution is a product of the binomial and trinomial distributions, written as:

$$p_s(v,d_1,d_2,d_3) = \binom{N}{v} \frac{(N-v)!}{d_1!d_2!d_3!} \left(\frac{1}{4}\right)^v \left(\frac{1}{4}\right)^{N-v} \tag{5.29}$$

and the overall BER in the presence of N crosstalk pulses for $M = 2$ is written as:

$$\begin{aligned} BER = \frac{n}{2(n-1)} \sum_{v=0}^{N} \sum_{d_1,d_2,d_3=0}^{d} &\ p_s(v,d_1,d_2,d_3) \\ &\times \begin{bmatrix} 1 - \{1 - P(X_0(d_1 t_s) > X_1(vt_s))\} \\ \{1 - P(X_0(d_2 t_s) > X_1(vt_s))\} \{1 - P(X_0(d_3 t_s) > X_1(vt_s))\} \end{bmatrix} \end{aligned} \tag{5.30}$$

where d_1, d_2, d_3 are the number of crosstalk in empty slot 1, 2, 3 respectively, and $d_3 = N - v - d_1 - d_2$. $X_0(d_z t_s)$ and $X_1(vt_s)$ are the random variables for empty slot z hit by d crosstalk pulses and signal slot hit by v crosstalk pulses respectively.

5.6.2.2 Only slots aligned (OSA)

The simplest method to generate the probability distribution of multiple crosstalk for the OSA case is by simulation, but for completeness, the analytical method is presented for $M = 1$. With the OSA constraint, there is a chance that all, some, or no crosstalk frames align with the signal.

For $M = 1$, and considering N crosstalk with f frames aligned with the signal frame, the total probability that v and d crosstalk pulses hit the signal slot and empty slot of the signal frame respectively is written as,

$$p_s(v,d|f) = \frac{1}{n^N} \binom{N}{f} \binom{f}{\ni} \binom{N-f}{\varsigma} \binom{N-f}{\varsigma_1} \left(\frac{1}{2}\right)^f \left(\frac{1}{2}\right)^{2(N-f)} \tag{5.31}$$

where $v = \ni + \varsigma$ and $d = \ni_1 + \varsigma_1$. $\ni$ and $\ni_1 = f - \ni$ are the number of crosstalk pulses from crosstalk with frames aligned with the signal frame that hit the signal slot and the empty slot in the signal frame respectively while ς and ς_1 are the number of crosstalk pulses from crosstalk with frames misaligned with the signal frame

that hit the signal slot and the empty slot in the signal frame respectively. In deriving the crosstalk distribution in eq. 5.31, we have considered that crosstalks with frames misaligned with the signal frame are each made up of an earlier transmitted frame (frame 1) and a later transmitted frame (frame 2) both overlapping the signal frame. Given that both crosstalk frame 1 and frame 2 are independent and that the overlap is symmetrical between the two slots of the signal frame, the distribution from crosstalk frame 1 and frame 2 on the signal frame have been treated as two independent binomial contributions, each with $(N - f)$ number of crosstalks involved in the process. The overall BER in the presence of N crosstalk pulses for $M = 1$ is written as:

$$BER = \frac{n}{2(n-1)} \sum_{f=0}^{N} \sum_{\ni=0}^{f} \sum_{\varsigma,\varsigma_1=0}^{N-f} p_s(v,d|f) \left[1 - \{1 - P(X_0(dt_s) > X_1(vt_s))\} \right] \qquad (5.32)$$

5.7 Multiple crosstalk results

Except where stated otherwise, the same physical parameters used for the single crosstalk model are maintained for the multiple crosstalk model (Table 5.2). In addition, the signal to crosstalk ratio R_{XT} as used in the multiple crosstalk results refers to signal to single crosstalk ratio, arising as it does typically from the demultiplexer crosstalk rejection. The OOK model follows the same model for multiple crosstalk sources in [20] and with perfect extinction ratio assumed (so that any advantage of DPPM is not overstated).

An example BER result obtained using the general formulation under the assumption of FA is shown in Fig. 5.10a for $M \leq 7$ and for $N \leq 5$, with signal to crosstalk ratio of 5 dB (possible in the case of asymmetric losses between the user transmission paths). As generally expected, the BER performance worsens with increasing number of crosstalk sources, and improves as the coding level increases. In Fig. 5.10b, the DPPM BER performance is shown to be better than OOK in the presence of multiple crosstalk sources. The DPPM BER results obtained under the FA assumption for 30 and 50 crosstalk sources are seen to be close to the BERs obtained using the crosstalk distributions facilitated by Monte Carlo simulations. By this result, and considering that most practical WDM systems consist of about 32 to 64 channels, we can infer that the FA assumption gives a good approximation of the BER.
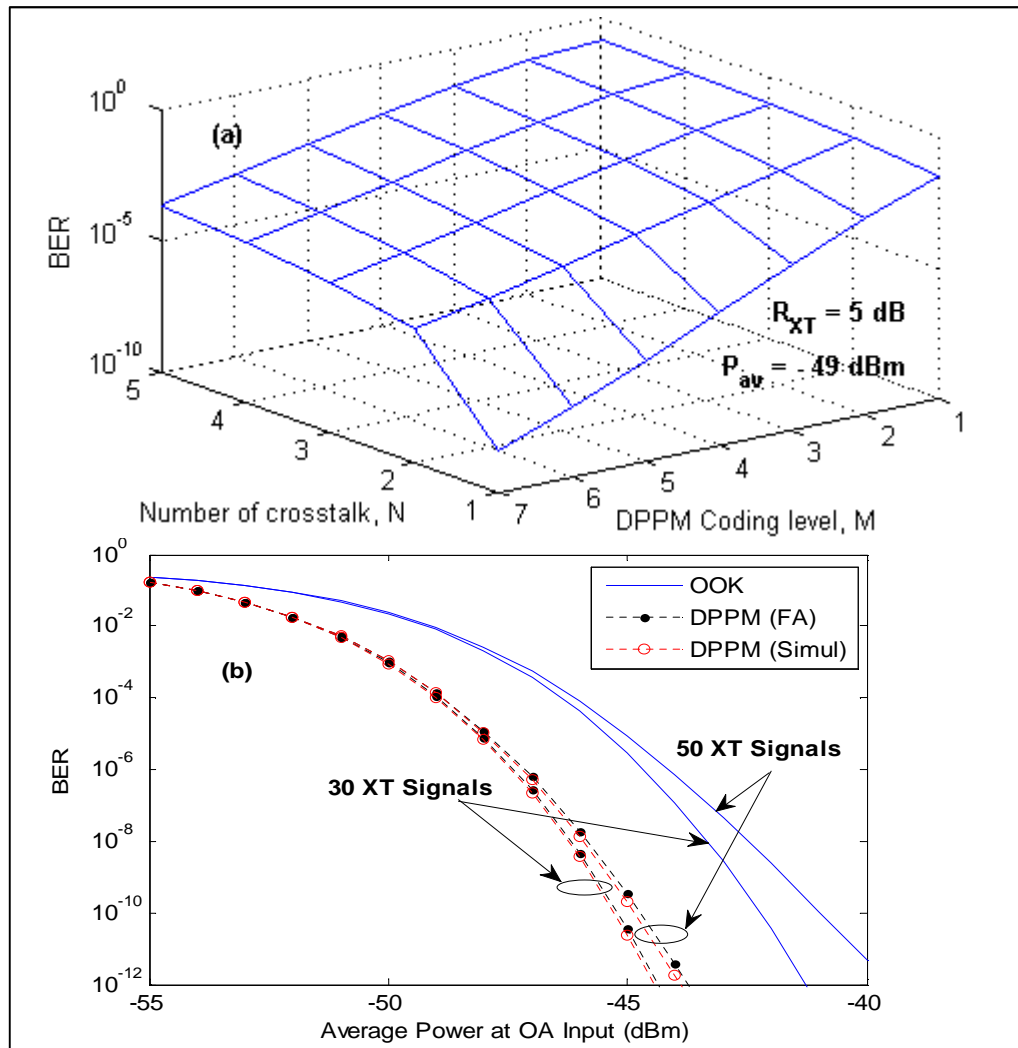
Fig. 5.10 Multiple crosstalk BER plots: (a) BER as a function of number of crosstalk N and coding level M for DPPM (FA) and (b) BER against average power at OA input for OOK and DPPM at $M = 2$ (1000000 Monte Carlo trials)

The result of DPPM power penalty analyses for multiple crosstalk for $M = 1$ and $M = 2$ is compared with power penalty for OOK in Fig. 5.11 for target BER of 10^{-9}. Clearly, DPPM predicts a reasonable penalty which is less than the OOK penalty for multiple crosstalk, even at low coding levels. The DPPM improvement in power penalty becomes better as the number of crosstalk sources increases and as the coding level increases from $M = 1$ to $M = 2$. In Fig. 5.11c, the FA is compared with OSA and simulation for $M = 1$ and only simulation for $M = 2$. Although the FA seems to overestimate the power penalty, the approximation gets better for $M = 2$. Additionally, it is computationally quicker than the other approaches and provides an upper bound for the system. These same trends in Fig. 5.11 are seen in Fig. 5.12, but with lower power penalties predicted for 10^{-3}. This

result is particularly of interest to modern high-sensitivity optical systems where
FEC is commonly used.
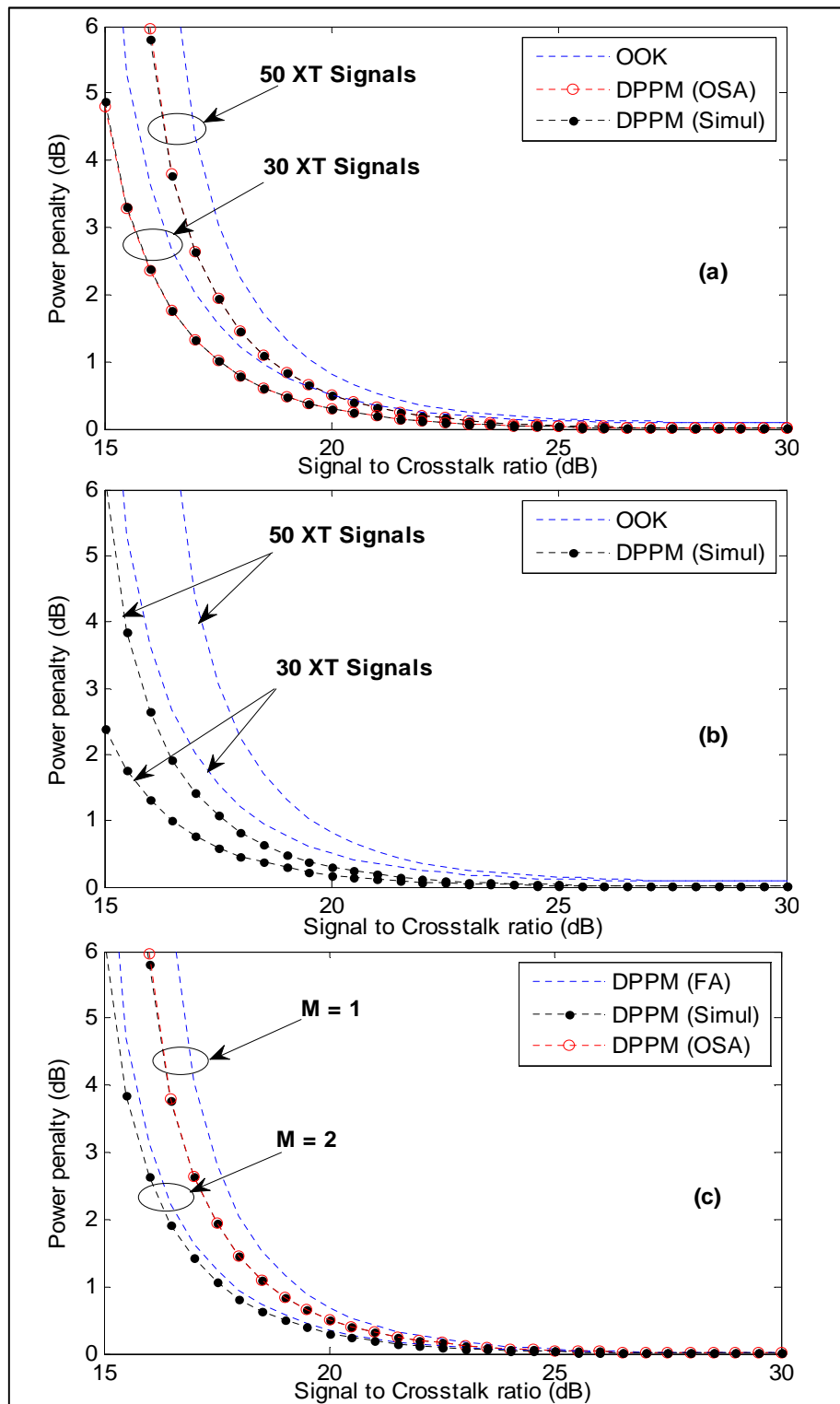
Fig. 5.11 Power penalty against Signal-to-crosstalk ratio for OOK and DPPM
(multiple crosstalk OSA and Simulation) at BER = 10^{-9}: (a) $M = 1$ (b) $M = 2$ and
(c) DPPM FA compared with OSA and/or Simulation (50 XT Signals)
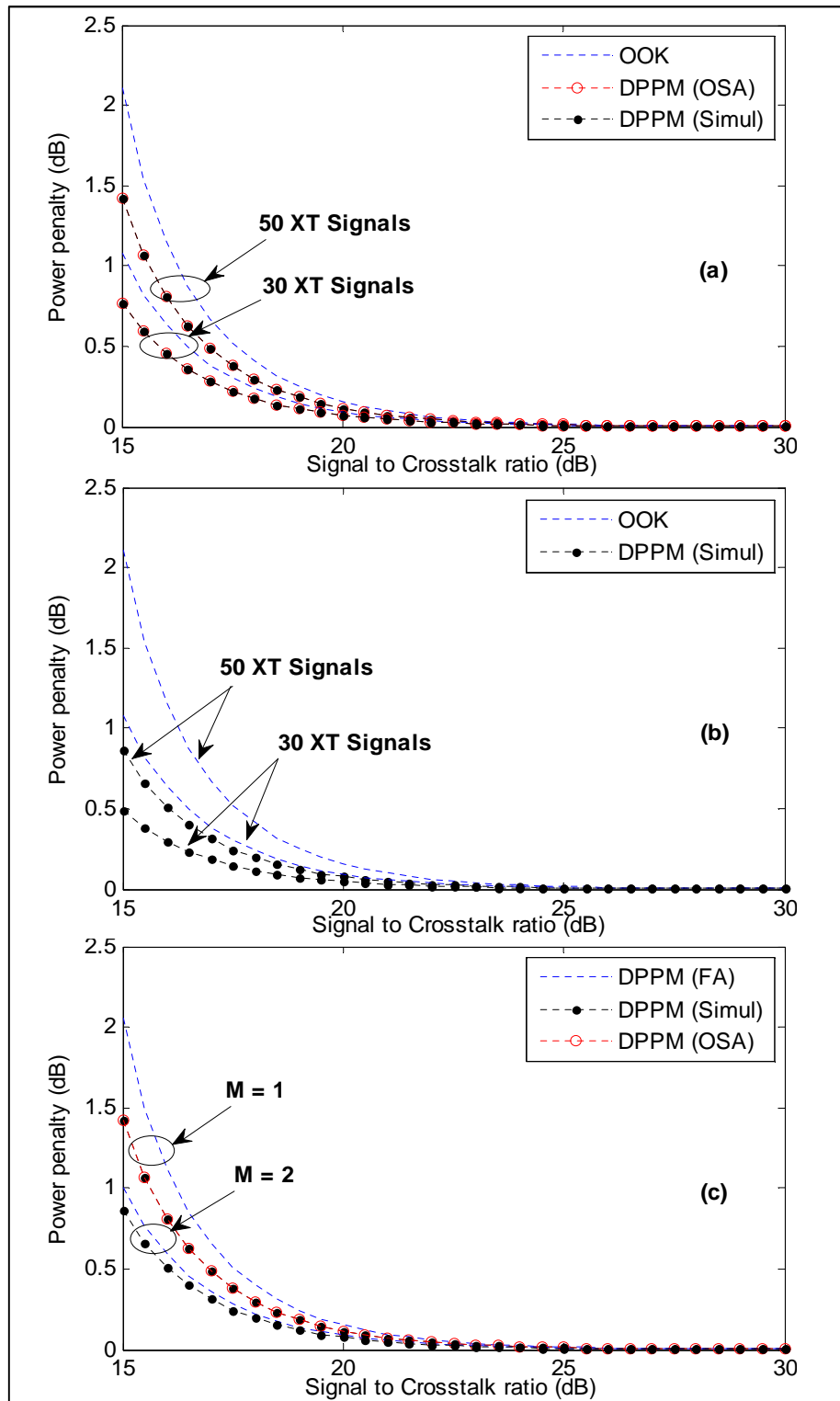
Fig. 5.12 Power penalty against Signal-to-crosstalk ratio for OOK and DPPM (multiple crosstalk OSA and Simulation) at BER = 10^{-3}: (a) $M = 1$ (b) $M = 2$ and (c) DPPM FA compared with OSA and/or Simulation (50 XT Signals)

5.8 Summary

Analyses of crosstalk for optically preamplified WDM DPPM systems are performed for the first time using the GA, CB and MCB. The FA case is found to marginally present the worst power penalty. However the accuracy penalty is justified by a significant reduction in calculation complexity. For multiple crosstalk, the probability distribution of the crosstalk is easily obtained using Monte Carlo simulation. However for a fixed coding level, it is possible to analytically find the probability distribution of crosstalk in the signal frame by considering all the different multinomial contributions from every possible combination of aligned and misaligned crosstalk frames. The approach using the OSA assumption predicts a sensible penalty compared to the approach with FA assumption and hence presents a better representation of a practical system. Furthermore, the MCB is recommended as the safest method of evaluation as it presents a tighter upper bound than the CB and is more sensitive to the optical amplification, though the GA is computationally quicker. The DPPM coding level $M = 2$ is a likely option for WDM DPPM free space and wireless systems because of its sensitivity improvement for a small bandwidth expansion over OOK, and when crosstalk is present this is further benefited by a reduced power penalty relative to OOK. With the model developed and the analysis performed in this chapter, we are a step closer to evaluating the performance of a full WDM DPPM network with hybrid fibre and turbulent FSO links. The combined effect of interchannel crosstalk and atmospheric turbulence in such a network is the topic of the next chapter.

5.9 References

1. Phillips, A. J., Cryan, R. A., Senior, J. M.: 'An optically preamplified intersatellite PPM receiver employing maximum likelihood detection'. *IEEE Photonics Technol. Lett.,* 1996, **8**, (5), pp. 691-693
2. Aladeloba, A. O., Phillips, A. J., Woolfson, M. S.: 'Performance evaluation of optically preamplified digital pulse position modulation turbulent free-space optical communication systems'. *IET Optoelectron.,* 2012, **6**, (1), pp. 66-74
3. Ohtsuki, T.: 'Performance analysis of indoor infrared wireless systems using PPM CDMA'. *Electronics and Commun. in Japan* 2002, **85**, (1), pp. 1-10
4. Leeson, M. S.: 'Pulse position modulation for spectrum-sliced transmission'. *IEEE Photonics Technology Letters, ,* 2004, **16**, (4), pp. 1191-1193
5. Miyazawa, T., Sasase, I.: 'BER Performance Analysis of Spectral Phase-Encoded Optical Atmospheric PPM-CDMA Communication Systems'. *J. Lightw. Technol.,* 2007, **25**, (10), pp. 2992-3000
6. Garrett, I.: 'Pulse-Position Modulation for Transmission Over Optical Fibers with Direct or Heterodyne Detection'. *IEEE Trans. Commun.,* 1983, **31**, (4), pp. 518-527
7. Phillips, A. J., Cryan, R. A., Senior, J. M.: 'Optically preamplified pulse-position modulation for fibre-optic communication systems'. *IEE Proc. - Optoelectron.,* 1996, **143**, (2), pp. 153-159
8. Liu, X., Chandrasekhar, S., Wood, T. H., Tkach, R. W., Winzer, P. J., Burrows, E. C., Chraplyvy, A. R.: 'M-ary pulse-position modulation and frequency-shift keying with additional polarization/phase modulation for high-sensitivity optical transmission'. *Opt. Express,* 2011, **19**, (26), pp. B868-B881
9. Selmy, H., Shalaby, H. M. H., Kawasaki, Z.-I.: 'Proposal and Performance Evaluation of a Hybrid BPSK-Modified MPPM Technique for Optical Fiber Communications Systems'. *J. Lightw. Technol.,* 2013, **31**, (22), pp. 3535-3545
10. Shinohara, H.: 'Broadband access in Japan: rapidly growing FTTH market'. *IEEE Commun. Mag.,* 2005, **43**, (9), pp. 72-78
11. Andrade, M. D., Kramer, G., Wosinska, L., Jiajia, C., Sallent, S., Mukherjee, B.: 'Evaluating strategies for evolution of passive optical networks'. *IEEE Commun. Mag.,* 2011, **49**, (7), pp. 176-184
12. Kramer, G., Pesavento, G.: 'Ethernet passive optical network (EPON): building a next-generation optical access network'. *IEEE Commun. Mag.,* 2002, **40**, (2), pp. 66-73
13. Bongtae, K., Byoung-Whi, K.: 'WDM-PON development and deployment as a present optical access solution'. *Conf. on Optical Fiber Commun. - incudes post deadline papers,* 2009, pp. 1-3
14. Ke, W., Nirmalathas, A., Lim, C., Skafidas, E.: '4 x 12.5 Gb/s WDM Optical Wireless Communication System for Indoor Applications'. *J. Lightw. Technol.,* 2011, **29**, (13), pp. 1988-1996
15. Aladeloba, A. O., Woolfson, M. S., Phillips, A. J.: 'WDM FSO Network with Turbulence-Accentuated Interchannel Crosstalk'. *J. Opt. Commun. Netw.,* 2013, **5**, (6), pp. 641-651
16. Gee-Kung, C., Chowdhury, A., Zhensheng, J., Hung-Chang, C., Ming-Fang, H., Jianjun, Y., Ellinas, G.: 'Key Technologies of WDM-PON for Future Converged Optical Broadband Access Networks [Invited]'. *IEEE/OSA J. of Optical Commun. and Networking,* 2009, **1**, (4), pp. C35-C50
17. Liu, L., Zhang, M., Liu, M., Zhang, X.: 'Experimental demonstration of RSOA-based WDM PON with PPM-encoded downstream signals'. *Chin. Opt. Lett.,* 2012, **10**, (7), pp. 070608
18. Caplan, D. O., Robinson, B. S.: 'WDM Mitigation of Nonlinear Impairments in Low-Duty-Cycle M-PPM Free-Space Optical Transmitters'. *Conf. Optical Fiber commun./National Fiber Optic Engineers Conf.,* 2008, pp. 1-3

19. Zuo, T. J., Phillips, A. J.: 'Performance of burst-mode receivers for optical digital pulse position modulation in passive optical network application'. *IET Optoelectron.,* 2009, **3**, (3), pp. 123-130

20. Monroy, I. T., Tangdiongga, E. *Crosstalk in WDM Communication Networks*. Norwell, Massachusetts, USA, : Kluwer Academic Publishers; 2002.

21. Ramaswami, R., Sivarajan, K. N., Sasaki, G. H. *Optical Networks: A Practical Perspective*. 3rd ed. Boston: Morgan Kaufmann Publishers; 2010.

22. Ma, R., Zuo, T. J., Sujecki, S., Phillips, A. J.: 'Improved performance evaluation for DC-coupled burst mode reception in the presence of amplified spontaneous emission noise and interchannel crosstalk'. *IET Optoelectron.,* 2010, **4**, (3), pp. 121-132

23. Al-Orainy, A. A., O'Reilly, J. J.: 'Error probability bounds and approximations for the influence of crosstalk on wavelength division multiplexed systems'. *IEE Proc. J. Optoelectron.,* 1990, **137**, (6), pp. 379-384

24. Ke, W., Nirmalathas, A., Lim, C., Skafidas, E.: 'Impact of Crosstalk on Indoor WDM Optical Wireless Communication Systems'. *IEEE Photonics Journal,* 2012, **4**, (2), pp. 375-386

25. Qinglong, Y., Liying, T., Jing, M.: 'Analysis of Crosstalk in Optical Satellite Networks With Wavelength Division Multiplexing Architectures'. *J. Lightw. Technol.,* 2010, **28**, (6), pp. 931-938

26. Kedar, D., Arnon, S.: 'Backscattering-induced crosstalk in WDM optical wireless communication'. *J. Lightw. Technol.,* 2005, **23**, (6), pp. 2023-2030

27. Ribeiro, L. F. B., Da Rocha, J. R. F., Pinto, J. L.: 'Performance evaluation of EDFA preamplified receivers taking into account intersymbol interference'. *J. Lightw. Technol.,* 1995, **13**, (2), pp. 225-232

28. Personick, S. D.: 'Applications for quantum amplifiers in simple digital optical communication systems'. *Bell Sys. Tech. J.,* 1973, **52**, (1), pp. 117-133

29. Phillips, A. J., Cryan, R. A., Senior, J. M.: 'An optically preamplified PPM intersatellite system described by a moment-generating function formulation'. *Microwave and Optical Technol. Letters,* 1995, **8**, (4), pp. 200-204

30. Sibley, M. J. N. *Optical Communications : components and systems*. 2nd ed. London: Macmillian Press Ltd; 1995.

31. Maru, K., Mizumoto, T., Uetsuka, H.: 'Demonstration of Flat-Passband Multi/Demultiplexer Using Multi-Input Arrayed Waveguide Grating Combined With Cascaded Mach-Zehnder Interferometers'. *J. Lightw. Technol.,* 2007, **25**, (8), pp. 2187-2197

32. Hirano, A., Miyamoto, Y., Kuwahara, S.: 'Performances of CSRZ-DPSK and RZ-DPSK in 43-Gbit/s/ch DWDM G.652 single-mode-fiber transmission'. *Optical Fiber Commun. Conf.,* 2003, pp. 454-456

33. Yu, C. X., Neilson, D. T.: 'Diffraction-grating-based (de)multiplexer using image plane transformations'. *IEEE J. Selected Topics in Quantum Electronics,,* 2002, **8**, (6), pp. 1194-1201

34. Majumdar, A. K.: 'Free-space laser communication performance in the atmospheric channel'. *J. Opt. Fiber Commun. Rep.,* 2005, **2**, pp. 345 - 396

35. Shilong, P., Jianping, Y.: 'IR-UWB-Over-Fiber Systems Compatible With WDM-PON Networks'. *J. Lightwave Technol.,* 2011, **29**, (20), pp. 3025-3034

36. Juanjuan, Y., Zheng, Z., Weiwei, H., Anshi, X.: 'Improved Performance of M-ary PPM Free-Space Optical Communication Systems in Atmospheric Turbulence due to Forward Error Correction'. *Intl. Conf. on Commun. Technol.* 2006, pp. 1-4

CHAPTER 6   Turbulence-Accentuated Interchannel Crosstalk in Hybrid Fibre and FSO WDM Systems using DPPM

6.1 Introduction

The optical fibre provides huge and unregulated bandwidth immune from electromagnetic interference, with low signal attenuation around the 1550 nm wavelength region [1], and is the medium of choice for high speed access networks. Optical fibre technology is well developed in access networks, and can potentially support high speed transmission to users in their homes and offices [2]. Thus optical fibre is commonly found in various communication links, including optical interconnects, point-to-point links between local area networks (LANs) and within passive optical networks (PONs) [3-5]. Other benefits of fibre networks include compatibility with most multiplexing/multiple access technology, and lower cost and attenuation compared to the previously used twisted-pair copper cables found in digital subscriber loop systems [1, 6]. In some cases however, it may be problematic to deploy a fibre link due to cost, physical barriers or for environmental reasons [7], or due to a need for fast deployment, and an alternative optical communication network may be required.

In many cases free space optical (FSO) communication links are easier and cheaper to deploy than optical fibre links [2, 8]. FSO communication systems have been widely applied in inter-satellite and deep space communications and have recently received more interest in terrestrial communication, with specific applications such as pre-deployed back up link, rapidly deployed disaster recovery link and enterprise connectivity e.g. LANs and wide area networks (WANs) [2, 4, 8]. Such systems provide extra flexibility and relative ease of upgrade as the user need changes, and have increasingly been proposed as promising solutions to high speed transmission in the last mile of optical access networks [9]. FSO communication, however, requires line of sight between transceivers which restricts the link penetration and coverage area. The requirement for line of sight could sometimes be advantageous, for example, in a multiple user connections

143

where many users occupy different cubicles in an office, it is easier to restrict each user's signal within the user's cubicle or cell, thereby reducing interferences between each user's signals [10]. In addition, there is also improved safety as any intrusion might block the signal and are easily detected [11, 12]. Generally, for terrestrial (atmospheric) applications, FSO communication systems performances are adversely affected by attenuation (due to atmospheric particles), beam spreading and turbulence-induced scintillation [13-16].

Wavelength division multiplexing (WDM) has application in both optical fibre and FSO systems [1, 2, 4]. With WDM PON, fixed wavelengths are assigned to each optical network unit (ONU), thus more fully exploiting the high transmission bandwidth available in the optical domain and avoiding the synchronisation and threshold acquisition required in the burst mode upstream of TDM/TDMA systems [17, 18]. Compared to TDM/TDMA PONs, WDM PON systems use demultiplexers to separate each ONU's data instead of power splitters, thus reducing the system loss and extending the network reach. As a result, WDM PON systems are increasingly being considered as the primary solution to the continuous rise in bandwidth demand in access networks [19, 20]. In contrast to space division multiplexing (SDM), WDM supports network resource sharing, which generally reduces implementation cost. Furthermore, unlike CDM and TDM where the system chip rate and bit rate may be higher than the end user's data rate, WDM systems enable simultaneous transmission by all users at full system bit rate only limited by the electronic processing speed [1].

In the previous chapter, interchannel crosstalk was considered for a WDM DPPM system, and the analysis could be applied for a fibre system or a non-turbulent FSO system. A HFFSO WDM system using DPPM, possibly presents a more feasible solution in some scenarios to high bandwidth users than a fibre or FSO only system. Such a system combines the numerous advantages of both fibre and FSO communication with digital pulse position modulation and WDM techniques and is analysed for the first time in the work presented in this chapter. Modelling the HFFSO WDM DPPM system is non-trivial; the combined effect of the different impairments on system performance is complex. Particularly, the random fluctuations in both signal and crosstalk powers due to turbulence under various DPPM coding levels could lead to power penalties higher than those reported in Chapter 5.

6.2 Network structure and description

The network components as shown in Fig. 6.1 for the upstream and Fig. 6.2 for the downstream include a transmitter module which comprises of a laser driver (LD) and laser for optical signal generation, the input message signal (data) and a PPM modulator (PPM Mod) and a receiver module made up of a photodetector (PD), electrical amplifier and filter (EA) and the integrate and compare circuitry (ICC) for system decision. Thus the system is intensity modulated and the signal is received by direct detection. The downstream collecting lens may include an optical bandpass filter (OBPF) (shown in Fig. 6.2b) to limit background ambient light, while the demultiplexer (demux) inherently performs the optical bandpass filtering in the upstream direction. With DPPM, the system does not require dynamic tracking of a threshold unlike for some OOK systems [21], and it could exist in a PON configuration and possibly include an optical amplifier (OA) to improve the receiver sensitivity and extend the network reach [18]. The optical line terminator (OLT) is linked to a remote node (RN) via a feeder fibre and optical signals are distributed to the various optical network units (ONUs) through a turbulent free space channel. An automatic pointing and tracking system including multiple lenses and focusable collimators or beam expanders [22, 23] is used to launch the light exiting from the fibre end at the remote node or the transmitter at the ONU to free space. The properties of the lenses used in the pointing and tracking subsystem will vary depending on the FSO link length. Different systems to achieve pointing, tracking and alignment can be found in [23-25]. By using an automatic tracking and pointing subsystem, a narrow transmit divergence angle is achieved through adjusting the position and focal lengths of the lenses [22, 23]. The signals are received via a collimator with collecting lens (CL) at the opposite end. The collecting lenses (CLs) are assumed to be widely spaced but appropriately orientated and aligned with the respective transmitting lenses such that signal from one wavelength is not received at another wavelength through the wrong collecting lens. In this way, it is easy to avoid intrachannel crosstalk. The optical amplifier, downstream demux and upstream multiplexer (mux) are conveniently located at a remote node, while the upstream demux and downstream mux are located at the OLT. This choice for the OA position limits

145

the possibility of fibre non-linear effects occurring during the downstream transmission since the signal would not be boosted before going into the fibre.
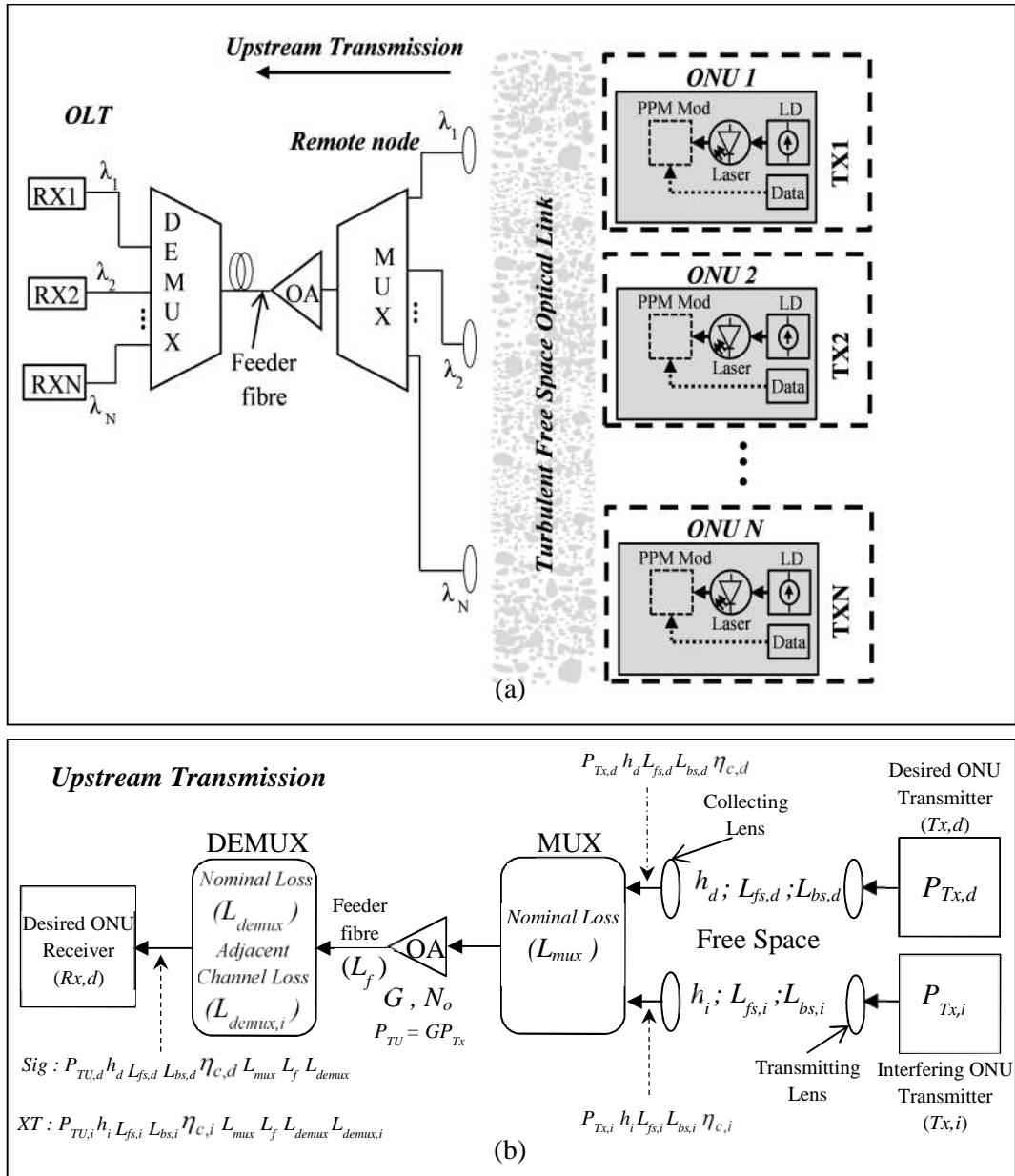
Fig. 6.1 Optically preamplified WDM DPPM upstream network: (a) system diagram and (b) functional diagram
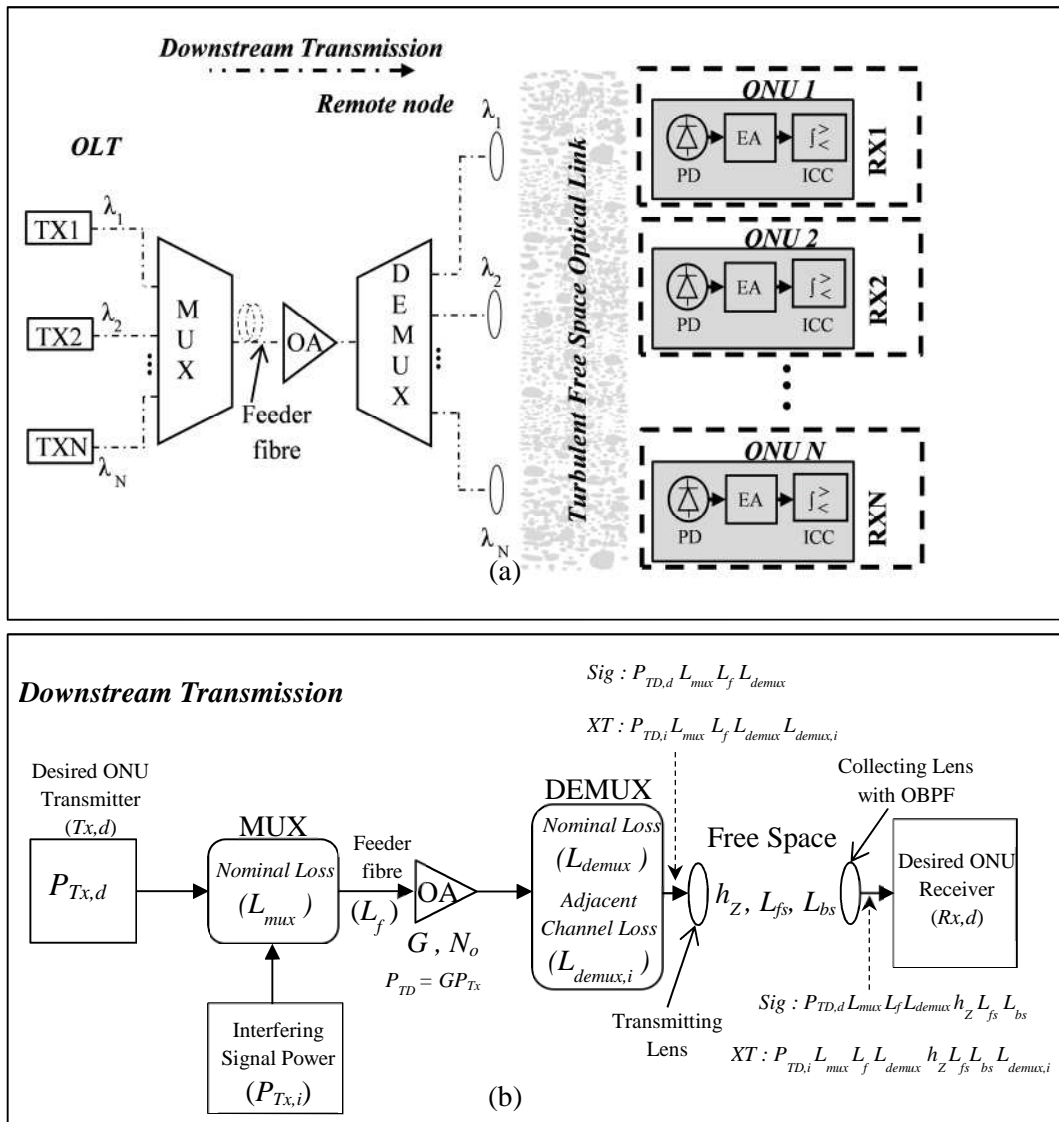
Fig. 6.2 Optically preamplified WDM DPPM downstream network: (a) system diagram (b) functional diagram

Interchannel crosstalk occurs due to the imperfect nature of the demux (in the OLT for upstream transmission or the remote node for downstream transmission). Additionally, turbulence puts more stringent demands on the rejection of non-signal wavelengths by the demux (as a mean signal-to-crosstalk ratio of e.g. 25 dB could vary widely above and below that value due to the independence of turbulence on signal and crosstalk paths). However in the upstream, the signals experience turbulence from different atmospheric links and perhaps different turbulence regimes before the interfering signal is coupled onto the path of the desired signal, hence the crosstalk is caused by a turbulent interfering signal and is more destructive. The downstream transmission is different though, as the

interfering signal is coupled onto the path of the desired signal before both signals are subjected to the same atmospheric turbulence. Thus the crosstalk is not worsened by the turbulence in the downstream.

6.3 Turbulence channel modelling

The effects of turbulence are characterized using the gamma-gamma (GG) pdf written as eq. (3.10), which can be re-written (conditional on h_Z) as [13, 16, 26]

$$p_{GG}(h_Z) = \frac{2(\alpha\beta)^{(\alpha+\beta)/2}}{\Gamma(\alpha)\Gamma(\beta)} h_Z^{((\alpha+\beta)/2)-1} K_{\alpha-\beta}\left(2\sqrt{\alpha\beta h_Z}\right) ; \qquad h_Z > 0 \qquad (6.1)$$

where $h_Z = h_d$ or h_i is the attenuation due to atmospheric turbulence for the desired signal or interferer respectively and the α and β parameters incorporating aperture averaging are written as eqs. (3.11) and (3.12) respectively for plane wave propagation. The Rytov variance σ_R^2 distinguishes the various link turbulence regimes (weak turbulence $\sigma_R^2 < 1$, moderate turbulence $\sigma_R^2 \approx 1$, strong turbulence $\sigma_R^2 > 1$ and saturated turbulence $\sigma_R^2 \to \infty$), and is given by $\sigma_R^2 = 1.23 C_n^2 k^{7/6} l_{fso}^{11/6}$ [13, 26], where C_n^2 is the refractive index structure constant, typically ranging from $\approx 10^{-17} m^{-2/3}$ to $\approx 10^{-13} m^{-2/3}$, $k = 2\pi/\lambda$ is the optical wave number and l_{fso} is the free space link length [13, 16]. The turbulence induced scintillation of the desired signal and interferer are each treated independently for the upstream as each is transmitted over different free space path, however, for the downstream transmission, both the signal and interferer exit the same transmitting lens and travel over the same physical path.

The fibre loss is $L_f = 10^{(-\alpha_f l_f)/10}$ and the free space loss (considered for clear air) is $L_{fs} = 10^{(-\alpha_{fso} l_{fso})/10}$ where α_f and α_{fso} are the attenuation coefficients of fibre and free space respectively, (in dB/km), and l_f is the fibre link length (in km). Free space attenuation however varies for different atmospheric conditions as discussed in Chapter 3, and under hazy, foggy, rainy and snowy conditions, signal attenuation is more severe and the FSO link length is limited. The nominal demux loss L_{demux} /multiplexer (mux) loss L_{mux} is about 3.5 dB [5, 27], while the interferer's demux loss $L_{demux,i}$ is the additional loss that interferer experiences upon coupling to the desired signal wavelength port, and also defines the signal to

crosstalk ratio (in the situation when the input signal and crosstalk power are equal). The free space transmission beam spreading loss in dB for a small transmitter aperture in the presence of turbulence is written as [13, 16, 22].

$$L_{bs} = 20\log_{10}\left(\frac{D_{RX}}{D_e}\right) \tag{6.2}$$

where D_{RX} is the receiving CL aperture diameter, D_e is the beam diameter at the CL due to diffraction and turbulence written as,

$$D_e = d_l\left[1+1.33\sigma_R^2\left(\frac{2l_{fso}}{k(d_l/2)^2}\right)^{5/6}\right]^{1/2} \tag{6.3}$$

$d_l \approx D_{TX} + \varphi_{TX}l_{fso}$ [16, 22] defines the beam diameter due to diffraction only and both D_{TX} and φ_{TX} are the transmitter aperture diameter and divergence angle respectively for either the desired or interfering signal.

A coupling loss is encountered at the interface between the free space link and the fibre link. Assuming that the fibre ends connected to the multiplexers are within the CL focal plane, the coupling efficiency η_c is given by [28]

$$\eta_c = 8a^2\int_0^1\int_0^1\left(\exp\left[-\left(a^2+\frac{A_{RX}}{A_c}\right)\left(x_1^2+x_2^2\right)\right]I_0\left(2\frac{A_{RX}}{A_c}x_1x_2\right)x_1x_2\right)dx_1dx_2 \tag{6.4}$$

where $a = 1.12$ is the coupling geometry parameter, expressed as the ratio of the CL radius to the back-propagated fibre mode radius, and optimum for a fully coherent incident plane wave in the absence of turbulence [28], $A_{RX} = \pi D_{RX}^2/4$ is the CL area, $A_c = \pi\rho_c^2$ is the spatial coherence area of the incident wave, with radius $\rho_c = (1.46C_n^2k^2l_{fso})^{-3/5}$, $I_0(\bullet)$ is a modified Bessel function of the first kind, order zero.

6.4 DPPM crosstalk modelling

A DPPM frame consists of $n = 2^M$ equal time slots of duration $t_s = M/nR_b$, where M is the coding level and R_b is the data rate. For example, at binary data rate of 2.5 Gbps, a DPPM frame with $M = 2$ contains four slots and the pulse in the frame represents a 2-bit word transmitted at slot rate of 5 GHz. In WDM DPPM systems, the bandwidth expands with increasing coding level and appropriate spacing is required between the wavelengths for systems with high

coding level. At $M = 2$, the bandwidth expansion of the system is minimum, thus this analysis is performed at $M = 2$ which represents a practical trade-off.

For analytical convenience, assuming that only slots of crosstalk and signal align during reception, for $M = 2$, $n_1 \in \{1, 2, 3, 4\}$ as shown in Fig. 5.4. In addition, the number of crosstalk pulses that can impair the desired signal ranges from 0 to 2, depending on the position of the pulse in the interfering signal frame and the pattern of (mis)alignment with the desired signal frame. In Chapter 5, this condition which neglects partial slot misalignment was referred to as only slots aligned (OSA), and leads to a quick approach which predicts sensible results for both single and multiple crosstalk sources.

In a practical WDM system, signals in all active wavelengths contribute some amount of crosstalk to signals on other wavelengths. The effects of crosstalk from adjacent wavelengths are typically more severe than crosstalk from other wavelengths further separated from the desired wavelength. Therefore, for immediate insight into a WDM DPPM system affected by turbulence, the simple case of a single adjacent interferer is considered in this analysis. However, the analysis is useful wherever we have the possibility of turbulence-accentuated crosstalk. A typical scenario where the single interferer model could be applied is in a system where one interferer is much nearer to the remote node compared to the other interferers. In such case, there is significant asymmetry in crosstalk power of the interferers and the single dominant interferer could be used for the system performance calculations. In addition, since it was shown in the previous chapter that the effect of a single interferer with high power is worse than that of many interferers with equivalent power, the joint pdf of multiple interferer's turbulences that has been weakened by the demux channel rejection when coupling on to the desired signal wavelength may be replaced by a single pdf of a stronger turbulence while the interfering signals are lumped into a single wavelength and then modelled as a single crosstalk with strong turbulence. This presents an upper bound on the system BER performance (see the result in Appendix C).

For the upstream transmission, the received DPPM rectangular pulse power at the photodetector input for the desired signal and the interferer are respectively written as

$$P_d(h_d) = P_{TU,d} h_d L_{fs,d} L_{bs,d} \eta_{c,d} L_{mux} L_f L_{demux} \tag{6.5}$$

$$P_i(h_i) = P_{TU,i} h_i L_{fs,i} L_{bs,i} \eta_{c,i} L_{mux} L_f L_{demux} L_{demux,i} \tag{6.6}$$

and the single polarisation ASE power spectral density (PSD) at the photodetector input for the desired signal and the interferer are respectively written as

$$N_o = 0.5(NF \times G - 1) h\upsilon L_f L_{demux} \tag{6.7}$$

$$N_{o,i} = 0.5(NF \times G - 1) h\upsilon_i L_f L_{demux} L_{demux,i} \tag{6.8}$$

where G and NF are the optical amplifier gain and noise figure respectively, h is Planck's constant, υ and υ_i are the optical frequencies of the desired signal and interferer respectively.

Also, for the downstream transmission, the received DPPM rectangular pulse power for the desired signal and the interferer are respectively written as

$$P_d(h_Z) = P_{TD,d} h_Z L_{mux} L_f L_{demux} L_{fs} L_{bs} \tag{6.9}$$

$$P_i(h_Z) = P_{TD,i} h_Z L_{mux} L_f L_{demux} L_{demux,i} L_{fs} L_{bs} \tag{6.10}$$

and the single polarisation ASE PSD at the photodetector input for the desired signal and the interferer are respectively written as

$$N_o = 0.5(NF \times G - 1) h\upsilon L_{demux} L_{fs} L_{bs} \tag{6.11}$$

$$N_{o,i} = 0.5(NF \times G - 1) h\upsilon_i L_{demux} L_{demux,i} L_{fs} L_{bs} \tag{6.12}$$

Following the same treatment as in Chapter 5, the general equations for the upstream transmission are derived below in eqs. (6.13) - (6.17), the equations for the downstream are recovered by replacing the attenuation due to atmospheric turbulence for the desired signal/interferer (h_d, h_i) with h_Z.

The means and variances of the random variables both representing the integration over the slot that contains only the signal pulse, only crosstalk pulse, both signal and crosstalk pulses and no pulses (i.e. empty slot) are derived and respectively written as:

$$\mu_{X_{sig,int}}(h_d, h_i) = \frac{LR' q N_o}{t_s} + Gq \left[sigR' P_d(h_d) + intR_i' P_i(h_i) \right] \tag{6.13}$$

$$\sigma^2_{X_{sig,int}}(h_d, h_i) = \sigma^2_{th-DPPM} + \left(\frac{LR' q^2 N_o (1 + R' N_o)}{t_s^2} \right) + Gq^2 R' \left[\left(1 + 2R' N_o \right) \frac{sigP_d(h_d)}{t_s} \right]$$
$$+ Gq^2 R_i' \left[\left(1 + 2R_i' N_{o,i} \right) \frac{intP_i(h_i)}{t_s} \right] \tag{6.14}$$

where $sig \in \{0,1\}$ and $int \in \{0,1\}$ depending on the presence of signal/crosstalk pulse in the slot or not, $R' = \eta/h\upsilon$, $R'_i = \eta/h\upsilon_i$, η is the photodetector quantum efficiency, q is the electron charge, $L = B_o m_t t_s$ is the product of spatial and temporal modes [14], B_o is the demux or OBPF channel bandwidth and m_t is the number of ASE noise polarisation states. The means and variances have been derived with modifications to account for crosstalk–ASE beat noise assuming the interferer and the desired signal experiences the same ASE noise at the amplifier output [29].

Given that each symbol has equal probability of being transmitted in a slot, the probability that a symbol is successfully received in the presence of crosstalk and atmospheric turbulence $P_{ws(l_s,r_s)}(h_d,h_i) = 1 - P_{we(l_s,r_s)}(h_d,h_i)$ where $P_{we(l_s,r_s)}(h_d,h_i)$ is the symbol error probability in the presence of crosstalk and turbulence, $l_s \in \{0,1,2\}$ and $r_s \in \{0,1\}$ denote the number of crosstalk occurring in the signal frame and signal pulse slot respectively. Following the analysis in Chapter 5, one can write that:

$$P_{ws(l_s,r_s)}(h_d,h_i) \geq \prod_{\substack{j=1 \\ j \neq \text{sig slot}}}^{n} P(X_{1,\text{int}} > X_j | h_d, h_i) \tag{6.15}$$

where X_j represents the content of the non-signal slot $X_{0,\text{int}}$, and

$$P_{we(l_s,r_s)}(h_d,h_i) \leq 1 - \left[1 - P(X_{0,0} > X_{1,\text{int}} | h_d, h_i)\right]^{n-1-(l_s-r_s)} \left[1 - P(X_{0,1} > X_{1,\text{int}} | h_d, h_i)\right]^{l_s-r_s} \tag{6.16}$$

Assuming that the random variables $X_{1,\text{int}}$ and $X_{0,\text{int}}$ are Gaussian, the expression $P(X_{0,\text{int}} > X_{1,\text{int}} | h_d, h_i)$ using the Gaussian approximation (GA), is of the general form [14]

$$P(X_{0,\text{int}} > X_{1,\text{int}} | h_d, h_i) = 0.5\,\text{erfc}\left(\frac{\mu_{X_{1,\text{int}}}(h_d,h_i) - \mu_{X_{0,\text{int}}}(h_d,h_i)}{\sqrt{2\left[\sigma^2_{X_{1,\text{int}}}(h_d,h_i) + \sigma^2_{X_{0,\text{int}}}(h_d,h_i)\right]}}\right) \tag{6.17}$$

6.5 BER analysis

In a WDM DPPM system with a single interferer, there may be no crosstalk pulse in the signal frame (for example, compare the signal frame in Fig. 5.4 with the crosstalk frame when $n_1 = 1$). Furthermore, one or two crosstalk pulse(s) may

possibly impair the signal frame (compare the signal frame in Fig. 5.4 with the crosstalk frame when $n_1 = 2$ or 3 respectively). However, only one crosstalk pulse can hit a single slot in the signal frame.

The BERs conditional on turbulence and crosstalk frame overlap (n_1) for the upstream and downstream are respectively written as

$$BER_{U_{l_s}}\left(h_d, h_i, n_1\right) = p_{f(l_s)}(n_1)\frac{n}{2(n-1)}\left[\ p_{s(l_s)}(1)P_{we(l_s,1)}\left(h_d, h_i\right) + p_{s(l_s)}(0)P_{we(l_s,0)}\left(h_d, h_i\right)\ \right] \quad (6.18)$$

and

$$BER_{D_{l_s}}\left(h_Z, n_1\right) = p_{f(l_s)}(n_1)\frac{n}{2(n-1)}\left[\ p_{s(l_s)}(1)P_{we(l_s,1)}\left(h_Z\right) + p_{s(l_s)}(0)P_{we(l_s,0)}\left(h_Z\right)\ \right] \quad (6.19)$$

where $p_{f(l_s)}(n_1)$ denote the probability of l_s crosstalk pulses hitting the signal frame (calculated the same as in Chapter 5), and n_1 is the number of slots in crosstalk frame 1 that overlap the signal frame. Also $p_{s(l_s)}(r_s)$ denote the probability of r_s out of l_s crosstalk pulses hitting the signal slot so that the probability that a crosstalk pulse hits the signal pulse slot $p_{s(l_s)}(1) = l_s/n$ and the probability that crosstalk pulse(s) hit an (unspecified) empty slot $p_{s(l_s)}(0) = (n - l_s)/n$. The no crosstalk symbol error probability $P_{we(0,0)}(h_d)$ is treated the same as in [14], $P_{we(l_s,1)}(h_d, h_i)$ and $P_{we(l_s,0)}(h_d, h_i)$ are calculated using eq. (6.16) for $r_s = 1$ and 0 respectively, and represent word error contributions when the interferer and the desired signal have experienced turbulence from different (i.e. assumed independent) atmospheric links as in the upstream. Both $P_{we(l_s,1)}(h_Z)$ and $P_{we(l_s,0)}(h_Z)$ are calculated using eq. (6.16) for $h_d \approx h_i \approx h_Z$ (i.e. where the interferer and the desired signal have travelled the same turbulence path like in the downstream), and for $r_s = 1$ and 0 respectively.

The overall BER in the presence of crosstalk and turbulence for the upstream is thus calculated by summing up all the error contribution calculated from eq. (6.18) for all values of l_s and averaging over all values of crosstalk frame overlap (n_1) and both the turbulence pdf's for the desired signal and the interferer. It is written as

$$\overline{BER_U} = \int_0^\infty \int_0^\infty \frac{1}{n}\sum_{n_1=0}^{n-1}\ \sum_{l_s=0}^{2} BER_{U_{l_s}}\left(h_d, h_i, n_1\right) p_{GG,d}\left(h_d\right)\ p_{GG,i}\left(h_i\right)\ \mathrm{d}h_d\ \mathrm{d}h_i \quad (6.20)$$

Also the overall BER in the presence of crosstalk and turbulence for the downstream is calculated by summing up all the error contribution calculated from eq. (6.19) for all values of l_s and averaging over all values of n_1 and the turbulence pdf for only the desired signal. It is written as

$$\overline{BER}_D = \int_0^\infty \frac{1}{n} \sum_{n_1=0}^{n-1} \sum_{l_s=0}^2 BER_{D_{l_s}}(h_Z, n_1) \, p_{GG,d}(h_Z) \, dh_Z \tag{6.21}$$

In deriving eqs. (6.20) and (6.21), we maintained the same assumption in Chapter 5 that signal and crosstalk are more likely to arrive at the receiver with relative frame misalignment, because signals are randomly transmitted in overlapping time. Thus an average BER for all form of misalignment has been taken. For analysis assuming fixed alignment or misalignment of crosstalk and signal frames, eqs. (6.20) and (6.21) are simplified by modifying them to exclude the requirement for averaging over all values of n_1, and then calculated for the value of n_1 that corresponds to the fixed alignment or misalignment.

6.6 Results and discussion

Bit error rate (BER), required optical transmission power and power penalty results are presented using parameters reported in Table 6.1. The DPPM coding level $M = 2$ is used for all calculations to keep the bandwidth expansion low while still maintaining the attractive features of DPPM. The required optical power referred to in this chapter represents the transmitter power at the OLT (for downstream transmission) and ONU (for upstream transmission). The transmission power at the ONU is restricted to 20 dBm to avoid exceeding the eye safety limits for free space (outdoor) transmission around the 1550 nm wavelength region [15, 30, 31]. Refractive index structure constant ranging from $C_n^2 = 10^{-16}$ m$^{-2/3}$ to 10^{-13} m$^{-2/3}$ are used for free space optical link length of 200 m to 2000 m, corresponding to Rytov variance (σ_R^2) range of 1.04×10^{-4} to 7.10 and covering all the turbulence regimes. Aperture averaging is incorporated in the turbulence model for scintillation mitigation through the use of eqs. (3.11) and (3.12). Amplifier saturation based effects, fibre dispersion and other nonlinearities are neglected in the analysis, and a perfect extinction is assumed for both OOK and DPPM calculations. Background ambient light power is considered negligible

in the proposed network which operates at 1550 nm and uses narrow field of view collecting lenses with small optical noise bandwidth [32]. The mux/demux channel bandwidth is assumed to be 76 GHz, with insertion loss of about 3.5 dB and adjacent channel spacing of 100 GHz in the C-band of the ITU (International Telecommunication Union) grid specification. Demux adjacent channel rejection values typically ranging from -15 dB to -45 dB have been demonstrated experimentally in [33-35] and are considered. As seen in Chapter 5, the impact of a single high power crosstalk is worse than that of many crosstalk of equivalent power. Thus in this chapter, only a single crosstalk source from a dominant interferer is considered. Each user corresponds to an ONU, so both terms are used interchangeably in the following discussion.

Table 6.1: Physical parameters used for calculations

Parameters	Description	Value
R_b	Binary data rate	2.5 Gbps
B_o	Demux or OBPF channel bandwidth	76 GHz
λ_{sig}	Desired signal wavelength	1550 nm
φ_{TX}	Transmission divergence angle	0.2 mrad
D_{RX}	Receiver collecting lens diameter	13 mm [31]
η	Receiver quantum efficiency	0.8
l_f	Feeder fibre link length	20 km
l_{fso}	Maximum free space link length	2 km
α_f	Fibre attenuation	0.2 dB/km
α_{fso}	Free space attenuation (clear air)	0.2 dB/km
G	Optical preamplifier gain	30 dB
NF	Optical preamplifier noise figure	4.77 dB
m_t	ASE noise polarisation states	2
L_{demux}	Signal demux/mux loss	3.5 dB [5, 27]

The upstream BER curves for a single interferer at both strong and weak turbulences are shown in Fig. 6.3 for signal and interferer FSO link lengths of 1500 m. For this particular result, we considered an optically preamplified receiver without any other losses, to clearly show the effects of crosstalk alone, turbulence alone and turbulent crosstalk. The Rytov variance (σ_R^2) is fixed for each particular curve and the transmitter power for the signal and interferer are assumed to be the same so only the demux adjacent crosstalk rejection loss ($L_{demux,i}$) is responsible for the crosstalk. The crosstalk effect is seen to be small without turbulence (as shown by the Sig,XT BER curves in Figs. 6.3a and 6.3b) even for a demux with poor adjacent channel rejection (15 dB). However in the presence of turbulence, either for the signal or for the interferer or both, the crosstalk effect is more prominent and results in bit error rate floor as seen in Fig. 6.3c. The error floor occurred at a much lower BER (not shown for $\sigma_R^2 = 0.35$) for non-turbulent signal with turbulent interferer (Sig,TurbXT) because the power of the turbulent interferer is reduced by the demux channel rejection ratio.

As a result of the random fluctuation in received irradiance, atmospheric turbulence can increase or decrease the value of the desired signal or interferer pulse at decision time. Therefore, the error floor occurs when turbulence has increased the interfering signal (and hence the crosstalk power) value in the empty slot or attenuated the desired signal pulse value in the signal slot, to a sufficiently significant extent. This happens at high signal power when the effect of (other) noise on the system is negligible. To understand this properly, firstly, consider the extreme situation of a noiseless (i.e. no ASE beat, thermal, shot etc) system. In such a system for the times the crosstalk power is even fractionally bigger than the signal power, due to turbulence, there is a perfect detection of crosstalk resulting in a BER, for the signal, of 0.5. Equally, once the signal is bigger than the crosstalk, there is perfect signal detection with BER equal to 0. Thus, the error floor is simply given by $0.5 \times prob\,(crosstalk\ power > signal\ power)$. This, under the assumption of equal long term average powers at the demux input, occurs for $h_d \leq L_{demux,i}$ for turbulent signal with non-turbulent interferer, $h_i \geq 1/L_{demux,i}$ for non-turbulent signal with turbulent interferer, and $h_i/h_d \geq 1/L_{demux,i}$ for turbulent signal with turbulent interferer. The BER value where the error floors occur is thus determined by both the turbulence strength and the demux channel rejection

(which directly controls the crosstalk power). Before the error floors occur, the system BER performance is limited by noise (ASE beat, thermal, shot etc.) and an increase in the signal-to-noise-ratio (SNR) of the system improves the BER. Similarly at low power, the noise dominates the signal and worsens the BER. However, in a noiseless system, the BER over the whole power range (e.g. in Fig. 6.3c) would be constant and equal to the BER value at which the system is limited by the combined effect of turbulence attenuation and crosstalk power.
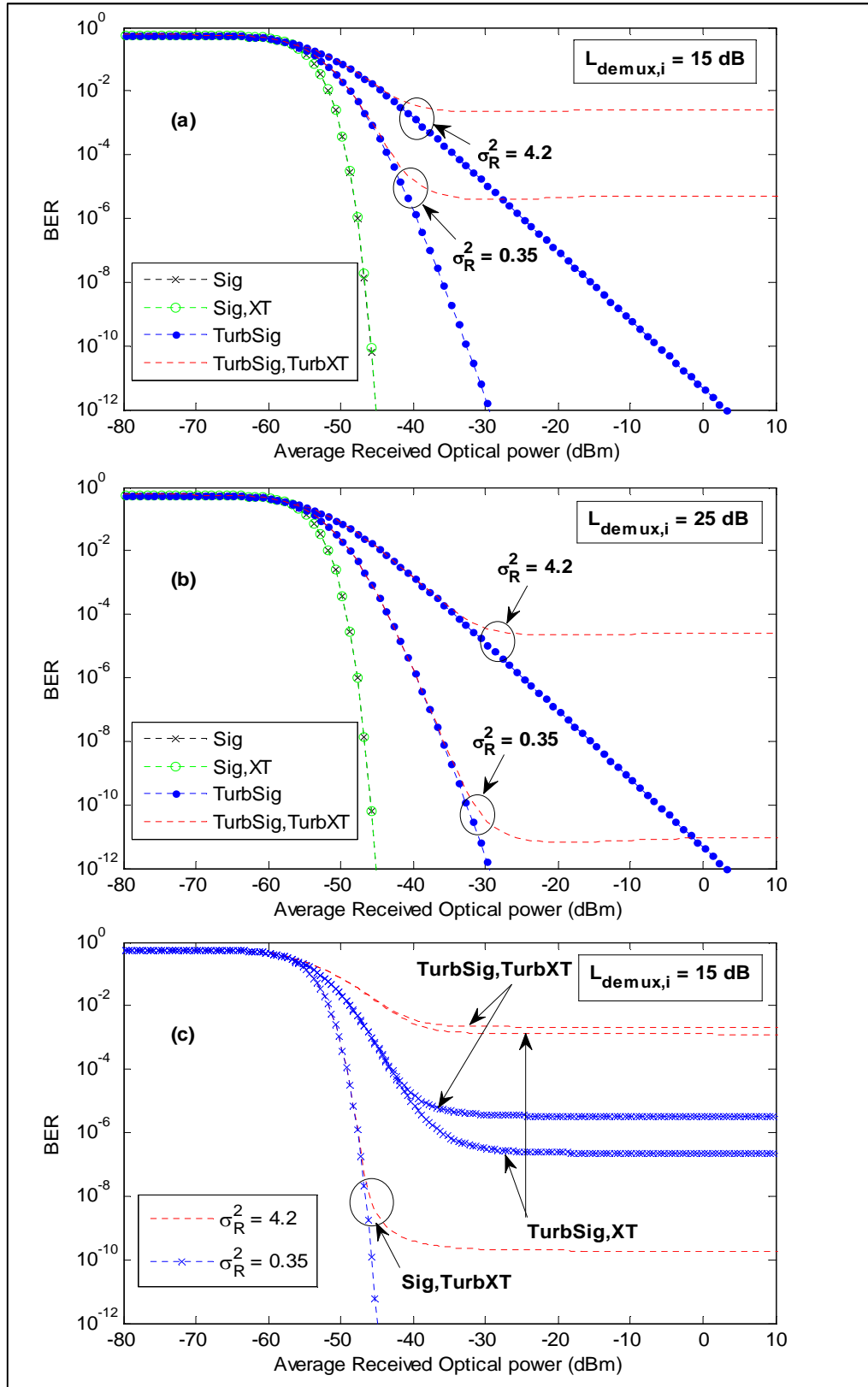
Fig. 6.3 Upstream BER versus Average Received Optical Power (dBm) for strong and weak turbulence regimes with σ_R^2 fixed for each curve: (a) $L_{demux,i}$ = 15 dB (b) $L_{demux,i}$ = 25 dB and (c) $L_{demux,i}$ = 15 dB
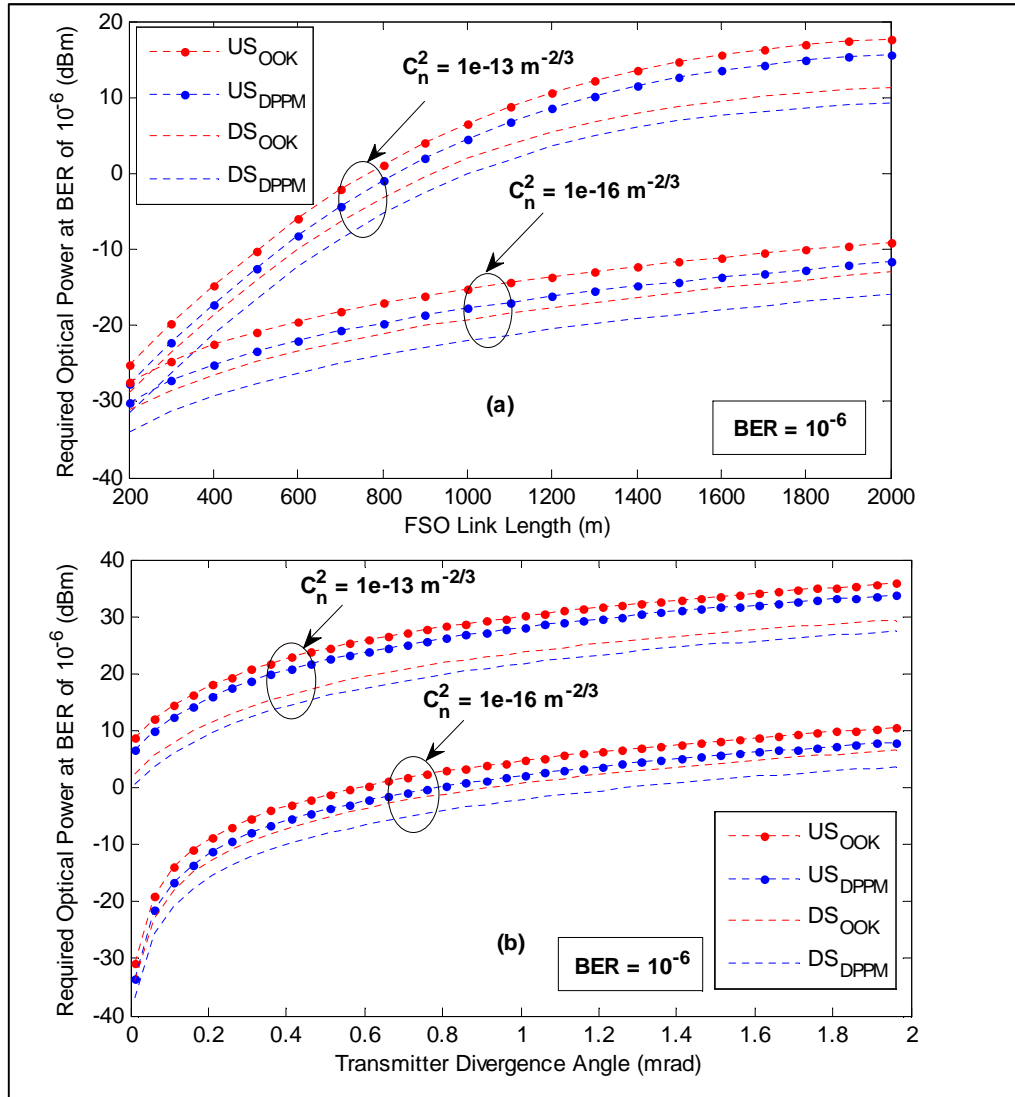
Fig. 6.4 Required Optical Power (dBm) for strong and weak turbulence regimes at $L_{demux,i}$ = 35 dB versus: (a) FSO Link Length (m), φ_{TX} = 0.2 mrad and (b) Transmitter Divergence Angle (mrad)

The upstream and downstream required optical power at target BER of 10^{-6} is shown in Fig. 6.4 as a function of FSO link length and transmitter divergence angle for both OOK and DPPM systems. The interferer demux rejection is 35 dB and both interferer and signal are at the same distance from the remote node. The required optical power for the DPPM system is seen to be lower than that of the OOK system for all turbulent regimes considered. This result is consistent with the findings in the non-turbulent model presented in Chapter 5, which show that DPPM requires less power compared to OOK in a WDM free space system. In Fig. 6.4a, the required optical power increases with the C_n^2 and FSO link length

due to the perceived increase in turbulence strength as either or both parameters increases. This is not always the case, as will be seen and explained in later results. However, the increase in required optical power with respect to transmitter divergence angle and C_n^2 in Fig. 6.4b is a continuous trend owing to increase in beam spreading loss.

In Fig. 6.5, the required optical power for upstream transmission is considered for various interferer and signal FSO link lengths at target BER of 10^{-6} and demux rejection of 35 dB. The result in Fig. 6.5 is of the same form as previously obtained OOK results [15], and reveals that the effect of turbulence-accentuated crosstalk is worse when the interferer is closer to the remote node compared to the desired signal. This is because the interfering signal experiences less loss on average and hence becomes stronger than the desired signal before the demux taken into account. Thus at certain interferer FSO link length, it is impossible to attain the target BER and an error floor occurs as seen in Fig. 6.5a. The target BER is achievable at reduced C_n^2 value of $10^{-16} \, \mathrm{m}^{-2/3}$ for every location within the FSO link distances considered in Fig. 6.5b, with the required optical power rising as the position of the desired ONU moves away from the remote node. Therefore, it is highly important for a network designer to determine the closest distance to the remote node each ONU should be in order to obtain the required system performance with adequate consideration to the demux adjacent channel rejection ratio. For example, using a demux with adjacent rejection ratio of 35 dB as shown in Fig. 6.5a, when the interfering user is 500 m away from the remote node, then the desired ONU cannot be more than 1000 m away from the remote node for the target BER to be met at all turbulence regimes. To avoid some of these issues, a power control algorithm (PCA) may be included in the system to monitor each ONU transmit power relative to the distance from the remote node and ensure that the same power is received at each user's collecting lens. The PCA could help in reducing ONU transmit powers and interferences among the ONUs as have been seen in RF mobile communications.
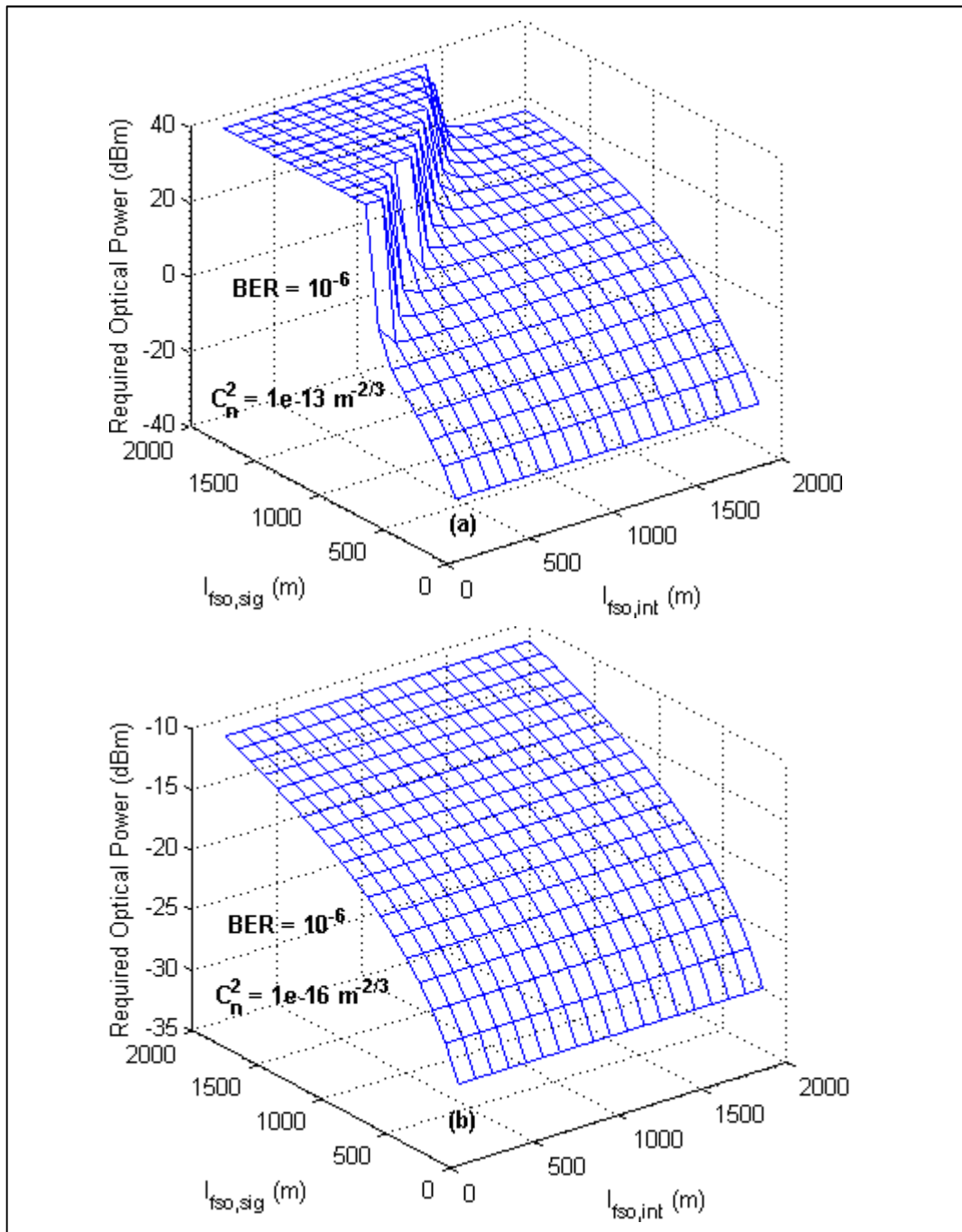
Fig. 6.5 Required Optical Power (dBm) for the upstream as a function of the FSO link lengths for signal and interferer (m) at $L_{demux,i}$ = 35 dB and target BER = 10^{-6}
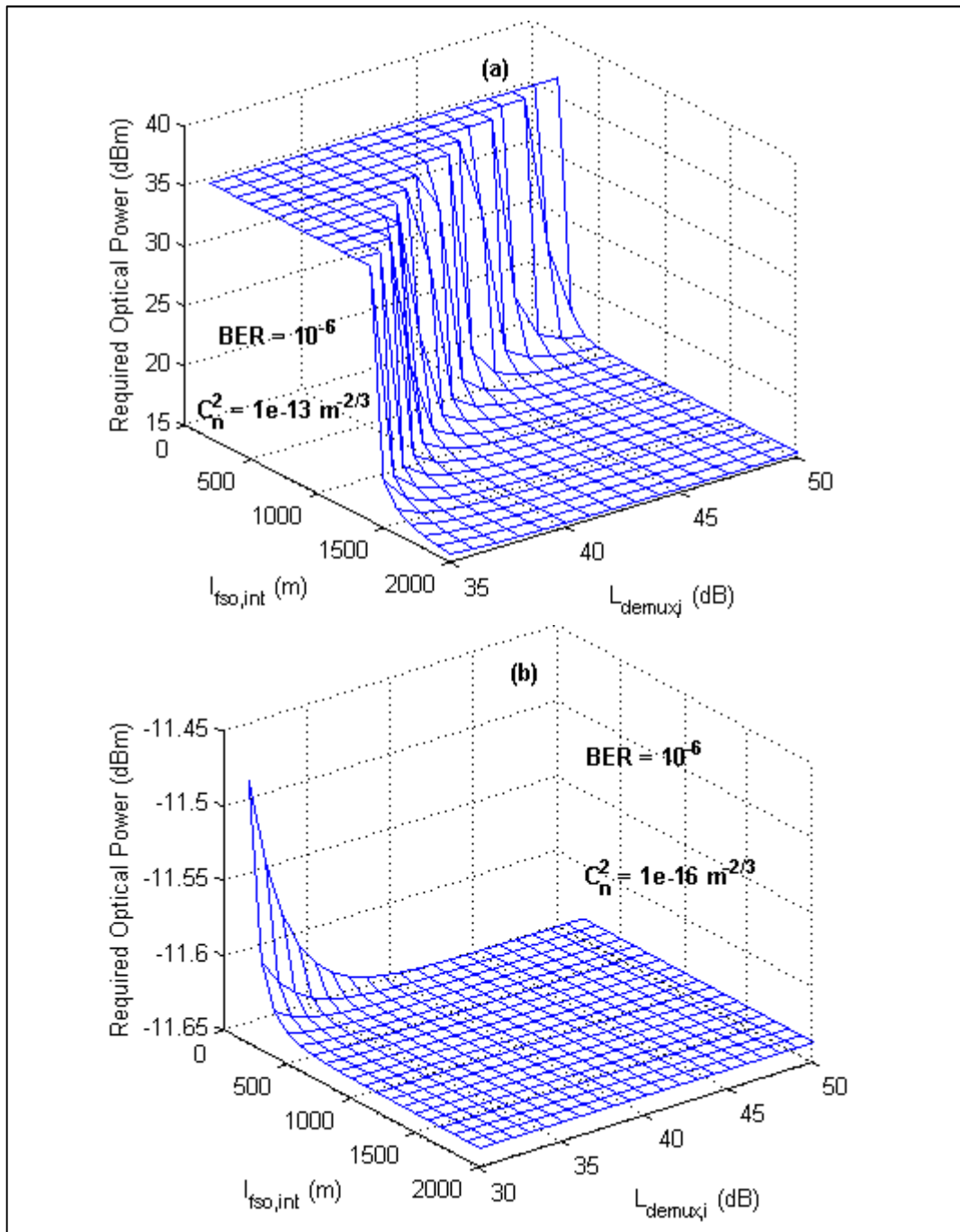
Fig. 6.6 Upstream Required Optical Power (dBm) as a function of demux channel
rejection and interferer's FSO link (m) at $l_{fso,sig}$ = 2000 m and target BER of 10^{-6}

In Fig. 6.6, the demultiplexer figure of merit in terms of adjacent channel
rejection is considered for various interferer's FSO link lengths at target BER of
10^{-6} and under different turbulence conditions. The FSO link length for the desired
signal is fixed at 2000 m which is the maximum FSO link length considered in
this analysis. It is shown in Fig. 6.6a that if the desired ONU is positioned at 2000

m away from the remote node, then for another ONU (interferer) to be at 500 m to the remote node, a demux with adjacent rejection ratio greater than 45 dB is required so that the target BER is met for all turbulence regimes. Alternatively, the interfering user may be located at 1500 m from the remote node and a demux with adjacent rejection ratio greater or equal to 35 dB is used to meet the targeted BER performance. The target BER is easily achieved at weak turbulence condition as seen in Fig. 6.6b.

The Rytov variance is related to scintillation index and is normally used for turbulence characterisation. It is directly related to the FSO link length and C_n^2 and gives an indication of the turbulence strength. Thus in Fig. 6.7, the required optical power for upstream transmission at target BER of 10^{-6} is examined for variable C_n^2 values and as a function of either FSO link length or demux loss (adjacent channel rejection). In Fig. 6.7a, with the desired user permanently positioned at 2000 m from the remote node, error floor are effectively seen gradually increasing as C_n^2 increases and/or interferer's distance from the remote node decreases, indicating positions where the target BER is not achievable. However, the floor disappears in Fig. 6.7b with both the desired user and interferer permanently positioned at 2000 m from the remote node.

As previously noted, the Rytov variance constantly increases with C_n^2 and FSO link length. However, it has been shown experimentally that the scintillation index and hence optical turbulence strength does not continuously increase with the Rytov variance [13, 36]. Generally, as the Rytov variance increases, the turbulence strength increases until a maximum is reached at a point referred to as the focusing regime [13] where the worst effect of random focusing is achieved. After this point, continued increase of the Rytov variance leads to loss of spatial coherence and a gradual decay in the scintillation index up to the saturated turbulence regime where it approaches unity [36]. This behaviour is responsible for the rise and fall in the required optical power along the C_n^2 axis in Fig. 6.7.
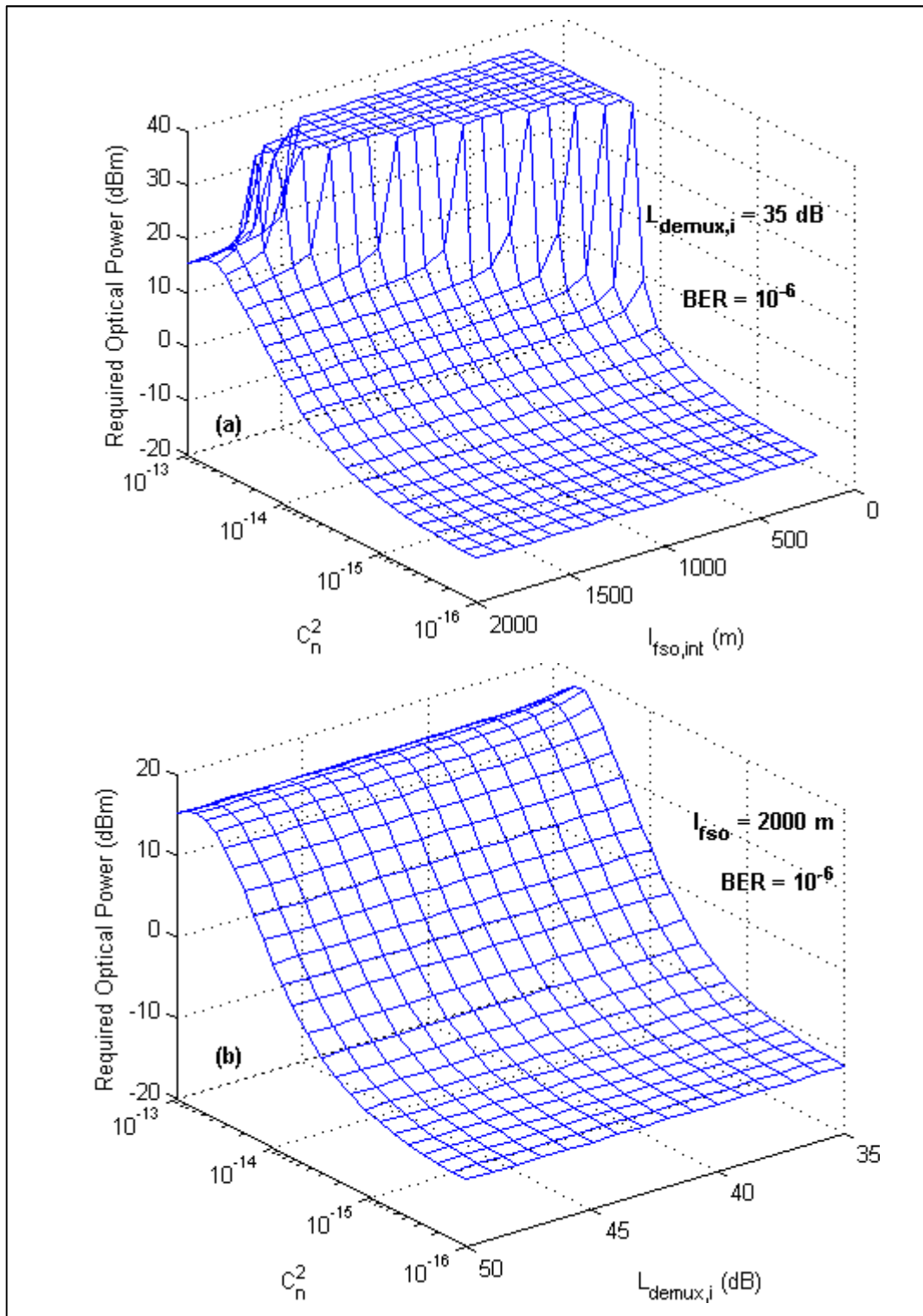
Fig. 6.7 Required Optical Power (dBm) for the upstream as a function of the refractive index structure constant (C_n^2) at target BER = 10^{-6}: (a) $l_{fso,sig}$ = 2000 m (b) $l_{fso,sig}$ and $l_{fso,int}$ = 2000 m
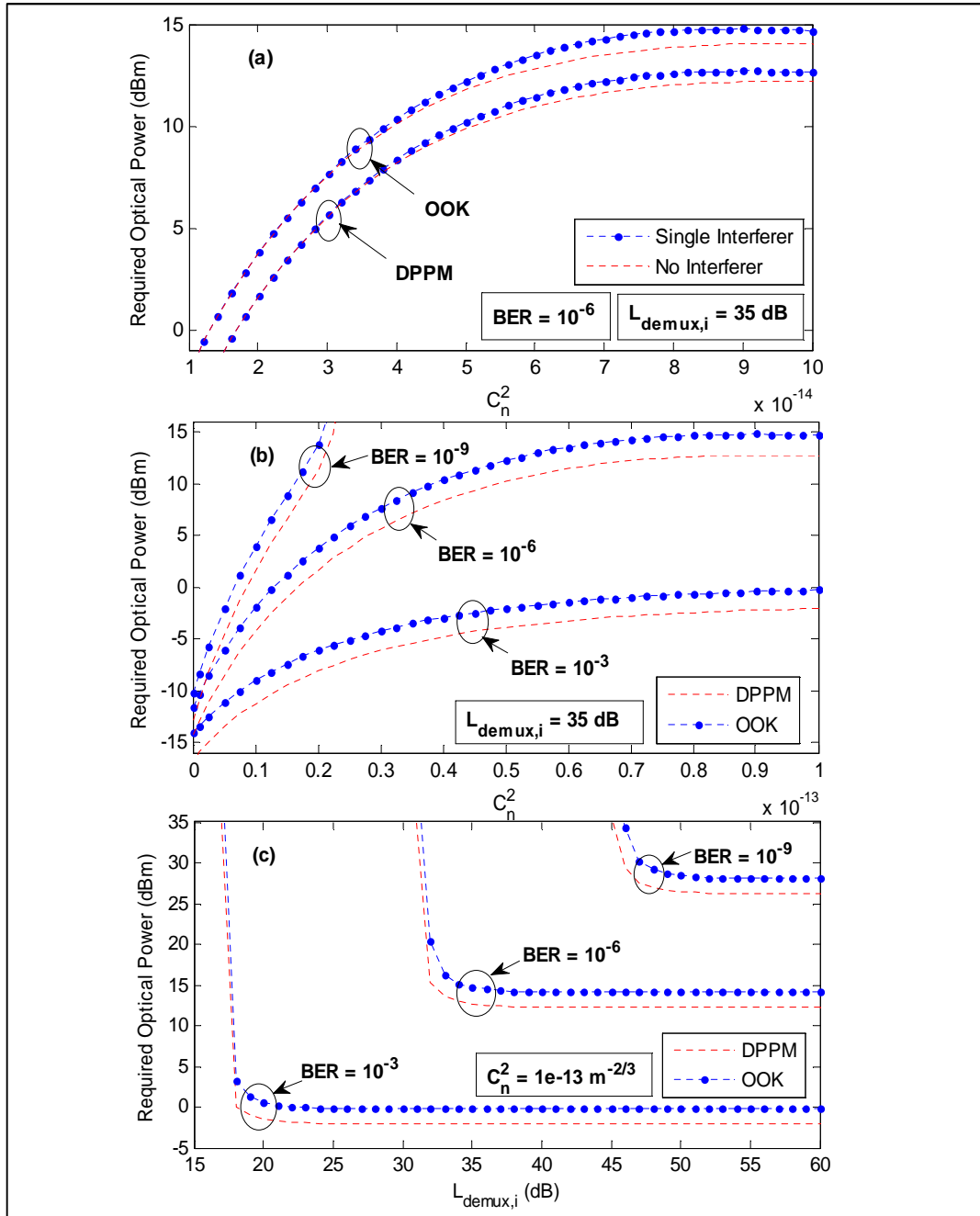
Fig. 6.8 Upstream Required Optical Power as a function of the refractive index structure constant (C_n^2) and demux adjacent channel rejection at l_{fso} = 1500 m

The required optical power as a function of the interferer demux loss and refractive index structure constant for DPPM system is compared with OOK system in Fig. 6.8. The FSO link lengths for the signal and interferer are fixed at 1500 m so that the system operation is moved closer to the focusing regime for the C_n^2 values considered. It is seen that the DPPM system requires lower optical power compared to the OOK system for all values of C_n^2 and $L_{demux,i}$ used in the analysis. In Fig. 6.8a, for target BER of 10^{-6} and $L_{demux,i}$ of 35 dB, the single

crosstalk effect is clearly seen worsening as the turbulence strength increases for both the OOK and DPPM systems. The system performance at different target BER values is examined for OOK and DPPM in Figs. 6.8b and 6.8c. The result in Fig. 6.8c shows that for target BERs of 10^{-9}, 10^{-6} and 10^{-3} to be met at all turbulence regimes, the system requires demultiplexer with adjacent channel rejection greater or equal to 46 dB, 32 dB and 18 dB respectively. However, to meet a BER of 10^{-9}, high power (above 20 dBm) would be required. With interleaved FEC implemented in turbulent systems as explained in Section 2.3, it becomes more feasible for practical FSO systems to operate at BER of 10^{-3}, and demultiplexers with 18 dB rejection are readily available.

The power penalty results are shown in Fig. 6.9 for $l_{fso,sig} = 1500$ m. Unlike the non-turbulent WDM DPPM versus OOK crosstalk results in the previous chapter, Figs. 6.9a and 6.9b indicate that the OOK system has slightly lower power penalty compared to the DPPM system under moderate to strong turbulence. As shown in Fig. 6.9a, with no interferer the DPPM power penalty is greater than the OOK power penalty by 0.2 dB, and increasing to 0.5 dB as the turbulence strength increases. This reduction in DPPM sensitivity over OOK systems in the presence of turbulence has been reported in [14], with no interferers. This is specifically because the turbulence pdf shifts more to the left with increasing σ_R^2 (see Fig. 3.7), thus more area of the pdf coincide with part of the instantaneous BER curve dominated by signal independent noise such as thermal noise, resulting in a reduction of the DPPM average sensitivity advantage over OOK as the turbulence strength increases. The difference between the power penalties of both systems is reduced in the presence of interferers (see Fig. 6.9a). And under no turbulence as seen in the result in Chapter 5 or under weak turbulence as seen in Figs. 6.9c and 6.9d, the power penalty for the DPPM system tends to be lower than that of the OOK system. As shown in Fig. 6.9d, an interferer that is closer to the remote node causes more crosstalk to other users farther away, even at low C_n^2 value. Thus in the absence of power control, user positioning should be considered as an important design parameter. Implementing a PCA ensures that the average signal-to-crosstalk ratio is independent of the user's position, and is almost the same value as $L_{demux,i}$, unlike the case shown in Fig. 6.9d. The use of PCA will be exemplified in Chapter 8.
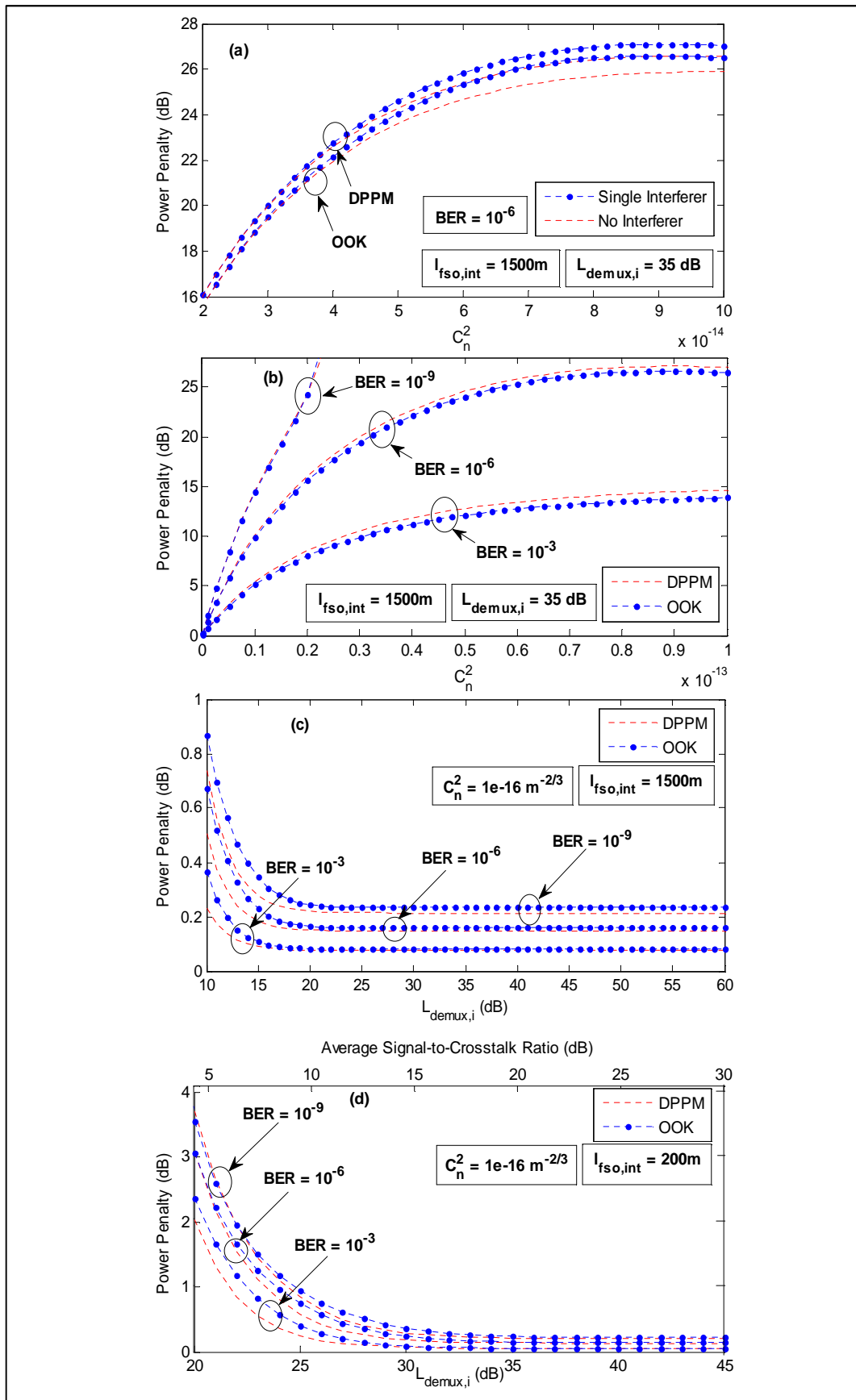
Fig. 6.9 Power penalty (dB) for the upstream as a function of the refractive index structure constant (C_n^2) and demux adjacent channel rejection at $l_{fso,sig} = 1500$ m

6.7 Summary

A hybrid fibre and FSO WDM DPPM network have been studied in this chapter and the effects of turbulence-accentuated interchannel crosstalk on the system performance analysed for the first time. For all turbulence regimes, it could be seen that DPPM systems required lower optical power compared to OOK systems. At coding level of 2, the DPPM scheme presented about 2 dB improvements in required average power over the OOK scheme. The existence of turbulence-accentuated crosstalk for the upstream transmission which somewhat restricts the relative distances between the remote node and both the interferer and the desired user for a specified target BER and demux adjacent rejection ratio was established in the results. Depending on the position of the interferer relative to the desired user, power penalties of about 0.2 dB – 3.0 dB for weak turbulence and above 20 dB for strong turbulence regimes was reported for 10^{-6} BER target. Error floor occur in turbulent WDM DPPM systems with crosstalk and the relationship between the turbulence and the crosstalk at the onset of the error floor was shown in our analysis. The achievable BER can be improved using interleaved FEC as discussed in Chapter 2 and by implementing a PCA. In the next chapter, we will consider another system performance metric referred to as the outage probability, before we finally consider a larger OCDMA WDM network with different OOCs used in each WDM wavelength.

6.8 References

1. Mukherjee, B.: 'WDM optical communication networks: progress and challenges'. *IEEE J. Selected Areas in Commun.,* 2000, **18**, (10), pp. 1810-1824
2. Ciaramella, E., Arimoto, Y., Contestabile, G., Presi, M., D'Errico, A., Guarino, V., Matsumoto, M.: '1.28 terabit/s (32x40 Gbit/s) wdm transmission system for free space optical communications'. *IEEE J. Selected Areas in Commun.,* 2009, **27**, (9), pp. 1639-1645
3. Forbes, M., Gourlay, J., Desmulliez, M.: 'Optically interconnected electronic chips: a tutorial and review of the technology'. *J. Electron. & Commun. Eng.,* 2001, **13**, (5), pp. 221-232
4. Forin, D. M., Beleffi, G. M. T., Curti, F., Corsi, N., De Sanctis, V., Sacchieri, V., Teixeira, A. J. L., et al.: 'On field test of a Wavelength Division Multiplexing Free Space Optics transmission at very high bit rates'. *9th Int. Conf. Telecommun.* 2007, pp. 77-80
5. Chang-Hee, L., Sorin, W. V., Byoung-Yoon, K.: 'Fiber to the Home Using a PON Infrastructure'. *J. Lightw.Technol.,* 2006, **24**, (12), pp. 4568-4583
6. Ramaswami, R., Sivarajan, K. N., Sasaki, G. H. *Optical Networks: A Practical Perspective*. 3rd ed. Boston: Morgan Kaufmann Publishers; 2010.
7. Pei-Lin, C., Shenq-Tsong, C., Shuen-Te, J., Shu-Chuan, L., Han-Hsuan, L., Ho-Lin, T., Po-Hsuan, H., et al.: 'Demonstration of 16 channels 10 Gb/s WDM free space transmission over 2.16 km'. *Digest of the IEEE/LEOS Summer Topical Meetings* 2008, pp. 235-236
8. Aladeloba, A. O., Phillips, A. J., Woolfson, M. S.: 'Improved bit error rate evaluation for optically pre-amplified free-space optical communication systems in turbulent atmosphere'. *IET Optoelectron.,* 2012, **6**, (1), pp. 26-33
9. Qianling, C., Brandt-Pearce, M., Wilson, S. G.: 'Optically Amplified Wireless Infrared MISO Systems'. *IEEE Global Telecommun.Conf.,* 2007, pp. 4505-4510
10. Barry, J. R. *Wireless Infrared Communications*. Boston: Kluwer Academic Publishers; 1994 1994.
11. Kedar, D., Arnon, S.: 'Urban optical wireless communication networks: the main challenges and possible solutions'. *IEEE Commun. Mag.,* 2004, **42**, (5), pp. S2-S7
12. Kahn, J. M., Barry, J. R.: 'Wireless infrared communications'. *Proc. IEEE,* 1997, **85**, (2), pp. 265-298
13. Andrews, L. C., Phillips, R. L. *Laser Beam Propagation Through Random Media*. 2nd ed: SPIE Press, Bellingham, Washington; 2005.
14. Aladeloba, A. O., Phillips, A. J., Woolfson, M. S.: 'Performance evaluation of optically preamplified digital pulse position modulation turbulent free-space optical communication systems'. *IET Optoelectron.,* 2012, **6**, (1), pp. 66-74
15. Aladeloba, A. O., Woolfson, M. S., Phillips, A. J.: 'WDM FSO Network with Turbulence-Accentuated Interchannel Crosstalk'. *J. Opt. Commun. Netw.,* 2013, **5**, (6), pp. 641-651
16. Majumdar, A. K.: 'Free-space laser communication performance in the atmospheric channel'. *J. Opt. Fiber Commun. Rep.,* 2005, **2**, pp. 345 - 396
17. Ansari, N., Zhang, J. *Media Access Control and Resource Allocation for Next Generation Passive Optical Networks*: Springer; 2013.
18. Zuo, T. J., Phillips, A. J.: 'Performance of burst-mode receivers for optical digital pulse position modulation in passive optical network application'. *IET Optoelectron.,* 2009, **3**, (3), pp. 123-130
19. Kazovsky, L., Shing-Wa, W., Ayhan, T., Albeyoglu, K. M., Ribeiro, M. R. N., Shastri, A.: 'Hybrid Optical-Wireless Access Networks'. *Proc. IEEE,* 2012, **100**, (5), pp. 1197-1225
20. Liaw, S. K., Lai, Y. T., Chang, C. L., Shung, O.: 'AWG-based WDM-PON monitoring system using an optical switch and a WDM filter'. *Laser Phys.,* 2008, **18**, (9), pp. 1052-1055

21. Ohtsuki, T.: 'Performance analysis of atmospheric optical PPM CDMA systems'. *J. Lightw. Technol.,* 2003, **21**, (2), pp. 406-411

22. Bloom, S., Korevaar, E., Schuster, J., Willebrand, H.: 'Understanding the performance of free-space optics'. *J. Opt. Netw.,* 2003, **2**, (6), pp. 178-200

23. Hai-Yin, H., Wan Chian, L., Hoa Le, M., Ghassemlooy, Z., Yi-Lin, Y., Shien-Kuei, L.: '2 x 80 Gbit/s DWDM Bidirectional Wavelength Reuse Optical Wireless Transmission'. *IEEE Photonics Journal,* 2013, **5**, (4), pp. 7901708-7901708

24. Ho, T.-H., Trisno, S., Smolyaninov, I. I., Milner, S. D., Davis, C. C.: 'Studies of pointing, acquisition, and tracking of agile optical wireless transceivers for free-space optical communication networks'. *Remote Sensing* 2004: Intl. Society for Optics and Photonics, pp. 147-158

25. Tidwell, T. L., Gregory, J. T., Chalfant III, C. H., Orlando, F. J., Leftwich, M.: 'Rapid acquisition, pointing and tracking optical system for free space optical communications'. US Patent 8, 160, 452 B1; 2012

26. Khalighi, M., Schwartz, N., Aitamer, N., Bourennane, S.: 'Fading Reduction by Aperture Averaging and Spatial Diversity in Optical Wireless Systems'. *J. Opt. Commun. Netw. ,* 2009, **1**, (6), pp. 580-593

27. Monroy, I. T., Tangdiongga, E. *Crosstalk in WDM Communication Networks*. Norwell, Massachusetts, USA, : Kluwer Academic Publishers; 2002.

28. Dikmelik, Y., Davidson, F. M.: 'Fiber-coupling efficiency for free-space optical communication through atmospheric turbulence'. *Appl. Opt.,* 2005, **44**, (23), pp. 4946-4952

29. Ma, R., Zuo, T. J., Sujecki, S., Phillips, A. J.: 'Improved performance evaluation for DC-coupled burst mode reception in the presence of amplified spontaneous emission noise and interchannel crosstalk'. *IET Optoelectron.,* 2010, **4**, (3), pp. 121-132

30. 'Safety of laser products - part 1: Equipment classification, requirements and user's guide, IEC-60825-1 (Incorporating amendments A1:1997 and A2:2001)', 2001.

31. Vetelino, F. S., Young, C., Andrews, L., Recolons, J.: 'Aperture averaging effects on the probability density of irradiance fluctuations in moderate-to-strong turbulence'. *Applied Optics,* 2007, **46**, (11), pp. 2099-2108

32. Kiasaleh, K.: 'Performance of APD-based, PPM free-space optical communication systems in atmospheric turbulence'. *IEEE Trans. Communs.,* 2005, **53**, (9), pp. 1455-1461

33. Yu, C. X., Neilson, D. T.: 'Diffraction-grating-based (de)multiplexer using image plane transformations'. *IEEE J. Sel.Topics Quantum Electron.,* 2002, **8**, (6), pp. 1194-1201

34. Maru, K., Mizumoto, T., Uetsuka, H.: 'Demonstration of Flat-Passband Multi/Demultiplexer Using Multi-Input Arrayed Waveguide Grating Combined With Cascaded Mach-Zehnder Interferometers'. *J. Lightw. Technol.,* 2007, **25**, (8), pp. 2187-2197

35. Hirano, A., Miyamoto, Y., Kuwahara, S.: 'Performances of CSRZ-DPSK and RZ-DPSK in 43-Gbit/s/ch DWDM G.652 single-mode-fiber transmission'. *Optical Fiber Commun. Conf.,* 2003, pp. 454-456

36. Andrews, L. C., Phillips, R. L., Hopen, C. Y. *Laser Beam Scintillation with Applications*: SPIE Press; 2001.

CHAPTER 7   Outage Probability in WDM FSO System with Turbulence–Accentuated Interchannel Crosstalk

7.1 Introduction

Optical signals propagating in the atmosphere are exposed to significant distortions in intensity and phase because of the inhomogeneous nature of atmospheric particles, and the consequent variations in the index of refraction over the atmospheric channel [1, 2]. This, as already discussed, is referred to as optical scintillation, and causes deep fades in intensity and random loss of signals [3-6]. In previous chapters, the scintillation effect of atmospheric turbulence has been considered entirely as an ergodic random process in which the same result is obtained for the BER whether the calculation is performed using ensemble (statistical) averages or by substituting ensemble averages with time averages. This is justified by the fact that the bit durations considered are shorter than the correlation time of the fluctuations by atmospheric turbulence which is in the range of 1 - 10 ms, such that over a bit period (and indeed typically over many bit periods), the instantaneous fluctuation effects remains approximately the same [7-9]. While scintillation is a slow time-varying process [4, 10], the instantaneous BER of a turbulence-affected system may sometimes fall below the target BER, causing some outages in the system which are not accounted for by the long term average BER [11]. Therefore, the outage probability of an FSO system requires proper consideration, and provides an alternative way (to the average BER) of considering the overall performance of an FSO system. In addition to the generic analysis of FSO communication outage probability performed in [1], the outage probability of other FSO systems including multiple-input-multiple-output (MIMO) and relay assisted multi-hop systems have also been studied in [10, 12-16]. This however represent the first time that the outage probability of a system with turbulence-affected interferer is studied.

7.2 Outage probability

The outage probability or probability of fade is another criterion for expressing the performance of turbulence-affected FSO systems. For a given pdf of the randomly fluctuating irradiance, the outage probability indicates the fractional duration of time [1] in which the (instantaneous) received irradiance in a system with fading channel is below the required irradiance to meet a predetermined target signal-to-noise ratio (SNR), bit error rate (BER) or a Gaussian Q – function (for example, durations x, y and z shown in Fig. 7.1). Unlike the average BER, the outage probability of the system presents the effect of short time outages during which the system may experience high error rate due to the fading characteristics of the atmospheric channel [17]. The target outage requirement in the optical transport network is about 0.001% (i.e. 5.25 minutes per year), while availability greater than 99% (i.e. less than 87.7 hours per year) is usually considered satisfactory in optical access network applications, e.g. LAN applications [18-20]. Thus for a HFFSO access network, the same outage requirement need to be maintained in both the fibre and the FSO parts of the link to ensure that the QoS is not degraded. Except where the FSO link is a repair to the core network or a back-up link in the access network, then users may be willing to accept a less reliable network as a temporary link during repair and maintenance than a total outage.
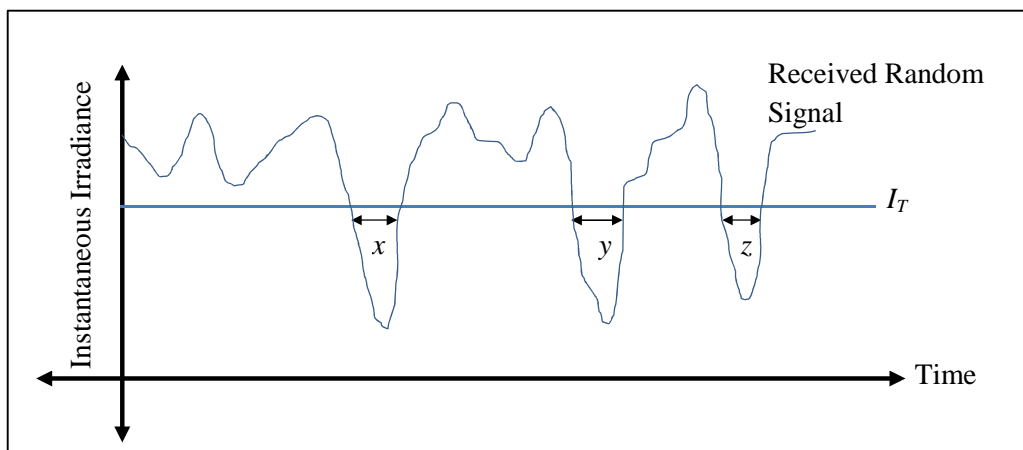
Fig. 7.1 Random signal received at the collecting lens

172

7.3 System and channel model

In a non-turbulent OOK NRZ system with 'optimal' threshold and no crosstalk, the BER is simply written as,

$$BER_{OOK} = \frac{1}{2}\,\text{erfc}\!\left(\frac{Q}{\sqrt{2}}\right) \quad \text{where} \quad Q = \frac{i_1 - i_0}{\sigma_1 + \sigma_0}, \tag{7.1}$$

and for non-turbulent DPPM system with integrate and compare receiver and no crosstalk,

$$BER_{DPPM,ICR} = \frac{n}{2(n-1)}\left\{1 - \left[1 - \frac{1}{2}\,\text{erfc}\!\left(\frac{Q}{\sqrt{2}}\right)\right]^{n-1}\right\} \quad \text{where} \quad Q = \frac{\mu_{X_1} - \mu_{X_0}}{\sqrt{\sigma_{X_1}^2 - \sigma_{X_0}^2}} \tag{7.2}$$

where i_d and σ_d^2 $(d = 0,1)$ are the mean and variance of a transmitted one or zero bit, and μ_{X_d} and $\sigma_{X_d}^2$ are the mean and variance of a transmitted pulse slot or empty slot. Equations (7.1) and (7.2) are modified accordingly in the presence of crosstalk to accurately determine the effective threshold above which the signal quality meets the required performance.

Using the transformation of random variables from eq. 3.6, the gamma-gamma (GG) pdf written as eq. (6.1) could be rewritten as [1, 21],

$$p_{GG}(I,\langle I \rangle) = \frac{1}{\langle I \rangle}\frac{2(\alpha\beta)^{(\alpha+\beta)/2}}{\Gamma(\alpha)\Gamma(\beta)}\left(\frac{I}{\langle I \rangle}\right)^{((\alpha+\beta)/2)-1} K_{\alpha-\beta}\!\left(2\sqrt{\alpha\beta\left(\frac{I}{\langle I \rangle}\right)}\right), \qquad I > 0 \tag{7.3}$$

where I is the instantaneous irradiance, $\langle I \rangle$ is the average or mean irradiance, and $h_Z = I/\langle I \rangle$ is the normalized optical field irradiance written as eq. 3.6 and implicitly expresses the signal attenuation due to atmospheric turbulence induced scintillation. In addition, the irradiance fluctuation in a turbulent FSO channel could be characterized by K-distribution and log-normal (LN) pdf, respectively written as [1, 21],

$$p_{KD}(I,\langle I \rangle) = \frac{1}{\langle I \rangle}\frac{2(\alpha)^{(\alpha+1)/2}}{\Gamma(\alpha)}\left(\frac{I}{\langle I \rangle}\right)^{((\alpha+1)/2)-1} K_{\alpha-1}\!\left(2\sqrt{\alpha\left(\frac{I}{\langle I \rangle}\right)}\right), \qquad I > 0 \tag{7.4}$$

$$p_{LN}(I,\langle I \rangle) = \frac{1}{I\sigma_L\sqrt{2\pi}}\exp\left[-\frac{\left\{\ln\!\left(\frac{I}{\langle I \rangle}\right)+\frac{1}{2}\sigma_L^2\right\}^2}{2\sigma_L^2}\right], \qquad I > 0 \tag{7.5}$$

$\sigma_L^2 = \exp[1/\alpha + 1/\beta] - 1$ is the log-amplitude variance which is made up of the large-scale and small-scale log-irradiance variances.

The outage probability in a turbulence-affected system without any interferer is written as [1],

$$P_{OUT}(\langle I \rangle) = P(I \le I_T | \langle I \rangle) = \int_0^{I_T} p_X(I, \langle I \rangle) dI \tag{7.6}$$

where I_T is the required instantaneous irradiance to achieve the predetermined performance threshold in a non-turbulent system, and $p_X(\bullet)$ represents the GG, KD or LN pdf.

For a turbulence-affected system with interferer (e.g. as shown in Fig. 6.1), we denote the average (turbulence free) irradiances for the data and crosstalk as $\langle I_d \rangle$ and $\langle I_i \rangle$ respectively, such that the independent turbulence pdfs of the signal and interferer is respectively written as $p_{X_d}(I_d, \langle I_d \rangle)$ and $p_{X_i}(I_i, \langle I_i \rangle)$ where I_d and I_i are the instantaneous irradiances of the signal and interferer both defined at the photodiode facet or as the equivalent irradiances referred back to the collecting lenses. Ideally, the system is expected to perfectly filter-out the irradiance of the interfering signal so that the desired signal is unimpaired. However, in most WDM FSO built systems, the desired signal is accompanied with some level of turbulence-affected crosstalk due to imperfections in the demultiplexer.

Independent of turbulence, the instantaneous BER of the system is a function of I_d and I_i, and for an OOK system the instantaneous BER can be written as,

$$BER_{inst}(I_d, I_i) = \frac{1}{4} \text{erfc}\left(\frac{Q(I_d, I_i)}{\sqrt{2}} \right) \tag{7.7}$$

$$Q(I_d, I_i) = \frac{i_{1,0}(I_d, I_i) - i_{0,1}(I_d, I_i)}{\sigma_{1,0}(I_d, I_i) + \sigma_{0,1}(I_d, I_i)} \tag{7.8}$$

where the exact value of BER_{inst} and Q in eqs. (7.7) and (7.8) depends on the point where I_d and I_i are defined in the system, and considering system gains and losses. Equation (7.8) implies that for a fixed Q, a relationship $I_d = f(I_i)$ exists, or equivalently, there is a signal-to-crosstalk ratio for a given I_d that is required to achieve a defined instantaneous BER target. For a DPPM system, this relationship is implicitly expressed in eq. (6.17) which can be re-written as,

$$P(X_{0,int} > X_{1,int} | I_d, I_i) = 0.5 \, \text{erfc}\left(\frac{\mu_{X_{1,int}}(I_d, I_i) - \mu_{X_{0,int}}(I_d, I_i)}{\sqrt{2[\sigma^2_{X_{1,int}}(I_d, I_i) + \sigma^2_{X_{0,int}}(I_d, I_i)]}} \right) \tag{7.9}$$

The relationship $I_d = f(I_i)$ defines a curve where the instantaneous BER is equal
to the target BER as it is illustrated in Fig. 7.2. Above the curve is the region
where the instantaneous BER is less than the target BER and below the curve is
the region where the instantaneous BER is greater than the target BER and
indicates the outage area.
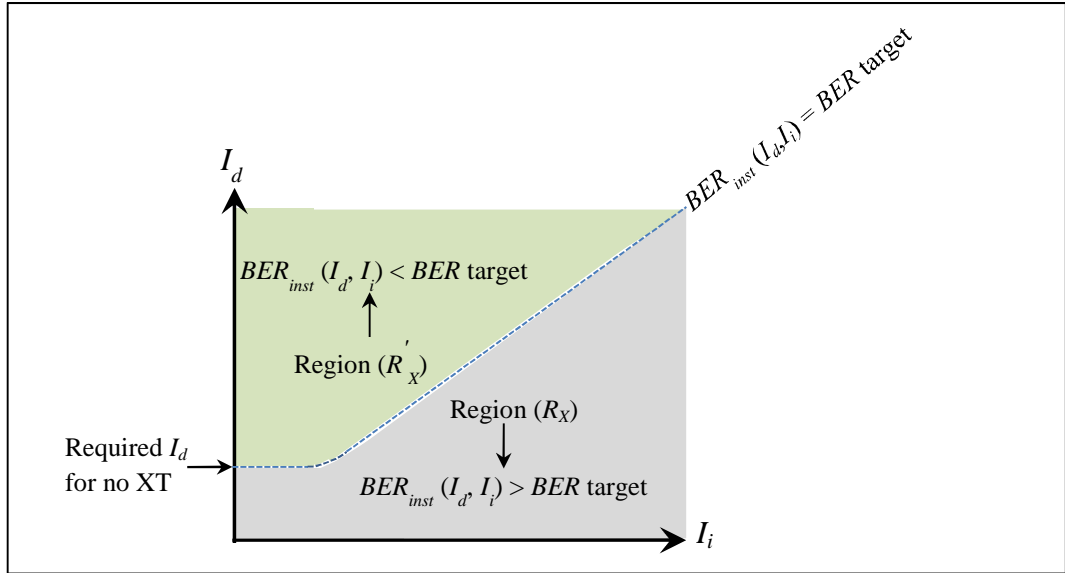
Fig. 7.2 Illustration of outage area (region R_X) for a turbulence-affected WDM
FSO system

The joint pdf of the turbulence on the desired signal and the interfering signal
is written as $p_{X_d X_i}\left(I_d, I_i, \langle I_d \rangle, \langle I_i \rangle\right)$. For a Rytov variance $\sigma_R^2 = 1.23 C_n^2 k^{7/6} l_{fso}^{11/6} \approx 4.2$
(indicating a strong turbulence), and $L_{demux,i} = 25$ dB, the joint pdf is shown in Fig.
7.3 as a function of both I_d and I_i using the GG distribution and for a target BER
of 10^{-3}. The red curve represents the points where the instantaneous BER is equal
to the target BER and the region below the curve is indicative of the outage area.
Note that both signal and interferer are assumed to have the same FSO link length
(l_{fso}) of 1500 m here.
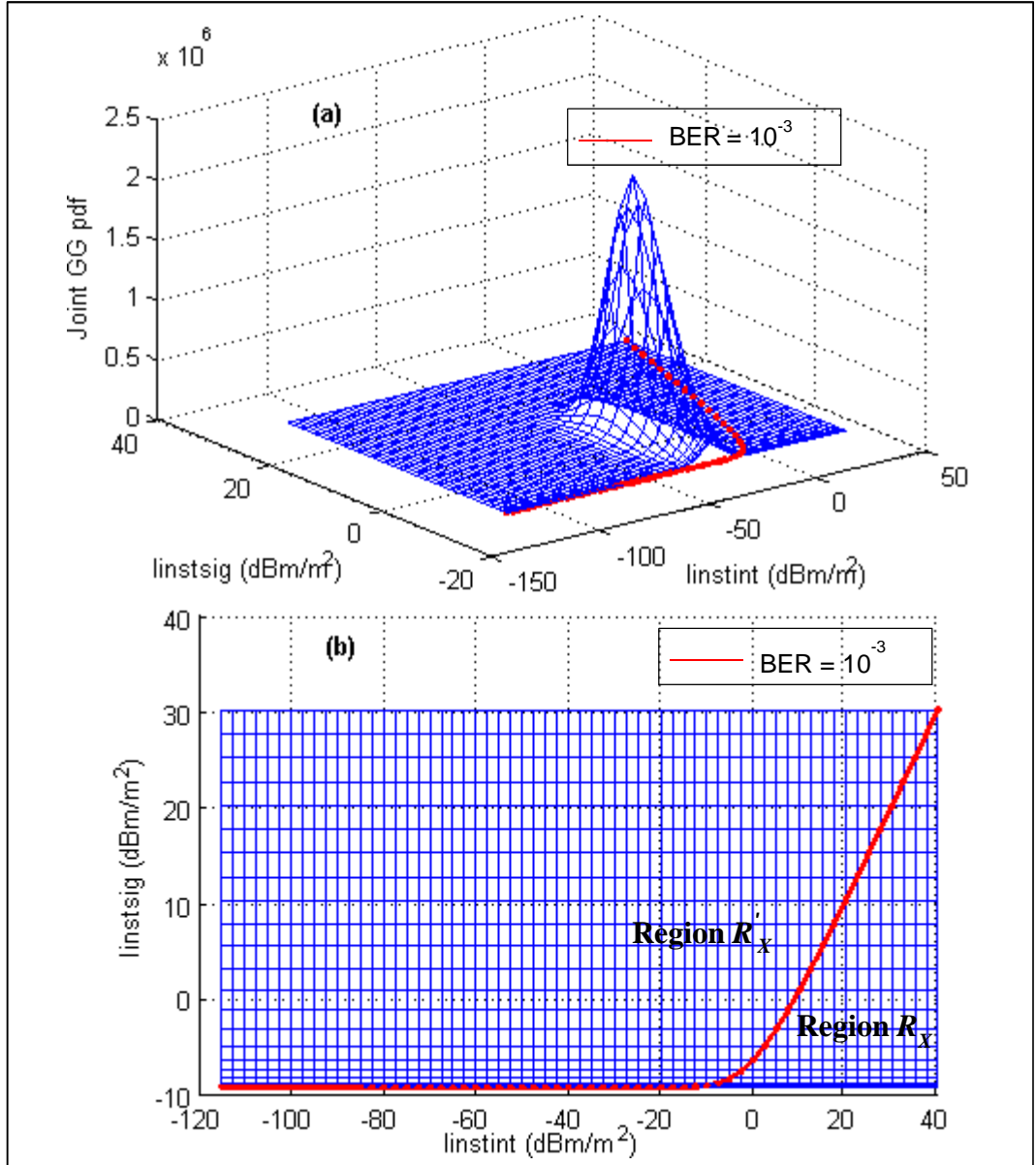
Fig. 7.3 Joint turbulence pdf of the desired signal and the interfering signal for C_n^2
$= 1 \times 10^{-13}$ m$^{-2/3}$, $l_{fso} = 1500$ m, $L_{demux,i} = 25$ dB, $\langle I_d \rangle = 10$ dBm/m^2 and target BER
of 10^{-3} in an OOK system, and using the GG pdf with parameters defined in Table
6.1, (the red curve signifies the points where the BER$_{inst}$ = BER target): (a) Joint
pdf (full view) and (b) top view

The outage probability is thus obtained by integrating the joint pdf over the
area that the instantaneous BER is greater than the BER target, and is written as;

$$P_{OUT}(\langle I_d \rangle, \langle I_i \rangle) = \iint_{R_X} p_{X_d X_i}(I_d, I_i, \langle I_d \rangle, \langle I_i \rangle) \, dI_d \, dI_i \qquad (7.10)$$

where R_X is the region in (I_d, I_i) space where $BER_{inst}(I_d, I_i) >$ BER target (e.g. as
shown in Figs. 7.2 and 7.3). Equation (7.10) could be simplified further as,

$$P_{OUT}\left(\langle I_d \rangle, \langle I_i \rangle\right) = \int_0^\infty \int_0^{I_{dT}(I_i)} p_{X_d}\left(I_d, \langle I_d \rangle\right) p_{X_i}\left(I_i, \langle I_i \rangle\right) dI_d \, dI_i$$

$$= \int_0^\infty p_{X_i}\left(I_i, \langle I_i \rangle\right) \left[\int_0^{I_{dT}(I_i)} p_{X_d}\left(I_d, \langle I_d \rangle\right) dI_d \right] dI_i \qquad (7.11)$$

where $I_{dT}(I_i)$ is the threshold instantaneous irradiance required to achieve a BER$_{inst}$ that is equal to the BER target and is dependent on the instantaneous irradiance of the interferer.

For quick insight into the outage probability analysis of a system with interferer, consider a non-amplified system with only thermal noise and ignoring component and path losses. Equation (7.8) for such a system could be written as,

$$Q\left(h_{turb,sig}, h_{turb,int}\right) = \frac{h_{turb,sig}\left[R_{sig}\left(P_1 - P_0\right)\right] + h_{turb,int}\left[R_{int}\left(P_{0XT} - P_{1XT}\right)\right]}{2\sigma_{th}} \qquad (7.12)$$

where R_{sig} and R_{int} are the responsivities of the signal and interferer, P_1 or P_0 and P_{1XT} or P_{0XT} are defined as the turbulence-free received power in a transmitted one or zero of the signal and interferer respectively, (i.e. the power received when $h_{turb,sig}$ and $h_{turb,int}$ are both equal to 1), σ_{th}^2 is the thermal noise variance, while $h_{turb,sig} = I_d / \langle I_d \rangle$ and $h_{turb,int} = I_i / \langle I_i \rangle$ are the attenuations due to turbulence induced scintillation on the desired signal and the interfering signal respectively. Assuming equal responsivity and extinction ratio (r) for signal and interferer, eq. (7.12) could further be simplified as

$$h_{turb,sig} = h_{turb,int} L_{demux,i} + \frac{\sigma_{th} Q\left(h_{turb,sig}, h_{turb,int}\right)(r+1)}{RP_{av}(r-1)} \qquad (7.13)$$

where we have used the relationships $P_1 = P_{av}\left(2r/(r+1)\right)$, $P_0 = P_{av}\left(2/(r+1)\right)$ and $P_{avXT} = P_{av} L_{demux,i}$, and P_{av} is the turbulence-free received average power. In addition, eq. (7.13) could also be written in terms of the instantaneous and mean irradiances as,

$$I_{dT}(I_i) = I_d = \frac{I_i \langle I_d \rangle L_{demux,i}}{\langle I_i \rangle} + \frac{\sigma_{th} Q\left(h_{turb,sig}, h_{turb,int}\right)(r+1)}{RA_{RX}(r-1)} \qquad (7.14)$$

where $P_{av} = \langle I_d \rangle A_{RX}$, and A_{RX} is the area of the receiving lens aperture.

The relationships in eqs. (7.13) and (7.14) are fully depicted in Fig. 7.4. for $Q(h_{turb,sig}, h_{turb,int})$ equivalent of BER$_{inst}$ = 10^{-3}. From both the equations and Fig. 7.4, it is clearly seen that the threshold instantaneous irradiance (I_{dT}) increases as

$h_{turb,int}$ increases. This is expected because higher threshold is required to counter the rise in attenuations due to turbulence induced scintillation on the interfering signal if a BER_{inst} equal to the BER target is to be achieved. Additionally, I_{dT} also increases as the mean irradiance $\langle I_d \rangle$ increases. This is because the interfering signal power also increases when the mean irradiance increases, necessitating an increase in the required I_{dT} to maintain a BER_{inst} that is equal to the BER target. Furthermore, the influence of aperture averaging on turbulence induced scintillation can be deduced from eq. (7.14) which shows that required I_{dT} could also be reduced by increasing the aperture area of the receiving lens.
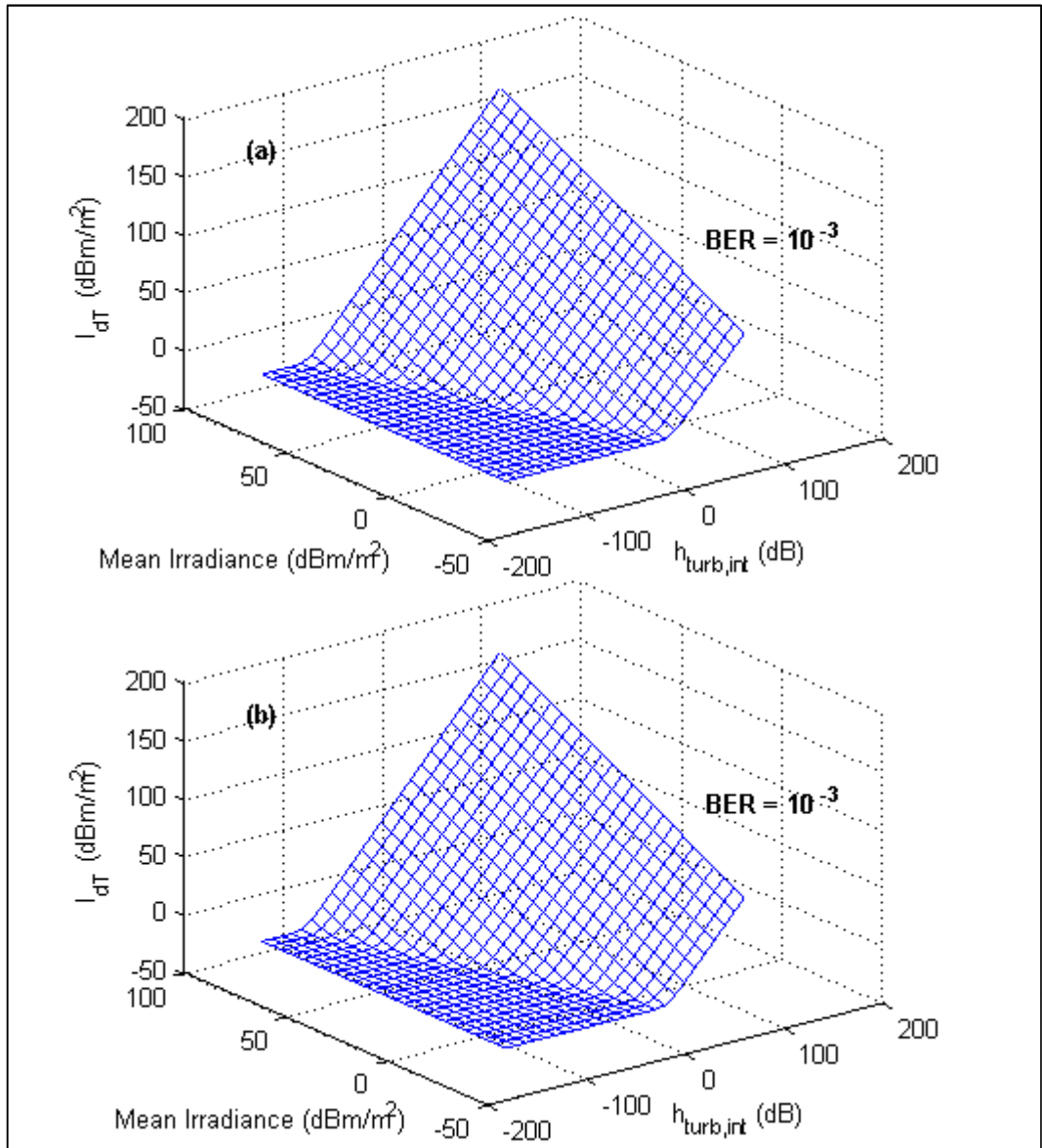
Fig. 7.4 Threshold instantaneous irradiance (I_{dT}) as a function of turbulence attenuation on interferer ($h_{turb,int}$) and mean irradiance, $C_n^2 = 10^{-13}$ m$^{-2/3}$, FSO Link Length = 1500 m and $L_{demux,i}$ = 35 dB: (a) OOK and (b) DPPM

7.4 Numerical results

In setting the target threshold for the instantaneous received irradiance, an (adaptive threshold) optically preamplified FSO receiver is considered with the input optical power defined at the receiver, thus only the effect of attenuation due to turbulence is taken into account. Except if it is stated otherwise, in the following results I_T for the system without interferer and I_{dT} for the system with an interferer are set to be consistent with a BER target of 10^{-3} (i.e. assuming interleaved FEC as discussed in Chapter 2 is implemented, and also to gives a qualitative feel for more stringent BER). It should be noted that while BER target of 10^{-3} may seem high, it has been shown by results in [22-24] that it is possible to reduce the BER and recover transmitted data using FEC as found in recent high-sensitivity optical communication systems. Perfect extinction is assumed, and the DPPM coding level is fixed at 2. Other parameters used in the analysis are taken from Table 6.1 and for straightforwardness the desired user and the interferer are both assumed to be at equal distances from the remote node.

The outage probability for both OOK and DPPM systems without interferer is shown in Fig. 7.5 using the GG, KD and LN turbulence distribution models. The Rytov variance σ_R^2 is approximately 4.2 (with $\alpha \approx 4.44$ and $\beta \approx 2.15$), thus the turbulence regime is characterized as strong. The result obtained using the LN pdf model is generally optimistic. As noted in Chapter 3, the LN pdf is commonly used in modelling weak turbulence conditions, but the difference between the pdf tails of the LN and GG distributions widens as the turbulence becomes stronger. On the other hand, the K-distribution is widely used in modelling strong to saturated turbulence conditions, but is only dependent on the α parameter. The KD is the limit of the GG when $\beta \to 1$. This explains the discrepancy shown in Fig. 7.5 between the GG and the KD outage probability curves when $\beta \approx 2.15$. The GG model however predicts a worse but more realistic result compared to the LN model. Fig. 7.5 clearly indicates that DPPM systems predict a better outage probability than OOK systems. In previous chapters, it was established that DPPM systems are more power efficient than OOK systems. For the same reason, DPPM systems are more resistant to turbulence induced outages which only occur when the received instantaneous power is below the target threshold.
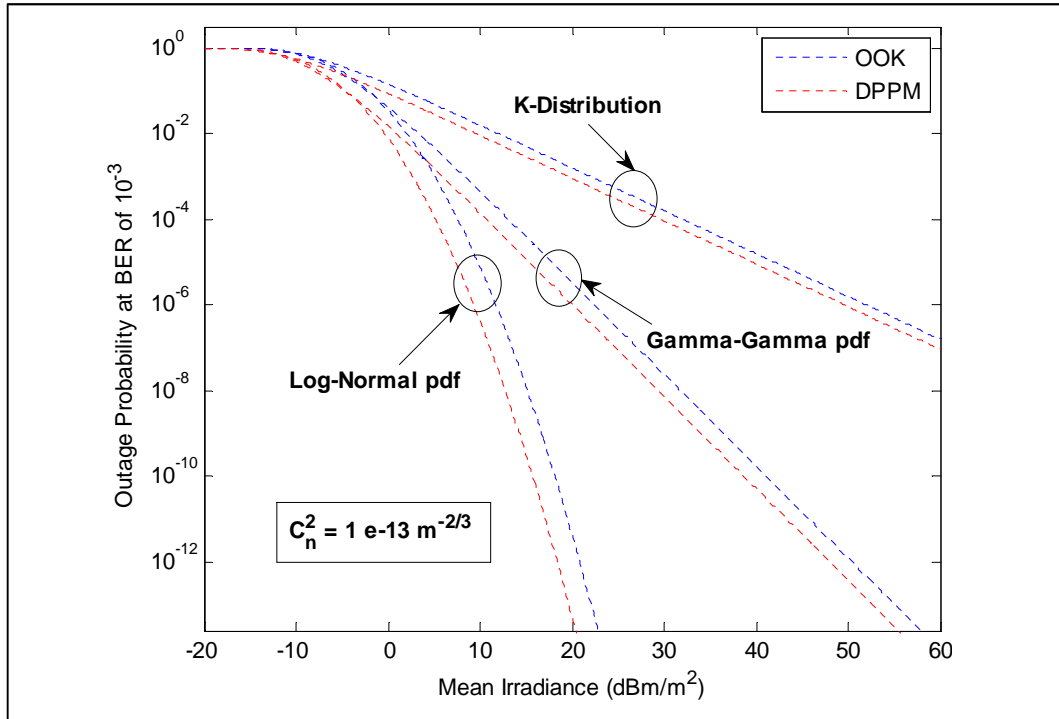
Fig. 7.5 Outage Probability versus Mean Irradiance for a turbulent system with no interferer: FSO Link Length = 1500 m and $C_n^2 = 10^{-13}$ m$^{-2/3}$

The remaining results are presented using the GG distribution model which has a closer fit to previously obtained simulation results [1, 25]. Fig. 7.6 shows the result of the outage probability as a function of the mean irradiance and FSO link length for both OOK and DPPM systems without interferer. Both results in Figs. 7.6a and 7.6b seem identical but a point to point comparison actually reveals that DPPM have a slightly lower outage probability compared to OOK as already shown in Fig. 7.5. For a fixed mean irradiance in Fig. 7.6, the outage probability increases with the FSO link length (and consequently, the Rytov variance (σ_R^2)). An increase in Rytov variance indicates increase in the strength of turbulence of the link, thus higher threshold instantaneous irradiance is required to achieve the BER target. A corresponding increase in the transmitter power (and implicitly the mean irradiance) is therefore necessary to reduce the likelihood of the system being in outage, as shown in Fig. 7.6, where the outage probability is decreasing as the mean irradiance is increasing.

180
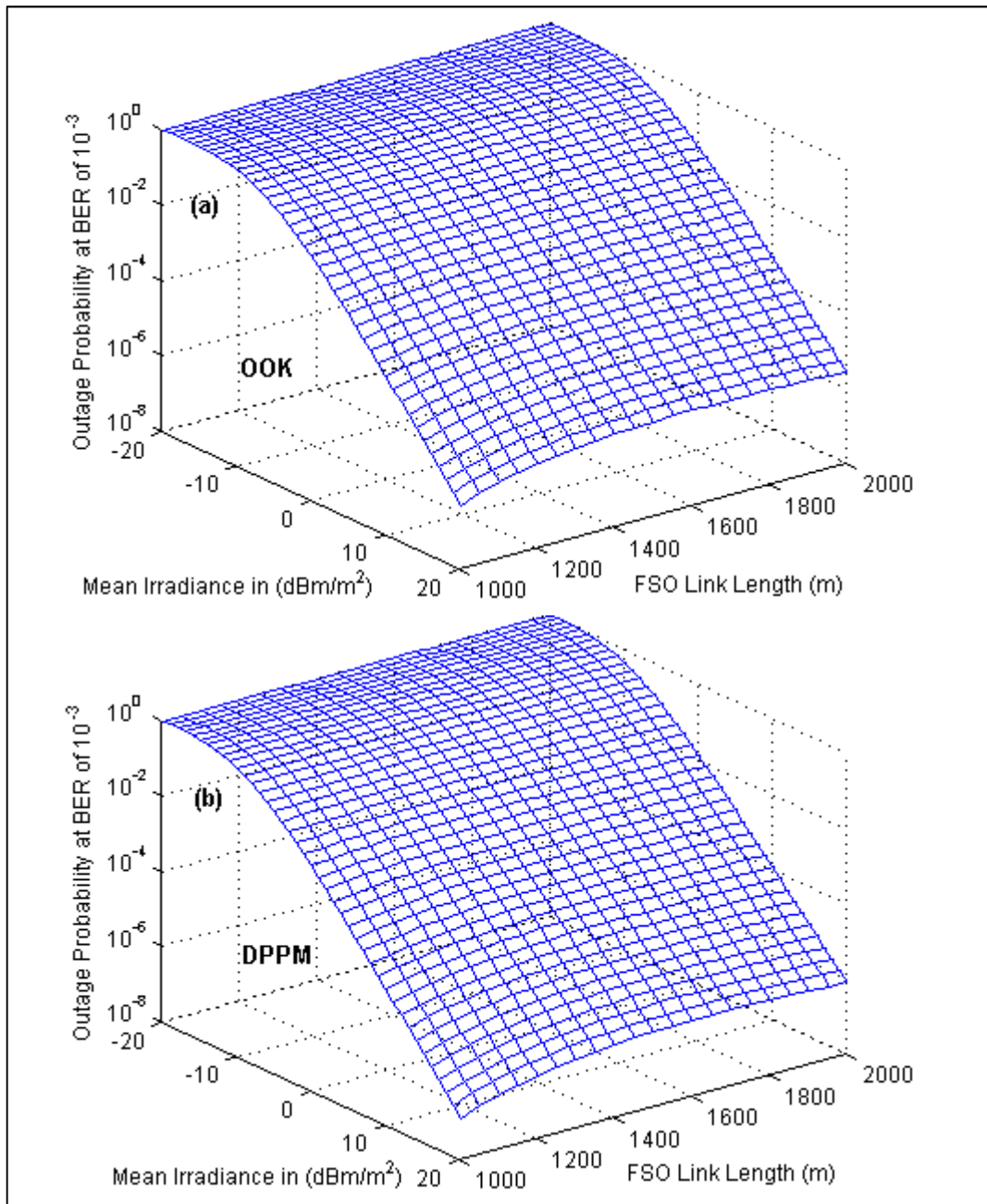
Fig. 7.6 Outage Probability as a function of FSO link length and mean irradiance
for a turbulent system with no interferer, $C_n^2 = 10^{-13}$ m$^{-2/3}$: (a) OOK and (b) DPPM

Figs. 7.7 and 7.8 show the outage probability result in the presence of a single
turbulent interferer for OOK and DPPM systems respectively. The system outage
performances with variation in the refractive index structure constant (C_n^2),
demultiplexer adjacent channel rejection ($L_{demux,i}$) and target BER are examined
for an FSO link length (l_{fso}) of 1500 m for both signal and interferer. With the
presence of interferer, error floors similar to those obtained for BER evaluations

in Chapter 6 and in [26] occur. As explained in Chapter 6, when a turbulence-affected signal is impaired by a turbulence-affected interferer, error floor occur at a probability of error determined by the turbulence attenuation on both the signal ($h_{turb,sig}$) and interferer ($h_{turb,int}$) as well as the demux adjacent channel rejection L_{demuxi}, and sets in once $h_{turb,int}/h_{turb,sig} \geq 1/L_{demux,i}$. This is also expressed in eq. (7.13) which shows that for a large value of P_{av}, the last term on the RHS of the equation tends to zero, and $h_{turb,sig} \approx h_{turb,int} L_{demux,i}$ gives the value of the error floor as evidently seen in Figs. 7.7a – 7.7b and 7.8a – 7.8b where the error floor position shifts with change in C_n^2 or/and L_{demuxi}. The error floor is independent of the predetermined threshold performance and target BER, (see Figs. 7.7c and 7.8c), however for a fixed mean irradiance, the outage probability worsens with decrease in target BER (increase in required threshold instantaneous irradiance) before the error floor occurs. It should be noted that DPPM system still retains a marginal advantage on outage probability over OOK systems even in the presence of interferers. However, this is only obtainable before the error floor sets in as the error floor occur at the same outage probability value for both the OOK and DPPM systems.
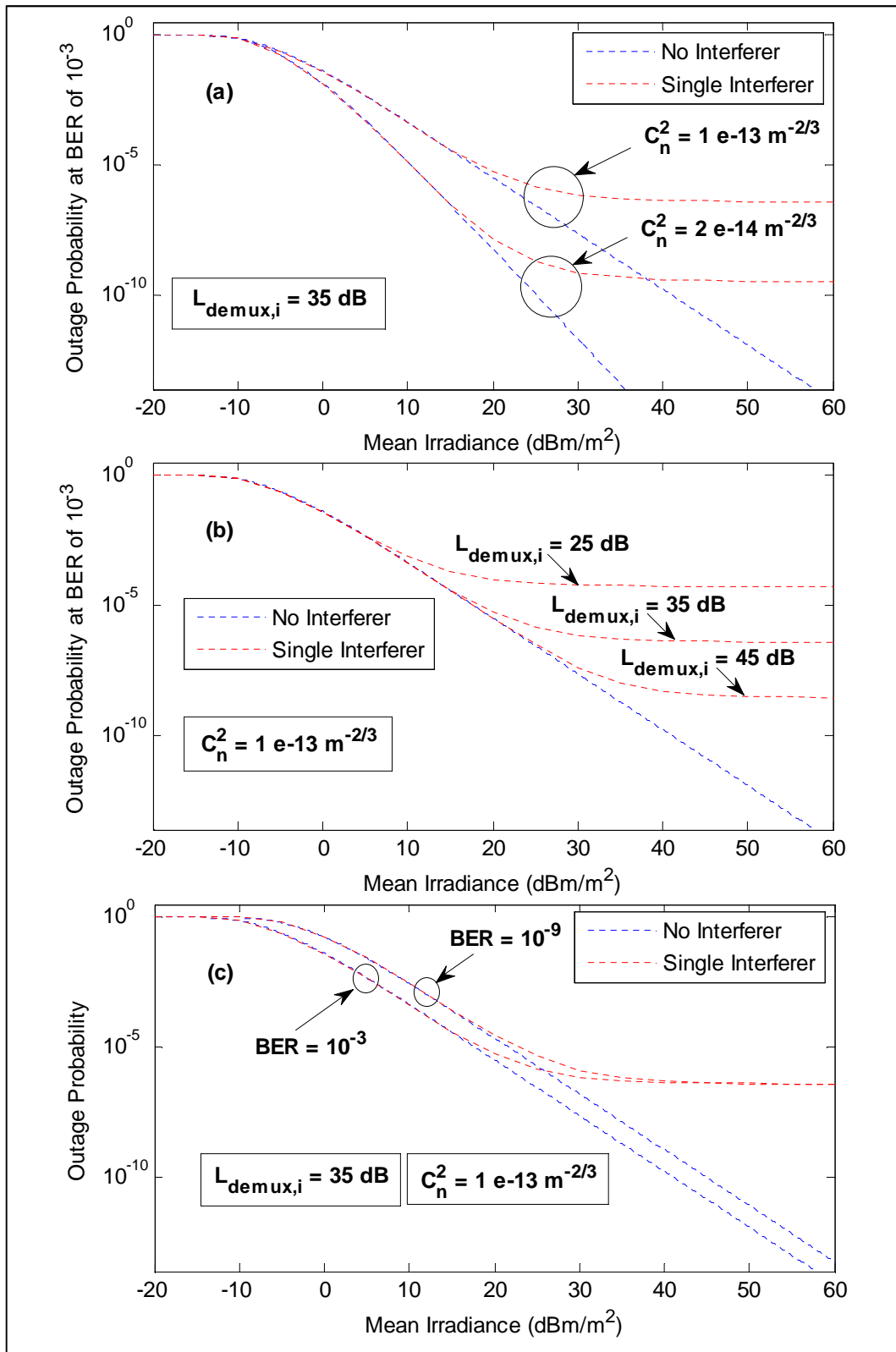
Fig. 7.7 OOK Outage Probability versus Mean Irradiance for a turbulent system (FSO Link Length = 1500 m): (a) for different values of C_n^2 (b) for different values of $L_{demux,i}$ and (c) for different values of the target BER
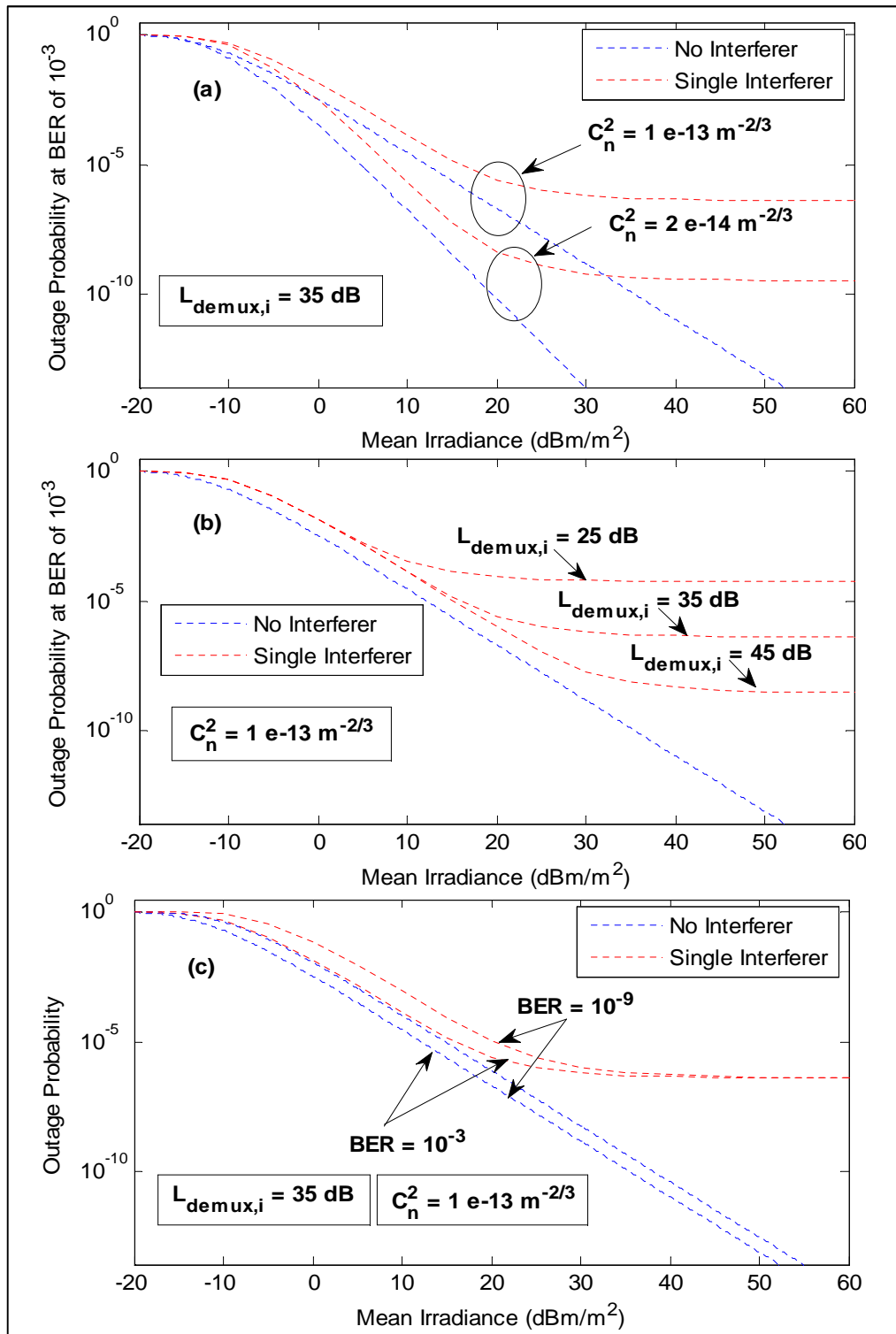
Fig. 7.8 DPPM Outage Probability versus Mean Irradiance for a turbulent system
(FSO Link Length = 1500 m): (a) for different values of C_n^2 (b) for different
values of $L_{demux,i}$ and (c) for different values of the target BER

The outage probability as a function of the mean irradiance and of either the
FSO link length or the demux adjacent channel rejection is shown in Figs. 7.9 and

7.10 for OOK and DPPM systems respectively. In Figs. 7.9a and 7.10a, the C_n^2 is fixed at 10^{-13} m$^{-2/3}$ with L_{demuxi} = 35dB. The outage probability is shown increasing as the FSO link length of both the desired user and the interferer (which is assumed equal in this chapter) is also increasing. The results in Figs. 7.9a and 7.10a are of similar trend to Fig. 7.6 for a system without interferer, except for the occurrence of error floors and higher outage probability values in Figs. 7.9a and 7.10a due to the presence of an interferer. The error floor becomes more prominent, and the achievable outage performance becomes increasingly limited as the FSO link length and Rytov variance (σ_R^2) (and implicitly the strength of the turbulence regime affecting the desired signal and the interfering signal) increases. The impact of the demux adjacent channel rejection is investigated in Figs. 7.9b and 7.10b for OOK and DPPM systems respectively. The FSO link lengths of the signal and interferer are fixed at 1500 m with C_n^2 = 10^{-13} m$^{-2/3}$, resulting in σ_R^2 = 4.2 and indicating a strong turbulence regime. As expected, in Figs. 7.9b and 7.10b, the outage probability is shown decreasing as the demux adjacent channel rejection is increasing. This is simply due to decrease in both the interferer's power and the accompanying scintillation effects. In both Figs. 7.9 and 7.10, it could be seen that the outage probability decreases as more power is transmitted, this further emphasises the need for a system with power efficient modulation scheme such as DPPM. It is important to note that although the BER at every point in Figs. 7.9 and 7.10 is 10^{-3}, the outage probability ranges from approximately 1 to 10^{-14}, depending on the mean irradiance, the level of turbulence and the demux adjacent channel rejection. This clearly highlights the importance of the outage probability analysis to transport or network layer design in turbulent FSO channel, as such analysis ensures that the system is stable and robust to turbulence induced fading. To further buttress this point, we compare the outage probability for a DPPM system with L_{demuxi} = 25dB and σ_R^2 = 4.2 (i.e. C_n^2 = 10^{-13} m$^{-2/3}$ and l_{fso} = 1500 m) as shown in Fig. 7.8b with the average BER calculated using the same parameters and shown in Fig 6.3b. Both results are obtained for an optically amplified receiver system with all losses ignored except the turbulence induced scintillation effect. The comparison shows that the required average received power to achieve an average BER of 10^{-3} is about -39.1 dBm while an average irradiance of about 6.5 dBm/m^2 (an equivalent of -32.3

dBm in average received power using receiving lens aperture diameter of 13 mm) is required to achieve an outage probability of 10^{-3}. Thus, in a high sensitive system that may require high degree of accuracy (e.g. in defence and security systems) it may be necessary to transmit more power than indicated by the average BER to ensure that the integrity of the received data is not compromised due to deep fades experienced in the atmospheric channel.
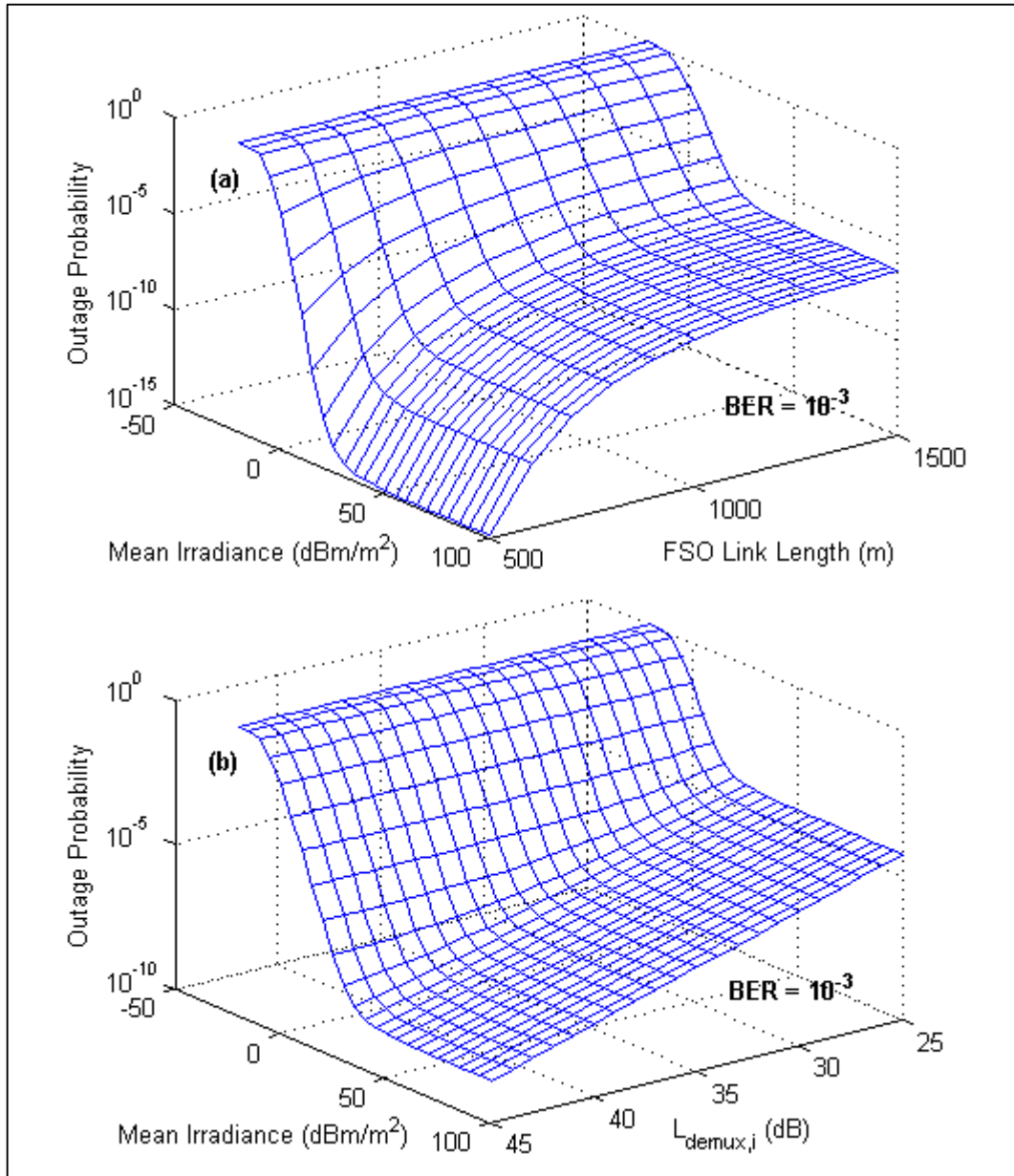
Fig. 7.9 Outage Probability for an OOK system at BER target of 10^{-3} and C_n^2 of 10^{-13} m$^{-2/3}$, as a function of the mean irradiance and: (a) the FSO Link Length ($L_{demux,i} = 35$ dB), and (b) the demux adjacent channel rejection ($l_{fso} = 1500$ m)
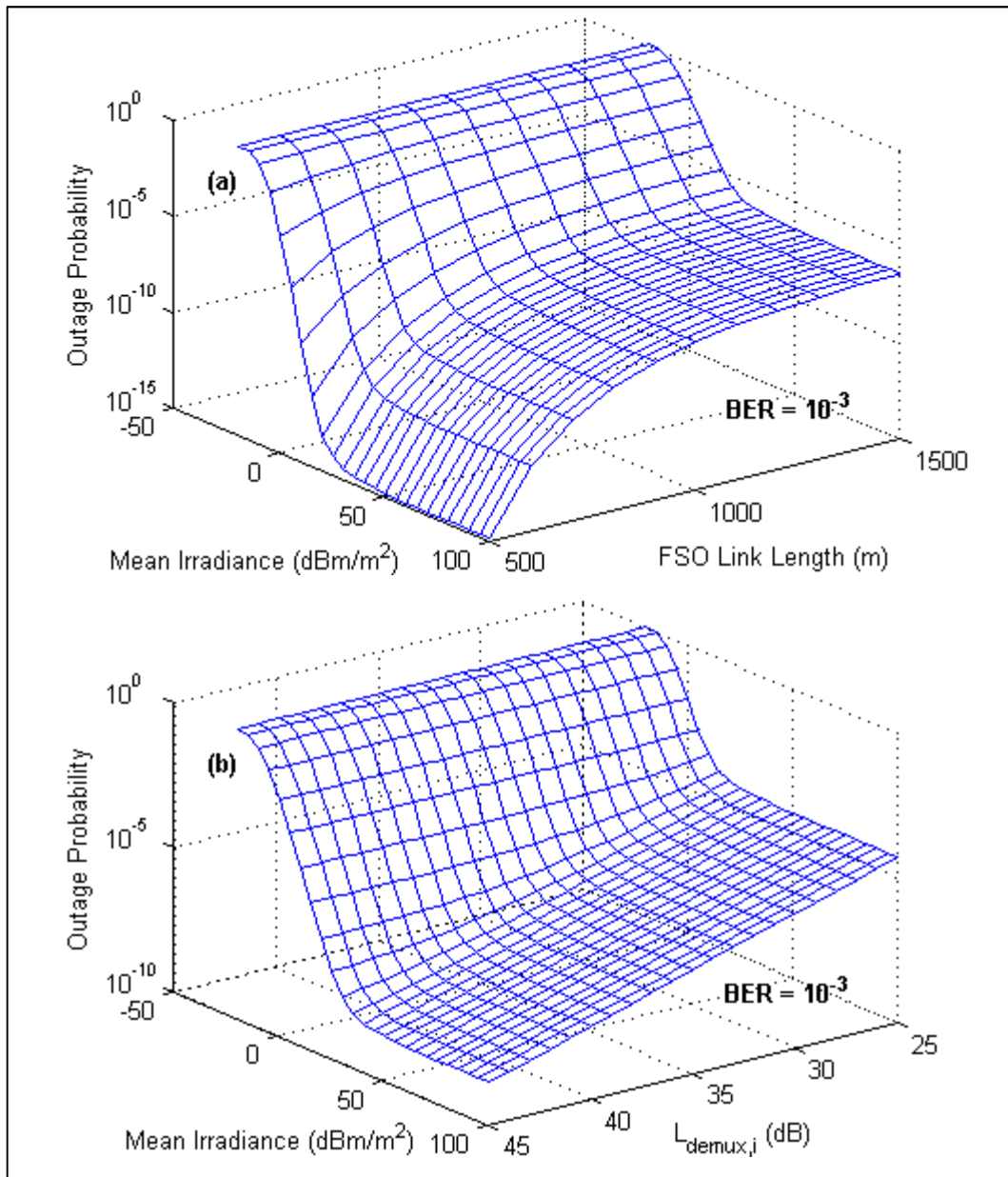
Fig. 7.10 Outage Probability for a DPPM system at BER target of 10^{-3} and C_n^2 of
10^{-13} m$^{-2/3}$, as a function of the mean irradiance and: (a) the FSO Link Length
($L_{demux,i}$ = 35 dB), and (b) the demux adjacent channel rejection (l_{fso} = 1500 m)

7.5 Summary

The analysis of outage probability for WDM FSO systems impaired by turbulence-accentuated interchannel crosstalk is performed in this chapter for both OOK and DPPM systems. The presented results show that systems with acceptable BER performance could suffer from high outages if the received instantaneous irradiance is not properly considered in the design of an FSO network. Predictably, the outage probability increases as the crosstalk power increases, and as the turbulence attenuation on the interfering or/and desired signal become stronger. As have been shown in previous chapters, the DPPM system presents an advantage in power efficiency over the OOK system. This advantage is marginally reduced in the presence of turbulence, although, in applications where the DPPM bandwidth expansion is not a direct concern, the DPPM power efficiency may be improved by increasing the DPPM coding level (*M*) above the value of 2 which has mainly been used in this thesis. Thus far we have investigated the performance of the hybrid fibre and FSO network for indoor application using CDMA, and for outdoor application using WDM. An outdoor WDM network incorporating CDMA for network scalability, which could be seamlessly integrated with the indoor CDMA network analysed in Chapter 4, is considered in the last chapter.

7.6 References

1. Andrews, L. C., Phillips, R. L. *Laser Beam Propagation Through Random Media*. 2nd ed: SPIE Press, Bellingham, Washington; 2005.
2. Zhu, X., Kahn, J. M.: 'Free-space optical communication through atmospheric turbulence channels'. *IEEE Trans. Commun.,* 2002, **50**, (8), pp. 1293-1300
3. Majumdar, A. K. Theory of Free-Space Optical (FSO) Communication Signal Propagation Through Atmospheric Channel. Advanced Free Space Optics (FSO). Springer Series in Optical Sciences. 186: Springer New York; 2015. pp. 21-30
4. Farid, A. A., Hranilovic, S.: 'Outage Capacity Optimization for Free-Space Optical Links With Pointing Errors'. *J. Lightw. Technol.,* 2007, **25**, (7), pp. 1702-1710
5. Andrews, L. C., Phillips, R. L., Hopen, C. Y. *Laser Beam Scintillation with Applications*: SPIE Press; 2001.
6. Perez, J., Zvanovec, S., Ghassemlooy, Z., Popoola, W. O.: 'Experimental characterization and mitigation of turbulence induced signal fades within an ad hoc FSO network'. *Opt. Express,* 2014, **22**, (3), pp. 3208-3218
7. Zhu, X., Kahn, J. M., Wang, J.: 'Mitigation of turbulence-induced scintillation noise in free-space optical links using temporal-domain detection techniques'. *IEEE Photonics Technology Letters,* 2003, **15**, (4), pp. 623-625
8. Zhu, X., Kahn, J. M.: 'Communication techniques and coding for atmospheric turbulence channels'. *J Optic Comm Rep,* 2007, **4**, (6), pp. 363-405

9. Razavi, M., Shapiro, J. H.: 'Wireless optical communications via diversity reception and optical preamplification'. *IEEE Trans. Wireless Commun.,* 2005, **4**, (3), pp. 975-983

10. Letzepis, N., Guillen i Fabregas, A.: 'Outage probability of the Gaussian MIMO free-space optical channel with PPM'. *IEEE Trans. Commun.,* 2009, **57**, (12), pp. 3682-3690

11. Chan, V. W. S.: 'Free-space optical communications'. *J. Lightwave Technol.,* 2006, **24**, (12), pp. 4750-4762

12. Young-chai, K., Alouini, M. S., Simon, M. K.: 'Outage probability of diversity systems over generalized fading channels'. *IEEE Trans. Commun.,* 2000, **48**, (11), pp. 1783-1787

13. Karimi, M., Nasiri-Kenari, M.: 'Outage analysis of relay-assisted free-space optical communications'. *IET Communications,* 2010, **4**, (12), pp. 1423-1432

14. Hasna, M. O., Alouini, M. S.: 'Outage probability of multihop transmission over Nakagami fading channels'. *IEEE Commun. Letters,* 2003, **7**, (5), pp. 216-218

15. Karagiannidis, G. K., Tsiftsis, T. A., Sandalidis, H. G.: 'Outage probability of relayed free space optical communication systems'. *Electronics Letters,* 2006, **42**, (17), pp. 994-995

16. Farid, A. A., Hranilovic, S.: 'Diversity Gain and Outage Probability for MIMO Free-Space Optical Links with Misalignment'. *IEEE Trans. Commun.,* 2012, **60**, (2), pp. 479-487

17. Ghassemlooy, Z., Popoola, W., Rajbhandari, S. *Optical Wireless Communications - System and Channel Modelling with MATLAB*. 1st ed. London: CRC Press; 2013.

18. Kim, I. I., Korevaar, E. J.: 'Availability of free-space optics (FSO) and hybrid FSO/RF systems'. *Int'l Symp. on the Convergence of IT and Commun.* 2001: Int'l Society for Optics and Photonics, pp. 84-95

19. Prokes, A.: 'Atmospheric effects on availability of free space optics systems'. *OPTICE,* 2009, **48**, (6), pp. 066001-066010

20. Xiao, X. *Technical, commercial and regulatory challenges of QoS: An internet service model perspective*. Massachusetts, USA: Morgan Kaufmann; 2008.

21. Aladeloba, A. O., Phillips, A. J., Woolfson, M. S.: 'Improved bit error rate evaluation for optically pre-amplified free-space optical communication systems in turbulent atmosphere'. *IET Optoelectron.,* 2012, **6**, (1), pp. 26-33

22. Anguita, J. A., Djordjevic, I. B., Neifeld, M. A., Vasic, B. V.: 'Shannon capacities and error-correction codes for optical atmospheric turbulent channels'. *J. Optical Networking,* 2005, **4**, (9), pp. 586-601

23. Djordjevic, I. B., Milenkovic, O., Vasic, B. V.: 'Generalized low-density parity-check codes for optical communication systems'. *J. Lightw. Technol.,* 2005, **23**, (5), pp. 1939

24. Djordjevic, I. B., Vasic, B. V., Neifeld, M. A.: 'LDPC coded OFDM over the atmospheric turbulence channel'. *Opt. Express,* 2007, **15**, (10), pp. 6336-6350

25. Flatté, S. M., Bracher, C., Wang, G.: 'Probability-density functions of irradiance for waves in atmospheric turbulence calculated by numerical simulation'. *Journal of the Optical Society of America* 1994, **11**, (7), pp. 2080-2092

26. Aladeloba, A. O., Woolfson, M. S., Phillips, A. J.: 'WDM FSO Network with Turbulence-Accentuated Interchannel Crosstalk'. *J. Opt. Commun. Netw.,* 2013, **5**, (6), pp. 641-651

CHAPTER 8   Optical CDMA over WDM in Hybrid Fibre and Turbulent FSO Network

8.1 Introduction

The passive optical network (PON) was experimented and standardized within the last two decades, and has topologically evolved at different times in attempt to open up the optical access networks. Compared to the copper-based access networks, the PON was major progress in providing higher bandwidth to the access networks [1]. Nevertheless, further upgrade is desired in the optical access networks to avoid capacity saturation and adequately provide for the increasing traffic demands [2], and optical CDMA could provide the additional capacity.

In a typical PON, only two wavelengths are used for signal transmission (one each for the upstream and downstream transmissions). Recent studies on PON propose wavelength division multiplexing (WDM) as the possible solution to providing higher bandwidth in PON [1-3]. Additionally, integrating WDM into PON provide a smooth and flexible upgrade path for the legacy PON and presents a platform for the coexistence of future and present PON devices [2]. Although WDM has attracted major interest in research and industry, commercial deployments of WDM systems have been slow. Advances in optical access technology and current traffic demands in access networks have eased some of the concerns over large scale WDM deployment in PON (such as high bandwidth market availability, undeveloped device technology and software support) [1]. The present challenge to commercial deployment is the high cost of equipment compared to existing TDM systems [3, 4]. Some of the schemes proposed to mitigate the cost of equipment in WDM PON are found in [5-7].

The wavelength grid for CWDM was provided by the ITU-T Recommendation G.694.2, supporting 18 channels from 1271 nm to 1611 nm at 20 nm wavelength spacing [8-10]. Appendix II of the same recommendation further relates to wavelength allocation for video distribution signal multiplexed with BPON, and with only 18 wavelength channels available, further capacity upgrade may be necessary to support large number of users in an access network [8, 9]. Optical

code division multiple access (OCDMA) technique has been studied and/or experimentally demonstrated for use in different channels [11-14], and can potentially combine with WDM to provide additional capacity in the access network. Hybrid WDM and OCDMA systems have been investigated for PON application in [9, 15-18]. In addition to the boost in capacity and high scalability, a hybrid WDM and OCDMA access network would benefit from the remarkable progress made in optical encoder/decoder device technology and enhanced system security, while still maintaining many advantages of the WDM PON [9, 10]. While such a hybrid system provides numerous advantages, there is a drawback in the average end user's data rate which is generally considerably lower than the system chip rate for each wavelength. However, in a more flexible multi-rate network, dedicated wavelengths could be provided for high data rate customers at a suitable cost.

The architecture of the PON is predominantly based on optical fibre. High percentages of homes in some Asian countries (e.g. Japan, Hong Kong and South Korea) are served by fibre to the home (FTTH) networks [19]. Currently in Europe, about 15 million subscribers have fibre terminating at their homes or buildings [20], as telecom operators are slowly upgrading from already installed copper twisted pair (using ADSL/VDSL). In the Middle East and Africa, the FTTH network is in the emerging and developing phase [21]. Some of the challenges to fast roll-out of fibre include installation cost, limited access to installation location and infrastructural or topographical barriers [22]. Free space optical (FSO) communication system is an alternative means of extending broadband services to users' homes within the access network, and in some cases are easier to set-up compared to optical fibre links [23-25]. However, both optical fibre and FSO technologies could potentially be combined to provide a robust and flexible solution to the high bandwidth demand in optical access networks. Optical fibre network incorporating FSO distribution links have been proposed and studied in [4, 11, 26, 27]. It is also possible in certain network arrangements to connect some ONUs to the remote node through a fibre distribution link while others ONUs are connected using FSO distribution link.

Interchannel crosstalk is a well reported impairment in WDM systems [28-30]. The effects of atmospheric turbulence and interchannel crosstalk in a HFFSO WDM system have been considered in [26, 27]. As established in [26, 27],

atmospheric turbulence in the FSO link of HFFSO WDM system causes random fluctuations of crosstalk signal, and significantly worsens its effect on the system. On the other hand, OCDMA systems are susceptible to multiple access interference (MAI), and have been well researched for turbulent FSO links and for fibre links [12-14, 31-33]. The influence of interchannel crosstalk in an all-fibre OCDMA over WDM on-off keying (OOK) system has been considered in [9, 34]. However, the combined impact of turbulence-accentuated interchannel crosstalk and multiple access interference (MAI) on the performance of such a system has not been previously considered, and hence is the basis of this work.

8.2 Network structure and description

A diagram of the proposed network is shown in Fig. 8.1. The same types of code sequence used in Chapter 4, the optical orthogonal codes (OOCs) are also used for this network. Each K users on the same wavelength use distinct OOCs from the same family, and a user corresponds to a single optical network unit (ONU) so both terms are used interchangeably in this analysis. In the downstream, coded signals are transmitted on multiple wavelengths from the optical line terminator (OLT) via a feeder fibre and distributed to individual ONUs by FSO link. At the ONUs, upstream coded signals are transmitted through a short fibre length and from a transmitting lens (TL) to the corresponding collecting lens (CL) at the remote node using the FSO link. Equally, downstream coded signals for each ONU are transmitted from the transmitting lens at the remote node to the receiver collecting lens (RCL) at the ONU through the same FSO link. A pointing and tracking subsystem is assumed to be located at the remote node to maintain appropriate alignment of the transmitting and collecting lenses. In an OCDMA network, signals from other users on the same wavelength (e.g. λ_1) as the desired user signal leads to multiple access interference (MAI) during reception. As these signals have been transmitted over a turbulent FSO link, turbulence induced scintillation could combine with MAI to further degrade the system [35]. In the hybrid WDM and OCDMA network shown in Fig. 8.1, optical signals from users on other wavelengths (e.g. λ_N) are also received by the desired user due to imperfect performance of the demultiplexer (demux) in the OLT for upstream transmission and in the remote node for downstream transmission. This type of

interference which could be accentuated by turbulence is referred to as interchannel crosstalk.
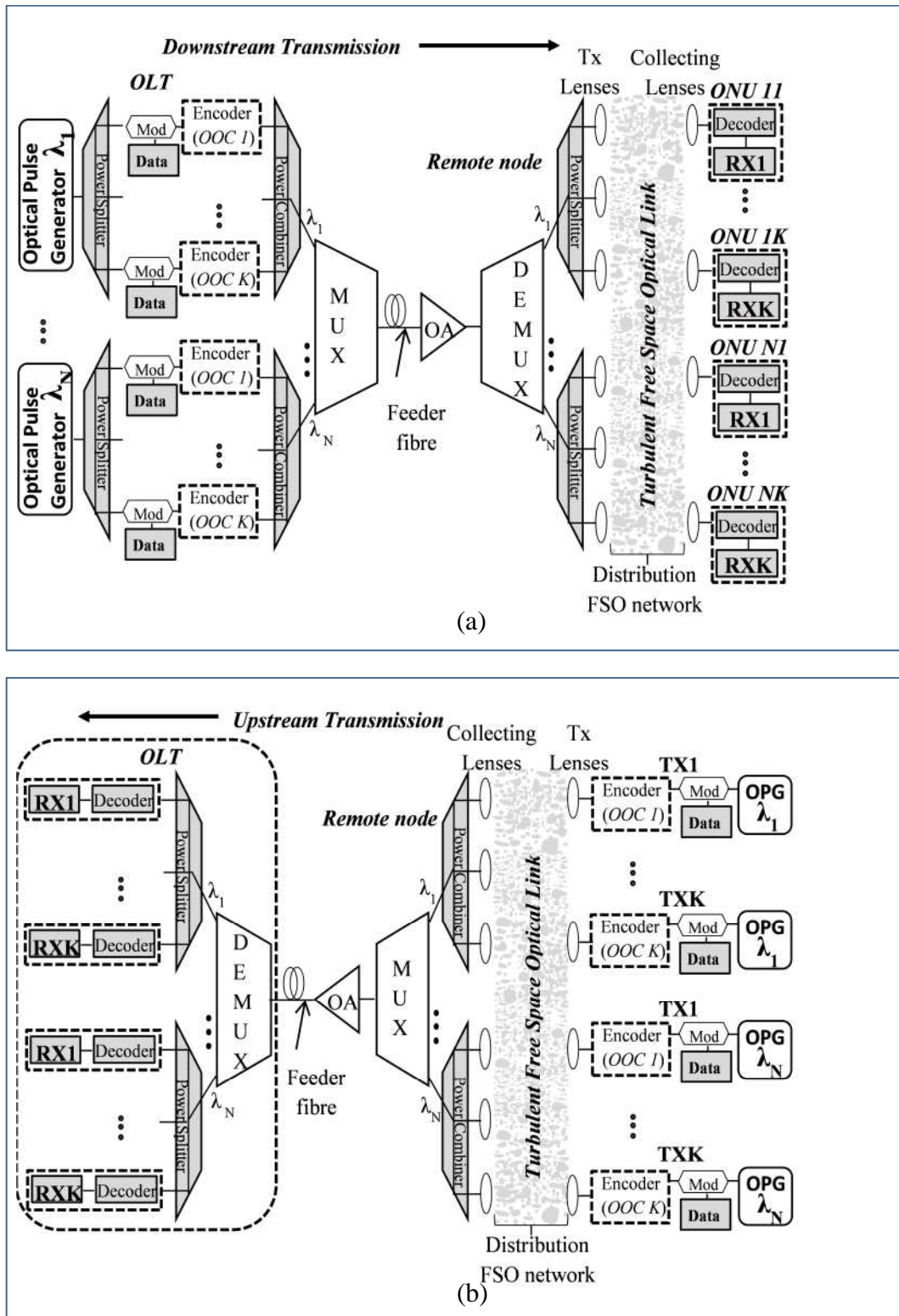
Fig. 8.1 Hybrid WDM and OCDMA Network with Optical fibre and FSO links:
(a) Downstream network diagram and (b) Upstream network diagram

8.2.1 Upstream transmission

Multiple ONUs limited by the number of OOCs share a dedicated wavelength and establish a point-to-point upstream transmission link with the OLT (see Fig. 8.1b). The operating wavelengths are assumed to be set around 1550 nm on the C-band of the ITU-T grid, thus benefiting from the low signal attenuation and developed optical device technology in those range of wavelengths. Each group of ONUs transmitting on a fixed wavelength uses the same laser transmitters operating at a set central wavelength. Optically encoded signals from the ONUs located at homes, buildings or kerb are transmitted upstream through a turbulent FSO link to the remote node. The optical signals for all the ONU on each wavelength are combined separately using a power combiner before the signals on all the wavelengths are multiplexed, amplified and conveyed to the OLT through a feeder fibre. At the OLT, the demux separates the signals according to their wavelengths and a power splitter divides each wavelength signal into the number of ONUs for further decoding and reception. Thus, similar to the system discussed in Chapter 4, encoding and decoding are performed in the optical domain for this network. OCDMA encoder/decoder technology has improved over the years with various classifications either in terms coding dimension (1D or 2D) or with respect to light source coherency [9]. The traditional fibre delay line and simple correlator are commonly used as 1D encoder/decoder [31, 36] as it is illustrated in Fig. 3.4, and sometimes they are used in combination with optical logic gates as either 1D or 2D encoder/decoder [33, 37, 38]. Multi-port encoder/decoder and high performing encoder/decoder based on superstructured fibre Bragg gatings (SSFBG) have also been proposed and demonstrated [9, 39, 40] and are realistic device options for the hybrid WDM and OCDMA network. The wave front of the signals transmitted by the ONUs are distorted by atmospheric turbulence as they propagate through the FSO link, causing additional beam spreading above the diffraction limited range [41]. Suitable positioning of the CLs at the remote node is necessary to avoid the optical beam from ONUs on one wavelength spreading into the field of view of the CLs meant for signals from another wavelength, and causing intrachannel crosstalk due to multipath effect. The signals collected at each CL is coupled into a short fibre to the power combiner, experiencing a coupling loss dependent on the back propagated mode profile of the fibre and the

coherence area of the beam [42]. Additionally, the signals experience free space attenuation and nominal losses due to the power combiner and multiplexer (mux) before the power is boosted by a fibre amplifier (e.g. (EDFA)). Besides, as we have seen in previous chapters, the optical amplifier introduces ASE noise which propagates with the signals to different OLT receivers. In this network, both signals and noise incur further losses due to attenuation in the feeder fibre and inherent demux and power splitter losses.

The imperfect nature of the OLT demux results in turbulent signals from undesired wavelengths being received on the desired user's wavelength as interchannel crosstalk. It is important to note that since the OOCs are reusable at different wavelengths, the crosstalk signals could possibly include signal of the same optical code as the desired user and signals of different optical code as the desired user. Thus in addition to MAI caused by turbulent signals from other users with different optical code but on the same wavelength, the desired user is also impaired by interchannel crosstalk caused by turbulent signals from other users with different optical code but on different wavelength, and interchannel crosstalk caused by turbulent signal from a single user with the same optical code but on different wavelength. As will be shown later in this analysis, the effect of interchannel crosstalk (interference from another wavelength) caused by the single user with the same optical code as the desired user is worse than the combined effect of interchannel crosstalk from the other users with different optical code from the desired user, provided that the number of users in each wavelength does not exceed the theoretical upper bound of a CDMA system.

Background ambient light enters the upstream system from all the RCLs at the remote node and is amplified just like the signals. However, ambient light mainly from the sun has lower power at 1550 nm wavelength compared to shorter wavelengths such as the visible light spectrum, and is non-directional, thus it is largely restricted by the narrow FOV of the fibre and lens system. It also encounters fibre coupling loss, demux/mux losses, splitter/combiner losses and fibre attenuation. Based on these considerations, and by the use of narrow field of view collecting lens that rarely points to the sun, and small channel optical noise bandwidth, the background ambient power reaching the upstream receiver is considered negligible in this analysis.

8.2.2 Downstream transmission

The downstream architecture is similar to the upstream but the system operation is different. Each wavelength at the OLT has a separate laser source which transmits the signal for the group of ONUs on its wavelength. As shown in Fig. 8.1a, the signal on each wavelength is split into the number of ONUs on the wavelength and separately encoded with the OOC for each ONU before being recombined for wavelength multiplexing. The multiplexed signals propagates through the feeder fibre to the remote node for optical amplification and demultiplexing before each wavelength's signal is split into each ONUs signal and further transmitted through the FSO link for decoding and reception. The downstream crosstalk arises from the imperfect performance of the demux at the remote node. Compared to the upstream transmission, there is additional splitter loss in the downstream, this is an optional operational cost that reduces the number of optical sources required at the OLT to the number of wavelengths (N), instead of one per user (i.e. NK) as is obtained in the upstream. Where cheap optical sources are available, it may be a better option to have one source per user in the downstream, and avoid the additional splitter loss. As discussed in Chapter 4, for unit auto and cross-correlational constraint, MAI could be eliminated in the downstream as long as the number of interferers in each wavelength is less than the ratio of the code length to the square of the code weight (i.e. $K - 1 < L_c/w^2$) [13]. Under such condition, a cyclic shift(s) for which there is no MAI between all the users always exist, and under the control of the OLT, each downstream signal is transmitted with the appropriate cyclic shift to ensure that no MAI exist between all the users. Furthermore, since crosstalk signals (interfering signals from other wavelength) originate before the turbulent FSO link, and propagate through the same physical FSO link with the desired ONU's signal, the effect of the crosstalk is not exacerbated by the turbulence (i.e. not exacerbated by the fact that turbulence for each is statistically independent, (see below)). Similar to the upstream consideration, the effect of background ambient light is considered negligible in the downstream as the ambient light is non-directional and encounters fibre coupling loss. Additionally, the RCL could be coated with a thin film optional optical bandpass filter (OBPF) to limit the amount of ambient light reaching the receiver.

8.3 Channel modelling

The location of each ONU could be quite distant from the others such that signals from each ONU propagate through a physically distinct FSO path to the remote node (e.g. where the users are located in different buildings that are far apart). Under such condition, each ONU's signal in the upstream direction as shown in Fig. 8.1b would have uncorrelated turbulence and hence require separate consideration. For computational ease, in this analysis we assume 0 km between the ONUs on the same wavelength (although realistically, the correlational length of turbulence is in the order of $\sqrt{l_{fso}\lambda}$ [41, 43]). This assumption is valid, for example, by changing the location of the power combiner in Fig. 8.1b from the position after the mux to a position before the transmitting lenses (TLs), and then replacing the set of TLs and CLs with a single TL and CL, such that different ONU's signals on the same wavelength which are combined together exit the same TL and propagate through the same physical FSO Link to the same CL before being multiplexed together with signals from other wavelength. This makes the analysis adaptable to a network extending indoors such as the one discussed in Chapter 4, and implies that different ONU's signals on the same wavelength experience similar optical turbulence behaviour over the atmospheric link (e.g. where the ONUs are located in a block of flats in the same building). Thus each group of ONUs on the same wavelength have the same time varying fluctuations and their turbulence induced scintillations are correlated in time and considered the same. In the downstream, the turbulence on the signal and the crosstalk is correlated irrespective of the distance between the ONUs. This is because if the ONUs are in the same building, the same TL and CL could be used for the signals on the same wavelength, which then travel through the same physical FSO link between the remote node and the building, accompanied by crosstalk, and is split into the number of ONUs on the wavelength after the CL. Alternatively, if the ONUs are far apart different TL and CL could be used as shown in Fig. 8.1a, in which case each ONU's signal accompanied by crosstalk, travel through distinct physical FSO link and is received independent of other ONU's signals.

8.3.1 Atmospheric channel modelling

The irradiance of the optical signal arriving at the CL is constantly fluctuating as optical energy is randomly redistributed across the beam due to turbulence induced scintillation along the FSO link. The strength of the turbulence is classified as weak, moderate, strong or saturated using the Rytov variance $\sigma_R^2 = 1.23 C_n^2 k^{7/6} l_{fso}^{11/6}$ [41], and atmospheric turbulence effect is commonly characterised by the gamma-gamma (GG) pdf $p_{GG}(h_Z) = f(\alpha, \beta, h_Z)$ (see eq. (6.1)), where the α and β parameters incorporating aperture averaging are written as eqs. (3.11) and (3.12) respectively. The free space attenuation in clear air is $L_{fs} = 10^{(-\alpha_{fso} l_{fso})/10}$ where $\alpha_{fso} = 0.2$ dB/km is the free space attenuation coefficient, while the beam spreading loss (L_{bs}) and coupling efficiency (η_c) are calculated using eqs. (6.2) and (6.3) respectively, as detailed in Chapter 6.

In the upstream direction, the turbulence induced scintillation effect on the ONUs that are on the desired signal wavelength is treated independently of the scintillation effect on other ONUs on the crosstalk wavelength as each group is assumed to be transmitted over a distinct free space path. However, for the downstream transmission, both the desired signal with interferers on the same wavelength and crosstalk exit the same transmitting lens and travel over the same FSO path, hence the turbulence effect is considered the same.

8.3.2 OCDMA modelling

Each ONU's data is recognized by a signature sequence represented in the form of optical orthogonal codes (OOCs) which is defined as $(L_c, w, \gamma_a, \gamma_c)$ where L_c is the code length, w is the code weight, γ_a is the maximum autocorrelation constraint and γ_c is the maximum cross-correlation constraint [13]. In order to limit the effect of MAI, unit values of γ_a and γ_c are considered. For chip duration T_c and chip rate $R_c = 1/T_c$, the impulse response of an OOC chip pulse is written as eq. (4.1), and the number of users K that a family of OOCs can simultaneously support is constrained by the Johnson bound [44, 45] , and is expressed as eq. (4.2). Thus K is the maximum number of OOCs and is the number of ONUs that can connect at the same time to a single wavelength in the network. The OOCs are also reusable on all other wavelengths in the network. An ONU transmits a one bit

by sending a pulse on each of w pulse mark chip positions and for a zero bit, no pulse is sent. With $\gamma_c = 1$, other ONUs with different OOC can only contribute a maximum of one pulse each to the pulse mark chip positions of another ONU and this is the cause of MAI. Although in a practical system, as a result of timing jitters and delays between the OOC signals in the same wavelength, there is a possibility that zero interfering pulse may be introduced in the pulse mark chip positions of the desired ONU. As explained in Chapter 4, considering such exact analysis is not only unfeasible, but also renders the analysis code specific. A general approach which results in an upper bound is to consider that any user can only interfere with the maximum cross-correlational constraint γ_c [45, 46].

8.3.3 Crosstalk modelling

Signals from undesired wavelengths propagate through the network and encounter power losses with respect to their transmission path. At the demux, a fractional part of such signals, dependent on the demux channel rejection couples on to the wavelength of the desired signal. For an OCDMA system, the pulses that contribute to crosstalk are those that are on the pulse mark chip positions of the desired ONU's signal. With $\gamma_c = 1$, other wavelength ONUs transmitting with different OOC from the desired ONU can contribute a maximum of one pulse to the pulse mark chip position of the desired user (provided that any time delay between the signals (τ) is a multiple of the chip duration T_c). However, an ONU in another wavelength, transmitting with the same OOC as the desired signal can contribute a maximum of w pulse(s) to the pulse mark chip positions of the desired user when $\tau = 0$, and a single pulse when $0 < \tau < L_c$ because the maximum autocorrelation between an OOC and its shifted version $\gamma_a = 1$.

8.4 BER evaluation and analysis

Additional to the losses encountered by the signals at the FSO distribution link, other network losses are also incurred at the remote node, feeder fibre link and OLT. The inherent power splitter/combiner loss L_s is 3 dB per 2-way split which is a total of 6 dB for each power splitter or combiner. The nominal demux loss (L_{demux})/multiplexer (mux) loss (L_{mux}) is about 3.5 dB [29], while $L_{demux,i}$ is the additional loss that a crosstalk signal experiences upon coupling to the desired signal wavelength port at the demux, and also defines the signal to crosstalk ratio

(in the situation when all the ONUs have the same transmitting power and experience equal losses). The fibre loss is $L_f = 10^{(-\alpha_f l_f)/10}$ where $\alpha_f = 0.2$ dB/km is the attenuation coefficient of fibre, and l_f is the fibre link length (in km).

The average optical received power at the OLT photodiode from an ONU on the desired signal wavelength and an ONU on the crosstalk wavelength are respectively written as

$$P_d(h_d) = GP_{TU,d}h_d L_{fs,d}L_{bs,d}\eta_{c,d}L_{s,2}L_{mux}L_f L_{demux} \tag{8.1}$$

$$P_i(h_i) = GP_{TU,i}h_i L_{fs,i}L_{bs,i}\eta_{c,i}L_{s,2}L_{mux}L_f L_{demux}L_{demux,i} \tag{8.2}$$

where $P_{TU,d}$ and $P_{TU,i}$ are the transmit power of an ONU on the desired signal wavelength and an ONU on the crosstalk wavelength respectively, and $L_{s,j}$ is the total loss for j number of power splitters or combiners. The single polarisation ASE power spectral density (PSD) at the OLT photodetector inputs from an ONU on the desired signal wavelength and an ONU on the crosstalk wavelength are respectively written as

$$N_o = 0.5(NF \times G - 1)h\upsilon L_f L_{s,1}L_{demux} \tag{8.3}$$

$$N_{o,i} = 0.5(NF \times G - 1)h\upsilon_i L_f L_{s,1}L_{demux}L_{demux,i} \tag{8.4}$$

where G and NF are the optical amplifier gain and noise figure respectively, h is Planck's constant, υ and υ_i are the optical frequencies of the desired signal and crosstalk signal respectively.

In the downstream, the average optical received power at the ONU (from the OLT transmitters) on the desired signal wavelength and on the crosstalk wavelength are respectively written as

$$P_d(h_Z) = GP_{TD,d}h_Z L_{mux}L_f L_{s,3}L_{demux}L_{fs}L_{bs}\eta_{c,d} \tag{8.5}$$

$$P_i(h_Z) = GP_{TD,i}h_Z L_{mux}L_f L_{s,3}L_{demux}L_{demux,i}L_{fs}L_{bs}\eta_{c,i} \tag{8.6}$$

where $P_{TD,d}$ and $P_{TD,i}$ are the OLT transmit power to the ONU on the desired signal wavelength and the ONU on the crosstalk wavelength respectively. The single polarisation ASE power spectral density (PSD) at the ONU photodetector inputs experienced on the desired signal wavelength and on the crosstalk wavelength are respectively written as

$$N_o = 0.5(NF \times G - 1)h\upsilon L_{demux}L_{s,1}L_{fs}L_{bs}\eta_{c,d} \tag{8.7}$$

$$N_{o,i} = 0.5(NF \times G - 1)h\upsilon_i L_{demux}L_{demux,i}L_{s,1}L_{fs}L_{bs}\eta_{c,i} \tag{8.8}$$

8.4.1 OOK BER analysis

In OOK OCDMA, a bit period T_b is divided into L_c equal chips of duration T_c, where L_c is the code length and the data rate $R_b = R_c / L_c$. As shown in Fig. 8.2, pulses equal to the code weight w are sent in pulse mark chip positions 1, 4 and 11 of the transmitting user's OOC for data one transmission, and no pulse is sent for data zero transmission.
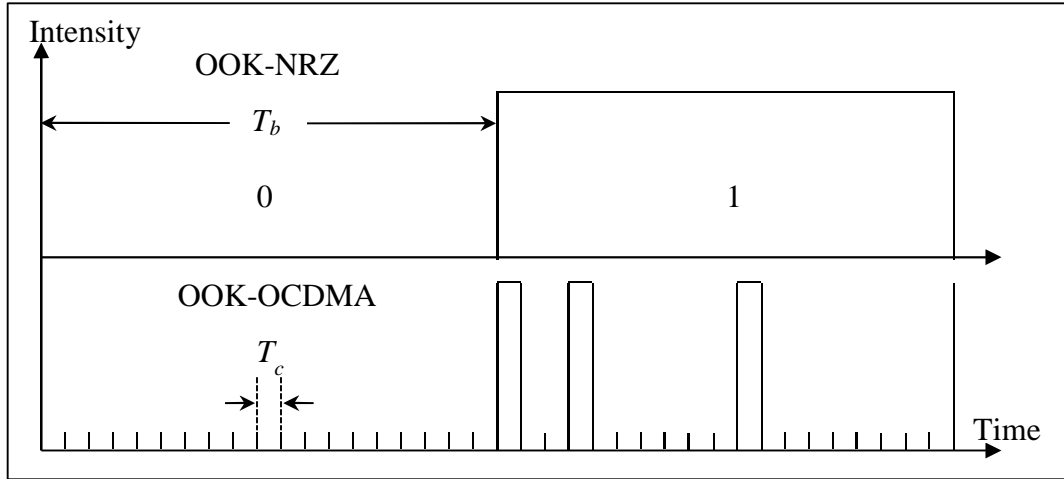
Fig. 8.2 Illustration of time waveform for OOK OCDMA signal with $L_c = 19$ and $w = 3$

The maximum number of ONUs contributing to MAI on the desired signal wavelength is $K - 1$ where K is the number of ONUs on a single wavelength. For $\gamma_a = \gamma_c = 1$, the probability of MAI occurring between one ONU and another is given by $p = w^2 / 2L_c$ [31], the factor of $1/2$ accounting for the fact that an interfering ONU may transmit data 1 or data 0.

8.4.1.1 Upstream transmission

In order to ease the understanding of the OOK upstream transmission BER calculations, a flowchart for the calculation processes is provided as Fig. 8.3. The peak received signal power for a pulse at the OLT from an ONU on the desired signal wavelength is conditional on the attenuation due to atmospheric turbulence for the desired signal, and is related to the average received power. It is written as

$$\mu_{p_{Sig}}(h_d) = \frac{2L_c P_d(h_d)}{w} \qquad (8.9)$$

For an ONU on a different wavelength from the desired signal wavelength, the peak received crosstalk power for a pulse at the OLT is conditional on the attenuation due to atmospheric turbulence for the crosstalk signal, and is written as

$$\mu_{P_{XT}}(h_i) = \frac{2L_c P_i(h_i)}{w} \tag{8.10}$$

where $P_d(h_d)$ and $P_i(h_i)$ are the OOK average power received at the OLT photodiode from an ONU on the desired signal wavelength and an ONU on the crosstalk wavelength respectively, and written as eqs. (8.1) and (8.2).
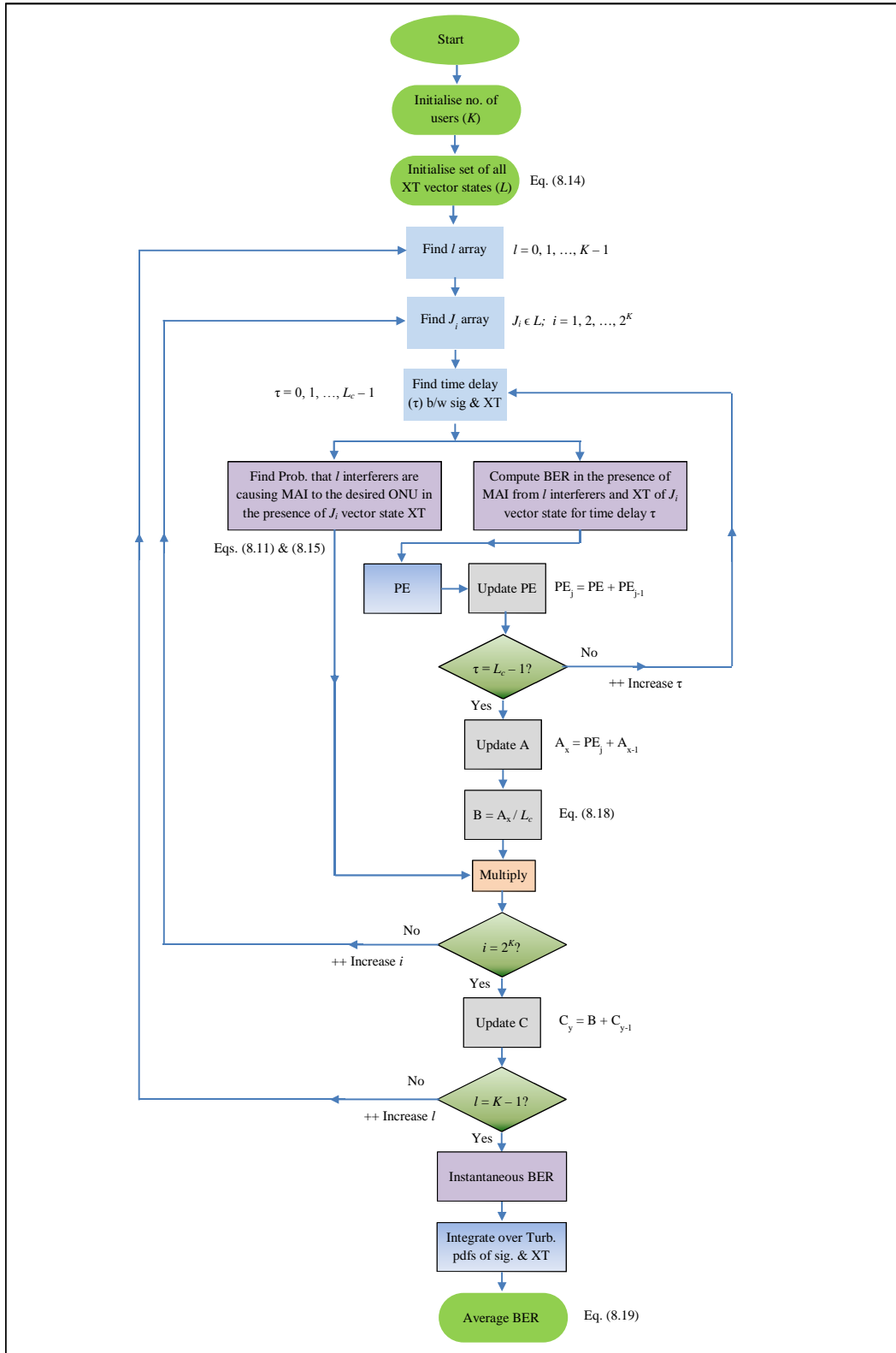
Fig. 8.3 Flowchart for upstream BER calculations in an OOK OCDMA over WDM network

Interference from the same wavelength (MAI)

The probability of a particular interference pattern occurring when l ONUs are causing multi-access interference to the desired ONU has a binomial distribution and is of the same form as eq. (4.18). It is written as [13]

$$P(l) = \frac{(K-1)!}{l!(K-1-l)!}(p_o)^l (1-p_o)^{K-1-l}, \quad p_o = \frac{w^2}{2L_c} \tag{8.11}$$

Because some ONUs may be inactive in the network at any particular time, l ranges from 0 to $K-1$ at the decision time.

Interference from different wavelength (Crosstalk)

The vector state of a typical crosstalk corresponding to the number of pulses contributed to the pulse mark chip positions of the desired user could be written as

$$J_i \equiv \big(\delta_i(1), \ \delta_i(2), \ ..., \delta_i(K)\big) \tag{8.12}$$

where $\delta_i(z) \in \{0,1,\Lambda\}$, $\Lambda = w$ for $\tau = 0$, $\Lambda = 1$ for $0 < \tau < L_c$ and τ is the time delay (in multiples of the chip duration T_c) between the signals on the desired wavelength and the signals on the crosstalk wavelength, and occur with the probability $p(\tau) = 1/L_c$. For the code parameter $\{L_c, w, \gamma_c, \gamma_a\} = \{19, 3, 1, 1\}$, using eq. (4.2), there are three ONUs in each wavelength (i.e. $K = 3$). Assuming the first ONU on the crosstalk wavelength uses the same OOC as the desired ONU, the elements of the crosstalk vector state $\delta_i(z)$ could further be define as

$$\delta_i(z) = \begin{cases} \Lambda, & \text{if 1st ONU is active} \\ 1, & \text{if 2nd or 3rd ONU is active} \\ 0, & \text{if any ONU is inactive} \end{cases} \tag{8.13}$$

A full set of all the crosstalk vector states (J_i) could be represented as L and written as

$$L = \begin{bmatrix} J_1 \\ J_2 \\ J_3 \\ J_4 \\ J_5 \\ J_6 \\ J_7 \\ J_8 \end{bmatrix} = \begin{bmatrix} 0 & 0 & 0 \\ \Lambda & 0 & 0 \\ 0 & 1 & 0 \\ 0 & 0 & 1 \\ \Lambda & 1 & 0 \\ \Lambda & 0 & 1 \\ 0 & 1 & 1 \\ \Lambda & 1 & 1 \end{bmatrix} \tag{8.14}$$

By representing the number of nonzero elements in J_i as $|J_i|$ and the sum of all the elements in J_i as l_{J_i}, the probability that $|J_i|$ ONUs are active on the

wavelength adjacent to the desired signal's wavelength and contributing l_{J_i} crosstalk pulses to the desired signal could be written as

$$P(l_{J_i}) = p_o^{|J_i|} (1 - p_o)^{K-1-|J_i|}, \qquad (8.15)$$

Note that eq. (8.15) is of similar form to eq. (8.11), the only difference is that the binomial term expressed as factorials in eq. (8.11) has been separately expressed as a set of vector states (see eq. (8.14)), to enable a proper consideration of the crosstalk contribution by the first ONU on the crosstalk wavelength, which uses the same OOC as the desired user and could contribute either 1 or w pulses to the pulse mark chip positions of the desired user depending on the value of τ.

Assuming that the random variables for the mean and variances of the desired signal, MAI and crosstalk are Gaussian, using the Gaussian approximation (GA), the mean and variances of the received signal (including MAI and crosstalk and conditional on turbulence attenuation) could be written respectively as

$$i_{b,XT}(l, l_{J_{i,\tau}}, h_d, h_i) = \frac{LR'qN_o}{T_c} + q\left[(wb+l)R'\mu_{P_{Sig}}(h_d) + l_{J_{i,\tau}}R_i'\mu_{P_{XT}}(h_i)\right] \qquad (8.16)$$

$$\sigma_{b,XT}^2(l, l_{J_{i,\tau}}, h_d, h_i) = \left(\frac{LR'q^2N_o(1+R'N_o)}{T_c^2}\right) + q^2R'\left[(1+2R'N_o)\frac{(wb+l)\mu_{P_{Sig}}(h_d)}{T_c}\right]$$
$$+ q^2R_i'\left[(1+2R_i'N_{o,i})\frac{l_{J_{i,\tau}}\mu_{P_{XT}}(h_i)}{T_c}\right] + \sigma_{th-OOK_C}^2 \qquad (8.17)$$

where $b = 0$ or 1 depending on the transmitted bit, $\sigma_{th-OOKC}^2$ is the OOK OCDMA thermal noise variance, $R' = \eta/h\upsilon$, $R_i' = \eta/h\upsilon_i$, η is the photodetector quantum efficiency, q is the electron charge, $L = B_o m_t T_c$ is the product of spatial and temporal modes, B_o is the demux channel bandwidth and $m_t = 2$ is the number of ASE noise polarisation states. Eq. (8.17) includes the thermal, ASE-shot, signal-shot, signal-spontaneous beat and spontaneous–spontaneous beat noise variances of the desired signal with MAI as well as crosstalk-shot and crosstalk-spontaneous beat noise variances. It is assumed that all the signals experience the same ASE noise at the amplifier output [47].

The OOK upstream bit error rate (BER) conditioned on the MAI, crosstalk and turbulence is written as

$$BER_{OOK\_U}(l, l_{J_i}, h_d, h_i) = \frac{1}{L_c}\sum_{\tau=0}^{L_c-1}\frac{1}{2}\left[\frac{1}{2}\text{erfc}\left(\frac{i_D - i_{0,XT}(l, l_{J_{i,\tau}}, h_d, h_i)}{\sigma_{0,XT}(l, l_{J_{i,\tau}}, h_d, h_i)\sqrt{2}}\right) + \frac{1}{2}\text{erfc}\left(\frac{i_{1,XT}(l, l_{J_{i,\tau}}, h_d, h_i) - i_D}{\sigma_{1,XT}l, l_{J_{i,\tau}}, h_d, h_i\sqrt{2}}\right)\right]$$
$$(8.18)$$

where i_D is the optimum decision threshold which is fixed over the number of multiple access interferers and crosstalk, but varies with the instantaneous irradiance of both signal and crosstalk. A search algorithm will be used to obtain this threshold in this chapter. The average OOK upstream BER is written as

$$\overline{BER}_{OOK\_U} = \int_0^\infty \int_0^\infty \sum_{l=0}^{K-1} \sum_{J_i \in L} P(l) P\left(l_{J_i}\right) BER_{OOK\_U}\left(l, l_{J_i}, h_d, h_i\right)$$
$$p_{GG,d}\left(h_d\right) p_{GG,i}\left(h_i\right) \mathrm{d}h_d \, \mathrm{d}h_i$$

(8.19)

8.4.1.2 Downstream transmission

The downstream system is with less restriction. Multiple access interference could be eliminated in the downstream if the product of the number interferers and the square of the code weight is less than the code length (i.e. $(K-1)w^2 < L_c$) [13]. Thus with proper code design and arrangement, the downstream desired user signal and crosstalk at the photodiode are each equivalent to the logically gated OR signal of all the ONU signals in their wavelengths [13]. Furthermore, the crosstalk effect is not turbulence-accentuated since the crosstalk signal propagates through the same physical FSO path with the desired signal and basically experiences the same turbulence effects.

The mean and variances of the received signal in the presence of crosstalk is conditional on turbulence attenuation and could be written respectively as

$$i_{sig,int}(h_Z) = \frac{LR^{'}qN_o}{T_c} + qw\left[sigR^{'}\mu_{P_{Sig}}(h_Z) + intR_i^{'}\mu_{P_{XT}}(h_Z) \right]$$

(8.20)

$$\sigma^2_{sig,int}(h_Z) = \sigma^2_{th-OOK_C} + \left(\frac{LR^{'}q^2N_o\left(1+R^{'}N_o\right)}{T_c^2} \right) + R^{'}q^2w\left[\left(1+2R^{'}N_o\right)\frac{sig\mu_{P_{Sig}}(h_Z)}{T_c} \right]$$
$$+ R_i^{'}q^2w\left[\left(1+2R_i^{'}N_{o,i}\right)\frac{int\mu_{P_{XT}}(h_Z)}{T_c} \right]$$

(8.21)

where $sig \in \{0,1\}$ and $int \in \{0,1\}$ depending on the presence of signal/crosstalk in the pulse mark chip position of the desired signal or not. $\mu_{P_{Sig}}(h_Z)$ and $\mu_{P_{XT}}(h_Z)$ are the same as eqs. (8.9) and (8.10) respectively, with $P_d(h_d)$ and $P_i(h_i)$ redefined as the OOK average power received at the ONU photodiode from the OLT transmitter on the desired signal wavelength and the OLT transmitter on the crosstalk wavelength respectively as in eqs. (8.5) and (8.6).

The probability that data 0 is received given that data 1 is transmitted in the presence of crosstalk and turbulence is written as

$$P(0|1, int, h_Z) = \frac{1}{2} \operatorname{erfc}\left(\frac{i_{1,int}(h_Z) - i_D}{\sigma_{1,int}(h_Z)\sqrt{2}}\right) \tag{8.22}$$

Also, the probability that data 1 is received given that data 0 is transmitted in the presence of crosstalk and turbulence is written as

$$P(1|0, int, h_Z) = \frac{1}{2} \operatorname{erfc}\left(\frac{i_D - i_{0,int}(h_Z)}{\sigma_{0,int}(h_Z)\sqrt{2}}\right) \tag{8.23}$$

Assuming independent and equiprobable data for both crosstalk and desired signal, the bit error rate for the OOK downstream system is

$$
\begin{aligned}
BER_{OOK\_D}(h_Z) &= \frac{1}{4} \sum_{int=0}^{1} \left[P(0|1, int, h_Z) + P(1|0, int, h_Z) \right] \\
&= \frac{1}{4} \left[P(0|1,0, h_z) + P(0|1,1, h_Z) + P(1|0,0, h_Z) + P(1|0,1, h_Z) \right]
\end{aligned}
\tag{8.24}
$$

The average BER for OOK downstream is written as

$$\overline{BER}_{OOK\_D} = \int_0^\infty BER_{OOK\_D}(h_Z) \, p_{GG,d}(h_Z) \, \mathrm{d}h_Z \tag{8.25}$$

8.4.2 DPPM BER Analysis

DPPM signalling results in bandwidth expansion beyond that of OOK systems by a factor $B_{exp} = 2^M/M$ [48], where M is the DPPM coding level. In DPPM OCDMA, a bit period T_b is divided into $B_{exp}L_c$ equal chips of duration T_c, where L_c is the code length, and the data rate $R_b = R_c/B_{exp}L_c$. For binary PPM OCDMA ($M = 1$), the normal chip duration in OOK OCDMA is subdivided into 2 equal parts to obtain the binary PPM OCDMA chip duration. As shown in Fig. 8.4, w pulses of T_c duration are sent in pulse mark chip positions 1, 4 and 11 of the first slot (followed by 0 pulses in the second slot) for data zero transmission. For data one transmission, the pulses are sent in pulse mark chip positions of the second slot while 0 pulses are sent in the first slot. The probability of MAI occurring in any slot of the desired ONU is given by $p_1 = w^2/\gamma_c n L_c$ [45], where $n = 2^M$ is the number of DPPM slots and $1/n$ is the probability of data being transmitted in any of the DPPM slots. In addition, the probability of MAI occurring in one of the empty slots of the desired ONU is given by $p_2 = w^2/(n-1)\gamma_c L_c$ [49].
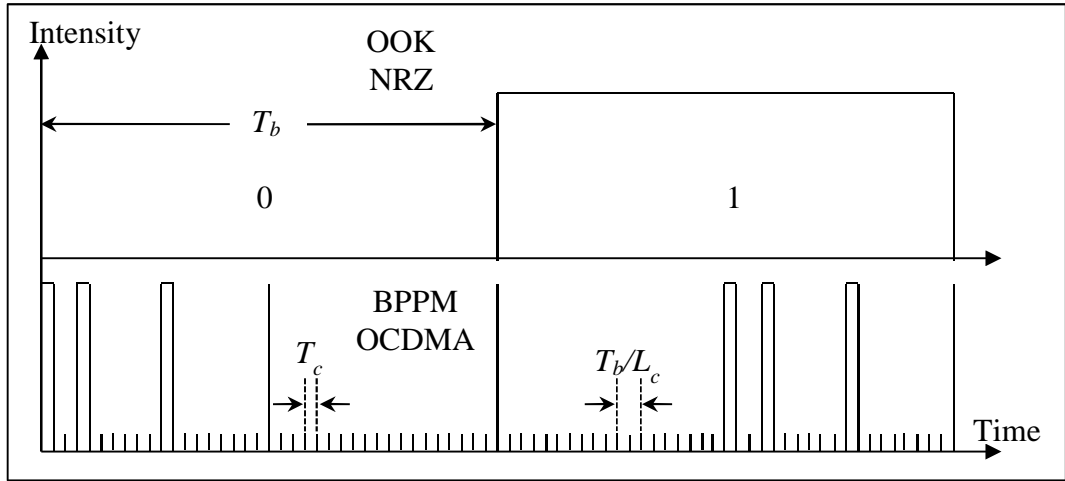
Fig. 8.4 Illustration of time waveform for binary DPPM OCDMA signal with $L_c = 19$ and $w = 3$

8.4.2.1 Upstream transmission

A flowchart for the DPPM upstream BER calculation processes is provided as Fig. 8.5, so as to facilitate the understanding of the BER analysis.

Interference from the same wavelength (MAI)

For DPPM, the probability of a particular interference pattern occurring when l_1 interferers are causing MAI in the slot conveying the desired signal pulses and l_0 interferers are causing MAI in an empty slot has a trinomial distribution and is of the same form as eq. (4.19). It is written as [45, 46, 49]

$$P(l_0, l_1) = \frac{(K-1)!}{l_0! l_1! (K-1-l_0-l_1)!} p_r(l_0, l_1) \tag{8.26}$$

where $p_r(l_0, l_1)$ is as defined by eq. (4.20) for $M = 1$ and eq. (4.21) for $M = 2$.
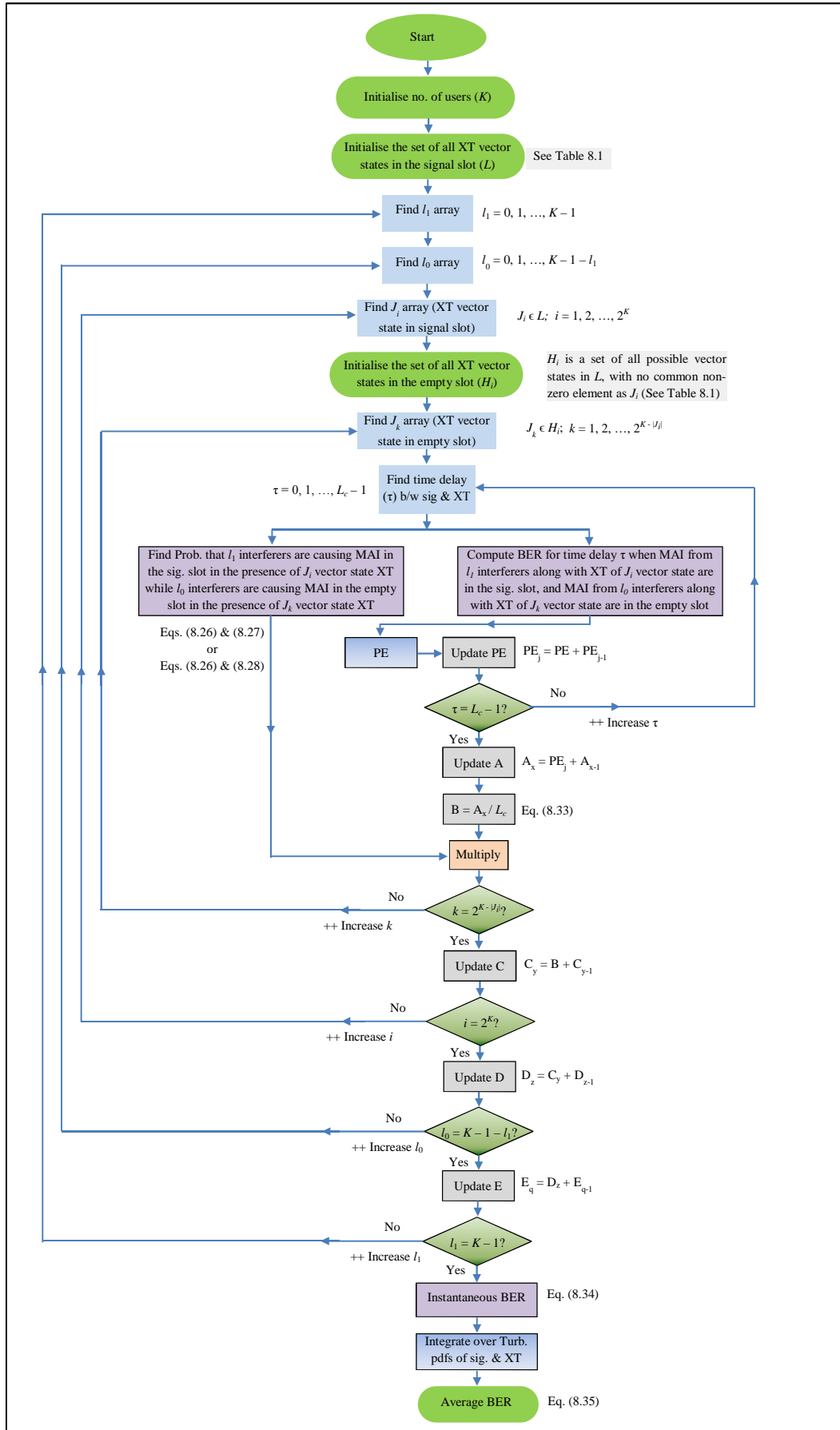
Fig. 8.5 Flowchart for upstream BER calculations in a DPPM network

Interference from the different wavelength (Crosstalk)
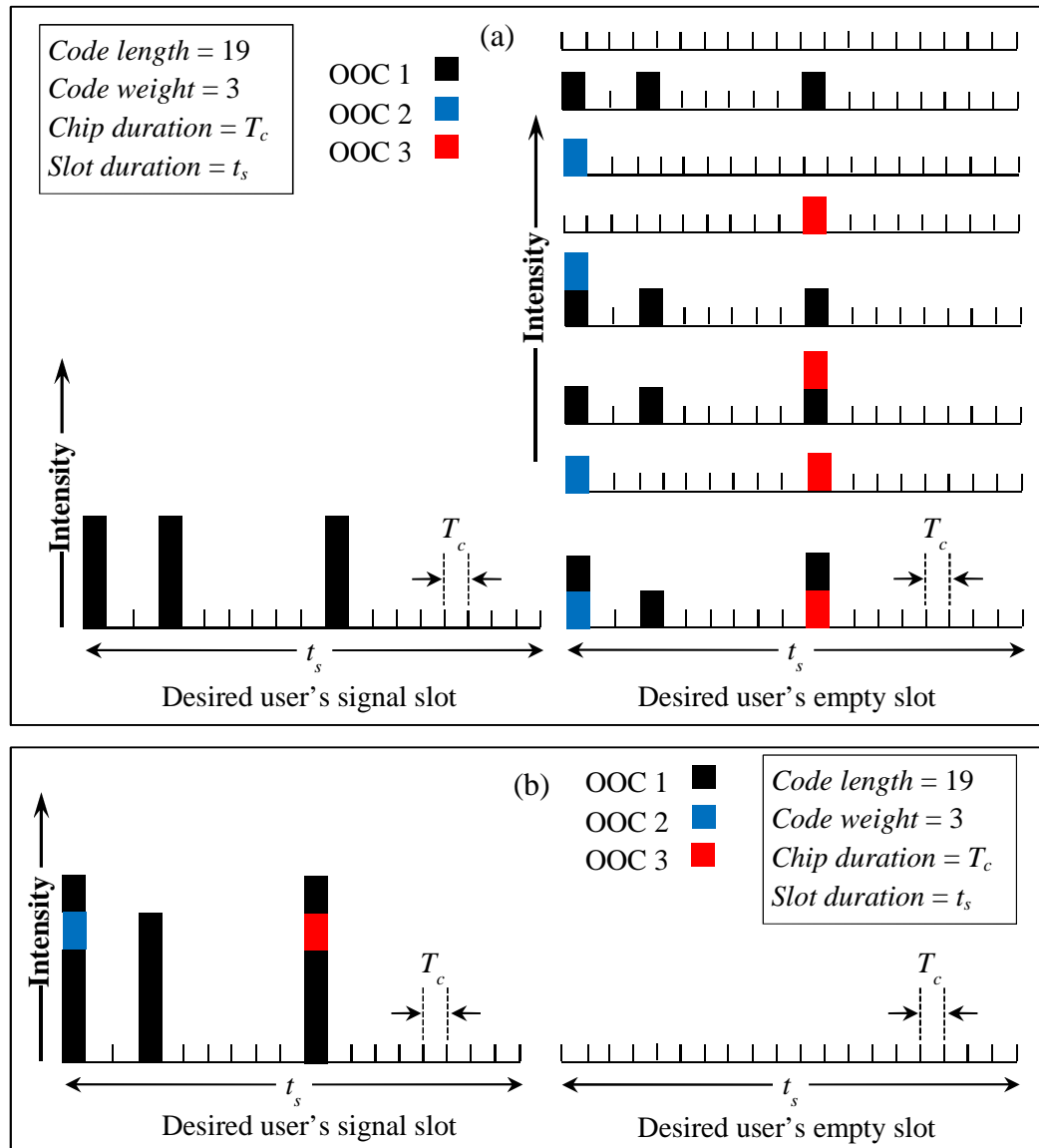
Fig. 8.6 Illustration of signal and crosstalk pulses on the pulse mark chip positions of the desired ONU which uses OOC 1 in a DPPM system with $\tau = 0$, $\Lambda = w$ and $P_{sig} = 3P_{XT}$: (a) all active ONUs on crosstalk wavelength transmit different data as the desired ONU (worst case) and (b) all active ONUs on crosstalk wavelength transmit the same data as the desired ONU (best case)

Consider an instance where $\tau = 0$ (i.e. $\Lambda = w$), and the desired ONU using OOC 1 has transmitted data 0 as shown in Fig. 8.6. The worst case occurs when active ONUs on the adjacent wavelength transmit data 1 as shown in Fig. 8.6a with the signal pulses three times greater than the crosstalk pulses (i.e. assuming demux adjacent rejection ratio of -4.77 dB). This represents crosstalk vector state 1 in

Table 8.1, with J_1 in the signal slot and H_1 in the empty slot. In this case, given that an ONU may be inactive at any time, there are eight possible ways in which the ONUs on the adjacent wavelength can introduce crosstalk pulses into the desired ONU's pulse mark chip position as shown by the pulses in the empty slot of the desired user in Fig. 8.6a. In the first incidence, all the crosstalk ONUs are inactive, so there is no pulse. In the second incidence, only ONU 1 is active and introduces three pulses because it uses the same OOC 1 with the desired ONU and $\tau = 0$. In the third and fourth occurrences, only ONU 2 and ONU 3 respectively are each active and introduces a single pulse because $\gamma_c = 1$. The fifth, sixth and seventh occurrences are when both ONUs 1 and 2, ONUs 1 and 3 and ONUs 2 and 3 respectively are active and in the last incidence, all the ONUs on the crosstalk wavelength are active.

The second case shown as Fig. 8.6b presents the best case as all the ONUs on the adjacent wavelength are active and transmitted data 0 as the desired ONU, thus there is no pulse in the empty slot of the desired user and no MAI at the correlator. This represents crosstalk vector state 8 in Table 8.1, with J_8 in the signal slot and H_8 in the empty slot. Between these two cases, there are other cases in which one ONU or two ONUs are active and have transmitted the same data as the desired ONU. In addition, there is a second instance where $0 < \tau < L_c$ (i.e. $\Lambda = 1$). Each of these incidences could be represented in vector state, and the whole events generally could be represented as a set of vector states.

The vector state of a typical crosstalk impairing the slot conveying the desired user's signal pulses could be written as $J_i \equiv (\delta_i(1),\ \delta_i(2),\ ...,\delta_i(K))$ while the vector state of a typical crosstalk impairing an empty slot of the desired user could be written as $J_k \equiv (\delta_k(1),\ \delta_k(2),\ ...,\delta_k(K))$. If the full set of all the crosstalk vector states impairing the slot carrying the desired user's signal pulses is represented as L in eq. (8.14), for every J_i in L, we may define a corresponding set H_i of all possible crosstalk vector states that could impair the desired user's empty slot. Thus H_i is the set of all the crosstalk vector states J_k impairing an empty slot of the desired user when J_i vector state of L is impairing the desired user's pulse slot. Table 8.1 depicts all the sets H_i of crosstalk vector state J_k in the desired user's empty slot given a particular crosstalk state vector J_i in the desired user's signal pulse slot. If

the number of nonzero elements in J_i and J_k are defined as $|J_i|$ and $|J_k|$ respectively, and the sum of all the elements in J_i and J_k are defined as l_{J_i} and l_{J_k} respectively, the probability distribution for J_i crosstalk vector state in the slot carrying the desired signal pulses and J_k crosstalk vector state in the desired user's empty slot could be written as

$$P(l_{J_i}, l_{J_k}) = p_1^{|J_i|+|J_k|} (1-2p_1)^{K-|J_i|-|J_k|} \qquad M=1 \qquad (8.27)$$

$$P(l_{J_i}, l_{J_k}) = p_1^{|J_i|} (1-p_1)^{K-|J_i|} p_2^{|J_k|} (1-p_2)^{K-|J_i|-|J_k|} \qquad M=2 \qquad (8.28)$$

It should be noted that eqs (8.27) and (8.28) are of the same form as eqs. (4.20) and (4.21) respectively. This is because the crosstalk is also a CDMA signal with the same probabilities of interference p_1 and p_2 between two OOCs.

Table 8.1 Set of crosstalk vector states for DPPM signal pulse slot and empty slot

L	H_i
$J_1 = \begin{bmatrix} 0 \\ 0 \\ 0 \end{bmatrix}$	$H_1 = \begin{bmatrix} 0 & \Lambda & 0 & 0 & \Lambda & \Lambda & 0 & \Lambda \\ 0 & 0 & 1 & 0 & 1 & 0 & 1 & 1 \\ 0 & 0 & 0 & 1 & 0 & 1 & 1 & 1 \end{bmatrix}$
$J_2 = \begin{bmatrix} \Lambda \\ 0 \\ 0 \end{bmatrix}$	$H_2 = \begin{bmatrix} 0 & 0 & 0 & 0 \\ 0 & 1 & 0 & 1 \\ 0 & 0 & 1 & 1 \end{bmatrix}$
$J_3 = \begin{bmatrix} 0 \\ 1 \\ 0 \end{bmatrix}$	$H_3 = \begin{bmatrix} 0 & \Lambda & 0 & \Lambda \\ 0 & 0 & 0 & 0 \\ 0 & 0 & 1 & 1 \end{bmatrix}$
$J_4 = \begin{bmatrix} 0 \\ 0 \\ 1 \end{bmatrix}$	$H_4 = \begin{bmatrix} 0 & \Lambda & 0 & \Lambda \\ 0 & 0 & 1 & 1 \\ 0 & 0 & 0 & 0 \end{bmatrix}$
$J_5 = \begin{bmatrix} \Lambda \\ 1 \\ 0 \end{bmatrix}$	$H_5 = \begin{bmatrix} 0 & 0 \\ 0 & 0 \\ 0 & 1 \end{bmatrix}$
$J_6 = \begin{bmatrix} \Lambda \\ 0 \\ 1 \end{bmatrix}$	$H_6 = \begin{bmatrix} 0 & 0 \\ 0 & 1 \\ 0 & 0 \end{bmatrix}$
$J_7 = \begin{bmatrix} 0 \\ 1 \\ 1 \end{bmatrix}$	$H_7 = \begin{bmatrix} 0 & \Lambda \\ 0 & 0 \\ 0 & 0 \end{bmatrix}$
$J_8 = \begin{bmatrix} \Lambda \\ 1 \\ 1 \end{bmatrix}$	$H_8 = \begin{bmatrix} 0 \\ 0 \\ 0 \end{bmatrix}$

The means and variances of the received signal (including MAI and crosstalk and conditional on turbulence attenuation) in the slot conveying the desired signal pulses and an empty slot are each written respectively as

$$i_{1,XT}(l_1, l_{J_{i,\tau}}, h_d, h_i) = \frac{LR'qN_o}{T_c} + q\left[(w+l_1)R'\mu_{P_{Sig}}(h_d) + l_{J_{i,\tau}}R_i'\mu_{P_{XT}}(h_i)\right] \qquad (8.29)$$

$$i_{0,XT}(l_0, l_{J_{k,\tau}}, h_d, h_i) = \frac{LR'qN_o}{T_c} + q\left[l_0 R'\mu_{P_{Sig}}(h_d) + l_{J_{k,\tau}}R_i'\mu_{P_{XT}}(h_i)\right] \qquad (8.30)$$

$$\sigma_{1,XT}^2(l_1, l_{J_{i,\tau}}, h_d, h_i) = \left(\frac{LR'q^2 N_o(1+R'N_o)}{T_c^2}\right) + R'q^2\left[(1+2R'N_o)\frac{(w+l_1)\mu_{P_{Sig}}(h_d)}{T_c}\right]$$
$$+ R_i'q^2\left[(1+2R_i'N_{o,i})\frac{l_{J_{i,\tau}}\mu_{P_{XT}}(h_i)}{T_c}\right] + \sigma_{th-DPPM_C}^2 \qquad (8.31)$$

$$\sigma_{0,XT}^2(l_0, l_{J_{k,\tau}}, h_d, h_i) = \left(\frac{LR'q^2 N_o(1+R'N_o)}{T_c^2}\right) + R'q^2\left[(1+2R'N_o)\frac{l_0\mu_{P_{Sig}}(h_d)}{T_c}\right]$$
$$+ R_i'q^2\left[(1+2R_i'N_{o,i})\frac{l_{J_{k,\tau}}\mu_{P_{XT}}(h_i)}{T_c}\right] + \sigma_{th-DPPM_C}^2 \qquad (8.32)$$

where $\mu_{P_{Sig}}(h_d)$ and $\mu_{P_{XT}}(h_i)$ are as defined in eqs. (8.9) and (8.10), with $P_d(h_d)$ and $P_i(h_i)$ redefined as the DPPM rectangular pulse power received at the OLT photodiode from an ONU on the desired signal wavelength and an ONU on the crosstalk wavelength respectively as in eqs. (8.1) and (8.2). $\sigma_{th-DPPMC}^2$ is the DPPM OCDMA thermal noise variance.

The DPPM upstream symbol error probability conditioned on the MAI, crosstalk and turbulence is given by

$$P_{WE-U}(l_1, l_0, l_{J_i}, l_{J_k}, h_d, h_i) = \frac{1}{L_c}\sum_{\tau=0}^{L_c-1}\frac{1}{2}\text{erfc}\left[\frac{i_{1,XT}(l_1, l_{J_{i,\tau}}, h_d, h_i) - i_{0,XT}(l_0, l_{J_{k,\tau}}, h_d, h_i)}{\sqrt{2\left\{\sigma_{1,XT}^2(l_1, l_{J_{i,\tau}}, h_d, h_i) + \sigma_{0,XT}^2(l_0, l_{J_{k,\tau}}, h_d, h_i)\right\}}}\right] \qquad (8.33)$$

The union bound of the instantaneous symbol error probability is derived as [14, 35, 50-52]

$$Pe_U(h_d, h_i) \le (n-1)\sum_{l_1=0}^{K-1}\sum_{l_0=0}^{K-1-l_1}\sum_{J_i\in L}\sum_{J_k\in H_i} P(l_1, l_0)\ P(l_{J_i}, l_{J_k})$$
$$P_{WE\_U}(l_1, l_0, l_{J_i}, l_{J_k}, h_d, h_i) \qquad (8.34)$$

The average DPPM upstream BER is written as

$$\overline{BER}_{DPPM\_U} = \frac{n}{2(n-1)}\int_0^\infty\int_0^\infty Pe_U(h_d, h_i)\, p_{GG,d}(h_d)\, p_{GG,i}(h_i)\,\mathrm{d}h_d\,\mathrm{d}h_i \qquad (8.35)$$

213

8.4.2.2 Downstream transmission

Similar to the OOK system, the mean and variances of the received DPPM signal in the presence of crosstalk are independent of MAI and conditional on turbulence attenuation. They are respectively written as

$$i_{sig,int}(h_Z) = \frac{LR'qN_o}{T_c} + qw \left[sigR'\mu_{P_{Sig}}(h_Z) + intR_i'\mu_{P_{XT}}(h_Z) \right] \tag{8.36}$$

$$\sigma_{sig,int}^2(h_Z) = \sigma_{th-DPPM_C}^2 + \left(\frac{LR'q^2N_o(1+R'N_o)}{T_c^2} \right) + R'q^2w \left[\left(1+2R'N_o \right) \frac{sig\mu_{P_{Sig}}(h_Z)}{T_c} \right]$$
$$+ R_i'q^2w \left[\left(1+2R_i'N_{o,i} \right) \frac{int\mu_{P_{XT}}(h_Z)}{T_c} \right] \tag{8.37}$$

where $sig \in \{0,1\}$ and $int \in \{0,1\}$ depending on the presence of signal/crosstalk in the pulse mark chip position of the desired signal or not. $\mu_{P_{Sig}}(h_Z)$ and $\mu_{P_{XT}}(h_Z)$ are the same as eqs. (8.9) and (8.10) respectively, with $P_d(h_d)$ and $P_i(h_i)$ redefined as the optical DPPM rectangular pulse power received at the ONU photodiode from the OLT transmitter on the desired signal wavelength and the OLT transmitter on the crosstalk wavelength respectively as in eqs. (8.5) and (8.6).

The probability that the random variable of the current in an empty slot is greater than the random variable of the current in the signal slot in the presence of crosstalk and turbulence is written as

$$P\left(i_{0,int}(h_Z) > i_{1,int}(h_Z) \right) = \frac{1}{2} \text{erfc} \left(\frac{i_{1,int}(h_Z) - i_{0,int}(h_Z)}{\sqrt{2\left\{ \sigma_{1,int}^2(h_Z) + \sigma_{0,int}^2(h_Z) \right\}}} \right) \tag{8.38}$$

where $int \in \{0,1\}$ depending on the presence of crosstalk in a slot in the desired ONU signal frame or not, and for slots with no signal or crosstalk, both the mean current and variance are independent of turbulence (i.e. $h_Z = 1$ for $i_{0,0}$ and $\sigma_{0,0}^2$). The instantaneous symbol error probabilities when the crosstalk pulse hits the signal slot and when the crosstalk hits an empty slot are respectively written as

$$P_{WE-D}(1,1,h_Z) \leq \frac{1}{n} \left[1 - \left\{ 1 - P\left(i_{0,0}(h_Z) > i_{1,1}(h_Z) \right) \right\}^{n-1} \right] \tag{8.39}$$

$$P_{WE-D}(1,0,h_Z) \leq \frac{n-1}{n} \left[1 - \left\{ 1 - P\left(i_{0,0}(h_Z) > i_{1,0}(h_Z) \right) \right\}^{n-2} \left\{ 1 - P\left(i_{0,1}(h_Z) > i_{1,0}(h_Z) \right) \right\} \right] \tag{8.40}$$

where $1/n$ is the probability of crosstalk signal impairing any slot in the desired signal frame and $(n-1)/n$ is the probability of crosstalk signal impairing any empty slot in the desired signal frame. The total instantaneous symbol error probability is written as

$$Pe_D(h_Z) = P_{WE-D}(1,1,h_Z) + P_{WE-D}(1,0,h_Z) \tag{8.41}$$

The average DPPM downstream BER is written as

$$\overline{BER}_{DPPM\_D} = \frac{n}{2(n-1)} \int_0^\infty Pe_D(h_Z) \; p_{GG,d}(h_Z) \, \mathrm{d}h_Z \tag{8.42}$$

8.5 Numerical results

Results are presented using the parameters reported in Table 8.2. In the result section, DPPM1 and DPPM2 refer to DPPM with $M = 1$ and DPPM with $M = 2$ respectively while OOK CDMA and DPPM CDMA are referred to as OOK_C and $DPPM_C$ respectively. Mux/Demux with adjacent channel spacing of 100 GHz in the C-band of the ITU (International Telecommunication Union) grid specification and inherent loss of about 3.5 dB [29] is considered. The mux/demux channel bandwidth is 70 GHz; we assume this to be the optical channel noise bandwidth. Adjacent channel rejection values between -15 dB and -45 dB [53, 54] are considered. Perfect extinction ratio is used in all calculations and the DPPM coding level is restricted to $M \leq 2$ so as to reduce the bandwidth expansion that is common with DPPM signalling. The thermal noise is estimated using baseline value $\sigma_{thBL} = 7 \times 10^{-7}$ A which is obtained from a model of a PIN receiver with $R_b = 2.5$ Gbps at BER of 10^{-12} assuming a sensitivity of -23 dBm [28], such that $\sigma_{th-OOK_C}^2 = R_c \sigma_{thBL}^2 / R_b$ for OOK_C system and $\sigma_{th-DPPM_C}^2 = B_{exp} \sigma_{th-OOK_C}^2$ for $DPPM_C$ system calculations. Typical OLT transmitter power is 10 dB [55], however, both the OLT and ONU transmitters may require to transmit more power (not more than 20 dBm for safety reasons [56]) to counter splitter/combiner losses and turbulence attenuation respectively. A splitter loss of 3 dB per 2-way split is assumed. Fibre dispersion and other nonlinearities, and optical amplifier saturation effects are neglected in the analysis. The results are based on the effect of users with dominant crosstalk power on a single adjacent wavelength. The impact of such high power single crosstalk source is more damaging compared to many other crosstalk sources with equivalent power. Except if it is stated

otherwise, the FSO link length (l_{fso}) of the ONUs on the desired wavelength and the ONUs on the crosstalk wavelength are assumed to be equal in the presented results, and in such case, the average signal-to-crosstalk ratio is equal to the demux adjacent signal rejection ($L_{demux,i}$). The Rytov variance $\sigma_R^2 = 1.23 C_n^2 k^{7/6} l_{fso}^{11/6}$ is used to characterise the strength of turbulence as weak $(\sigma_R^2 < 1)$, moderate $(\sigma_R^2 \approx 1)$, strong $(\sigma_R^2 > 1)$ and saturated $(\sigma_R^2 \to \infty)$, thus in the following result discussion, the turbulence is referred to as strong turbulence and weak turbulence when the FSO link length (l_{fso}) and the C_n^2 values used in obtaining the particular plot results in σ_R^2 value greater than 1 and σ_R^2 value less than 1 respectively. The number of users in each wavelength (K) is fixed at 3 for all the results shown below, except if it is stated otherwise for any particular plot.

Table 8.2: System parameters used for calculations

Parameters	Description	Value
R_b	Binary data rate	132 Mbps
B_o	Demux channel bandwidth	70 GHz
λ_{sig}	Desired signal wavelength	1550 nm
φ_{TX}	Transmission divergence angle	0.2 mrad
D_{RX}	Receiver collecting lens diameter	13 mm
η	Receiver quantum efficiency	0.8
l_f	Feeder fibre link length	20 km
l_{fso}	Maximum free space link length	1.5 km
L_c	Code length	19
w	Code weight	3
K	Number of ONUs per wavelength	3
G	Optical preamplifier gain	30 dB
NF	Optical preamplifier noise figure	4.77 dB

The upstream BER results for OOK_C system are compared with the results for $DPPM_C$ systems in Fig. 8.7 for $\sigma_R^2 = 4.2$ (i.e. with $l_{fso} = 1500$ m and $C_n^2 = 1 \times 10^{-13}$ $m^{-2/3}$, indicating strong turbulence regime), and with a poor adjacent channel rejection ($L_{demux,i} = 15$ dB). In the absence of turbulence as in Fig. 8.7a, $DPPM_C$ shows an improved BER performance compared to OOK_C, and even a better improvement is shown for $M = 2$ (DPPM2). The trend is the same when there is no crosstalk in the system, for example, the TurbSig BER results in Fig. 8.7c. However, the improvement recorded in this case is less than that seen in Fig. 8.7a. As stated in Chapters 6 and 7, there is a reduction in power efficiency shown by DPPM in turbulent systems compared to non-turbulent systems. This happens because the turbulence pdf is skewed or shifts more to the left with increasing Rytov variance (and consequently turbulence strength) as shown in Fig. 3.7, thus more area of the pdf coincide with part of the instantaneous BER curve where the thermal noise is dominant, resulting in an average BER which is dominated by the left tail of the pdf where both DPPM and OOK evenly converge to 0.5, and a consequent reduction in DPPM average sensitivity advantage over OOK as the turbulence becomes stronger. The combined effects of turbulence and crosstalk in a CDMA system result in error floors which are marginally raised compared to those seen in Chapter 6. This is shown in Fig. 8.7b for cases where only the signal is affected by turbulence (TurbSig,XT), and only the crosstalk is affected by turbulence (Sig,TurbXT), and also shown in Fig. 8.7c for the case where both the signal and crosstalk are affected by turbulence (TurbSig,TurbXT). In systems with strong turbulence and crosstalk, the $DPPM_C$ advantage over OOK_C is limited to the areas of the BER curve before the error floor occurs. However, the error floor is lowered (particularly for the $DPPM_C$ system with $M = 2$) for the case where the turbulence affects only the crosstalk (Sig,TurbXT) as is shown in Fig. 8.7b. This is because the signal is turbulence free and the turbulence attenuation on the crosstalk is reduced by the value of $L_{demux,i}$, as could be deduced from eq. (7.13) where the crosstalk term is written as $h_{turb,int} L_{demux,i}$.
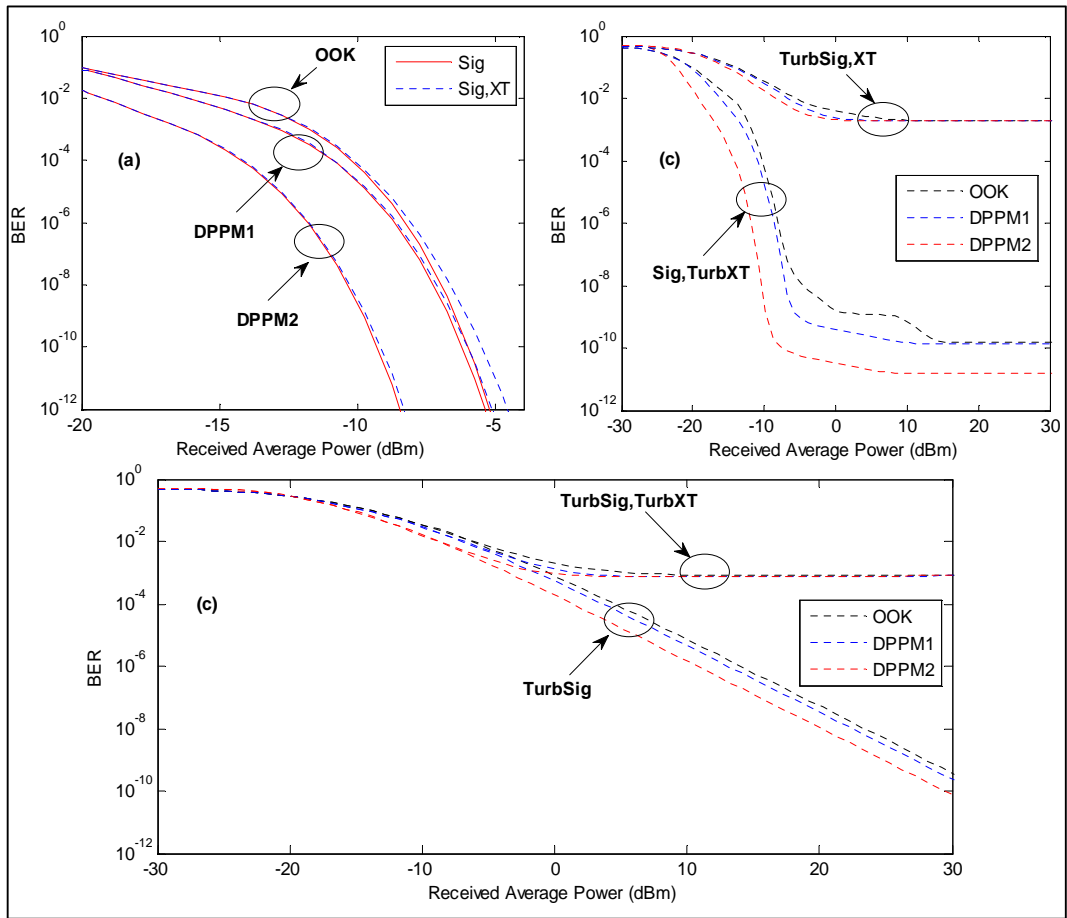
Fig. 8.7 Upstream BER versus Received Average Power (dBm) for OOK$_C$ and DPPM$_C$ systems using M = 1 (DPPM1) and M = 2 (DPPM2) with l_{fso} = 1500 m, C_n^2 = 1 x 10^{-13} m$^{-2/3}$ and $L_{demux,i}$ = 15 dB: (a) Sig and Sig,XT, (b) TurbSig,XT and Sig,TurbXT, and (c) TurbSig and TurbSig,TurbXT
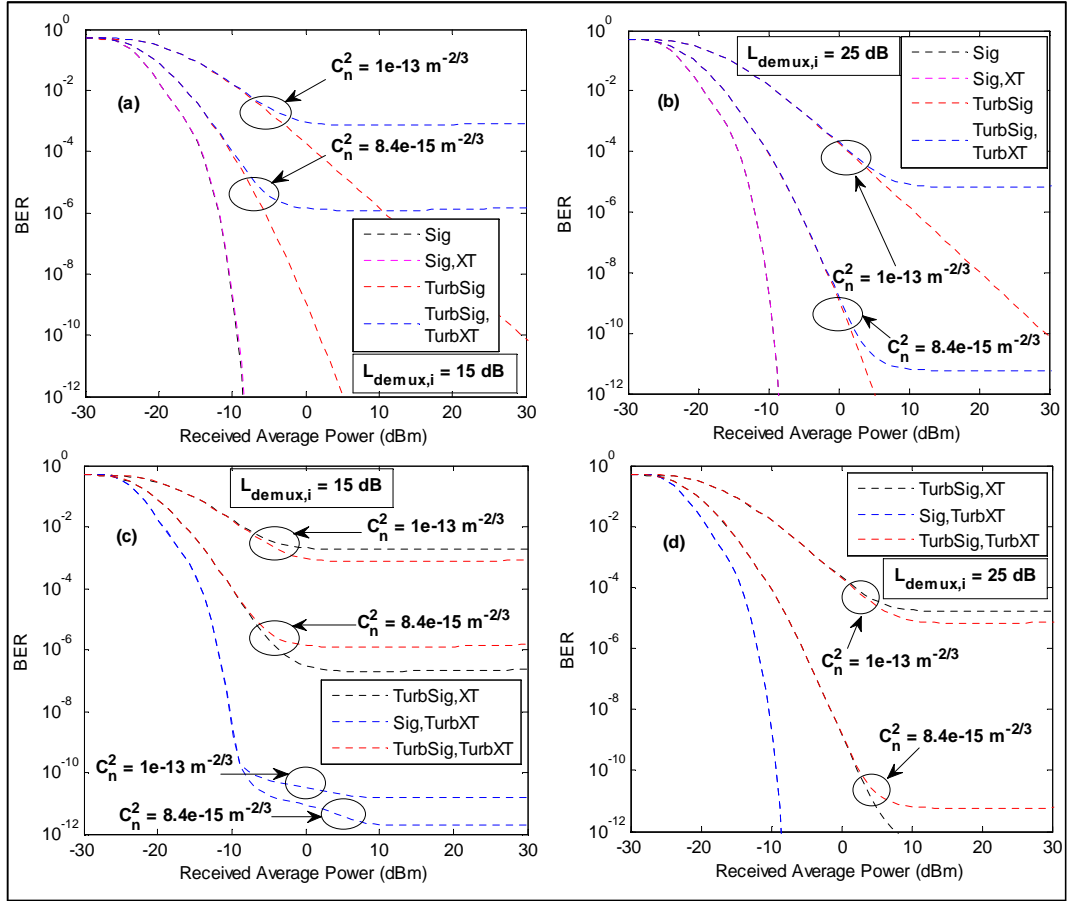
Fig. 8.8 Upstream BER versus Received Average Power for DPPM$_C$ system ($M = 2$) with $l_{fso} = 1500$ m and C_n^2 values of 1×10^{-13} m$^{-2/3}$ and 8.4×10^{-15} m$^{-2/3}$: (a) $L_{demux,i} = 15$ dB, (b) $L_{demux,i} = 25$ dB, (c) $L_{demux,i} = 15$ dB and (d) $L_{demux,i} = 25$ dB

Fig. 8.8 shows the result of the upstream BER for a DPPM$_C$ system using $M = 2$ with C_n^2 values of 1×10^{-13} m$^{-2/3}$ and 8.4×10^{-15} m$^{-2/3}$, which correspond to $\sigma_R^2 \approx 4.2$ and 0.35 for $l_{fso} = 1500$ m and indicate strong and weak turbulence regimes respectively. $L_{demux,i}$ is fixed for each sub-figure while C_n^2 is varied to show the impact of turbulence on the network BER performance. The BER is shown worsening with increase in turbulence strength in Figs. 8.8a – 8.8d, with the error floors raised for BER curves at strong turbulence conditions. A comparison of Figs. 8.8a and 8.8b and Figs. 8.8c and 8.8d shows the effect of crosstalk at both strong and weak turbulence regimes. The BER is improved and error floor lowered in Figs. 8.8b and 8.8d compared to Figs. 8.8a and 8.8c respectively, as the crosstalk at the desired ONU is reduced by using a demux with $L_{demux,i} = 25$ dB. In Figs. 8.8c and 8.8d, the error floor for TurbSig,XT is raised above that for TurbSig,TurbXT at $C_n^2 = 1 \times 10^{-13}$ m$^{-2/3}$. This is as a result of high crosstalk power

in the TurbSig,XT case because the crosstalk is not turbulence affected and does not experience turbulence-related losses such as increased beam spreading and coupling losses.
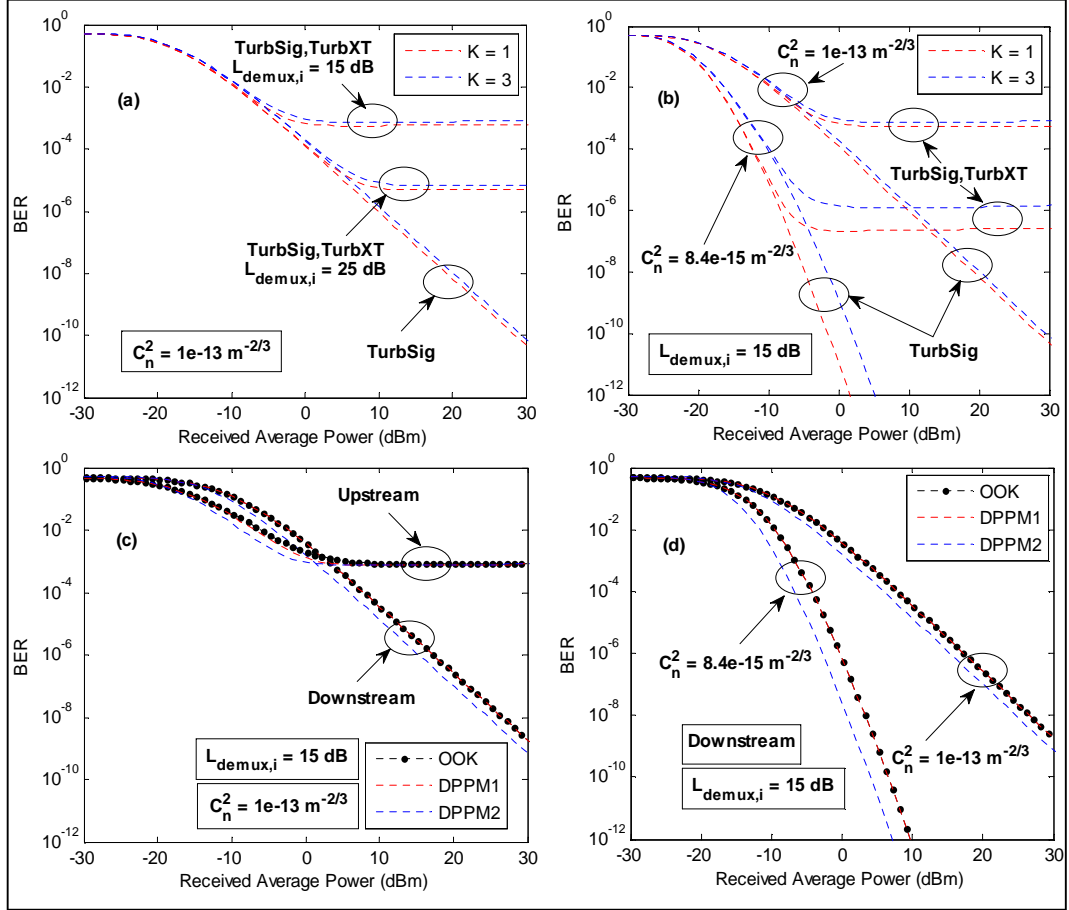
Fig. 8.9 BER versus Received Average Power with l_{fso} = 1500 m: (a) upstream DPPM$_C$ system (M = 2) with fixed C_n^2 and varying $L_{demux,i}$, (b) upstream DPPM$_C$ system (M = 2) with fixed $L_{demux,i}$ and varying C_n^2, (c) upstream and downstream for DPPM$_C$ and OOK$_C$ systems with both $L_{demux,i}$ and C_n^2 fixed and (d) downstream for DPPM$_C$ and OOK$_C$ systems with fixed $L_{demux,i}$ and varying C_n^2

The effects of MAI on the upstream BER at both strong and weak turbulences are shown in Figs. 8.9a and 8.9b, with demux adjacent channel rejections of 15 dB and 25 dB. The impact of MAI (as seen by the difference between K = 1 and K = 3 curves) is marginal at strong turbulence in Figs. 8.9a and 8.9b, and more pronounced in Fig. 8.9b at weak turbulence, with raised error floor in the presence of MAI. However, it should be noted that MAI in the system is dependent on the CDMA code parameters $\{L_c, w, \gamma_c, \gamma_a\}$ = {19, 3, 1, 1} used for this analysis, and

some changes in the parameters may worsen the MAI effects, for example, as shown in Fig. 8.10 where the code length has been increased to accommodate 4 users according to eq. (4.2). MAI is dominant in this case, and results in error floor in the absence of crosstalk as shown by the TurbSig curves for $K = 4$, and also results in a slight raise in the error floor above that of Figs. 8.9a and 8.9b for the TurbSig,TurbXT case. Note that for OOCs with $\gamma_c = \gamma_a = 1$, error floors could be eliminated by choosing code parameters that satisfy the inequality $K \leq w$.

The upstream BER is compared with the downstream BER at strong turbulence in Fig. 8.9c for both OOK_C and $DPPM_C$ systems. Turbulence-accentuated crosstalk and MAI which do not exist in the downstream, results in error floor in the upstream. The upstream BER is however better than the downstream BER before the error floor occurs. This is because of extra splitting loss experienced by the downstream signals as shown by the network architecture in Fig. 8.1a, which is optional and could be avoided by using one transmitting source per ONU instead of a single transmitting source for all ONUs on the same wavelength. Similar to the upstream, $DPPM_C$ with $M = 2$ results in improved BER compared to OOK_C in the downstream, as shown in Figs. 8.9c and 8.9d. In the absence of MAI and with the crosstalk not worsened by turbulence in the downstream, the performance of the downstream system is primarily affected by optical scintillation as shown by the BER results in Fig. 8.9d.
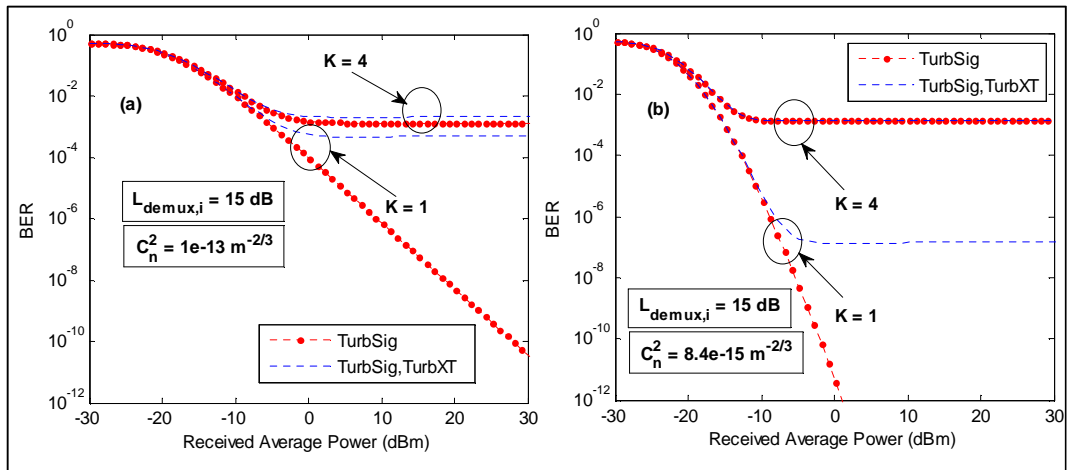
Fig. 8.10 Upstream BER versus Received Average Power for $DPPM_C$ system ($M = 2$) with $l_{fso} = 1500$ m, $L_{demux,i} = 15$ dB, and using the code parameter $\{L_c$, w, γ_c, $\gamma_a\} = \{25, 3, 1, 1\}$: (a) $C_n^2 = 1 \times 10^{-13}$ m$^{-2/3}$ and (b) $C_n^2 = 8.4 \times 10^{-13}$ m$^{-2/3}$
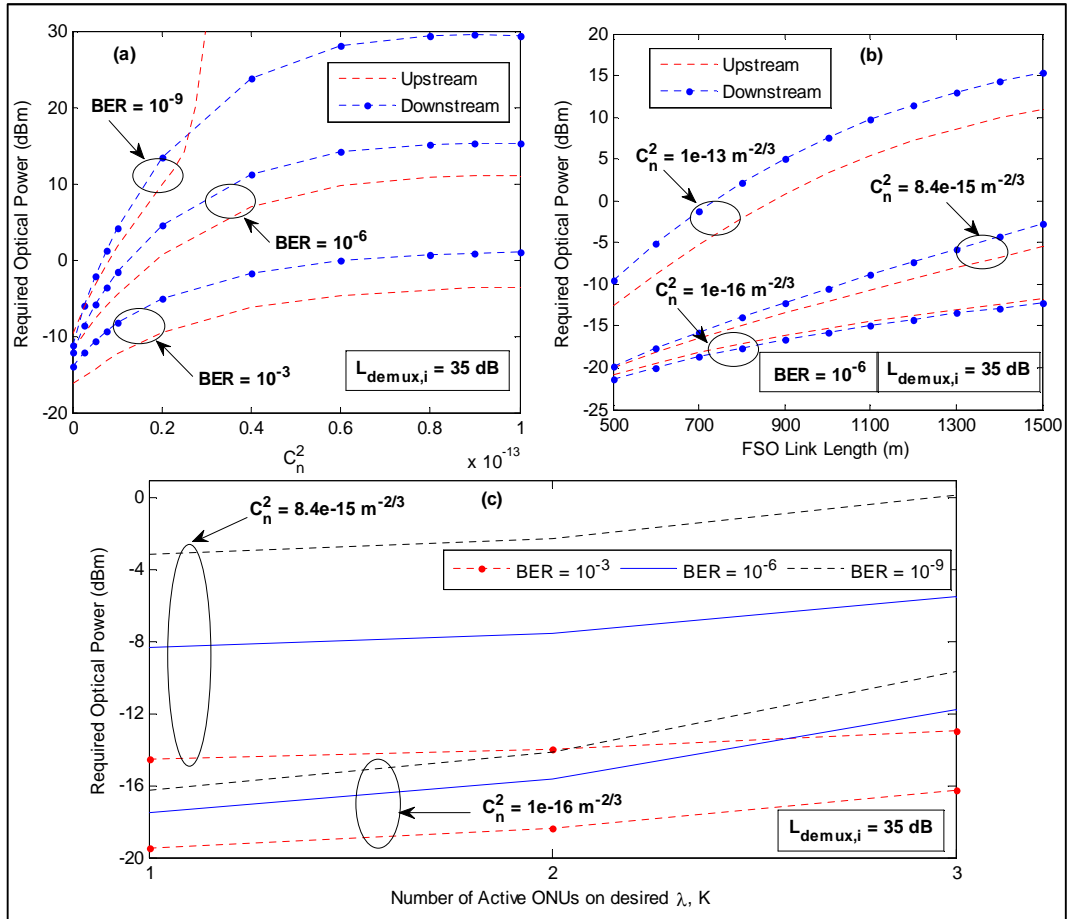
Fig. 8.11 Required Average Power (dBm) for OCDMA WDM DPPM system with $L_{demux,i} = 35$ dB: (a) against C_n^2 for upstream and downstream with $l_{fso} = 1500$ m, (b) against FSO link length (l_{fso}) for upstream and downstream, (c) against number of active ONUs on the desired wavelength for upstream with $l_{fso} = 1500$ m

The required average transmitter power for the upstream and downstream operations for DPPM$_C$ system using $M = 2$ is shown in Fig. 8.11 for a demux with improved adjacent channel rejection ($L_{demux,i} = 35$ dB). The required optical power is shown in Fig. 8.11a increasing in both the upstream and downstream systems as the C_n^2 (and consequently, the turbulence strength) and the target BER increases. In the upstream, target BER of 10^{-9} is not achievable for high values of C_n^2 (strong turbulence regimes) with $L_{demux,i} = 35$ dB because of the error floor. A demultiplexer with better adjacent channel rejection (e.g. above 45 dB as shown in Fig. 6.8c for non-CDMA WDM FSO system) could do better. However, such target BER is achieved at high ONU and OLT transmitter powers (above 20 dBm for the downstream as shown in Fig. 8.11a) which may introduce non-linear

effects in the system and will raise concerns for eye safety. Target BERs of 10^{-6} and 10^{-3} are achievable for all C_n^2 values in Fig. 8.11a and at average transmitter powers less than 20 dBm. The required average transmitter power is reduced for short FSO link lengths as shown in Fig. 8.11b because of decreasing σ_R^2 (and turbulence strength) as FSO link length decreases. The OLT is required to transmit more power compared to the ONU in Figs. 8.11a and 8.11b. This is because unlike the upstream transmission, a single transmitter at the OLT provides power which is split for downstream transmission to the three ONUs on the same wavelength. The extra splitting loss in the downstream is 6 dB. However at a very weak turbulence and low crosstalk power, the upstream required average transmitter power exceeds the downstream because of the presence of MAI (which is the dominant source of impairment under such conditions) in the upstream. This is shown in Fig. 8.11b and occurs for low target BERs (BER $\leq 10^{-6}$) which are achieved at relatively high optical power when the effect of MAI is more pronounced. For higher target BER values that are achieved at low power when the system is dominated by signal independent thermal noise instead of MAI (e.g. BER of 10^{-3}), the required optical power for the downstream remains greater than that for the upstream as shown in Fig. 8.11a for low C_n^2 values. The increase in upstream required optical power due to MAI at weak turbulence is clearly shown in Fig. 8.11c at different target BER values.

The system power penalty is shown in Fig. 8.12a for different FSO link lengths. The power penalty at very weak turbulence ($C_n^2 = 1 \times 10^{-16}$ m$^{-2/3}$) is dominantly contributed by MAI, and ranges from about -5.7 dB for target BER of 10^{-3} and l_{fso} of 500 m to 6.9 dB for target BER of 10^{-9} and l_{fso} of 1500 m. In strong turbulence conditions, the power penalty exceeds 25 dB for target BER of 10^{-6} and l_{fso} of 1500 m, and BER of 10^{-9} is not achievable for $l_{fso} > 800$ m. The power penalty caused by MAI alone (i.e. relative to when one ONU is active on the desired wavelength) for various target BER values is shown in Fig. 8.12b. The effect of MAI is less prominent at strong turbulence conditions with a maximum power penalty contribution of about 1 dB when the 3 ONUs are active and at target BER of 10^{-6}. No result is shown for target BER of 10^{-9} at strong turbulence conditions, as previously shown, such BER is not achievable at l_{fso} of 1500 and C_n^2 of 1×10^{-13} m$^{-2/3}$. The effect of MAI is more prominent at weak turbulence

conditions and for C_n^2 of 1×10^{-16} m$^{-2/3}$, a power penalty of about 6.6 dB is predicted for target BER of 10^{-9} when the 3 ONUs are active. This value is 0.3 dB less than the power penalty of 6.9 dB stated above for all the system impairments under the same condition, probably due to minor contributions from crosstalk and the much weakened turbulence.
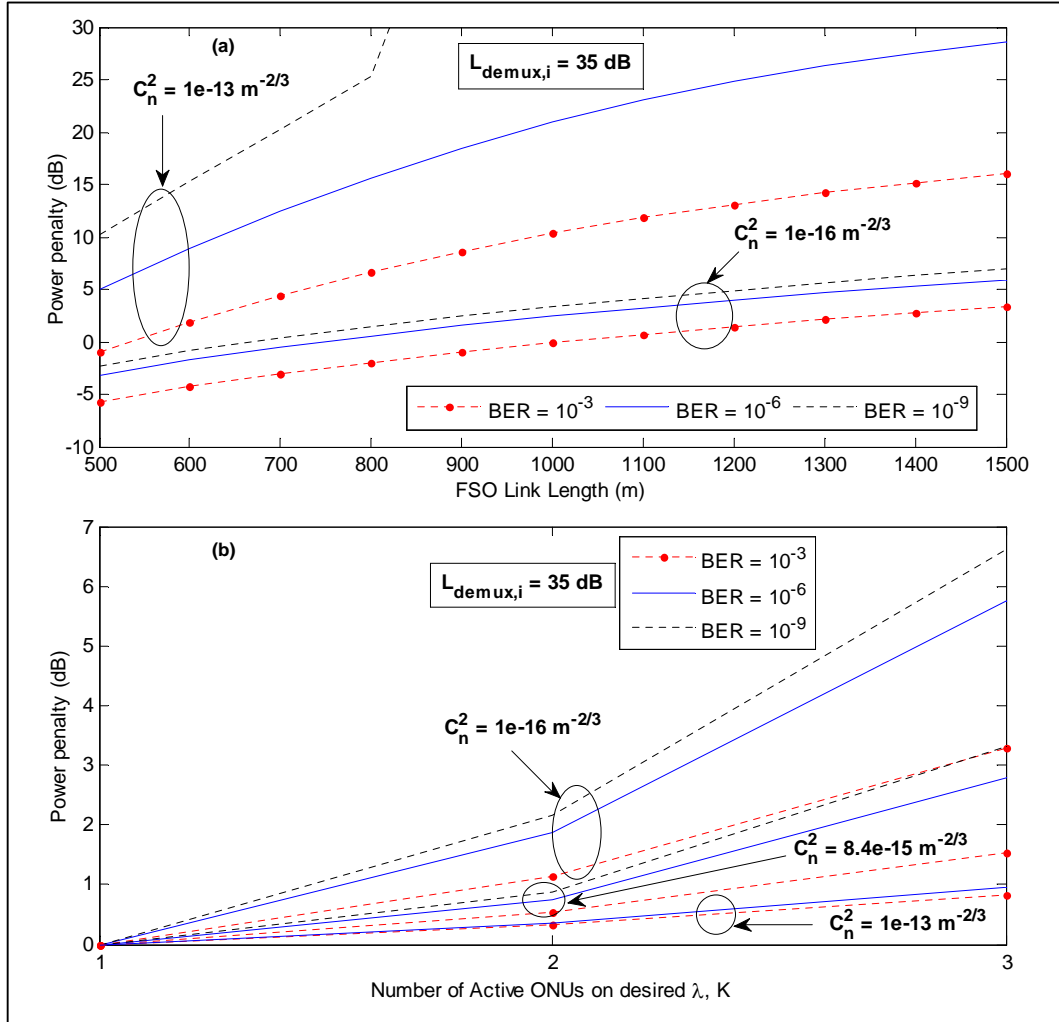
Fig. 8.12 Upstream Power penalty (dB) for DPPM$_C$ system for varying C_n^2 and $L_{demux,i} = 35$ dB: (a) against FSO link length, (b) against number of active ONUs on the desired wavelength with $l_{fso} = 1500$ m

In Fig. 8.13, the assumption that the FSO link lengths of all ONUs are equal is removed, and results for the upstream required optical power are presented with and without power control algorithm (PCA), for different values of the FSO link length for ONUs on the crosstalk wavelength $l_{fso,int}$ and different values of the FSO link length for ONUs on the desired wavelength $l_{fso,sig}$. The power control procedure could be initiated from the remote node under the control of the OLT,

which tries to estimate each ONU's distance from the remote node in order to determine the required transmit power from such distance to achieve the defined quality of service. Implementation of PCA saves transmit power for both the ONU and the OLT and helps in the reduction of interferences between ONUs in the system by ensuring that equal power is received from each ONU irrespective of the distance from the remote node. Figs. 8.13a and 8.13b show the upstream required optical power without PCA and with PCA respectively, for various distances of the ONUs on the desired signal wavelength and the ONUs on the crosstalk wavelength, with $C_n^2 = 1 \times 10^{-13}$ m$^{-2/3}$, $L_{demux,i} = 35$ dB and for target BER of 10^{-6}. The result in Fig. 8.13a (without PCA) is of the same trend with Fig. 6.5a for the HFFSO WDM DPPM system considered in Chapter 6, with more power required when the ONU on the desired wavelength is farther away from the remote node. Furthermore, the effect of crosstalk is also accentuated when the interfering ONUs are closer to the remote node compared to the desired ONU, resulting in the target BER not being achieved in some area due to the occurrence of error floor. As explained in Chapter 6, this is majorly due to decrease in average signal-to-crosstalk ratio because of asymmetric losses experienced by the desired ONU and the interfering ONU when they are at unequal distances (with the interfering ONU being closer to the remote node). With power control implemented, the average-signal-to-crosstalk ratio is approximately constant and equal to $L_{demux,i}$ for all distances, thus the error floor does not occur, and the required optical power is lower for the points of unequal distances between the interfering and the desired ONUs as shown in Fig. 8.13b. In implementing a power control, the system determines the required transmitter power (P_{TXmin}) independent of the net link path loss to achieve the set QoS or BER. For downstream operation, the average transmitted power from the OLT to the ONU on the desired wavelength $P_{TD,d}$ is included in the data frame sent to each ONU as power control information (PCI) [57], the PCI is detached at the ONU, and the ONU estimates the received average power $P_d(h_Z)$. The net link path loss at the ONU distance in dB is obtained as $PL_{net} = P_{TD,d} - P_d(h_Z)$ as can be deduced from eq. (8.5) which is expressed in linear power. Finally, the OLT transmitter power to the ONU at that distance with power control is set as $P_{TXmin} + PL_{net}$. This is then embedded into the upstream data as PCI for the OLT. The process is the same but

performed differently for upstream since the path loss for upstream and downstream may differ, and it is repeated each time the ONU distance changes significantly for mobile users.
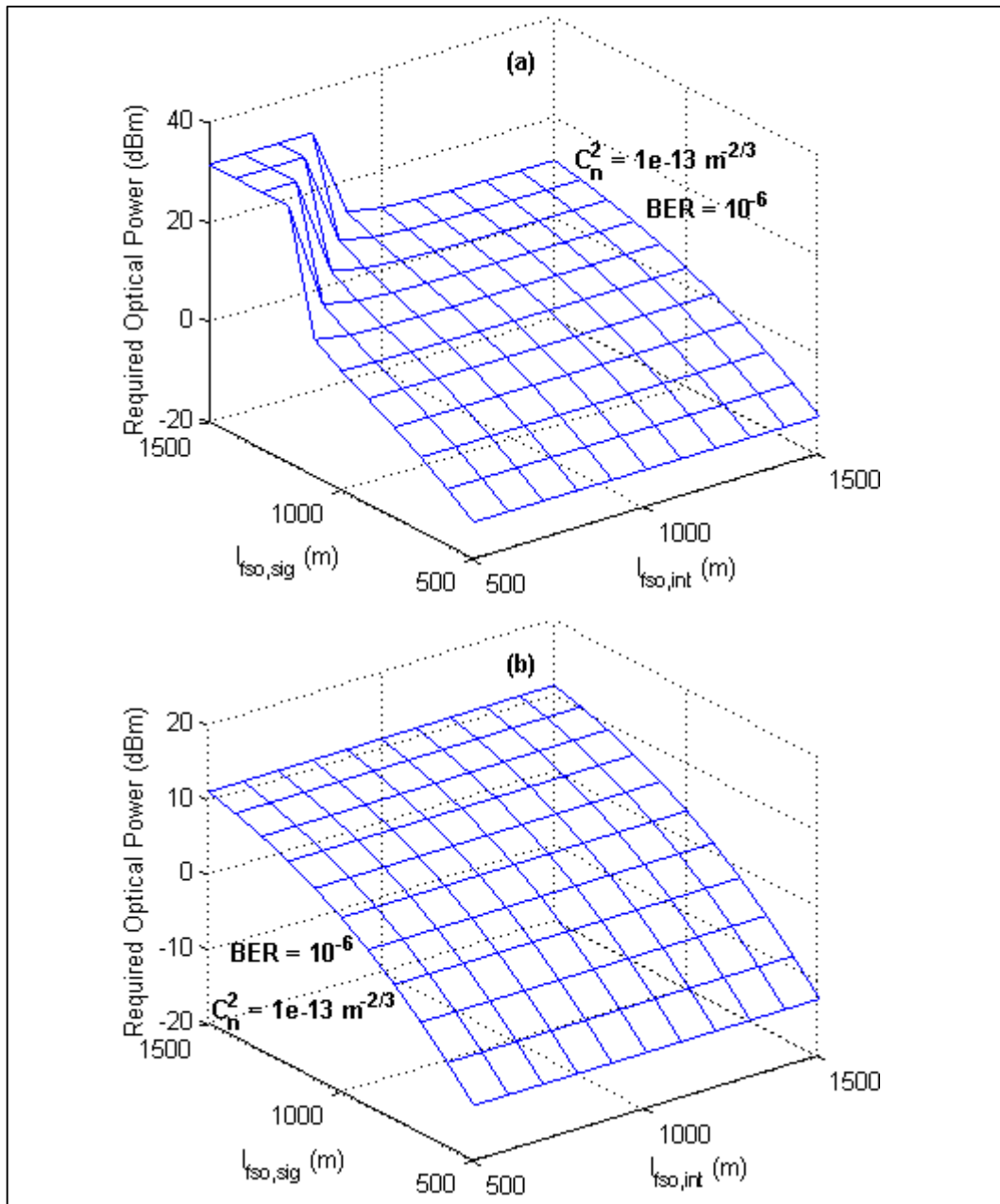
Fig. 8.13 Upstream Required Optical Power (dBm) as a function of the FSO link lengths for signal and interferer (m) at $L_{demux,i}$ = 35 dB and target BER = 10^{-6}: (a) Without power control algorithm and (b) With power control algorithm

8.6 Summary

The analysis of a novel network of hybrid WDM and OCDMA systems including both fibre and FSO links is performed in this chapter for both OOK and DPPM systems. Obtained results show the superiority of DPPM over OOK with regard to average power performance. The error floor in this system is raised above that which is seen in Chapter 6 because of the presence of MAI. Depending on the CDMA code parameters used in the network design, MAI alone could limit the network performance and may result in error floors at high BER values. However, by using a code weight that is equal to or greater than the number of users, the effect of MAI is reduced, and is predominantly noticed only in weak turbulence conditions. At the target BER of 10^{-6}, the required average transmitter power for both the downstream and upstream systems is less than 20 dBm and considered safe, but the OLT is required to transmit more power than the ONUs because of the additional (but optional) power splitting in the downstream. The effect of turbulence-accentuated crosstalk is shown to be mitigated using power control in this chapter. The primary advantages of this network over the HFFSO WDM network analysed in Chapter 6 are the increase in user capacity and better utilization of wavelength, although at the expense of reduced data rate per user. However, increase in data rate per user is possible, and will require additional processing speed. This network can easily be extended to an indoor environment and the data rate of 132 Mbps used in the analysis is comparable to current data rate in most indoor wireless systems. With stiff competition among service providers, and increasing demand for reduction in the cost per data rate by users, the proposed network is a sensible option to service providers and would help in satisfying the users need at reduced cost because no licence fee is required for the optical frequency band, and the cost of the network components is borne by many users compared to the HFFSO WDM system discussed in Chapter 6.

8.7 References

1. Banerjee, A., Park, Y., Clarke, F., Song, H., Yang, S., Kramer, G., Kim, K., et al.: 'Wavelength-division-multiplexed passive optical network (WDM-PON) technologies for broadband access: a review [Invited]'. *J. Opt. Netw.,* 2005, **4**, (11), pp. 737-758

2. Andrade, M. D., Kramer, G., Wosinska, L., Jiajia, C., Sallent, S., Mukherjee, B.: 'Evaluating strategies for evolution of passive optical networks'. *IEEE Commun. Mag.,* 2011, **49**, (7), pp. 176-184

3. Bongtae, K., Byoung-Whi, K.: 'WDM-PON development and deployment as a present optical access solution'. *Conf. on Optical Fiber Commun. - incudes post deadline papers,* 2009, pp. 1-3

4. Kazovsky, L., Shing-Wa, W., Ayhan, T., Albeyoglu, K. M., Ribeiro, M. R. N., Shastri, A.: 'Hybrid Optical-Wireless Access Networks'. *Proc. IEEE,* 2012, **100**, (5), pp. 1197-1225

5. Xu, Z., Wen, Y. J., Zhong, W.-D., Chae, C.-J., Cheng, X.-F., Wang, Y., Lu, C., et al.: 'High-speed WDM-PON using CW injection-locked Fabry-Pérot laser diodes'. *Opt. Express,* 2007, **15**, (6), pp. 2953-2962

6. Wooram, L., Mahn Yong, P., Seung Hyun, C., Jihyun, L., Byoung Whi, K., Geon, J.: 'Bidirectional WDM-PON based on gain-saturated reflective semiconductor optical amplifiers'. *IEEE Photonics Technol. Lett.,* 2005, **17**, (11), pp. 2460-2462

7. Liu, L., Zhang, M., Liu, M., Zhang, X.: 'Experimental demonstration of RSOA-based WDM PON with PPM-encoded downstream signals'. *Chin. Opt. Lett.,* 2012, **10**, (7), pp. 070608

8. 'Spectral grids for WDM applications: CWDM wavelength grid', International Telecommunication Union (ITU) Telecommunication Recommendation G.694.2, 2003.

9. Kitayama, K., Xu, W., Wada, N.: 'OCDMA over WDM PON-solution path to gigabit-symmetric FTTH'. *J. Lightw.Technol.,* 2006, **24**, (4), pp. 1654-1662

10. Galdino, L., Raddo, T. R., Sanches, A. L., Bonani, L. H., Moschim, E.: 'Performance comparison of hybrid 1-D WDM/OCDMA and 2-D OCDMA towards future access network migration scenario'. *14th Int'l Conf. on Transparent Optical Networks (ICTON)* 2012, pp. 1-4

11. Sasaki, K., Minato, N., Ushikubo, T., Arimoto, Y.: 'First OCDMA Experimental Demonstration over Free Space and Optical Fiber Link'. *Optical Fiber Commun. Conf./National Fiber Optic Engineers Conf.* 2008; San Diego,: Optical Society of America, pp. OMR8

12. Jazayerifar, M., Salehi, J. A.: 'Atmospheric optical CDMA communication systems via optical orthogonal codes'. *IEEE Trans. Commun.,* 2006, **54**, (9), pp. 1614-1623

13. Ghaffari, B. M., Matinfar, M. D., Salehi, J. A.: 'Wireless optical CDMA LAN: digital design concepts'. *IEEE Trans. Commun.,* 2008, **56**, (12), pp. 2145-2155

14. Ohtsuki, T.: 'Performance analysis of atmospheric optical PPM CDMA systems'. *J. Lightw. Technol.,* 2003, **21**, (2), pp. 406-411

15. Xu, W., Wada, N., Hamanaka, T., Miyazaki, T., Cincotti, G., Kitayama, K.: 'OCDMA over WDM Transmission'. *9th Int'l. Conf. on Transparent Optical Networks* 2007, pp. 110-113

16. Wang, X., Wada, N., Miyazaki, T., Cincotti, G., Kitayama, K.-i.: 'Hybrid WDM/OCDMA for next generation access network'. *Proc. SPIE 6783,* 2007, pp. 678314-678328

17. Huang, J.-F., Chang, Y.-T., Hsu, C.-C.: 'Hybrid WDM and optical CDMA implemented over waveguide-grating-based fiber-to-the-home networks'. *Optical Fiber Technology,* 2007, **13**, (3), pp. 215-225

18. Ashour, I. A. M., Shaari, S., Menon, P. S., Bakarman, H. A.: 'Optical code-division multiple-access and wavelength division multiplexing: hybrid scheme review'. *J. Comput. Sci.,* 2012, **8**, (10), pp. 1718-1729

19. Shumate, P. W.: 'Fiber-to-the-Home: 1977 - 2007'. *J. Lightw. Technol.,* 2008, **26**, (9), pp. 1093-1103
20. 'FTTH subscribers in Europe: nearly 15 million homes!', Fibre to the Home Council Europe Press Release, Feb. 2015. Available Online: http://www.ftthcouncil.eu [cited 29/04/2015].
21. Natalija, G., Michel, R., Carlo Maria, R.: 'Broadband Networks in the Middle East and North Africa: Accelerating High-Speed Internet Access', 2014. Available Online: http://www.worldbank.org2014 [cited 29/04/2015].
22. Pei-Lin, C., Shenq-Tsong, C., Shuen-Te, J., Shu-Chuan, L., Han-Hsuan, L., Ho-Lin, T., Po-Hsuan, H., et al.: 'Demonstration of 16 channels 10 Gb/s WDM free space transmission over 2.16 km'. *Digest of the IEEE/LEOS Summer Topical Meetings* 2008, pp. 235-236
23. Leitgeb, E., Gebhart, M., Birnbacher, U.: 'Optical networks, last mile access and applications'. *J Optic Comm Rep,* 2005, **2**, (1), pp. 56-85
24. Ciaramella, E., Arimoto, Y., Contestabile, G., Presi, M., D'Errico, A., Guarino, V., Matsumoto, M.: '1.28 terabit/s (32x40 Gbit/s) wdm transmission system for free space optical communications'. *IEEE J. Selected Areas in Commun.,* 2009, **27**, (9), pp. 1639-1645
25. Willebrand, H. A., Ghuman, B. S. *Free-space optics: enabling optical connectivity in today's networks*. Indiana USA: Sams Publishing; 2002.
26. Aladeloba, A. O., Woolfson, M. S., Phillips, A. J.: 'WDM FSO Network with Turbulence-Accentuated Interchannel Crosstalk'. *J. Opt. Commun. Netw.,* 2013, **5**, (6), pp. 641-651
27. Mbah, A. M., Walker, J. G., Phillips, A. J.: 'Performance Evaluation of Turbulence-Accentuated Interchannel Crosstalk for Hybrid Fibre and FSO WDM Systems using Digital Pulse Position Modulation'. *IET Optoelectronics,* 2016, **10**, (1), pp. 11-20
28. Ramaswami, R., Sivarajan, K. N., Sasaki, G. H. *Optical Networks: A Practical Perspective*. 3rd ed. Boston: Morgan Kaufmann Publishers; 2010.
29. Monroy, I. T., Tangdiongga, E. *Crosstalk in WDM Communication Networks*. Norwell, Massachusetts, USA, : Kluwer Academic Publishers; 2002.
30. Ke, W., Nirmalathas, A., Lim, C., Skafidas, E.: 'Impact of Crosstalk on Indoor WDM Optical Wireless Communication Systems'. *IEEE Photonics Journal,* 2012, **4**, (2), pp. 375-386
31. Salehi, J. A.: 'Code division multiple-access techniques in optical fiber networks. I. Fundamental principles'. *IEEE Trans. Commun.,* 1989, **37**, (8), pp. 824-833
32. Salehi, J. A., Brackett, C. A.: 'Code division multiple-access techniques in optical fiber networks. II. Systems performance analysis'. *IEEE Trans. Commun.,* 1989, **37**, (8), pp. 834-842
33. Mashhadi, S., Salehi, J. A.: 'Code-division multiple-access techniques in optical fiber networks - part III: optical AND logic gate receiver structure with generalized optical orthogonal codes'. *IEEE Trans. Commun.,* 2006, **54**, (8), pp. 1457-1468
34. Gharaei, M., Lepers, C., Gallion, P.: 'Impact of Crosstalk in Capacity Performance of WDM/OCDMA System'. *National Fiber Optic Engineers Conf.* 2010: Optical Society of America, pp. JThA49
35. Ohba, K., Hirano, T., Miyazawa, T., Sasase, I.: 'A symbol decision scheme to mitigate effects of scintillations and MAIs in optical atmospheric PPM-CDMA systems'. *IEEE Global Telecommuns. Conf.* 2005, pp. 1999-2003
36. Azizoglu, M., Salehi, J. A., Li, Y.: 'Optical CDMA via temporal codes'. *IEEE Trans. Commun.,* 1992, **40**, (7), pp. 1162-1170
37. Ghaffari, B. M., Salehi, J. A.: 'Multiclass, Multistage, and Multilevel Fiber-Optic CDMA Signaling Techniques Based on Advanced Binary Optical Logic Gate Elements'. *IEEE Trans. Commun.,* 2009, **57**, (5), pp. 1424-1432
38. Ng, E. K. H., Sargent, E. H.: 'Optimum threshold detection in real-time scalable high-speed multi-wavelength optical code-division multiple-access LANs'. *IEEE Trans. Commun.,* 2002, **50**, (5), pp. 778-784

39. Kataoka, N., Wada, N., Xu, W., Cincotti, G., Sakamoto, A., Terada, Y., Miyazaki, T., et al.: 'Field Trial of Duplex, 10 Gbps x 8-User DPSK-OCDMA System Using a Single 16 x 16 Multi-Port Encoder/Decoder and 16-Level Phase-Shifted SSFBG Encoder/Decoders'. *J. Lightw. Technol.,* 2009, **27**, (3), pp. 299-305

40. Kataoka, N., Cincotti, G., Wada, N., Kitayama, K.: 'Demonstration of asynchronous, 40Gbps x 4-user DPSK-OCDMA transmission using a multi-port encoder/decoder'. *Opt. Express,* 2011, **19**, (26), pp. B965-B970

41. Andrews, L. C., Phillips, R. L. *Laser Beam Propagation Through Random Media.* 2nd ed: SPIE Press, Bellingham, Washington; 2005.

42. Dikmelik, Y., Davidson, F. M.: 'Fiber-coupling efficiency for free-space optical communication through atmospheric turbulence'. *Appl. Opt.,* 2005, **44**, (23), pp. 4946-4952

43. Zhu, X., Kahn, J. M.: 'Free-space optical communication through atmospheric turbulence channels'. *IEEE Trans. Commun.,* 2002, **50**, (8), pp. 1293-1300

44. Fan, C., Salehi, J. A., Wei, V. K.: 'Optical orthogonal codes: design, analysis and applications'. *IEEE Trans. Info. Theory,* 1989, **35**, (3), pp. 595-604

45. Khazraei, S., Pakravan, M. R.: 'Analysis of generalized optical orthogonal codes in optical wireless local area networks'. *IEEE J. Sel. Areas Commun.,* 2009, **27**, (9), pp. 1572-1581

46. Khazraei, S., Pakravan, M. R.: 'Analysis of Generalized Optical Orthogonal Codes in Wireless Optical Networks Using BPPM'. *15th IEEE Intl. Conf. on Networks* 2007, pp. 170-175

47. Ma, R., Zuo, T. J., Sujecki, S., Phillips, A. J.: 'Improved performance evaluation for DC-coupled burst mode reception in the presence of amplified spontaneous emission noise and interchannel crosstalk'. *IET Optoelectron.,* 2010, **4**, (3), pp. 121-132

48. Sibley, M. J. N. *Optical Communications : components and systems.* 2nd ed. London: Macmillian Press Ltd; 1995.

49. Shalaby, H. M. H.: 'Performance analysis of optical CDMA communication systems with PPM signaling'. *IEEE Global Telecommun. Conf.* 1993, pp. 1901-1905

50. Shalaby, H. M. H.: 'A comparison between the performance of number-state and coherent-state optical CDMA in lossy photon channels'. *IEEE J. Selected Areas in Commun.,* 1995, **13**, (3), pp. 592-602

51. Dang, N. T., Pham, A. T.: 'Performance improvement of FSO/CDMA systems over dispersive turbulence channel using multi-wavelength PPM signaling'. *Opt. Express,* 2012, **20**, (24), pp. 26786-26797

52. Luu, T. A., Dang, N. T., Pham, A. T.: 'Performance analysis of optical atmospheric Turbo-coded 2-D CDMA systems with PPM signaling'. *8th Asia-Pacific Symp. on Info. and Telecommun.Technol. (APSITT)* 2010, pp. 1-6

53. Maru, K., Mizumoto, T., Uetsuka, H.: 'Demonstration of Flat-Passband Multi/Demultiplexer Using Multi-Input Arrayed Waveguide Grating Combined With Cascaded Mach-Zehnder Interferometers'. *J. Lightw. Technol.,* 2007, **25**, (8), pp. 2187-2197

54. Yu, C. X., Neilson, D. T.: 'Diffraction-grating-based (de)multiplexer using image plane transformations'. *IEEE J. Sel.Topics Quantum Electron.,* 2002, **8**, (6), pp. 1194-1201

55. Prat, J. *Next-generation FTTH passive optical networks: research towards unlimited bandwidth access.* Springer Science, 2008.

56. 'Safety of laser products - part 1: Equipment classification, requirements and user's guide, IEC-60825-1 (Incorporating amendments A1:1997 and A2:2001)', 2001.

57. Sheth, A., Han, R.: 'An Implementation of Transmit Power Control in 802.11b Wireless Networks'. *Technical Report CU-CS934-02, University of Colorado,* 2002.

CHAPTER 9 Conclusions and Future Work

9.1 Concluding summary

This thesis is focused on the performance of hybrid fibre and free space optical (HFFSO) communication systems in optical access networks, and a modelling of the effects of multiple access interference, crosstalk, atmospheric turbulence and amplified spontaneous emission noise in such systems has been presented. A historical overview of fibre and free space optical communication systems and an introduction of optical fibre access networks were provided in Chapter 1, with an emphasis on the potential importance of HFFSO access networks. Devices and processes involved in signal generation, transmission and reception, and the modulation schemes employed in the system modelling, namely OOK and DPPM, were discussed in Chapter 2, along with a brief review of passive optical networks and the physical channels used for optical communications.

The performance evaluation methods used in optical communication system BER modelling, including the GA, CB, MCB and SPA, and the various techniques used in the implementation of multi-user services in optical access networks were discussed in Chapter 3. Factors that can impair a HFFSO system, including attenuation and dispersion in fibre, beam spreading, coupling and scintillation-induced losses in free space, MAI, optical crosstalk, and other system noises were also discussed in Chapter 3, with the gamma-gamma and log-normal pdf models used to characterise the effect of atmospheric turbulence.

In Chapter 4, a model of an optically amplified HFFSO network using CDMA for multi-user service delivery in an indoor environment was presented and analysed using the performance evaluation methods discussed in Chapter 3. Previous indoor CDMA systems have been unamplified and analysed using mainly the GA, which does not provide a full description of the signal and noise processes in an optically amplified system. Therefore an MGF formulation including multi-user contributions was derived for use in the CB, MCB and SPA BER calculations for both OOK NRZ and DPPM systems. The BER calculation complexity is somewhat increased using the MGF based methods, which require a recalculation of the s parameter for each interfering user in the system before averaging over the number of interferers. The BER results showed that the CB

maintains an upper bound on the system BER and the SPA gives a BER lower than the other methods regardless of the amplifier gain. The MCB BER changes with amplifier gain, moving closer to the SPA at low gain ($G = 8$) and closer to the CB at high gain ($G = 26$), but could exceed the CB when the system is dominated by non-Gaussian MAI due to the fact that its original derivation assumes non-negligible Gaussian noise [1, 2]. The GA is less reliable than the MGF methods because it sometimes predicts BER which exceeds known upper bounds (CB and MCB), and for a CDMA system with unpredictable MAI states, the CB could be recommended as the safest method for system BER evaluation because it maintained an upper bound for all parameters used in the analysis in Chapter 4. Lower average power is required to meet target BER in the DPPM CDMA system compared to the OOK CDMA system, and lower transmit power is required from user devices in an optically amplified system compared to a non-amplified system.

Having shown the efficient power utilization of DPPM in the CDMA system considered in Chapter 4, which could seamlessly be integrated with an outdoor access network using WDM for network scalability, Chapter 5 considers a (non-CDMA) WDM DPPM system impaired by interchannel crosstalk. A model for the estimation of the performance of such a system, along with evaluation methods using the GA and the MGF-based methods were both developed for the first time in the work presented in Chapter 5. A novel analysis applicable to any physical channel was derived, and was applied to a non-turbulent WDM FSO system for a better and a quick insight into the performance of such systems. Under the assumptions of frame alignment (FA), only slot alignment (OSA) and slot misalignment (SM) between the desired signal and crosstalk, results were obtained for a system impaired by (i) a single crosstalk source and (ii) multiple crosstalk sources, using the GA, and both the CB and MCB where computational processing time and calculation complexity permits. Compared to the OSA case, the FA case presents a marginally higher BER and power penalty for both single and multiple crosstalk sources, while the SM case (considered only for single crosstalk for analytical and computational convenience) results in a lower BER and power penalty. The performance of the GA and the CB remains the same as in Chapter 4, but in the absence of MAI, the MCB is found to be more consistent compared to when MAI is dominant in the system as seen in Chapter 4. The

DPPM system maintained a lower BER and lower power penalty compared to OOK, in the absence of MAI and turbulence, only when the coding level (M) is greater than 1. When $M = 1$, the BER curves (and also the power penalty curves) for both the DPPM and OOK systems coincide.

The applicability of the model developed in Chapter 5 to practical outdoor FSO systems was demonstrated in Chapter 6 where the model was used to analyse a novel HFFSO WDM network using DPPM, and impaired by both atmospheric turbulence and interchannel crosstalk. The network structure includes a feeder fibre connecting the OLT to a remote node from where the signals are distributed to different ONUs on distinct wavelengths through a turbulent FSO link. The GG pdf, which is a close fit to simulation data [3-6], was used to characterise atmospheric turbulence from weak to saturated turbulence regimes, and the impacts of beam spreading and air-fibre coupling losses on the system performance were considered. The analysis performed in Chapter 6 was simplified by the GA, and exemplified how design parameters such as the free space link distance of the interferer and the desired signal from a remote node, transmitter divergence angle and the demultiplexer adjacent channel rejection, and atmospheric turbulence parameters such as refractive index structure constant could affect the performance of the system. BER results for cases where both the signal and crosstalk are affected by turbulence (TurbSig,TurbXT), only the signal is affected by turbulence (TurbSig,XT) and only the crosstalk is affected by turbulence (Sig,TurbXT) were presented. The results showed that the effect of crosstalk is accentuated in the upstream of the WDM FSO network due to the presence of turbulence and that the combination of both impairments results in an error floor in the upstream system. The system using DPPM (with $M = 2$) presented a lower BER and required optical power compared to the OOK system but has a power penalty advantage over OOK only for very weak turbulence.

An outage probability analysis for a network with both signal and interferer affected by turbulence, such as in the WDM FSO network considered in Chapter 6 was performed in Chapter 7 for both OOK and DPPM systems. To the best of the author's knowledge, the work presented in Chapter 7 represents the first time the outage probability of a system with turbulence-affected signal and turbulence-affected interferer is investigated. The results indicated that a system with acceptable BER could experience deep fades due to turbulence which generally

affects the quality of service. Such fading increases as either the crosstalk power or turbulence attenuation on the interfering signal or turbulence attenuation on the desired signal becomes stronger. It was also shown in Chapter 7 that DPPM is more tolerant to turbulence induced fades compared to OOK.

In Chapter 8, an extensive outdoor OCDMA over WDM network, which could easily be integrated with the indoor hybrid fibre and optical wireless CDMA system analysed in Chapter 4, was proposed and investigated using the GA for quick computation. The result showed that the presence of MAI in the system results in raised error floors, and higher power is required for the downstream transmission at target BERs for moderate to strong turbulence conditions. The MAI contribution to the system performance is more prominent at weak turbulence conditions for the parameters used in the analysis. A power control algorithm was also implemented in this chapter, and it showed to be promising in suppressing the error floor caused by turbulence-accentuated crosstalk due to asymmetric loss between the desired ONU and the interfering ONU.

9.2 Conclusions

The work done in this thesis shows the potential of HFFSO networks to provide high speed broadband services in an optical access network. The following conclusions can be drawn from the theoretical analysis and computational modelling performed in this thesis:

i. A HFFSO network is a promising solution to an all optical access network and could provide limited mobility to user devices in an indoor environment. However, there is a safety concern on the use of lasers in an indoor FSO system, and user mobility may only be achieved with the aid of a tracking and beam steering mechanism.

ii. An optically amplified upstream transmission could ease the difficulty in satisfying the stringent transmitter power required from user devices in indoor FSO systems due to concerns for eye and skin safety.

iii. Several evaluation methods have been used in this thesis because of their different strengths in terms of reliability, simplicity and computational time, and also to check that the behaviour of the models correspond to already established trends from similar analysis performed with these

methods. The MCB and CB are usually more trusted because they are upper bounds, but once turbulence is involved in the analysis, the calculation complexity and computational time with the MGF-based methods becomes high and the GA (which shows better consistency for turbulence affected systems than for non-turbulent systems) is used for quicker analysis.

iv. Optically amplified DPPM receivers in HFFSO networks can provide sensitivity improvement over equivalent OOK NRZ receivers of up to 2.8 dB at coding level of two ($M = 2$) with minimal bandwidth expansion and depending on the turbulence conditions. However, in CWDM systems where the DPPM bandwidth expansion is not problematic, greater sensitivity improvements can be achieved by increasing the DPPM coding level.

v. The reduction in the sensitivity advantage of DPPM systems over OOK systems in the presence of turbulence is attributed to the behaviour of the turbulence pdf which is skewed to the left and has its peak shifting more to the left with increasing Rytov variance (and consequently turbulence strength). This means that more area of the pdf coincides with part of the instantaneous BER curve where the thermal noise is dominant, resulting in an average BER which is dominated by the left tail of the pdf where both DPPM and OOK instantaneous BER evenly converge to 0.5 (i.e. the limit of the instantaneous BER as the instantaneous power tends to zero), and a consequent reduction in DPPM average sensitivity advantage over OOK as the turbulence becomes stronger.

vi. The effects of interchannel crosstalk are exacerbated by optical scintillation in the upstream of a HFFSO WDM system, and results in error floors. The error floor is raised when CDMA is incorporated into the system, resulting in both crosstalk and MAI combining with turbulence-induced scintillation to impair the system.

vii. A full estimation of the effects of turbulence-induced scintillation in a WDM system with an FSO link requires an assessment of its outage probability which is worsened by increasing strength of turbulence and crosstalk power.

viii. A HFFSO WDM access network with a feeder fibre link length of 20 km and a distributive FSO link length of 1500 m can provide high speed broadband services to users at acceptable BER and safe transmit power for all turbulence regimes and in clear atmospheric conditions. Such a network would, however, require an automatic pointing, acquisition and tracking subsystem, and an implementation of a power control algorithm may be necessary to enhance its performance.

ix. The required transmitter power is dependent on the system losses which varies based on the network architecture and level of turbulence. Higher power is required from the ONUs than the OLT in the HFFSO WDM network described in Chapter 6 because of air-fibre coupling losses incurred in the upstream transmission but not the downstream transmission (as signals are directly coupled to the photodetector in the downstream), while in the OCDMA over WDM HFFSO network described in Chapter 8, more power is required from the OLT than the ONUs because of more splitter losses and losses incurred in coupling the signal from air to fibre (which could be extended indoors) in the downstream transmission.

9.3 Proposals for future work

The scope of this thesis has been covered, with regard to the primary objectives set out at the beginning of the research work. However optical communications is a wide research area the totality of which cannot be covered within the time limit of the research. Other related research works that could be performed to extend the work carried-out in this thesis are now recommended.

▪ Through the use of additional power splitters/combiners or by adjusting the positions of existing ones, the outdoor HFFSO networks proposed in Chapters 6 and 8 could be merged with the indoor system described in Chapter 4 to form a larger all optical access network. Such extended network architecture may include a fibre-FSO(outdoor)-fibre-FSO(indoor) link connection and an evaluation of its performance is recommended as future work.

▪ In an OCDMA over WDM network, the code cardinality and network user capacity could be improved by the use of prime codes or more

complex encoding in two dimensions [7, 8]. As the effect of MAI increases with number of users, evaluating the combined impact of MAI, crosstalk and turbulence-induced scintillation in such a system is an interesting research topic.

▪ In addition to aperture averaging, the use of saturated optical amplifiers [9] and diversity schemes such as multiple-input-multiple-output (MIMO) [10-12] have been proposed as turbulence mitigation methods, and could be incorporated into the networks analysed in this thesis for further investigations.

▪ The bandwidth utilization of DPPM could be improved without reducing the average power advantage by hybridizing DPPM modulation with BPSK [13]. Similar multilevel modulation techniques with higher signal constellation, which use direct detection, such as differential phase shift keying (DPSK) [14, 15] could also be used in combination with DPPM for DWDM systems. The models developed in this thesis could be extended to investigate the effects of turbulence-affected interfering signals with the hybrid modulation technique. For such a direct detection (e.g. using MZI based balanced receiver) DPPM DPSK system, the effects of interchannel crosstalk is two dimensional, with the crosstalk capable of causing error in the pulse position as well as the differential phase of the pulse.

▪ The methodology used in this thesis involved only analytical and computational modelling, experimental verification of the results is recommended as future work for full system characterization. One of the major challenges anticipated during experimentation is the issue of timing recovery (for transmitter and receiver clock synchronisation), and a very likely solution is the use of a phase-locked loop (PLL) to lock-in the slot and frame frequency components as long as they are obtainable from the transmitted PPM signal. For DPPM systems transmitting square pulses in a full slot, a pre-processing of the detected signal is necessary to ensure that a strong frequency component at the slot frequency is present in the input signal to the PLL [16, 17].

▪ The behaviour of FSO links has been considered under the assumption of a clear air atmosphere, which is the predominant atmospheric condition over a one year cycle. In more than 10% of time per annum, the

atmospheric conditions consist of mist, rain, snow or fog, or a mixture of any of these conditions [18]. The design of FSO systems that can sustain the required availability in all weather conditions is of high practical interest. Straightforwardly, additional link margin could be provided to enable the system to cope with an increase in attenuation under unclear air atmospheric conditions. However, since these conditions are constantly changing, a variable optical attenuator controlled using real-time data obtained from hydrometric and visibility measuring devices could be included in the system for safety reasons.

- Diffused downstream transmission could be implemented for the indoor hybrid fibre and wireless optical system, since air-fibre coupling is not required in the downstream. Such a system could be susceptible to multipath dispersion [19] and may require more downstream transmit power but could also improve user mobility. Investigation of the effects of multipath dispersion/distortion in such a system could be a topic for future work.

9.4 References

1. Lam, A. W., Hussain, A. M.: 'Performance analysis of direct-detection optical CDMA communication systems with avalanche photodiodes'. *IEEE Trans. Commun.,* 1992, **40**, (4), pp. 810-820

2. O'Reilly, J. J., Mitchell, J. E.: 'Simplified derivation of the modified Chernoff upper bound'. *IEE Proc. Commun.,* 2005, **152**, (6), pp. 850-854

3. Andrews, L. C., Phillips, R. L. *Laser Beam Propagation Through Random Media*. 2nd ed: SPIE Press, Bellingham, Washington; 2005.

4. Abdi, A., Kaveh, M.: 'On the utility of gamma PDF in modeling shadow fading (slow fading)'. *IEEE Vehicular Technol. Conf.* 1999; Houston, TX, pp. 2308-2312

5. Vetelino, F. S., Young, C., Andrews, L., Recolons, J.: 'Aperture averaging effects on the probability density of irradiance fluctuations in moderate-to-strong turbulence'. *Applied Optics,* 2007, **46**, (11), pp. 2099-2108

6. Al-Ahmadi, S., Yanikomeroglu, H.: 'On the approximation of the generalized-K PDF by a Gamma PDF using the moment matching method'. *IEEE Wireless Commun. and Networking Conf.* 2009; Budapest, Hungary: IEEE, pp. 1-6

7. Yang, G.-C., Kwong, W. C.: 'Performance comparison of multiwavelength CDMA and WDMA+ CDMA for fiber-optic networks'. *IEEE Trans. Commun.,* 1997, **45**, (11), pp. 1426-1434

8. Shurong, S., Yin, H., Wang, Z., Xu, A.: 'A New Family of 2-D Optical Orthogonal Codes and Analysis of Its Performance in Optical CDMA Access Networks'. *J. Lightwave Technol.,* 2006, **24**, (4), pp. 1646-1653

9. Abtahi, M., Lemieux, P., Mathlouthi, W., Rusch, L. A.: 'Suppression of turbulence-induced scintillation in free-space optical communication systems using saturated optical amplifiers'. *J. Lightw. Technol.,* 2006, **24**, (12), pp. 4966-4973

10. Navidpour, S. M., Uysal, M., Kavehrad, M.: 'BER Performance of Free-Space Optical Transmission with Spatial Diversity'. *IEEE Trans. on Wireless Commun.,* 2007, **6**, (8), pp. 2813-2819

11. Tsiftsis, T. A., Sandalidis, H. G., Karagiannidis, G. K., Uysal, M.: 'Optical wireless links with spatial diversity over strong atmospheric turbulence channels'. *IEEE Trans. Wireless Commun.,* 2009, **8**, (2), pp. 951-957

12. Khalighi, M., Schwartz, N., Aitamer, N., Bourennane, S.: 'Fading Reduction by Aperture Averaging and Spatial Diversity in Optical Wireless Systems'. *J. Opt. Commun. Netw. ,* 2009, **1**, (6), pp. 580-593

13. Selmy, H., Shalaby, H. M. H., Kawasaki, Z.-I.: 'Proposal and Performance Evaluation of a Hybrid BPSK-Modified MPPM Technique for Optical Fiber Communications Systems'. *J. Lightw. Technol.,* 2013, **31**, (22), pp. 3535-3545

14. Ho, K.-P. *Phase-modulated optical communication systems*. New York, USA: Springer Science & Business Media; 2005.

15. Cancela, L. G., Pires, J. J.: 'Impact of intrachannel crosstalk on the performance of direct-detection DPSK optical systems'. *Quantum Electronics and Laser Sci. Conf.* 2005: Optical Society of America, pp. JThE48

16. Chen, C.-C., Gardner, C. S.: 'Performance of PLL synchronized optical PPM communication systems'. *IEEE Trans. Commun.,* 1986, **34**, (10), pp. 988-994

17. Davidson, F. M., Sun, X.: 'Slot clock recovery in optical PPM communication systems with avalanche photodiode photodetectors'. *IEEE Trans. Commun.,* 1989, **37**, (11), pp. 1164-1172

18. Kvicera, V., Grabner, M., Fiser, O.: 'Propagation characteristics obtained on parallel terrestrial FSO links at 860 nm and 1550 nm'. *2nd Int'l Workshop on Optical Wireless Commun.* 2013: IEEE, pp. 40-44

19. Barry, J. R. *Wireless Infrared Communications*. Boston: Kluwer Academic Publishers; 1994 1994.

$n_1 = 1, 2, …, n$ → Initialise n_1

$t_1 = t_c, 2t_c, …, mt_c$ → Initialise t_1

$t_2 = mt_c − t_1$ → Find t_2

No XT pulse in sig. frame
Find P(0) XT in sig. frame and compute final state weighted BER (B_o)

Only one t_1 partial XT pulse in sig. frame
Find P(t_1) XT in sig. frame
Find P(t_1) XT in sig. slot & compute initial state weighted BER
Find P(t_1) XT in empty slot & compute initial state weighted BER
Multiply
Final state weighted BER (B_1)

Only one t_2 partial XT pulse in sig. frame
Find P(t_2) XT in sig. frame
Find P(t_2) XT in sig. slot & compute initial state weighted BER
Find P(t_2) XT in empty slot & compute initial state weighted BER
Multiply
Final state weighted BER (B_2)

One t_1 and one t_2 partial XT pulse in sig. frame
Find P(t_1, t_2) XT in sig. frame
Find P(t_2) XT in sig. slot while t_2 XT in empty slot & compute initial state weighted BER
Find P(t_1) XT in sig. slot while t_1 XT in empty slot & compute initial state weighted BER
Find P(t_1, t_2) XT in empty slots while no XT in sig. slot & compute initial state weighted BER
Multiply
Final state weighted BER (B_3)

One t_1 and two t_2 partial XT pulses in sig. frame
Find P($t_1, 2t_2$) XT in sig. frame
Find P($2t_2$) XT in sig. slot while $2t_2$ XT in empty slots & compute initial state weighted BER
Find P(t_1) XT in sig. slot while t_1 and t_2 XT in empty slots & compute initial state weighted BER
Find P($t_1, 2t_2$) XT in empty slots while no XT in sig. slot & compute initial state weighted BER
Multiply
Final state weighted BER (B_4)

Two t_1 and one t_2 partial XT pulses in sig. frame
Find P($2t_1, t_2$) XT in sig. frame
Find P(t_2) XT in sig. slot while t_2 XT in empty slots & compute initial state weighted BER
Find P(t_1) XT in sig. slot while t_1 and t_2 XT in empty slots & compute initial state weighted BER
Find P($2t_1, t_2$) XT in empty slots while no XT in sig. slot & compute initial state weighted BER
Multiply
Final state weighted BER (B_5)

Two t_1 and two t_2 partial XT pulses in sig. frame
Find P($2t_1, 2t_2$) XT in sig. frame
Find P(t_1) XT in sig. slot while t_1 and $2t_2$ XT in empty slots & compute initial state weighted BER
Find P(t_2) XT in sig. slot while $2t_1$ and t_2 XT in empty slots & compute initial state weighted BER
Find P($2t_1, 2t_2$) XT in empty slots while no XT in sig. slot & compute initial state weighted BER
Multiply
Final state weighted BER (B_6)

Sum all final state weighted BERs (B = $B_1 + B_2 + B_3 + B_4 + B_5 + B_6$)

Update B — $B_i = B + B_{i-1}$

$t_1 = mt_c$?
No → ++ Increase t_1
Yes →

Update C — $C_j = B_i + C_{j-1}$

Eq. (5.15) — $D = C_j / m$

Eq. (5.14)

PE → Update PE — $PE_k = PE + PE_{k-1}$

$n_1 = n$?
No → ++ Increase n_1
Yes →

Eq. (5.16) — Overall BER — PE_k / n

Appendix B: Steps for the Monte Carlo simulations

❖ Choose coding level M, number of slots $n = 2^M$.

❖ Choose number of crosstalk sources N

❖ Assign integer numbers ranging from 1 to n as slot numbers for signal and crosstalk sources

❖ Assign a specific slot number as the slot containing the pulse in the signal frame

❖ Define the number of crosstalk sources that contribute a crosstalk pulse to slot i of the signal frame as $k_i \in \{0, 1, …, N\}$; ($i \in \{1, 2, …, n\}$).

❖ Create n dimensional matrix of size $N+1$ to represent bins. Each bin corresponds to a position $\{k_1, k_2, …, k_n\}$ in an n dimensional matrix and is incremented when exactly $k_1, k_2, …, k_n$ number of crosstalk sources contribute a crosstalk pulse each to slot numbers 1, 2, …, n of the signal frame respectively.

❖ Perform T trials

❖ In each trial:

  ➢ for each crosstalk,
    • generate a random integer number (z) from 1 to n to represent the slot number in the signal frame that aligns with the nth slot in crosstalk frame 1
    • generate a random integer number (x) from 1 to n to represent the slot number in crosstalk frame 1 that contains the crosstalk pulse
    • generate a random integer number (y) from 1 to n to represent the slot number in crosstalk frame 2 that contains the crosstalk pulse
    • slot number in signal frame in which crosstalk frame 1 contributes a crosstalk pulse is found as: $x + z - n$
    • slot number in signal frame in which crosstalk frame 2 contributes a crosstalk pulse is found as: $x + z$

❖ At the end of each trial:

  ➢ obtain $k_1, k_2, …, k_n$ as the counts in slot 1, 2, …, n of the signal frame respectively
  ➢ increment the bin that corresponds to position $\{k_1, k_2, …, k_n\}$ in the n dimensional matrix

❖ At the end of final trial:

  ➢ probability of $k_1, k_2, …, k_n$ crosstalk sources contributing crosstalk pulses to slot 1, 2, …, n of the signal frame respectively is obtained by dividing the content of the bin corresponding to position $\{k_1, k_2, …, k_n\}$ in the n dimensional matrix by the number of trials T.

Example for coding level $M = 1$ (i.e. $n = 2$)

❖ Coding level $M = 1$ and number of slots $n = 2$

❖ Choose number of crosstalk sources N

❖ Assign integer numbers ranging from 1 to *2* as slot numbers for signal and crosstalk sources

❖ Assign a specific slot number as the slot containing the pulse in the signal frame

❖ Define the number of crosstalk sources that contribute a crosstalk pulse to slot 1 of the signal frame as $k_1 \in \{0, 1, …, N\}$ and the number of crosstalk sources that contribute a crosstalk pulse to slot 2 of the signal frame as $k_2 \in \{0, 1, …, N\}$.

❖ Create bins of row $N+1$ and column $N+1$ in a 2 dimensional matrix. Each bin corresponds to $\{row, column\} = \{k_1, k_2\}$ and is incremented when exactly k_1 and k_2 number of crosstalk sources contribute a crosstalk pulse each to slot numbers 1 and 2 of the signal frame respectively.

❖ Perform T trials

❖ In each trial:

➢ for each crosstalk,
  - generate a random integer number (z) from 1 to 2, to represent the slot number in the signal frame that aligns with the nth slot in crosstalk frame 1
  - generate a random integer number (x) from 1 to 2, to represent the slot number in crosstalk frame 1 that contains the crosstalk pulse
  - generate a random integer number (y) from 1 to 2, to represent the slot number in crosstalk frame 2 that contains the crosstalk pulse
  - slot number in signal frame in which crosstalk frame 1 contributes a crosstalk pulse is found as: $x + z - 2$
  - slot number in signal frame in which crosstalk frame 2 contributes a crosstalk pulse is found as: $x + z$

❖ At the end of each trial:

➢ obtain k_1 and k_2 as the counts in slot 1 and slot 2 of the signal frame respectively
➢ increment the bin that corresponds to $\{row, column\} = \{k_1, k_2\}$

❖ At the end of final trial:

probability of k_1 and k_2 crosstalk sources contributing crosstalk pulses to slot 1 and slot 2 of the signal frame respectively is obtained by dividing the content of the bin corresponding to $\{row, column\} = \{k_1, k_2\}$ by the number of trials T

Appendix C: BER comparison of the impact of two crosstalk sources and a single crosstalk source of equivalent power
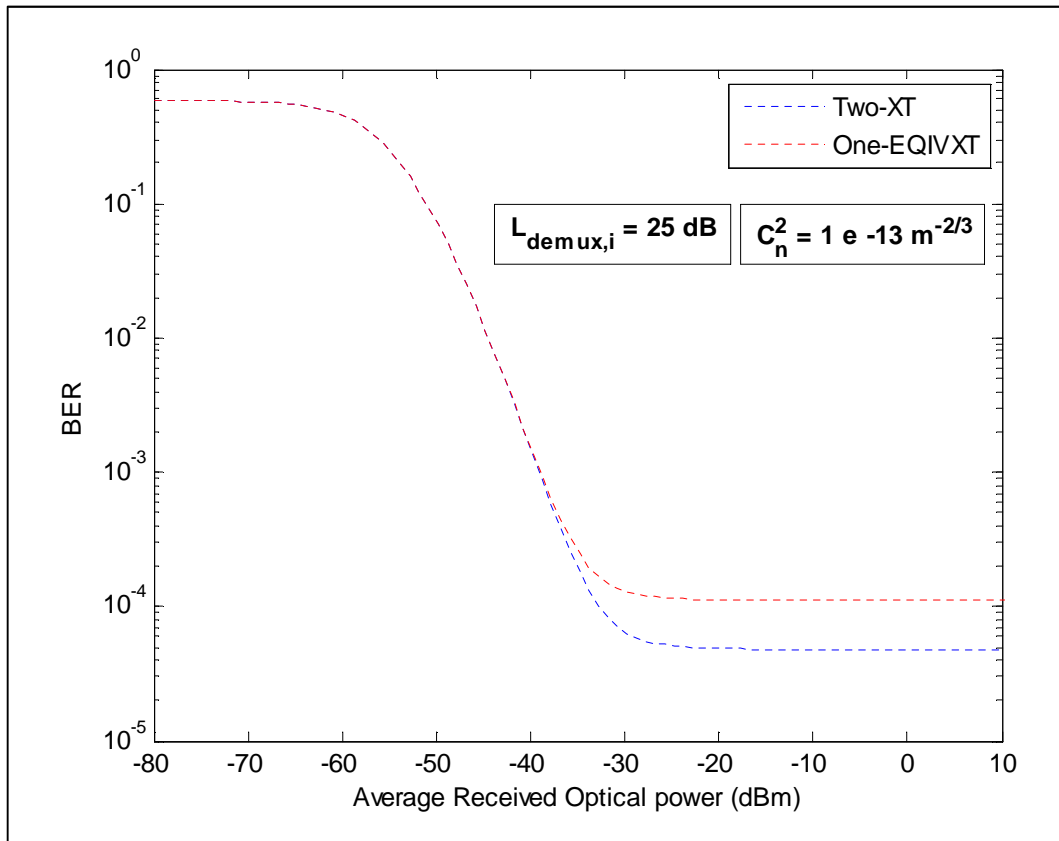
BER comparison of the impacts of two crosstalk sources and a single crosstalk source of equivalent power in a turbulent FSO WDM DPPM system under the FA assumption ($M = 2$, $l_{fso,sig} = l_{fso,int} = 1500$ m and signal-single-crosstalk ratio = $L_{demux,i}$)